THE WATER INSTITUTE
OF THE GULF®

Identifying Sediment Sources and Optimizing Placement of Dredge Material to Protect Critical Infrastructure – Port of Lake Charles

PREPARED BY THE WATER INSTITUTE OF THE GULF

Produced for and funded by: The Port of Lake Charles

05/30/2019

INTEGRATING APPLIED RESEARCH | LINKING KNOWLEDGE TO ACTION | BUILDING PARTNERSHIPS

ABOUT THE WATER INSTITUTE OF THE GULF

The Water Institute of the Gulf is a not-for-profit, independent research institute dedicated to advancing the understanding of coastal, deltaic, river and water resource systems, both within the Gulf Coast and around the world. This mission supports the practical application of innovative science and engineering, providing solutions that benefit society. For more information, visit www.thewaterinstitute.org.

SUGGESTED CITATION

The Water Institute of the Gulf (2019). Identifying Sediment Sources and Optimizing Placement of Dredge Material to Protect Critical Infrastructure – Port of Lake Charles. The Water Institute of the Gulf. Prepared for and funded by the Port of Lake Charles. Baton Rouge, LA.

Preface

This report covers data collection, analysis, and modeling conducted by The Water Institute of the Gulf (the Institute) in the Calcasieu Ship Channel (CSC) and Calcasieu Lake for the Port of Lake Charles in 2017-2018.

The observational data collection described herein was conducted for three purposes. First, to support the numerical modeling work examining sediment transport in the CSC by providing fixed station and boat-based data for model setup and calibration/validation. Second, the data collection was designed to quantify the sediment inputs and outputs to the CSC and within the CSC to examine the magnitude and sourcing of material deposited in the channel. The goal was to develop a quantified sediment budget to understand sedimentation rates and sources, a tool that can be applied to develop strategies that might reduce sediment deposition in the channel, reducing dredging needs. The data collection effort built upon previous projects that the Institute performed to support the Louisiana Coastal Protection and Restoration Authority (CPRA) in their planning for a salinity control structure in the lower reaches of the CSC. The third objective was an initial examination of whether sediment resuspension by ship wakes is occurring within the CSC. All data collected for the project will be provided in raw and processed form along with metadata suitable for server data basing for future use.

The objectives of the numerical predictive modeling effort are to (1) understand the sediment dynamics in the CSC, namely, sediment sources, sediment character, and infilling rates along the channel length; (2) examine sediment dynamics in the CSC under relative sea level rise conditions; and (3) evaluate the impacts to dredging of hydrologic alterations to the channel. Model runs were conducted to compare predictions about depositional hotspots with those derived from the observational data. The results were then used to refine model parameters to better constrain scenarios about how altering the present dredge disposal site configuration will impact the sediment budget and dredging needs.

After a discussion of methods and findings, the report closes with a set of technical recommendations that reflect on ways to better understand the sediment dynamics of the Calcasieu Channel-Lake system, and to further improve the numerical modeling capabilities and predictions of sedimentation.

Table of Contents

List of Figures

List of Tables

Acknowledgements

Several team members of The Water Institute of the Gulf supported this research effort and report production including Mead Allison, Diana Di Leonardo, Justin Ehrenwerth, Christopher Esposito, Ehab Meselhe, Michael Miner, Cyndhia Ramatchandirane, Dallon Weathers, and Brendan Yuill. Additional Institute staff provided assistance during the data collection effort, particularly for fieldwork, including Ryan Clark, Andrea Jerabek, Leland Moss, and Sequoia Riley. The authors would also like to acknowledge Tulane University undergraduate students and Institute interns Amanda Cuesta and Nuri Melancon, who helped with fieldwork and processing samples in the laboratory, as well Tulane University graduate student Daniel Culling for assistance with fieldwork. The authors also thank Austin Feldbaum of the Coastal Protection and Restoration Authority (CPRA) for joining the field crew during several campaigns.

Austin Feldbaum, Chris Allen, Wes Leblanc, Jennifer Mouton, James Pahl, Leigh Anne Sharpe, and Mike Miller of the CPRA provided guidance on the scope of work.

A special thanks to Frank Hughes at Spicer Hughes Marina in Hackberry, LA for allowing the Institute to deploy instruments on the marina's dock for the duration of the data collection campaign.

Tracy Falk, Jeff Corbino, and Rick Broussard from New Orleans District, U.S. Army Corps of Engineers provided helpful comments on draft versions of the report.

This report was edited and formatted by Amy Wold of the Institute.

1.0 Chapter 1: Project Introduction and Background

1.1. OVERVIEW

The Calcasieu Ship Channel (CSC) has become an important economic driver in Lake Charles and in the southwest Louisiana region. The CSC is a 68-mile long, deep-draft commercial waterway located in southwest Louisiana, from Lake Charles into the Gulf of Mexico (Figure 1). Beginning in the 1920s, the CSC was channelized by straightening, widening, and deepening the Calcasieu River to its current dimensions of 400 ft wide by 40 ft deep. Maintaining the adequate channel dimensions to accommodate ship traffic that is increasing in both volume and maximum vessel size requires a rigorous dredging plan. Thus, there is a need to carefully investigate the sediment dynamics along the length of the CSC and surrounding areas in order to understand the sources and character of the sediment and design a feasible and effective dredging strategy. The goal of the present project is to assist the Port of Lake Charles in strategizing to maintain its deep-draft commercial competitiveness through the 21st Century, while at the same time minimizing its environmental footprint and keeping dredging and dredge material disposal area maintenance costs to a minimum. This observational and modeling effort provides the necessary scientific underpinning to develop an integrated plan in the future that may include novel strategies that use dredge material to limit future dredging needs and qualify as beneficial use, and green infrastructure (e.g., ecosystem habitat improvements). Some of these strategies are outlined in the recommendations section.

Prior to the work presented in this current report, The Water Institute of the Gulf (the Institute) conducted a feasibility study to support the Louisiana Coastal Protection and Restoration Authority (CPRA) Calcasieu Ship Channel Salinity Control Project (Ramatchandirane et al., 2014). The Salinity Control Project (Figure 1) was designed to scope a set of structures that would regulate the connectivity between the CSC and the surrounding estuary to limit future increases in salinity in the marshes surrounding Calcasieu Lake while maintaining competitive commercial navigational capacity. With the tentatively selected decision on the configuration and set of control structures, the combined data collection and modeling approach was moved forward to support the design phase of the project with an emphasis on sediment transport, sources, and sinks in the system (Allison et al., 2018). This latter phase was the springboard to the present project for the Port of Lake Charles that continued and supplemented the CPRA-funded data collection effort and focused on the dredging implications of the Salinity Control project and the sediment budget of the system.

This report is divided into 5 chapters:

1. Project Introduction and Background
2. Data Collection and Analysis
3. Delft 3D Numerical Modeling
4. Explore Regulatory Efficiencies
5. Overall Report Summary and Recommendations

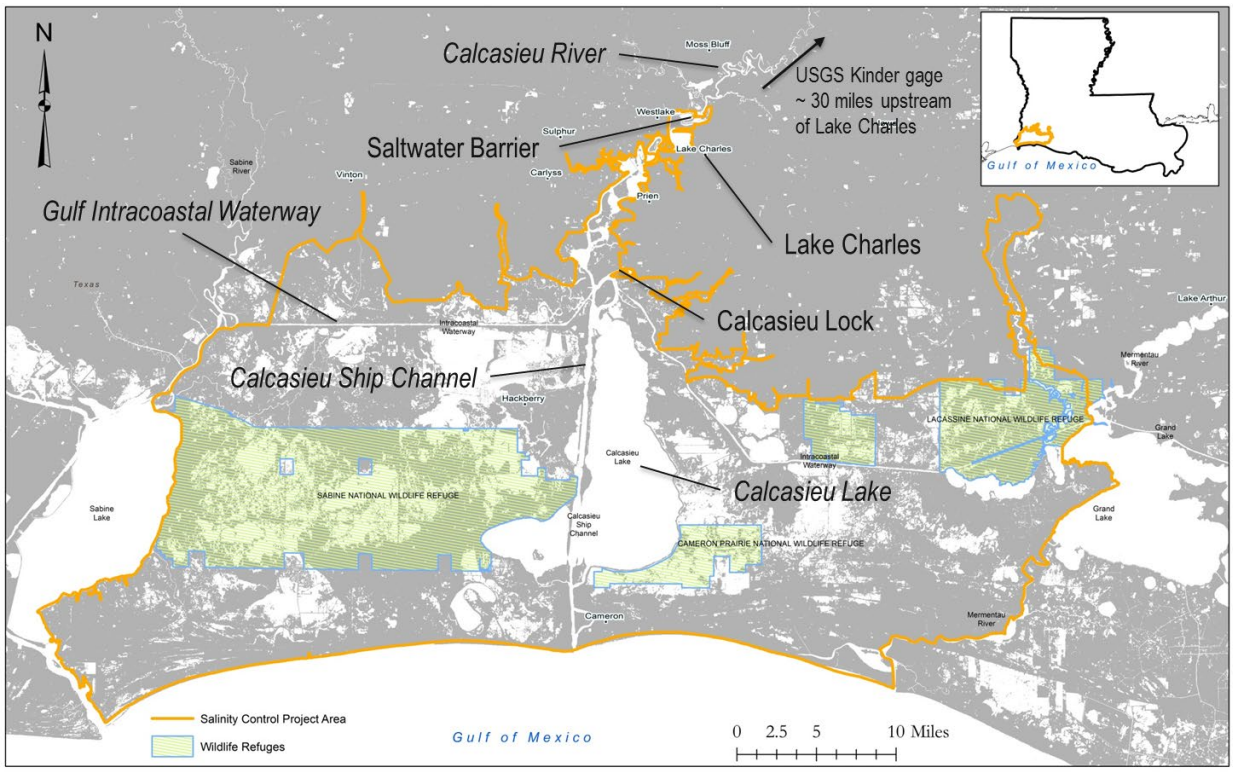

Figure 1. The Calcasieu Ship Channel and Lake system in southwest Louisiana as outlined in the Coastal Master Plan 2017 (Modified from CPRA, 2017).

1.2. GEOLOGICAL HISTORY OF CHENIER PLAIN

The Louisiana coast is divided into two major geomorphic zones: the Mississippi River Delta in southeast Louisiana and the Chenier Plain in southwest Louisiana. The Chenier Plain (approximately 1,930 square miles) is up to 19 miles wide and extends for nearly 125 miles from Sabine Pass at the Louisiana/Texas border to Southwest Pass at Vermilion Bay (Figure 2). It is a low energy (wind and wave) and microtidal environment, that experiences frequent storm impacts. The Chenier Plain is characterized by thin shore-parallel sand and shell-rich ridges (up to 13 ft), often lined by oak trees (hence the Cajun name “chenier” from the French word “chêne” for oak) that are interspersed between mudflats and marsh.

The formation of the Chenier Plain is linked to the history of the Mississippi River. The delta lobes that developed the Louisiana coast in the last ~10,000 years are shown in Figure 2. During periods when the river migrated west, westerly longshore transport carried the large quantities of fine-grained fluvial sediment supply to the Chenier Plain, driving the progradation (seaward expansion) of the shoreline. Meanwhile, when the river migrated to the east, the sediment supply was reduced leaving wave energy to dominate. This process eroded some of the prograded mudflats and reworked localized sandy and shelly material into beach ridge deposits (McBride et al., 2007). Over time, some of these mudflats became vegetated and naturally converted to marsh.

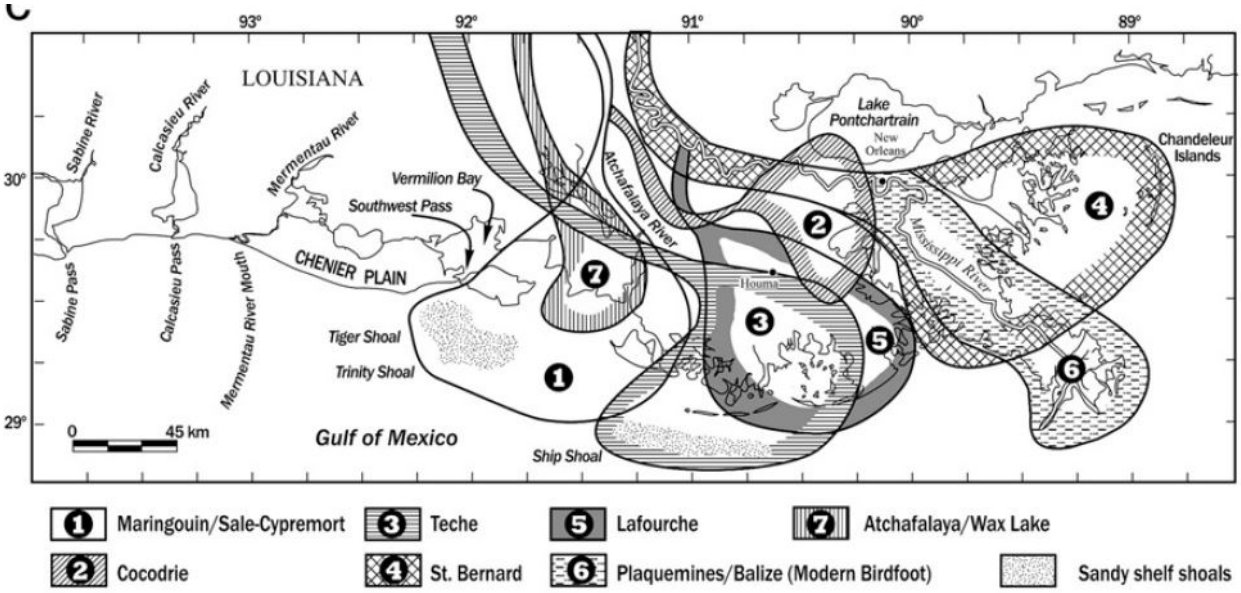

Figure 2. Map of the Louisiana coast, highlighting the extent of the Chenier Plain to the west of the Mississippi River delta complex. The different delta lobes are also shown. Figure from (McBride et al., 2007).

When the Mississippi River was partially diverted to the Atchafalaya River in the 1940s, two new deltas, Atchafalaya and Wax Lake, developed from the new influx of sediment over the next few decades (Figure 3). During periods of high discharge, the sediment plume from the Mississippi River combines with the sediment plume from the Atchafalaya River to form a highly concentrated "mud stream" of fine-grained material that is transported westward and settles along the southwest Louisiana shelf (Wells & Roberts, 1980). Winter cold fronts remobilize this fluid mud and resuspend the material, which is then deposited along the Chenier Plain shoreline (e.g., Kineke et al., 2006). The presence of high concentrations of sediment on the Western Louisiana shelf raises the possibility that the marine sediment input to the CSC and Calcasieu Lake via tidal exchange is significant.

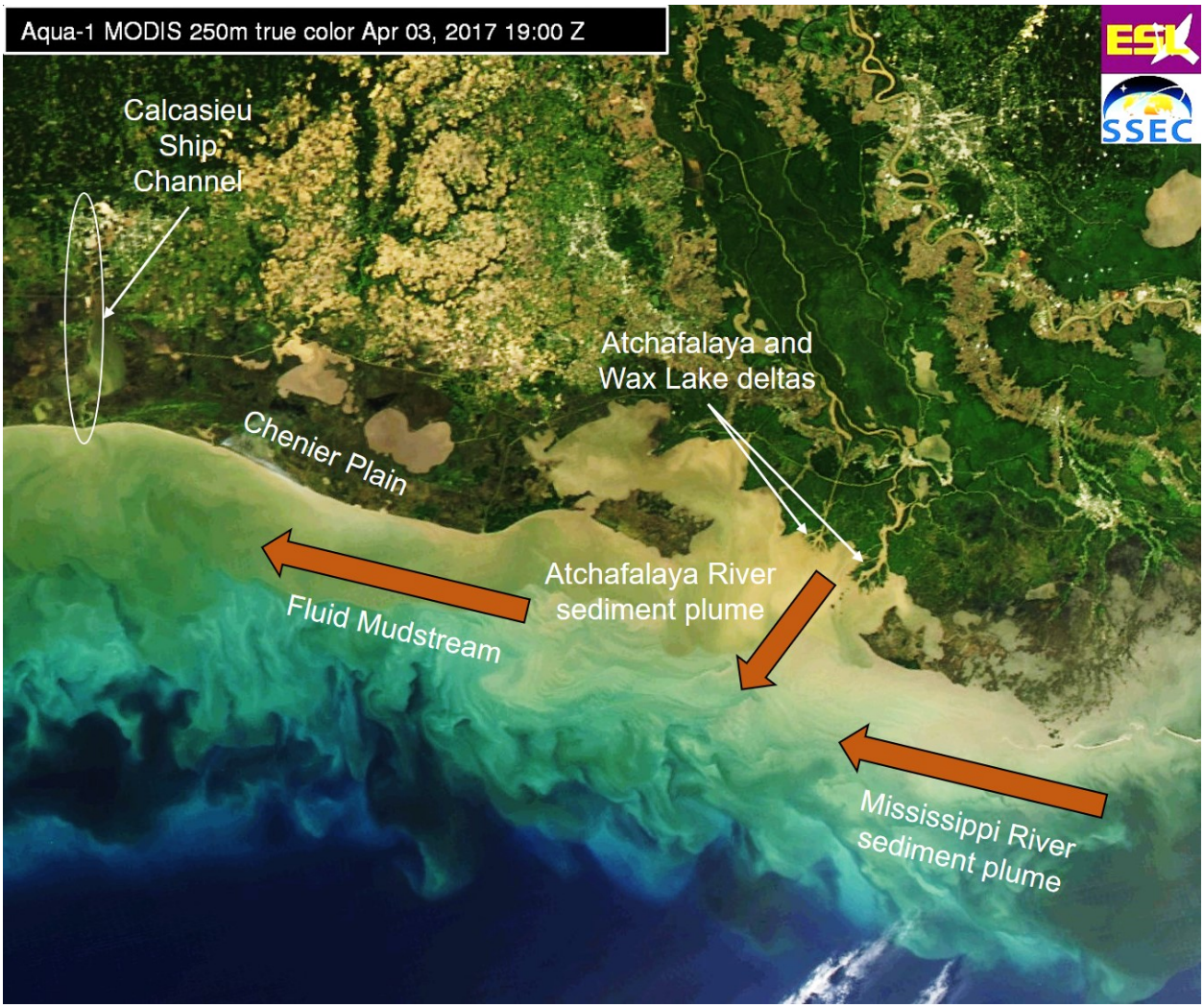

Figure 3. Fluid mudstreams from the Mississippi and Atchafalaya rivers feed the Chenier Plain. MODIS image from the Earth Scan Lab at Louisiana State University.

1.3. SALT WEDGE AND FLOC DYNAMICS

Estuarine conditions form where freshwater from rivers and saltwater from the ocean mix. The interaction between the river flow and ocean tide create unique hydrodynamics and sediment dynamics. Due to the density differences between fresh and salt water, estuarine flow stratification and development of a salt wedge is common. A salt wedge occurs when less dense freshwater flows on top of more dense saltwater (Figure 4). Landward tidal flow can also cause flow convergence, especially near the bed. Flow convergence occurs when river water flows downstream toward the ocean, but the tide flows upstream, creating an area of salinity intermediate between fresh and salt water.

The introduction of saltwater near the bed encourages a process known as flocculation where fine river sediment aggregates into larger flocs made up of multiple individual particles (Al Ani et al., 1991; Burban et al., 1989; Dyer & Manning, 1999; Kranck & Milligan, 1992; Manning et al., 2006). Flocs are larger and settle through the water column faster than individual particles of fine sediment. Faster settling of sediment increases sediment deposition on the bed. The zone of high turbidity and settling caused by

these processes is often termed the estuarine turbidity maximum or ETM (e.g., McLachlan et al., 2017; Ralston et al., 2012; Small & Prahl, 2004). In maintained ship channels, the ETM can be a place requiring significant amounts of repeat dredging due to high sedimentation rates.

Sediment and hydrodynamic processes in the ETM are difficult to measure because the ETM does not exist at a fixed location but moves along the channel with changes in river discharge and tide. Flocculation is similarly difficult to characterize due to the fragile nature of flocs and the difficulty of in-situ measurements. Some success has been seen using in-situ cameras (e.g., Dyer & Manning, 1999; Manning et al., 2006; Wolanski et al., 1996, 1998) and laser scattering measurements (eg. Agrawal & Pottsmith, 2000; Mikkelsen & Pejrup, 2000, 2001).

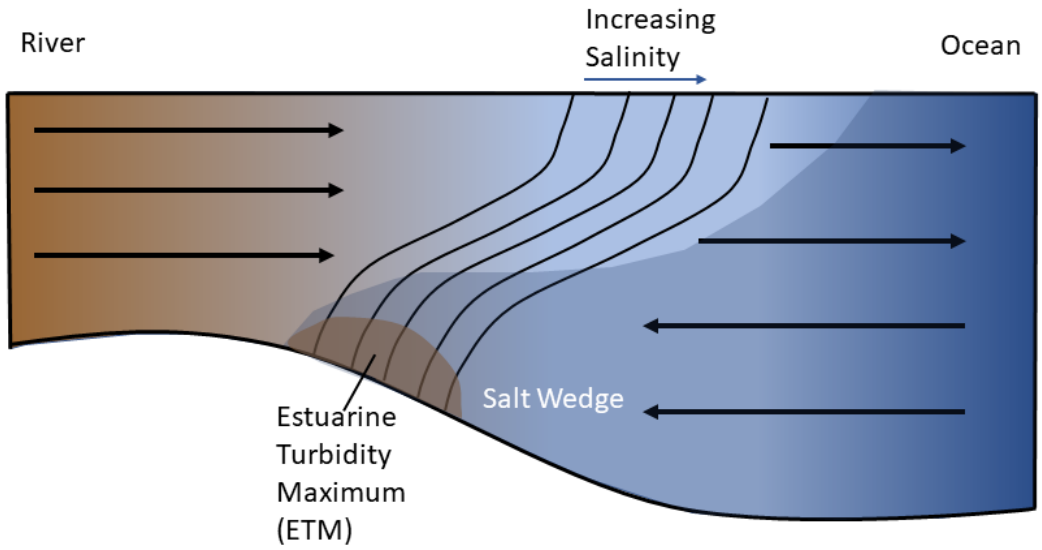

Figure 4. Conceptual diagram of a river estuary and the estuarine turbidity maximum.

1.4. DEFINING UNCERTAINTY IN THE SEDIMENT BUDGETS

Two estimates of total sediment input and output to the Calcasieu Lake system are presented in this report. The first, referred to as the Analytical Budget, is based entirely on observational data. The Analytical Budget is the research team's best attempt to quantify sediment inputs and outputs to the CSC system during the duration of the study, and to use them to contextualize the historical record of dredging in the Calcasieu Ship Channel. The analytical budget is described in detail in Chapter 2, Section 2.4.

The Modeled Budget (Section 3.3 of Chapter 3) is based on the Water Institute's Delft3D model. This model is based on the observational data, and the "base case" Delft3D model comes close to replicating the Analytical model. However, the primary value of the numerical sediment budget is in comparing alternative scenarios to the base case.

Throughout the text describing both the Analytical and the Modeled Budgets, we have referred to the uncertainty in the observational data that is used to create the Analytical Budget and to inform the Delft3D model. Uncertainty expresses the limitations inherent in any measurement of variable processes; these types of uncertainties typically decrease with repeated measurements and more thorough

understanding of the processes under study. Reports of uncertainty bounds express the range of values for a measurement that are known to some degree of confidence. Large uncertainty bounds do not necessarily indicate a lack of confidence in the measurement, but rather may indicate high variability in a process.

Potential sources of sediment considered in the report were bank retreat (also discussed at length in Fischenich, 2004) and inputs from the Calcasieu River, surrounding bayous, and the Gulf of Mexico. The USACE has identified that a fluid mud layer also exists in this channel. Indeed, the Water Institute observed such a layer, though our study was not designed to quantify it. The fluid mud layer in the CSC deserves further study and consideration and the Water Institute hopes to be able to collaborate with the USACE in the future to focus research to better understand this part of the dynamic CSC system. The Water Institute also acknowledges that the GIWW is a potentially significant source of sediment the CSC that is unquantified in the analytical budget. The GIWW West boundary does have a defined sediment input condition in the modeled budget, however the observational data is not present to validate the sediment input at this model boundary. An additional possibility for sediment deposition that deserves further investigation in the channel is a soft geologic layer that has become unconfined due to the excavation at the edges of the ship channel. In this scenario, the weight of the overlying sediments causes this layer to be extruded into the channel, contributing to dredging needs with limited to no surface expression.

2.0 Chapter 2: Data Collection and Analysis

2.1. INTRODUCTION AND BACKGROUND

The main data collection effort for the Port of Lake Charles project focused on twin goals of 1) examining, through the use of analytical sediment budgeting, how sediment exchange in the system impacts CSC dredging needs and frequency, and 2) providing data to setup and calibrate the predictive modeling effort. To this end, the data collection campaign focused on addressing the following questions:

1) What are the sediment sources to the CSC-Lake system?

2) What is the historical record of CSC dredging and how has it varied from reach-to-reach and over time? Is there evidence in this record of locations where dredging "hot spots" coincide with the sediment sources quantified in #1, such that a causal link can be established?

3) Do ship wakes of vessels traversing the CSC resuspend a significant amount of sediment along the flanks of the channel? Is it specific to vessel size? Does this represent a significant mechanism for introducing sediment to the CSC?

2.1.1. Field Description

The Calcasieu River is a small and flashy river (Figure 5), which drains largely rural and forested land north of Lake Charles, Louisiana and forms the inland limit of the Calcasieu Lake and CSC system. Average annual discharge of the Calcasieu River at the United States Geological Survey (USGS) gaging station at Kinder, LA (USGS 08015500) is about 2,000-2,500 cubic feet per second (cfs). Lake Charles, the CSC, and Calcasieu Lake receive water and sediments from fringing marshes and associated bayous, that empty into the lake, and one small bayou (Kelso Bayou) that enters directly into the CSC. Water and constituent exchange also occur with the Gulf of Mexico at the southern end of the CSC, and through the Gulf Intracoastal Waterway (GIWW; Figure 6). The Calcasieu Basin experiences a mixed tide-microtidal regime. The channel is tidally modulated from the Gulf of Mexico up to Lake Charles and the lowermost reaches of the Calcasieu River. Differing water velocities from a top and bottom layer of water flow are often observed in this tidal channel, including in salt wedge conditions (Ramatchandirane et al., 2014).

Two existing structures mitigate saltwater intrusion into the Calcasieu/Sabine and Mermenteau basins (Figure 1). The Calcasieu Lock is located in the GIWW, 2 miles east of the CSC. The Calcasieu Saltwater Barrier, 2.5 miles north of the I-10 bridge, prevents saltwater intrusion north of the CSC into Calcasieu River.

Before entering the Gulf of Mexico, the CSC cuts straight through Calcasieu Lake, which is approximately 82 mi^2 in area including West Cove (Figure 6). The lake is connected to the CSC via several pathways: West Fork (WFRK), East Fork (EFRK), inlets between the dredged material disposal sites that border the eastern side of the channel, and sheet flow along a shallow submerged levee where the main lake connects to West Cove.

Two bayou exchange points for water and sediment are identified in this study – Kelso Bayou and Grand Bayou. Kelso Bayou empties into the CSC at Hackberry, LA, approximately 5.6 miles south of the

GIWW. It is a small channel, 100 ft wide by 10-12 ft deep, and drains marshes west of the channel. Grand Bayou and other weirs and water control structures (e.g., Peconi Bayou, Mangrove Bayou, Lambert Bayou, and No-Name Bayou) are operated by CPRA and modulate flow between the southeast marshes and Calcasieu Lake. The flow and water quality of the latter features were not examined in the present study, but they are utilized in the analytical sediment budget calculations in Section 2.4.

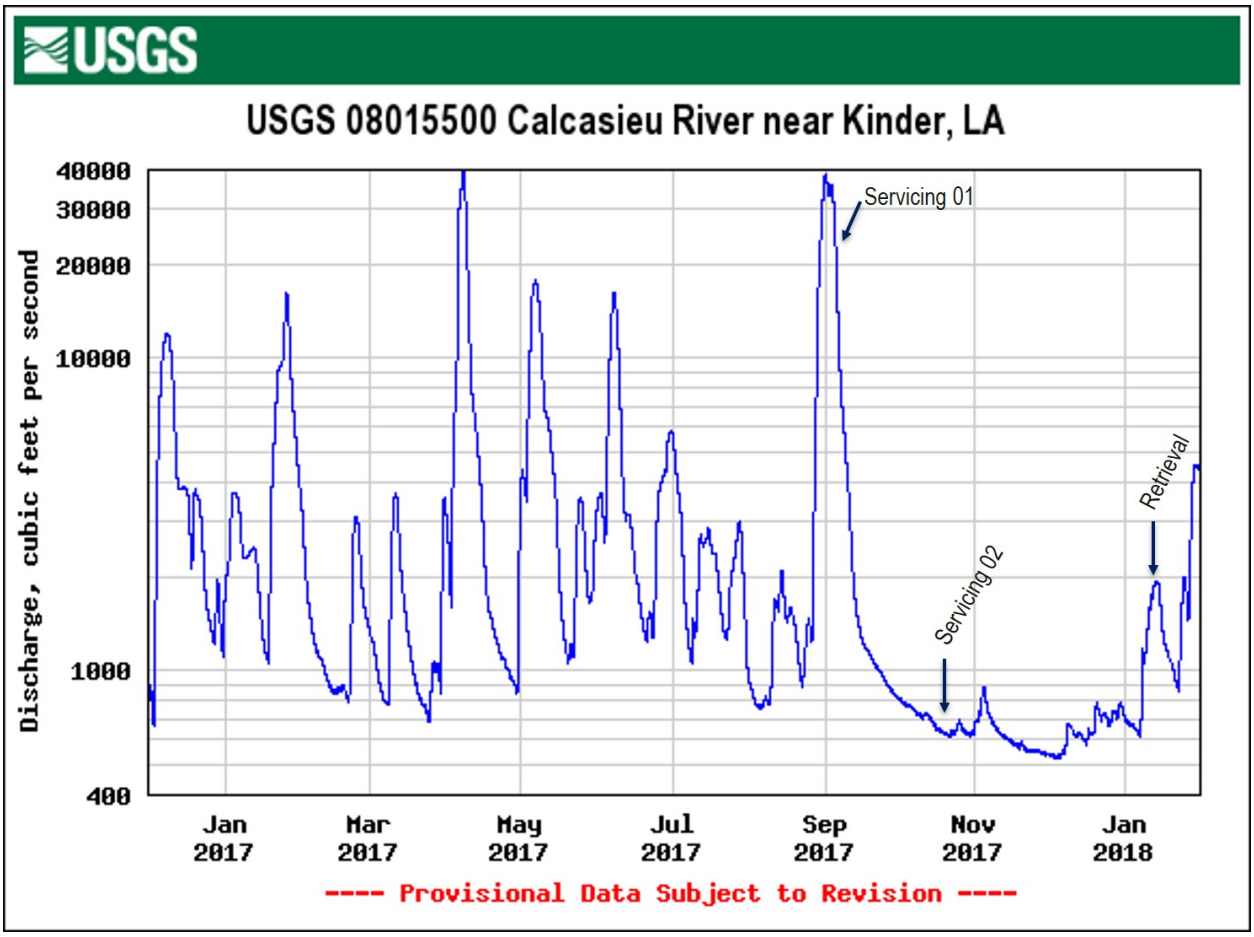

Figure 5. Calcasieu River water discharge at the USGS gage at Kinder, LA (USGS 08015500) during 2017 and study period. Field campaign servicing trips are indicated.

The wind and wave climate in this region is generally mild (Appendix A). Tropical storms and hurricanes in the summer and autumn can produce extreme variations in water levels and the highest wave energies in the system, especially in Calcasieu Lake. Meanwhile, winter to spring cold fronts produce lower magnitude fluctuations in water level (but can exceed the astronomical tidal variation), but the strong pre- and post-frontal winds produce the greatest significant wave heights outside of tropical systems. Tropical storms Cindy and Harvey both made landfall near Cameron, LA during the period of this study, on June 22, 2017 and August 30, 2017, respectively. Their impacts on the water and sediment budget are investigated in Section 2.4.3.

2.1.2. Field Data Collection Campaign

The field data collection campaign was primarily designed to identify and quantify water and sediment input, burial, and export at key water and suspended sediment exchange points in the CSC and Calcasieu Lake (Figure 6) for modeling needs as well as to derive the analytical sediment budget presented in Section 2.4. In addition, the field campaign included collecting channel bathymetry in the upper reaches of the CSC, as well as short-term, high-resolution hydrodynamic and suspended sediment monitoring to investigate the effects of ship wake on channel margin sediment resuspension and sourcing to the CSC.

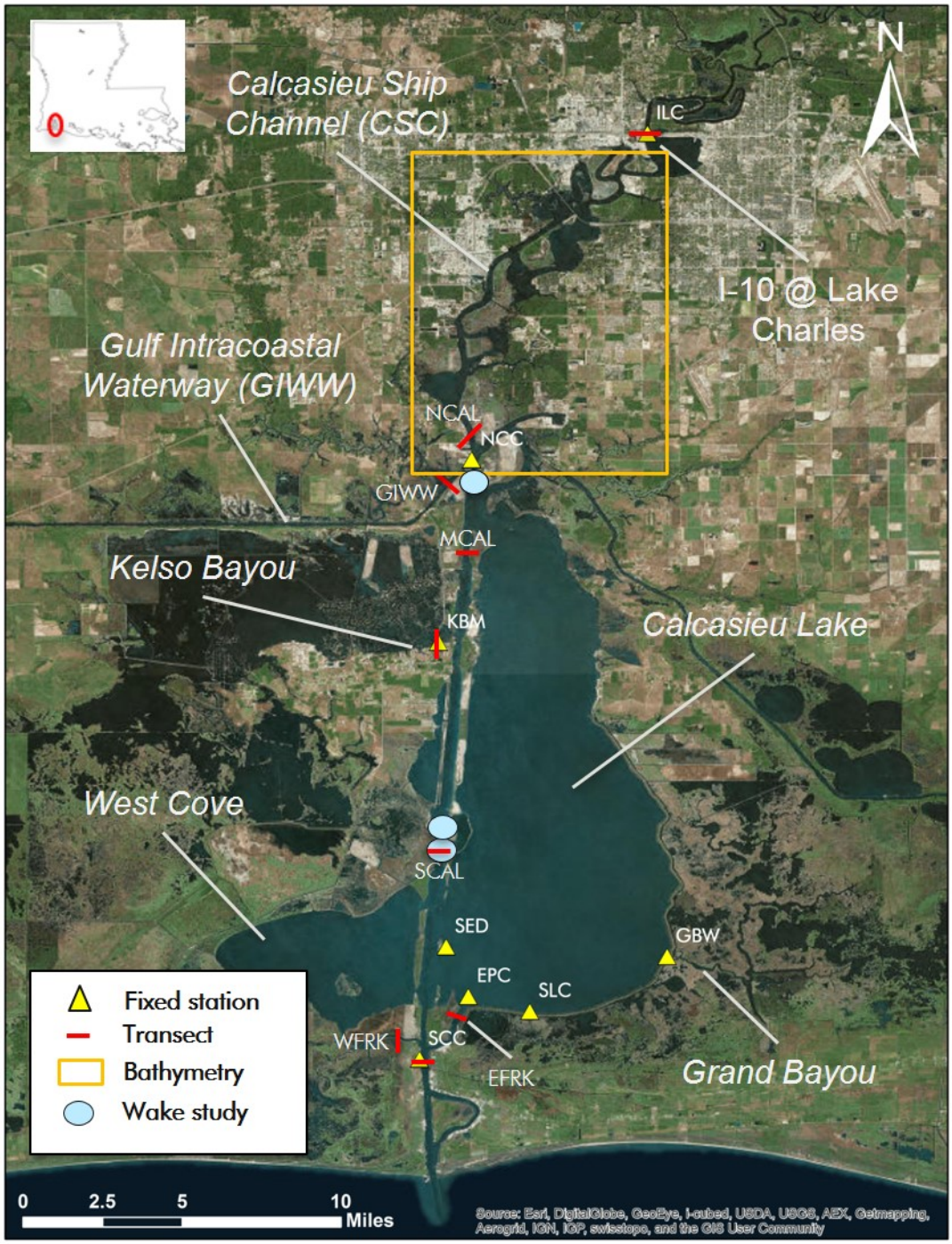

Figure 6. Map of the Calcasieu Ship Channel in southwest Louisiana, showing the fixed and boat-based data collection sites. The four types of collected data are represented here, fixed stations (yellow triangles), boat-based survey transects (red lines), channel bathymetry surveys (orange box), and the ship wake resuspension study stations (blue circles).

Two Institute boats were used in this study, the *R/V Lake Itasca* and the *R/V Silver Mullet* (Figure 7), both aluminum workboats, 26 feet and 22 feet in length, respectively. The field data collection campaign began

in September 2017 and ended in January 2018 (Table 1) and included four distinct tasks summarized in Figure 6: fixed stations, boat survey transects, upper CSC bathymetry survey, and short-term deployments for the ship wake resuspension study. Each of the following sections in this report describes these data collection activities and are followed by the analytically derived sediment budget.

Figure 7. Photographs of the *R/V Lake Itasca* (left) and the *R/V Silver Mullet* (right).

Table 1. Field data collection campaign schedule.

Fieldwork trip purpose	Date
Servicing trip 01 + boat-based surveys	Week of 09/05/2017
Servicing trip 02 + boat-based surveys	10/18/2018-10/27/2018
Instrument retrieval	Week of 01/08/2018

Table 2. Station list and description for each data collection activity including instruments used.

Station ID	Station Location		Instruments	Data
Boat-based transect surveys	ILC NCAL GIWW MCAL	SCAL EFRK WFRK SCC	ADCP, Van Dorn sampler CTD, LISST	Cross-channel discharge, @ thalweg: 3-point suspended sediment, water column profiles for conductivity, temperature, depth, optical backscatter (turbidity), volumetric grain size
ILC	I-10 Bridge @ Lake Charles (USGS station 08017044)		AWS, YSI	Suspended sediment, water level, salinity, turbidity, temperature
NCC	North Calcasieu channel (immediately south of the GIWW)		YSI	Water level, salinity, turbidity, temperature
KBM	Kelso Bayou marina		YSI, H-ADCP	Water level, salinity, turbidity, temperature, discharge
SED	Southeast dredge channel		AQD, YSI	Current profile, waves, water level, salinity, turbidity, temperature
EPC	East Pass channel		AQD, YSI	Current profile, waves, water level, salinity, turbidity, temperature
SLC	South Calcasieu Lake		ADV, YSI	Current velocity, waves, water level, salinity, turbidity, temperature
GBW	Grand Bayou weir		RBR duo	Water level, turbidity
SCC	South Calcasieu channel (USGS station 08017118)		AWS, 2 YSIs, 2 H-ADCP	Suspended sediment, water level, salinity, turbidity, temperature, discharge
Multibeam bathymetry survey	Upper CSC		Reson Seabat 7125	Channel bathymetry
Ship wake study	Areas 1 and 3 (near SCAL) and area 2 (near NCC)		RBR duo, YSI, AQD	Water level, turbidity

ADCP = Acoustic Doppler current profiler; CTD = Conductivity, depth, temperature; LISST = Laser in-situ scatterance and transmissometry; AWS = Automated water sampler; YSI = multi-parameter water quality sonde by Xylem; H-ADCP = Horizontal ADCP; AQD = Aquadopp current profiler; ADV = Acoustic Doppler velocimeter RBR duo = water level and turbidity logger by RBR

2.2. CONTINUOUS DATA COLLECTION

A suite of fixed instruments was deployed along the CSC and in Calcasieu Lake (Figure 6) to examine water and sediment exchange at key points in the system. Data collection began in December 2016, funded by the CPRA to investigate effects of the planned Calcasieu Salinity Control Structure Project on local hydrology. The present funding from the Port of Lake Charles allowed extending the station record, at these same locations, from September 2017 to the end of 2017. This provided a full year of data for model calibration and analytical sediment budgeting. Each fixed station was instrumented with a sonde that recorded water level, salinity, and turbidity. Two automated and programmable water samplers were deployed to collect suspended sediment samples for turbidity calibration of the sonde data: one at the northern end of the CSC under the I-10 bridge by the Port of Lake Charles (ILC) and another near the mouth of the channel, immediately south of the lake (SCC; Figure 6). Three current and wave sensors were deployed in the lake (at SED, EPC, and SLC) to capture wave conditions associated with specific meteorological events (e.g., frontal and tropical). Side-looking horizontal acoustic Doppler current profilers (H-ADCPs) were deployed at KBM to measure the water discharge of Kelso Bayou and at SCC to measure discharge through the confined southern section of the CSC (Figure 6). A log of all fixed station instrument files can be found in Appendix B.

Table 3. Fixed station coordinates in NAD83 UTM 15N.

Station Type	Station Name	Easting	Northing	Latitude	Longitude
Fixed	GBW	477078.1	3303511.5	29.86194	-93.23733
Fixed	SLC	471056.0	3300764.6	29.83703	-93.29961
Fixed	SED	467378.8	3304037.1	29.86647	-93.33777
Fixed	EPC	468346.8	3301533.3	29.84390	-93.32768
Fixed	SCC	466176.6	3298360.9	29.81521	-93.35004
Fixed	NCC	468559.1	3328618.3	30.08833	-93.32628
Fixed	KBM	467050.8	3319347.1	30.00463	-93.34164
Fixed	ILC	476337.6	3345138.7	30.23759	-93.24593

2.2.1. Station Coordinates and Elevation (Trimble RTK GPS)

High precision position and water surface elevation data were collected at each fixed station site on each visit using a Trimble R8 RTK system; the GPS antenna was mounted on top of a 6.5 ft survey pole (Figure 8). Correction factors were provided in real time via mobile internet through the LSU Center for Geoinformatics (C4G) (http://c4gnet.lsu.edu/c4g). Survey points were taken by continuously recording position and elevation (Trimble Access "topo-point" method) until 5 seconds of sufficiently accurate data (±1.2 inches x, y, z location) had been collected. The horizontal datum of the survey was Universal Transverse Mercator (UTM) Zone 15N in the North American Datum of 1983 (NAD83). The vertical datum was the North American Vertical Datum of 1988 (NAVD88) and was calculated referencing the 2012a Geoid (Geoid12A). Both the horizontal and vertical units are in meters. All water levels were corrected to the NAVD88 in Geoid 12A. These data are reported in Tables 3 and 4 and in metadata files provided with the digital data.

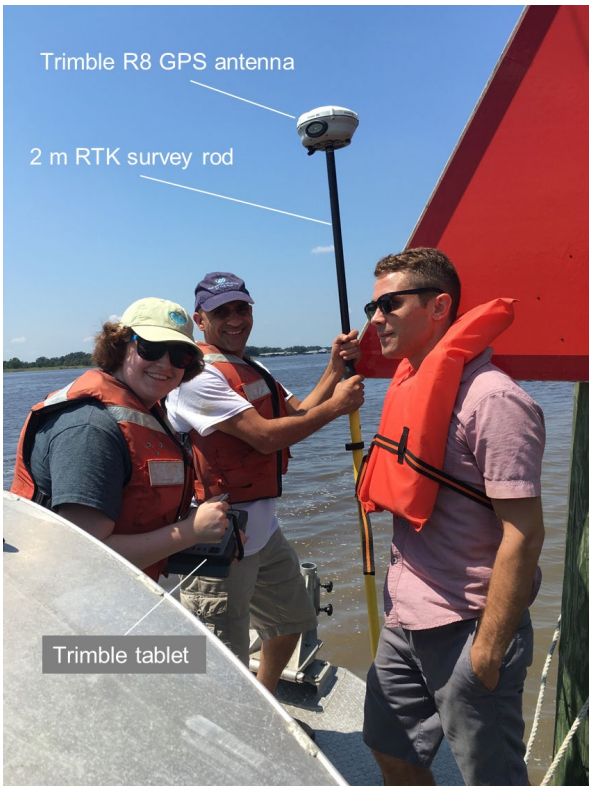

Figure 8. Photograph of RTK GPS survey of water surface elevation.

2.2.2. Multiparameter Hydrological and Water Quality Sondes (YSI)

Nine multiparameter hydrological and water quality sondes (8 EXO2 YSI and 1 OMS YSI) (Figure 9) were deployed at each station in the arrangement catalogued in Table 2, except at SCC where two EXO2 YSIs were deployed, each at different depths (Figure 6 and Table 2). The YSIs are a product of Xylem, Inc. (https://www.ysi.com/EXO2 and https://www.ysi.com/600OMS-V2). The parameters that were measured at all stations were water level, conductivity, temperature, and turbidity (Table 2). Data were continuously recorded at 12-minute and 15-minute, for the EXO2 YSI and OMS YSI, respectively. All recorded data were then averaged hourly. The sondes were serviced (cleaning and battery replacement) according to the schedule in Table 1 and calibrated with standard solutions provided by the manufacturer on service trip 01. Water level data were adjusted using local sea level pressure station data to account for local barometric changes. Quality control included statistical filtering, as well as inter-comparison with nearby USGS water quality and hydrological stations. An example of processed YSI data is shown in Figure 10.

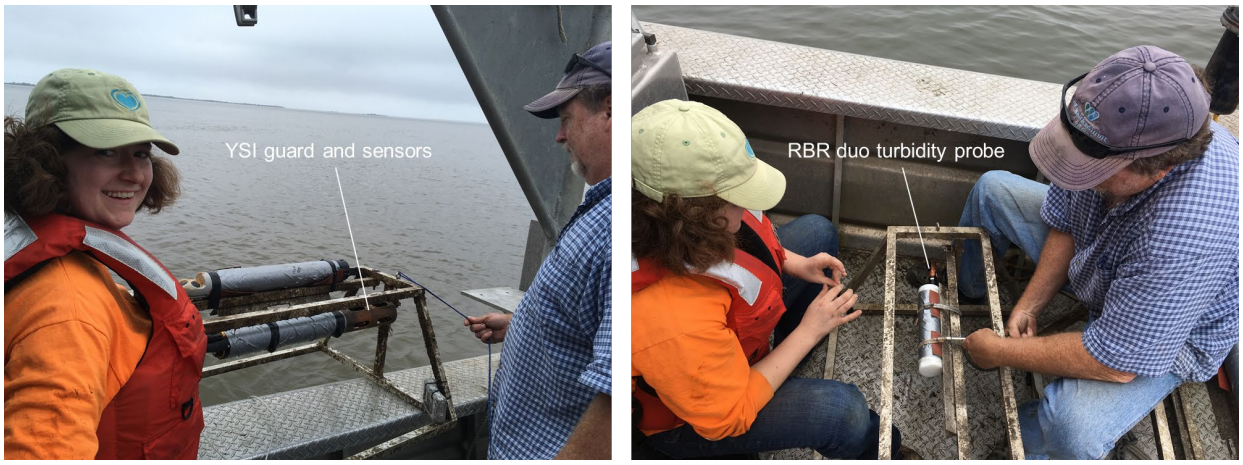

Figure 9. Photographs of hydrological and water quality sonde deployments.

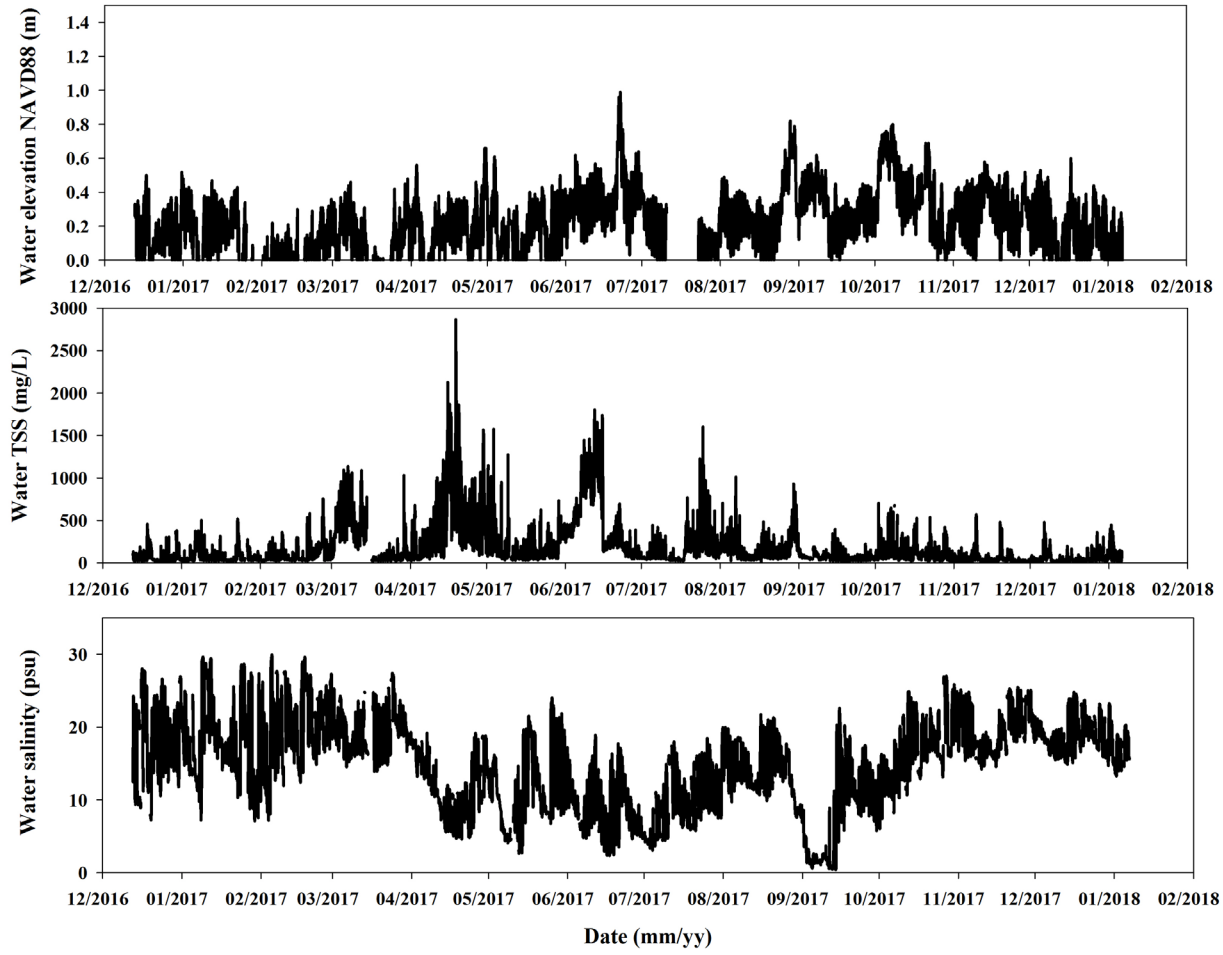

Figure 10. Example of processed hydrological data, water elevation, TSS (total suspended solids), and salinity at EPC (December 2016 – January 2018).

2.2.3. Automated Water Samplers for Suspended Sediment (AWS)

Automated water samplers (AWS) from Campbell Scientific (https://www.campbellsci.com/pvs4120c) were deployed at stations ILC and SCC (Figure 11). The hose intake was aligned with respect to elevation/depth to the YSI turbidity sensor for calibration (Section 2.2.4). This calibration sought to define an empirical relationship between turbidity and suspended sediment concentration. At SCC, the intake was aligned with the top YSI. A datalogger was interfaced with the water sampler and was set to trigger a water sample every 48 hours at 0:00 UTC. At each sample, the datalogger recorded the sample bottle number, the time of sample, and the system status. Prior to each sample event, the sampler sequence flushed out the intake hose to remove debris and biofouling. Water samples were filled to 800 mL and 400 mL, at ILC and SCC, respectively. The AWS was powered by a 12V battery, which was recharged by a solar panel.

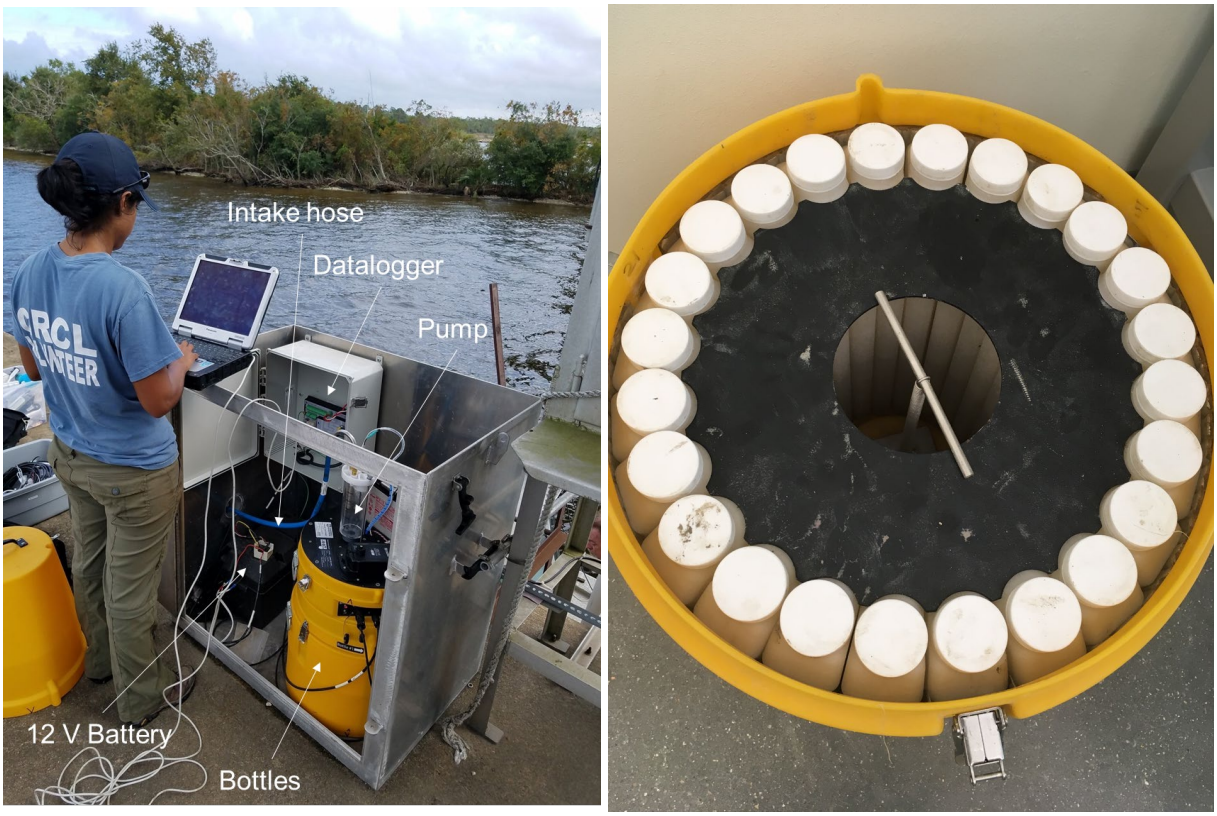

Figure 11. Photographs of the AWS deployed at station ILC. Left, an Institute employee is offloading data from the datalogger. Right, the water bottles from the AWS, each are numbered 1-24. During deployment the bottle caps were removed.

2.2.4. Turbidity Sensor Calibration to Total Suspended Sediment (TSS)

Sonde turbidity values were converted to total suspended solids (TSS) in mg/L using correlations derived from local water samples. In addition to the water sampler bottles collected for suspended sediment at ILC and SCC, 1-liter Nalgene water bottles were collected at each fixed station during each servicing trip. All water samples were filtered on Millipore polycarbonate 0.4 µm membrane filters using a vacuum pump. The filters were then oven-dried at 60ºC overnight before being weighed.

The suspended sediment mass was then correlated with each sonde turbidity value (Figure 12). Linear regression models were derived for each of the water samplers, equations (1) and (2) for ILC and SCC, respectively, where x is the turbidity sensor value in FNU. All other stations (NCC, KBM, SED, EPC, SLC, and GBW) were grouped together as "Other YSIs". The linear regression model for these upper channel and lake turbidities is shown in equation (3). Because the turbidity to TSS relationships for the ILC and "Other YSIs" were determined to be similar (Figure 12), the values from these stations were combined and equation (4) was derived. These regression equations were then used to calculate continuous TSS for all sondes, specifically, equation (2) was applied to the turbidity time-series of both YSIs (top and bottom) at SCC, and equation (4) was applied to the turbidity time-series of all other stations.

$$TSS = 1.22x + 2.21, r^2 = 0.86 \quad (1)$$

$$TSS = 1.19x - 4.67, r^2 = 0.95 \quad (2)$$

$$TSS = 1.19x + 0.63, r^2 = 0.83 \quad (3)$$

$$TSS = 1.17x + 5.25, r^2 = 0.87 \quad (4)$$

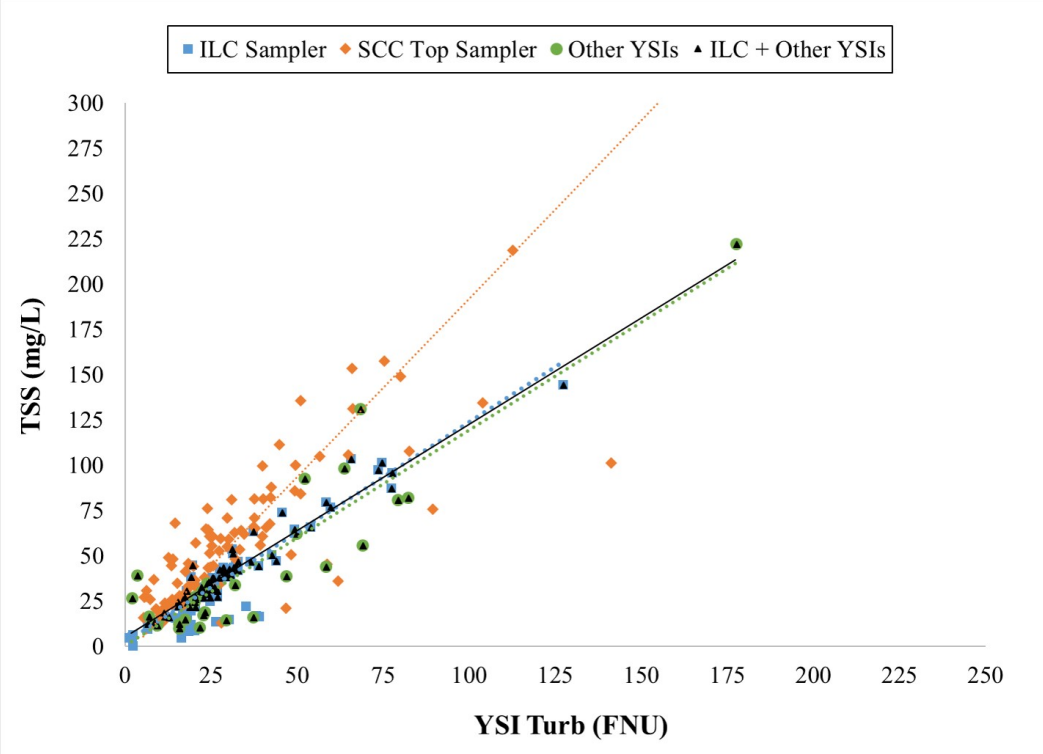

Figure 12. YSI turbidity sensor correlation with total suspended sediment (TSS). TSS was measured from the collected water bottles at each fixed station and from the AWS. Linear regressions were derived for each set of bottles, the ILC AWS (blue squares), the SCC top AWS (orange diamonds), all other fixed station YSIs and RBR (green circles). The ILC and "other YSIs" were combined (black triangles).

2.2.5. Horizontal Current Sensors (H-ADCPs)

Horizontal acoustic Doppler current profilers (H-ADCPs, also called "side-lookers") were placed at two sites to measure water discharge continuously (Figure 13). The H-ADCPs were SL-500s from Sontek, Inc. (https://www.sontek.com/productsdetail.php?SonTek-SL-8) operating at a frequency of 500 kHz. They have a range of 5-656 ft and a cell resolution of up to 10 cells. The velocity is measured to an accuracy of ± 1% of measured velocity. Water velocity profile data were collected horizontally in 9.8 ft and 36 ft size bins for KBM and SCC, respectively, both with a 5 ft blanking distance from the transducers. The profile spanned the width of KBM (9.8 ft x 10 cells), and the SCC profile used the full extent of the instrument to cover approximately 50% of the channel (36 ft x 10 cells). Data were collected and logged for 10 minutes every 30 minutes. At SCC, the top and bottom H-ADCPs were set 15 minutes apart from each other to reduce beam cross-talk interference.

At site KBM, one H-ADCP was deployed at 3-6 ft depth. At SCC, two H-ADCPs were installed, the "top" at 3-6 ft depth, and the "bottom" at 10-13 ft depth in an attempt the capture the salt wedge conditions. Because the transducer beams expand with distance from the transducer, the depths of deployment were determined by considering three factors: 1) the top H-ADCP transducer beams could not be cut off by the water surface at the lowest tide, 2) the bottom H-ADCP transducer beams could not be truncated by the channel bottom, 3) the top and bottom H-ADCP transducer beams should overlap as least as possible.

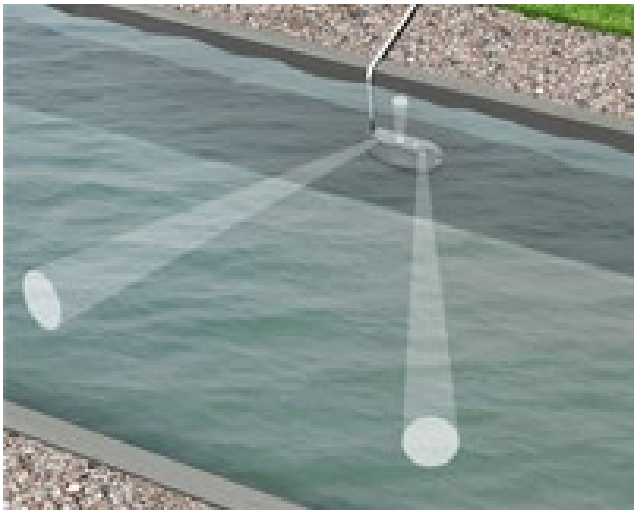

Figure 13. H-ADCP deployment. Left, visual schematic of a deployed H-ADCP where the two acoustic transducers record water velocities at one fixed depth (image from Sontek: http://www.sontek.com/productsdetail.php?SonTek-SL-8). Right, Institute employees service and clean one of the bio-fouled H-ADCPs at SCC.

2.2.6. Wave and Current Sensors (Aquadopps and ADV)

Two side-looking 1 MHz Nortek Aquadopp current profilers and one upward-looking Sontek Argonaut acoustic Doppler velocimeter (ADV) were used in this study to measure currents and waves in Calcasieu Lake (stations SED, EPC, and SLC). The instruments were generally deployed at least 30 ft from any platforms or pilings to minimize potential hydrodynamic influence from any structures contaminating the data set.

The Aquadopp was mounted horizontally on a deployment platform with the transducers facing upward, 0.85 ft above the seabed (Figure 14). The ADV was mounted on a tripod with the sensor prongs facing upward (Figure 14). Aquadopp current profile data and wave data were collected vertically in 1.64 ft and 6.56 ft bins, respectively, both starting from a 1.3 ft blanking distance above the transducers up to the air-water interface. ADV current and wave data were collected as single point data over a sampling volume of 0.015 in^3. The Aquadopps and the ADV were configured to log hourly current profile data from samples collected at 1 Hz and averaged over 60 seconds. The Aquadopp hourly current profile data was then depth-averaged. Hourly wave data were collected in bursts of 1024 samples at 1 Hz. Storm software, also provided by Nortek, was used for data processing and visualization. Example processed data are shown in Figure 15 and Figure 16.

Figure 14. Photographs of current and wave instruments. Left, Aquadopp on sled mount resting on the vessel deck, right, ADV mounted on a bottom-deployed tripod.

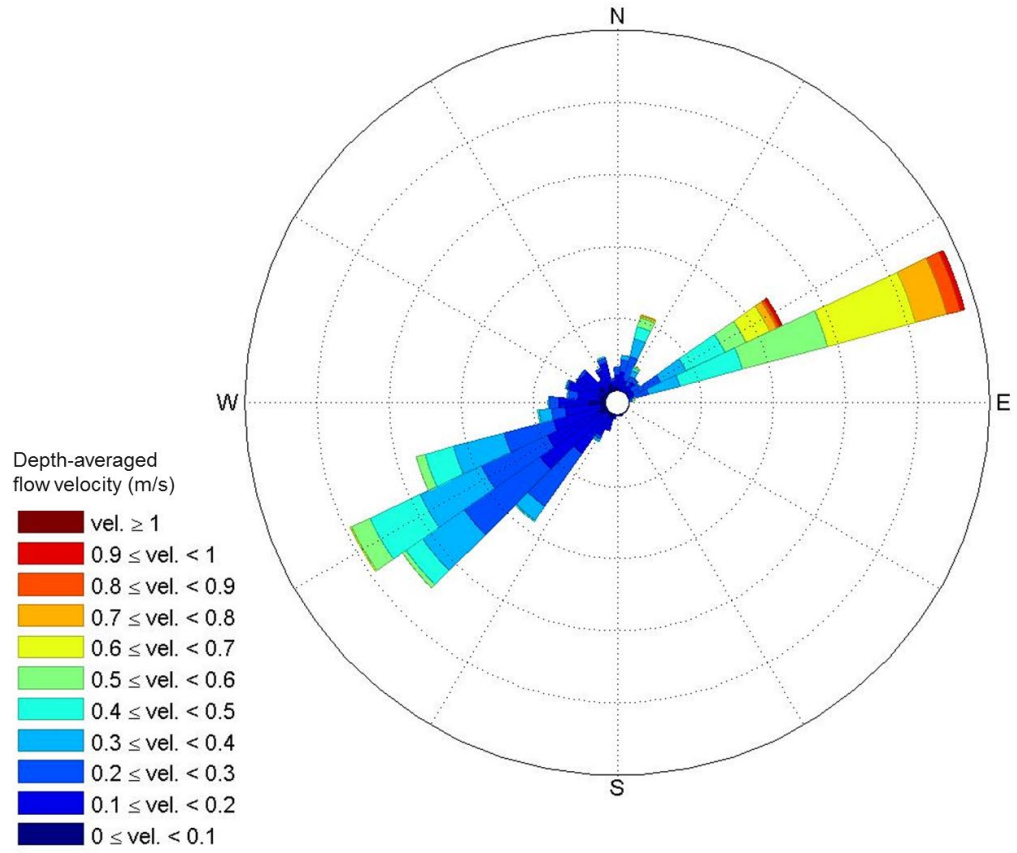

Figure 15. Example of a velocity flow rose at EPC from 03/16/2017 to 5/10/2017, where the compass direction indicates the direction the water is flowing toward.

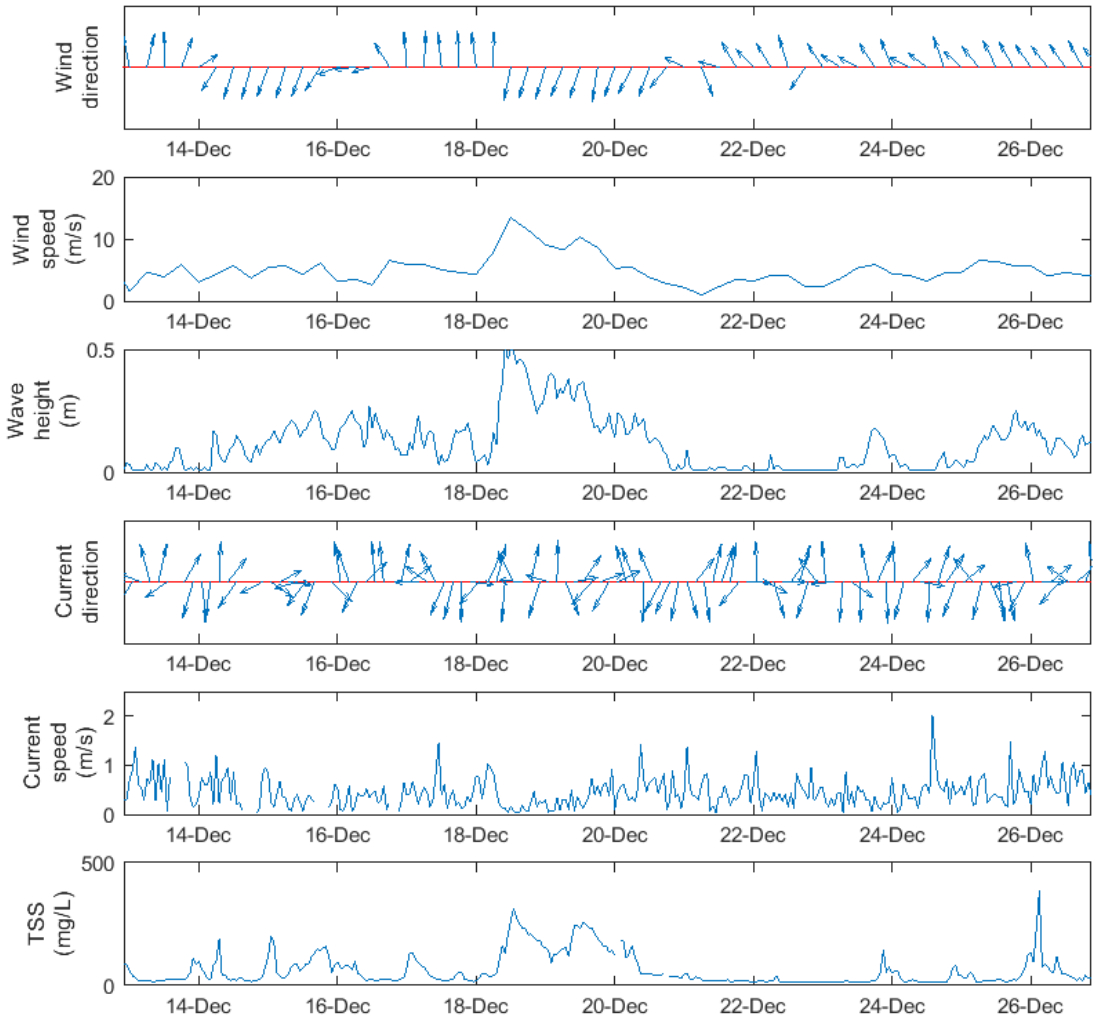

Figure 16. Example of processed wave data from station SED along with wind and TSS plots: wind data was obtained from the National Data Buoy Center (station CAPL1 8768094). This data is from December 2016.

2.3. BOAT-BASED SURVEYS

The boat-based survey transects served three purposes. First, cross-sectional (2D) current velocities were used to calculate discrete discharges along the CSC (Figure 6 and Table 4) at distinct times that can be utilized for model comparison (calibration and validation). Second, water column depth profiles and water samples were taken at the thalweg of each cross-sectional transect to characterize key water quality parameters (e.g., salinity, suspended sediment concentration) for the water column, and are also utilized for calibration of the model (Table 4). Finally, cross-sectional current velocities at stations KBM and SCC were used to calibrate the H-ADCPs at those stations (which measure velocity cross-channel at only one depth) to derive a full channel cross-section integration of water and sediment discharge over the time series (see Section 2.4.1).

Table 4. Boat-based transect survey locations and thalweg coordinates in NAD83 UTM 15N.

Transect	Location description	Easting	Northing	Latitude	Longitude
ILC	In the CSC, south of I-10 bridge at Lake Charles	476238.9	3345147.0	30.23767	-93.24695
NCAL	In the CSC, north of GIWW	468476.3	3329884.4	30.09976	-93.32717
GIWW	In the GIWW, west of the CSC	467807.5	3327848.6	30.08137	-93.33405
MCAL	In the CSC, south of the first lake inlet	468288.9	3324159.8	30.04809	-93.32895
KBM	In Kelso Bayou, west of the CSC	467040.6	3319372.3	30.00485	-93.34175
SCAL	In the CSC, north of lake opening	467054.6	3309074.1	29.91192	-93.34129
EFRK	In East Fork, channel between CSC and Calcasieu Lake	467839.8	3300482.8	29.83440	-93.33289
WFRK	In West Fork, channel between CSC and West Cove	465680.7	3299404.7	29.82462	-93.35521
SCC	In the CSC, south of Calcasieu Lake, north of channel mouth	466251.4	3298385.3	29.81543	-93.34927

2.3.1. Cross-Sectional Water Current Velocities and Discharge (ADCP)

A pole-mounted (down-looking) RD Instruments 600 kHz Workhorse Monitor ADCP was used to collect water velocity profile data along the series of boat-based transects that are listed in Table 4. The ADCP was bow-mounted on the *R/V Lake Itasca* (Figure 17) or *R/V Silver Mullet* to collect velocity data away from the hydrodynamic influence of the boat, including hull wake. Data from the cross-channel transects were used to determine 2D velocity characteristics at each transect at each survey time. WinRiver II software provided by RD Instruments was utilized for data processing and visualization. Positioning was acquired with the Trimble RTK system described in Section 2.2.1, while stream velocity measurements were based on bottom-tracking mode in the WinRiver software.

The vertical distribution of the data was at 1.6 ft depth bins that spanned the water column starting from the draft of the transducer (1-1.5 ft below the water surface depending on wave conditions) plus a blanking distance of 4.75 ft until the river/sea bed was reached. There was also a blanking zone at the bed of 3-6 ft. The measurement software, WinRiver II, extrapolated measurements into these vertical blanking areas in a similar fashion to the stream channel edge areas mentioned above. Duplicate transects were collected in opposing directions at the planned transect lines to account for the potential magnetic compass measurement bias induced from traversing the channel in one direction versus the other.

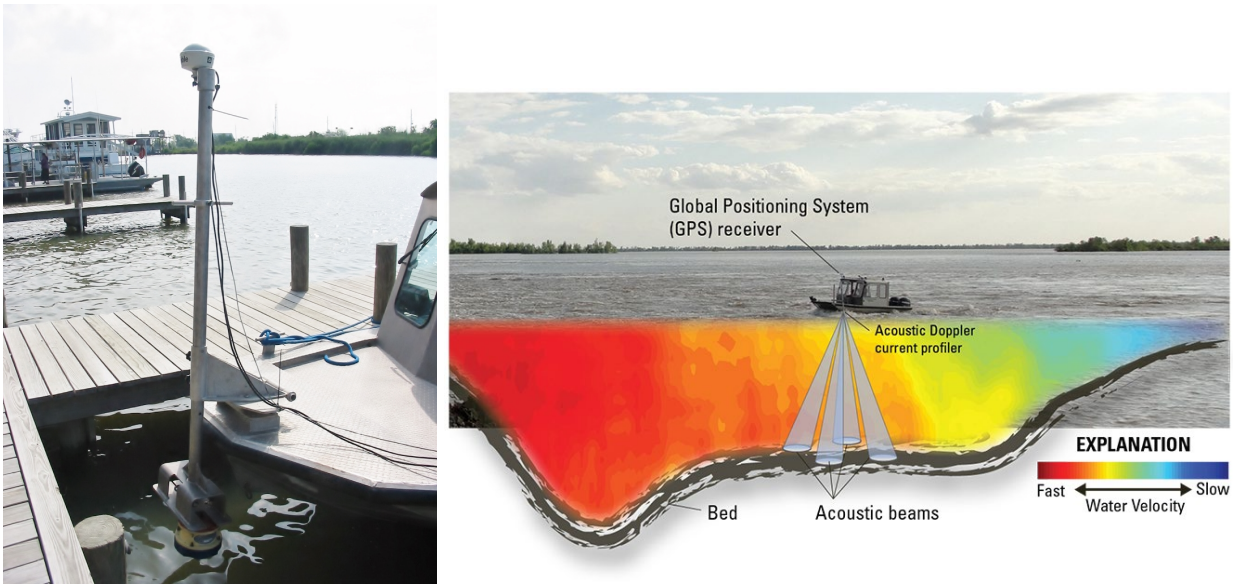

Figure 17. Example of ADCP deployment and boat survey transect. Left, photograph of ADCP instrument and GPS pole-mounted on *R/V Lake Itasca*. Right, visual schematic of boat survey superimposed with ADCP transect data at a channel cross-section (image from Mathworks: https://www.mathworks.com/company/newsletters/articles/analyzing-and-visualizing-flows-in-rivers-and-lakes-with-matlab.html)

The WinRiver II software provided an integrated downstream (i.e., towards the Gulf) or upstream total water discharge by utilizing the measured zone and extrapolating (within the WinRiver software) for the four areas of the channel cross-section not measured (e.g., surface water above the sensor, the near bottom, and the right and left banks too shallow to survey). The depth of the sensor was measured and the distances to the banks were input for each survey by the operator. Figure 18 demonstrates an example cross-section as visualized in WinRiver II. A log of all ADCP transects can be found in Appendix C.

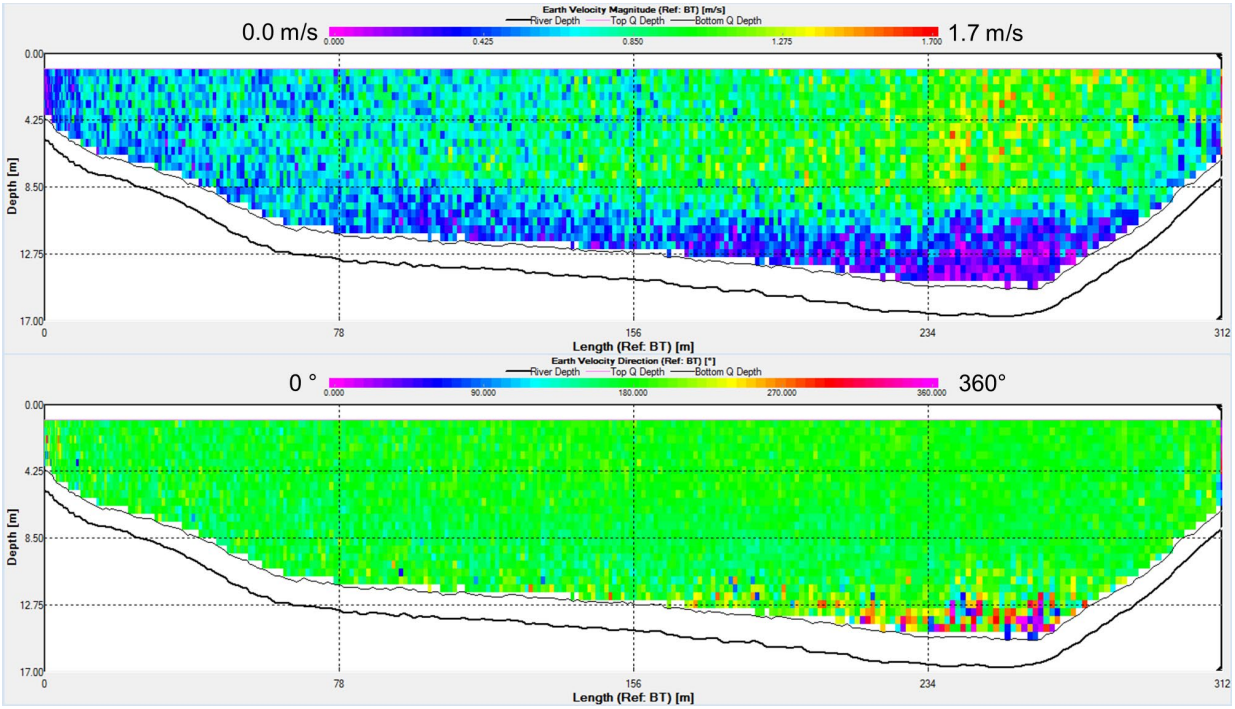

Figure 18. Example of an ADCP channel cross-section transect at station SCC from East to West on March 14, 2017. The top plot shows flow velocity magnitude and the bottom plot shows flow compass direction.

2.3.2. Water Column Profile Casts

Water column profile casts were conducted at the thalweg (maximum depth) of each ADCP transect (Figure 19 and Table 4). One water column profiling instrument, one volumetric in-situ grain size instrument, and one suspended sediment water sampler were deployed on the profiler for each cast. The sub-sections below describe each instrument in more detail. A log of all CTD/LISST casts can be found in Appendix D.

Figure 19. Photograph of a CTD/LISST cast at a transect station. Left, the casting instrument profiler is being deployed. Right, the LISST is attached to the CTD profiler frame and the Van Dorn sampler is attached above the frame.

Conductivity Temperature Depth (CTD)

Casts were conducted at each transect using a Seabird SBE-19 plus CTD (conductivity/temperature/depth) water column profiler (Figure 19). The unit recorded time-synchronized data at a 4 Hz frequency for the following instruments built into the profiler:

a) Microcat CT sensor (records water conductivity and temperature)
b) Paroscientific DigiQuartz pressure sensor
c) Pump flow-through system with pH and dissolved oxygen sensors
d) 5 cm path length transmissometer (optical turbidity)
e) Campbell Scientific OBS-3 optical backscatter turbidity sensor

At the onset of each cast, the profiler was held at the water surface for ~45 seconds prior to lowering it to the bottom to allow the pump to flush water through the system. Only data from the downcast are reported, as the potential for the instrument to touch the bottom and disturb sediment may have contaminated sensor readings during the upcast. Data are presented in tabular form with the following columns:

Col 1 Time (s)
Col 2 Water depth (m)
Col 3 Salinity (PSU)
Col 4 Temperature (°C)
Col 5 OBS-3 backscatterance (nephelometric turbidity units [NTU])

Col 6 Beam transmission (fractional percentage with 100% = 1)
Col 7 Sound velocity (m/s)
Col 8 Converted OBS (mg/L)

Figure 20 is an example of the turbidity data (transmissometer and OBS) from the SCC station. Note the reversed response of the two optical systems; increasing suspended sediment concentration reduces optical beam transmission (%) but increases optical backscatterance (NTUs).

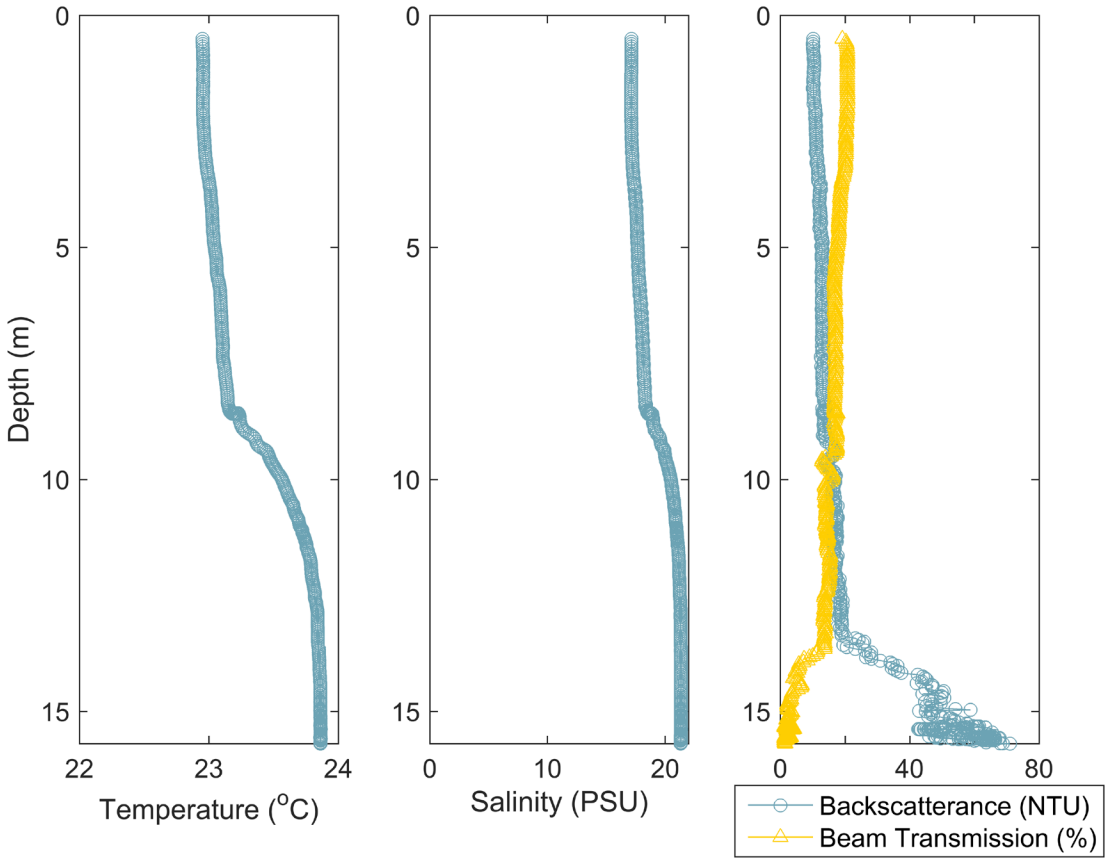

Figure 20. Example of processed data recovered from the CTD profiler from SCC on October 20 2017. From left to right, temperature, salinity, and turbidity. In the turbidity plot, data for both the optical backscatterance sensor and transmissometer are shown. Note the inverse relationship between optical beam transmission (less transmission with increasing sediment concentration) and optical backscatterance data (greater transmission with greater concentration).

Volumetric Grain Size in Suspension (LISST)

A Sequoia Scientific Laser In Situ Scattering and Transmissometry (LISST) sensor was attached to the CTD profiler frame and operated during each cast to measure in-situ particle size and concentration (Figure 19).

The LISST 100-X model (type C) uses laser diffraction from suspended particles to measure in-situ particle size (disaggregated and flocculated combined) over a size range of 1.9 to 380 µm (using the random particle shape inversion method (Agrawal et al., 2008). This unit was operated with an 80% path

reduction module (PRM) to compensate for the relatively high turbidities in the CSC; without the module, the unit saturates at concentrations above about 100 mg/L. The LISST was set to sample at 10 Hz, averaging over 10 samples to generate output data at 1 Hz. Depth was measured by an internal pressure sensor separate from that of the CTD profiler.

Raw LISST data are a measure of the laser scattering across 32 ring detectors. The raw data are combined with background scatter data (zscat file described below) to generate particle size distributions using MATLAB-based processing scripts provided by Sequoia Scientific. Processed LISST data takes the form of a volume distribution, the ratio of the volume of sediment (µl) to the volume of water (L) in the measured sample volume, distributed across 32 size bins. The resulting grain size distribution represents the in-situ grain sizes; flocculated muds are measured as their aggregate size (Agrawal et al., 2008). Due to the variety of grain shapes in sediments, the random particle size model was used to process the LISST data (Agrawal et al., 2008). The efficiency of laser transmission can change with time, thus, the LISST is frequently calibrated using particle free water. Background scatter measurements of distilled water were taken in triplicate and then averaged to generate the zscat file used in post-processing. Next, to account for the reduced path length of the PRM, a simple multiplication correction was applied to both the volume concentrations and the beam attenuation. Using the corrected concentration data, other grain size metrics were calculated, including the median grain size, mean grain size, and the grain size standard deviation.

LISST data processing yields a 46-column data table that is stored in ASCII digital files provided with this report. Columns 7-38 (or G through AL in Excel) contain the particle size distribution, expressed in volume concentration (µL/L) for each size bin. The data file also contains supporting information such as date, time, laser transmission, and battery voltage. The volume concentration in four grain size classes (2-32 µm clay and fine silt, 32-62 µm coarse silt, 62-125 µm very fine sand and >125 µm fine to coarse sand) are also delineated. Each column is labeled with the data and units.

LISST data can be visualized in several ways. Figure 21 shows depth profiles from SCC, demonstrating the ability of the LISST to measure both the particle size and particle concentration. Particle concentration in each of the previously mentioned size classes is also shown.

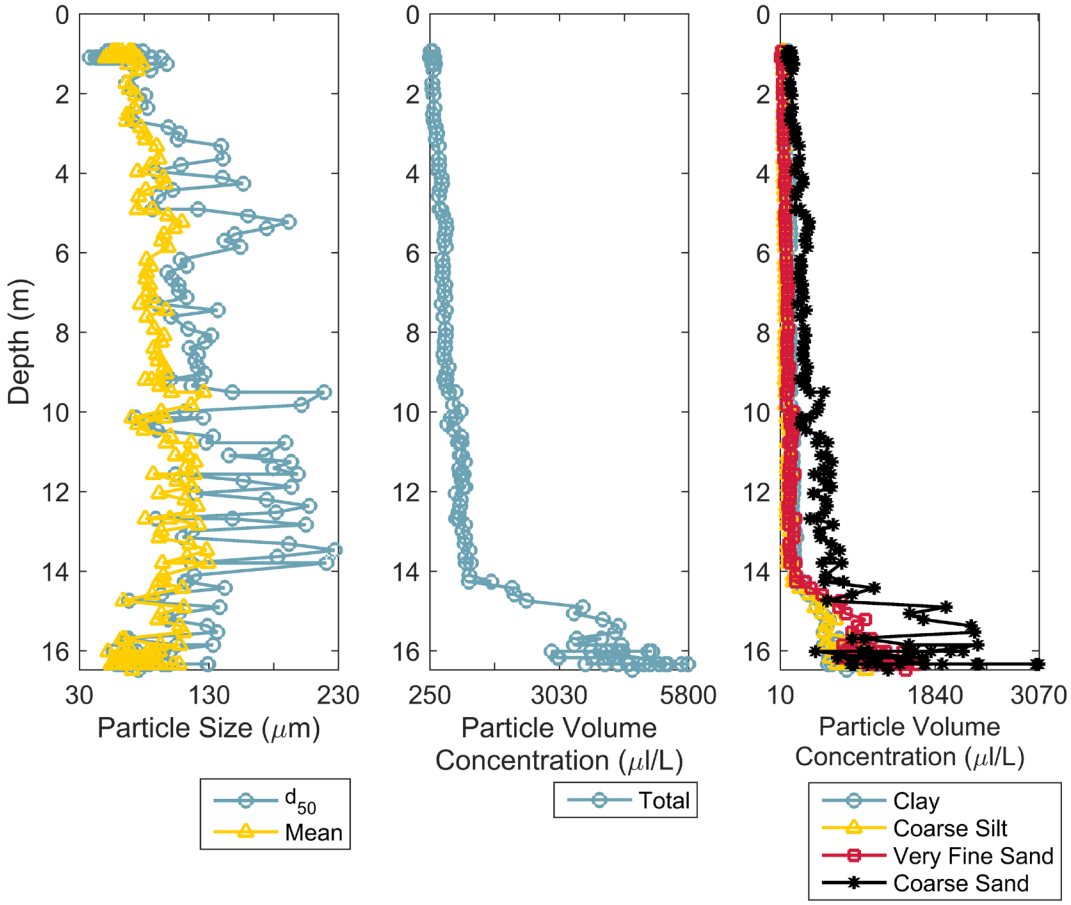

Figure 21. Example of processed (all data points, no depth filtering) LISST water column profiles from SCC on October 20, 2017. The mean and median (D50) particle size (left plot), total particle volume (middle plot), and particle volumes in size classes (right plot) at station SCC, demonstrate how LISST data may be visualized. These size classes reflect a combination of discrete and aggregate particles.

Suspended Sediment Water Sampling (Van Dorn)

Suspended sediment point samples were collected with a Van Dorn water sampler obtained from the Wildlife Supply Company in Yulee, FL (Figure 22). The Van Dorn sampler is a vertically deployed, PVC 2.2-liter sampler that captures a water mass from a specific depth (read from the wire guide) using a trigger messenger sent down the wire. The winch wire on the *R/V Lake Itasca* is 150 ft in length, which defines maximum sampling depth. Generally, one station was occupied in each cruise at the thalweg of each cross-sectional transect where CTD/LISST casts were also being conducted. Sampling was done following standard USGS methods of samples at 0.5, and 0.9 water depth, with the exception that water surface samples were collected in lieu of samples at 0.1 water depth. Samples in the Van Dorn were shaken and transferred to 1-liter sample bottles for return to the laboratory.

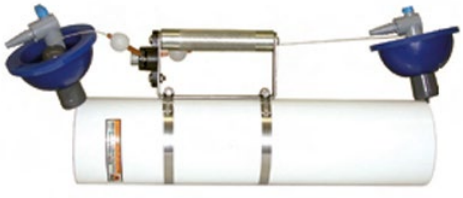

Figure 22. The 2.2-liter Van Dorn bottle water sampler used for suspended sediment sampling.

Water samples from the Van Dorn water sampler were analyzed for suspended sand and mud concentration. The sand fraction was removed, and the volume was measured by pouring the sample through a 62.5 µm (4 φ) sieve into a graduated cylinder. The remaining suspended sediment was vacuum-filtered onto pre-weighed 0.4 µm polycarbonate filters. The sand fraction and mud fraction (<63 µm) were oven dried at 60° C overnight. After cooling to room temperature, the dry weights were measured. Total suspended sediment concentration (in mg/L) was determined using the total of the measured sediment weights and the volume of the water sample. A log of all suspended sediment water samples can be found in Appendix E.

2.3.3. Multibeam Bathymetry

Multibeam bathymetric surveys were collected from the *R/V Itasca* to build a bathymetric basemap of the channel floor in the Upper CSC (Figure 23; magnified inserts Figure 24) for use in numerical model setup.

The Reson Seabat 7125 is a dual frequency system (200 kHz and 400 kHz), data utilized for this study were the higher resolution 400 kHz data. At the higher frequency, data were collected from 512 individual beams over a 165-degree swath with a 0.5-degree separation between each beam. The vertical resolution at both frequencies was 0.6 cm.

Positioning, heading, and attitude data (heave, pitch, roll, and yaw) were provided by an Applanix POS M/V 320 inertial guidance system mounted inside the hull of the vessel. It was operated in Real Time Kinematic (RTK) mode with real time correctors provided through the GulfNet real time virtual reference network. The reference network had correctors with a zero-length baseline and as such, no error was due to rover-base station separation. In a tightly coupled solution, the RTK corrected elevations/depths are about 2 cm in horizontal accuracy and 3 cm in vertical accuracy. The inertial measurement unit (IMU) of the POS M/V provided roll, pitch, and yaw corrections in millisecond (ms) time intervals to correct measurements to within ±0.01 degree. Once calibrated, the dual GPS antenna setup provided headings corrected to within ±0.02 degrees accuracy. Heave was measured to within 5 cm, and with the TrueHeave™ algorithm employed by the POS M/V, the precision dropped to 2 cm. The POS M/V also provided time synchronization for all data (e.g. motion, position, depth) at a 1 ms interval.

The horizontal datum of the survey was Universal Transverse Mercator (UTM) Zone 15N in the North American Datum of 1983 (NAD83). The vertical datum was the North American Vertical Datum of 1988 (NAVD88) and was calculated referencing the 2012 Geoid (Geoid12). Both the horizontal and vertical units are in meters.

Data from the multibeam system were collected in QINSy hydrographic acquisition software at a rate of 15 Hz. This dataset was post-processed using the Qimera software. Post-processing includes removal of multiples, other noise, and navigation drop-outs. Sound velocity correction was applied based on velocity measurements collected with the Conductivity, Temperature, Depth (CTD) instrument during the survey periods. Soundings were merged with horizontal and vertical positioning data, as well as inertial data to generate channel bathymetry grids.

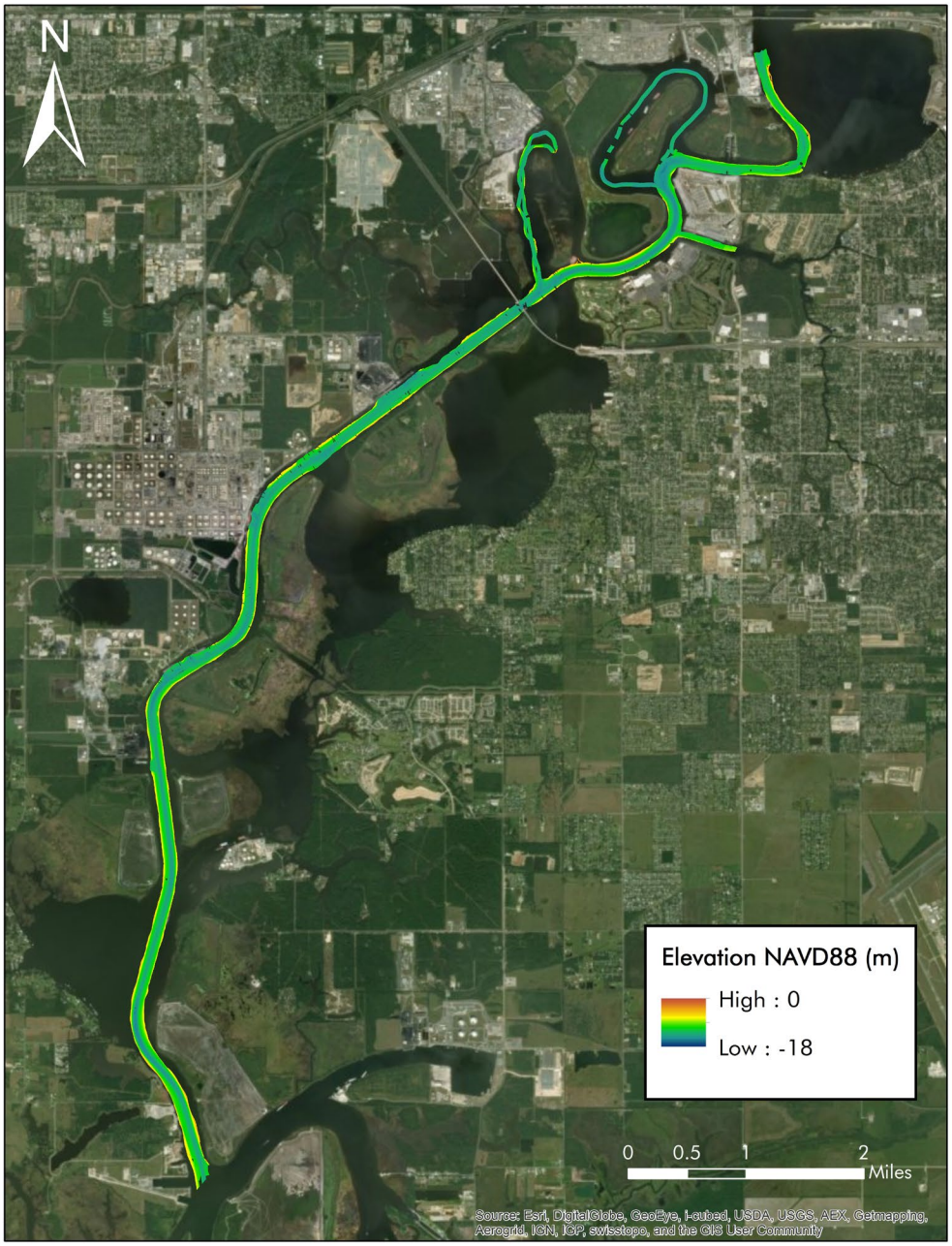

Figure 23. Multibeam bathymetry map of the Upper CSC collected in the present study (full surveyed coverage).

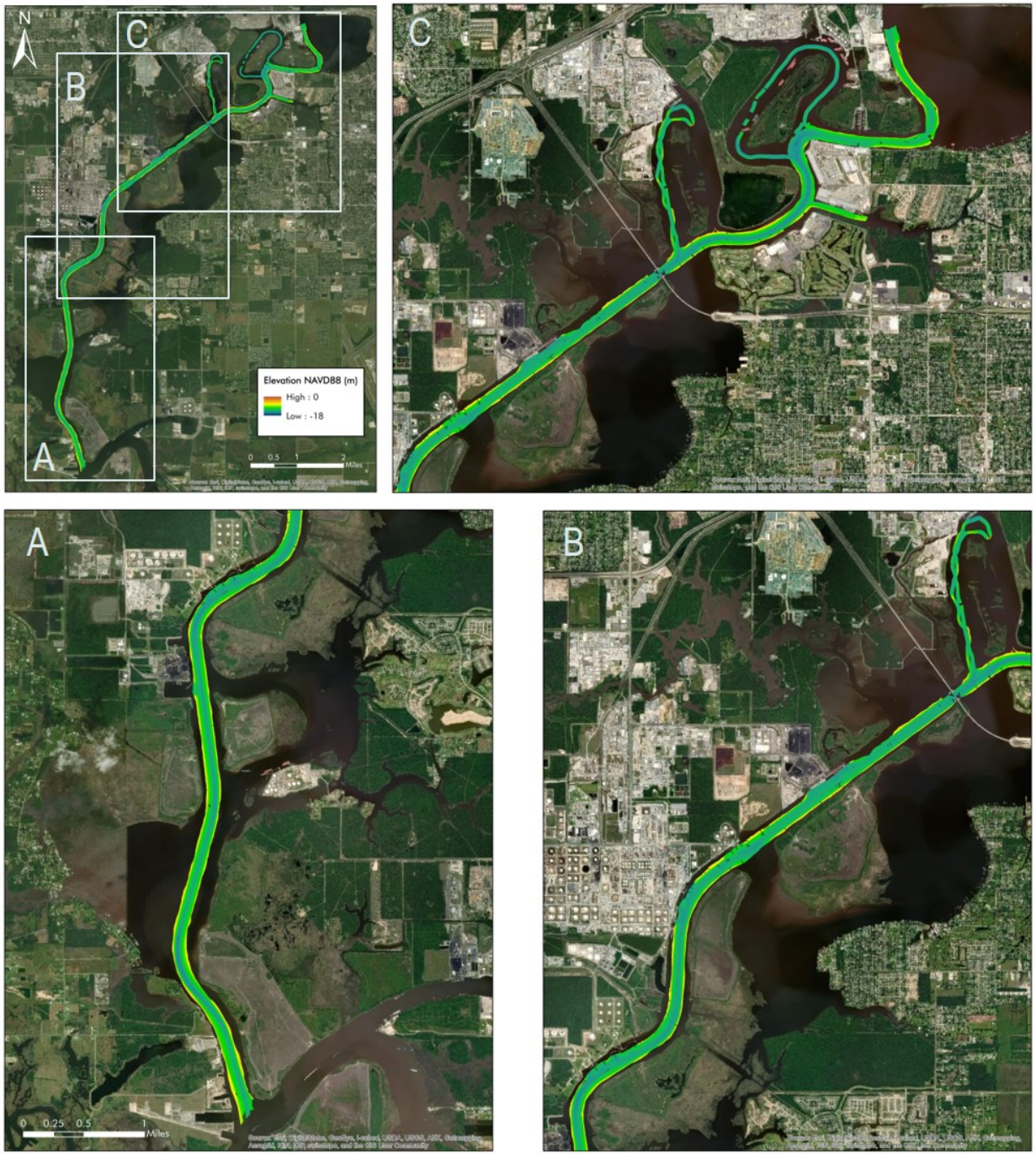

Figure 24. Subset views of sections of the Upper CSC multibeam bathymetry conducted in the CSC.

2.4. ANALYTICAL SEDIMENT BUDGET

The previous sections of this data report on the CSC are an accounting of the results from instrument measurements. The primary value of these results, and a discussion of their use, is presented in the numerical modeling report found in Chapter 3. The modeling value of the data is primarily in grid setup and calibration/validation, as well as to assess model bias. However, the present section developing an analytical sediment budget goes beyond these goals and is interpretative – an attempt to gain insight and conclusions about sediment sources, sinks, export magnitudes and timing in the CSC, and their potential impact on dredging needs. In the budgeting procedure outlined below, we develop a methodology to (1) quantify the potential sources of new sediment reaching the Lake-CSC study area (e.g., riverine, offshore, basinal), (2) examine what the data reveal about the exchange of sediments between subareas of the Lake-CSC coastal basin, and (3) quantify the historical bank line retreat rates along the unarmored shoreline of the CSC.

While the primary goal of the analytical sediment budget exercise is to annualize the magnitude of specific sediment sources, exchanges between source areas, and burial sites in the basin, this exercise offers additional comparative utility to the model results. That is, as part of a validation exercise to determine whether the numerical sediment flux models adequately capture all the relevant processes that supply sediment to the CSC, model runs were designed to encompass the first 8 months that the analytical budget is constructed (see below for those methods), and their agreement tested.

Figure 25. Map of CSC with channel river mile markers.

Several sediment input and output pathways are identified for the CSC estuary system (Figure 25 and Figure 26). The analytical sediment budget was derived by utilizing the observational data collected in the present project (and the earlier CPRA project) at key input and output exchange points, as well as sediment core geochronologies from Calcasieu Lake and West Cove collected in the earlier CPRA project (Allison et al., 2018). All budget numbers are scaled to an annualized mass flux value using a methodology described below in Section 2.4.1. The analytical sediment budget involves three elements shown schematically in Figure 26, each of which are outlined in detail in the methodology and results reported in subsequent sections:

1. New Sediment Inputs:
    - *Calcasieu River*: the river discharges through a tidally modulated exit directly into the northern section of the CSC
    - *Kelso Bayou*: a tidally modulated channel that discharges directly into the western side of the CSC near Hackberry, Louisiana
    - *Southeast Marshes*: several weir structures control the water and sediment exchange between the Cameron marshes and Calcasieu Lake
    - *Gulf of Mexico*: the tidally modulated marine input directly into the CSC through the Cameron jetties

2. Sediment Exchange Points between Calcasieu Lake/West Cove and the CSC:
    - *East Fork*: tidally modulated channel between the CSC and Calcasieu Lake
    - *West Fork*: tidally modulated channel between the CSC and West Cove
    - *Dredge Material Containment Area Barrier Gaps*: the exchange between the CSC and Calcasieu Lake and West Cove through gaps in the dredge placement area banks that line the CSC

3. Sediment Storage (Burial) Sites:
    - *Calcasieu Lake and West Cove*: the mass of sediment buried in the lake (Calcasieu Lake and West Cove)
    - *Calcasieu Ship Channel*: the mass of sediment buried in the CSC, and then removed periodically by dredging

Anthropogenic sediment sources (from the dredge material containment areas) were not included in the initial budgeting exercise, but an assessment of their possible magnitude was added later based on a comparison of the sediment sources described above the and historical dredging records. Hence, the anthropogenic sediment source results are presented in a later section (4.2).

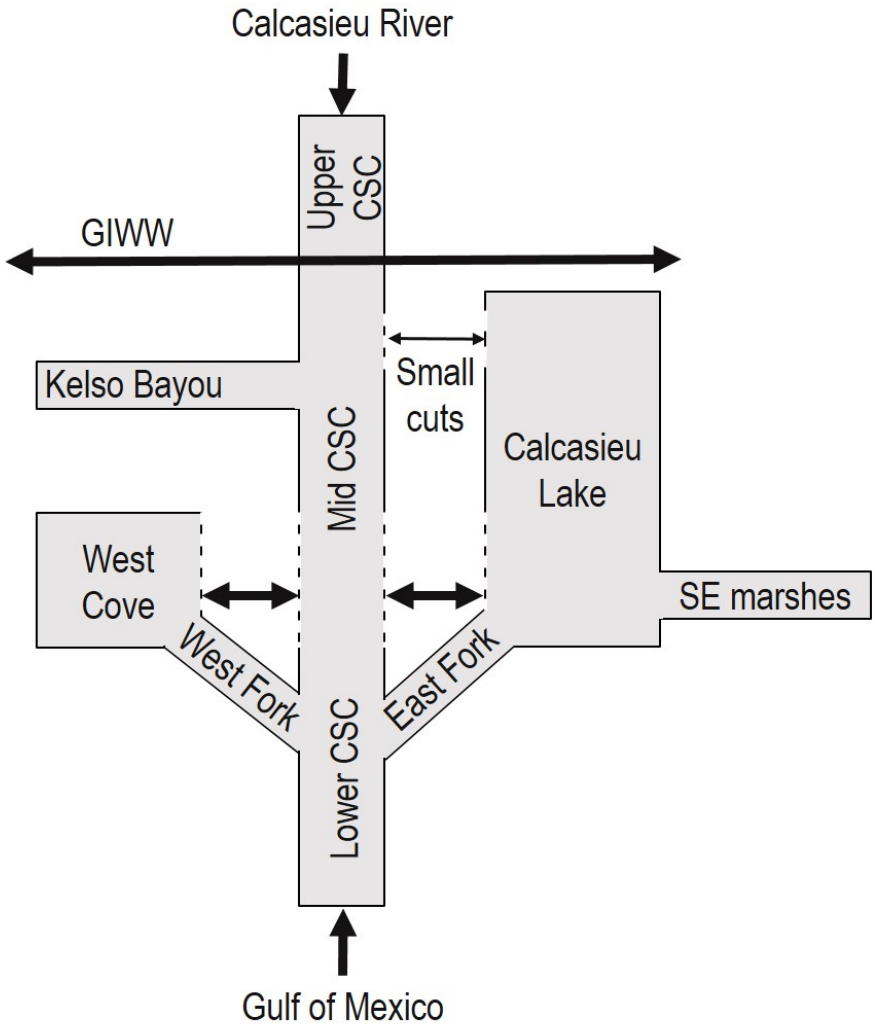

Figure 26. Schematic diagram of the inputs and exchange points to the CSC from adjacent water bodies. These are the key points that are the focus of the mass flux quantification in the analytical sediment budget.

2.4.1. Sediment Inputs to the Calcasieu Ship Channel

Deriving Water and Sediment Discharge from the Fixed Station Data

Calculating mass sediment fluxes on an annual basis to the CSC requires first calculating water fluxes from the station dataset. While each station's data from the present study had individual characteristics as outlined in following sections, the time-series of water and sediment discharge at ILC (Calcasieu River), KBM (Kelso Bayou), SCC (Gulf exchange), and East Fork channel (Figure 6 and Figure 26) were calculated using some universal methods. The water discharges at these stations were calculated using the USGS Index Velocity Method (IVM) (Levesque & Oberg, 2012) and the IVM for tidally affected areas (Ruhl & Simpson, 2005). The IVM calibrates continuous measurements of velocity to the mean channel velocity using discrete boat-based ADCP transect surveys of the full channel cross-section that were made during each site visit in the present study (Section 2.3.1). When combined with stage measurements from the fixed time-series gages, the continuous velocity measurements can be used to estimate continuous

discharge. Water velocities for this sediment budget were measured using either an upward-looking Nortek Aquadopp (East Fork) (Section 2.2.6) or a side-looking, RD Instruments H-ADCP (ILC, KBM, SCC) (Section 2.2.5). Stage was measured using a YSI (Section 2.2.2) at each of these stations.

In larger channels, such as the CSC at SCC, the H-ADCP is limited in the percentage of the total channel cross-section over which it can measure. Conversely, the Aquadopp measures a depth profile of current velocity and direction in one location in the channel. Calibration of these in-situ measurements with the ADCP transect surveys allows extrapolation of the mean velocity for the full channel cross-section.

Figure 27 shows an example of the index velocity calculation at Kelso Bayou (Station KBM). The cross-sectional average velocity from the boat-based ADCP is correlated with the H-ADCP velocity data from the same date and time. A linear regression of several corresponding ADCP transects and H-ADCP velocities gives an equation that can be applied to the H-ADCP velocity time-series to calculate a calibrated water velocity time-series.

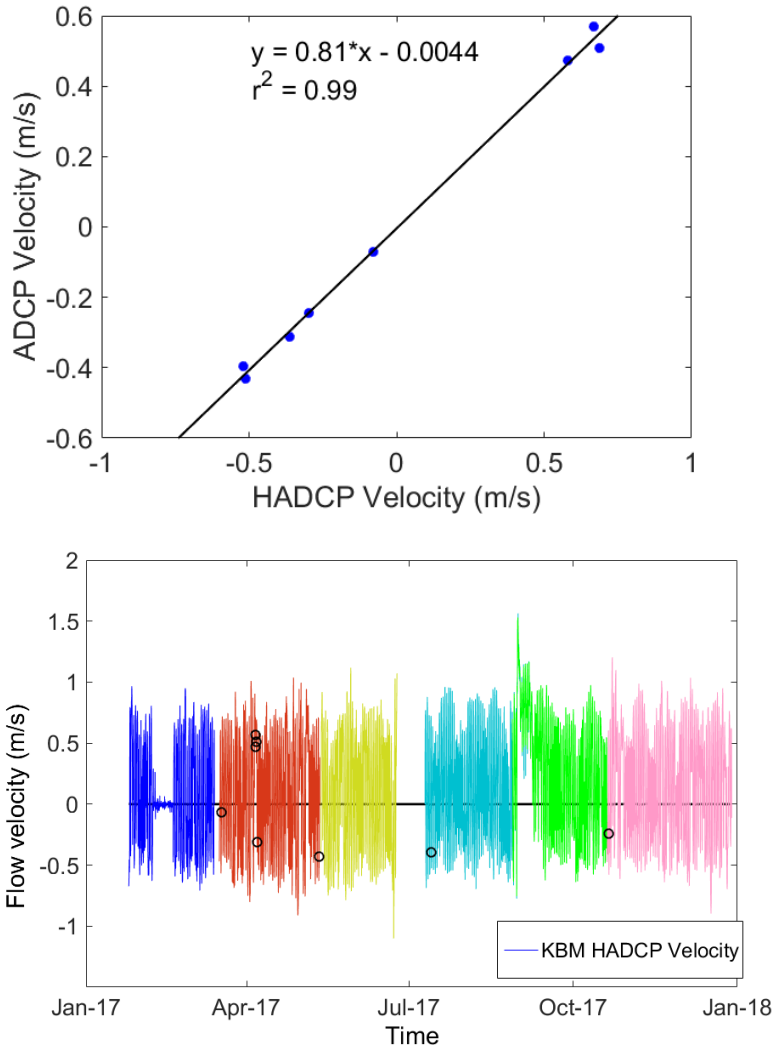

Figure 27. Example (station KBM) of conversion of H-ADCP velocities to cross-sectional averaged water velocities utilizing boat-based ADCP transects. Left, linear regression of cross-sectionally averaged H-ADCP and boat-based ADCP velocity to derive a conversion equation. Right, the boat-based ADCP transect average velocities (black circles) are plotted along with the calculated cross-sectional average velocity for the H-ADCP velocity time-series derived from the regression, where each color corresponds to a redeployment of the instrument after servicing.

To obtain the cross-sectional area, the shape of the channel bottom and sides was extracted from the boat-based ADCP transects. As water levels fluctuate, however, so does the cross-sectional area. A time-series of cross-sectional area was calculated from the vertically referenced (NAVD88) water elevations from the YSI data. Figure 28 shows a diagram of the KBM cross-sectional area, indicating the range of water elevations, and hence, area at this station during this study's deployment period. With the time-series for the calibrated H-ADCP velocity and the corrected channel cross-sectional area, the two time-series were multiplied to calculate instantaneous water discharge (Figure 29, top).

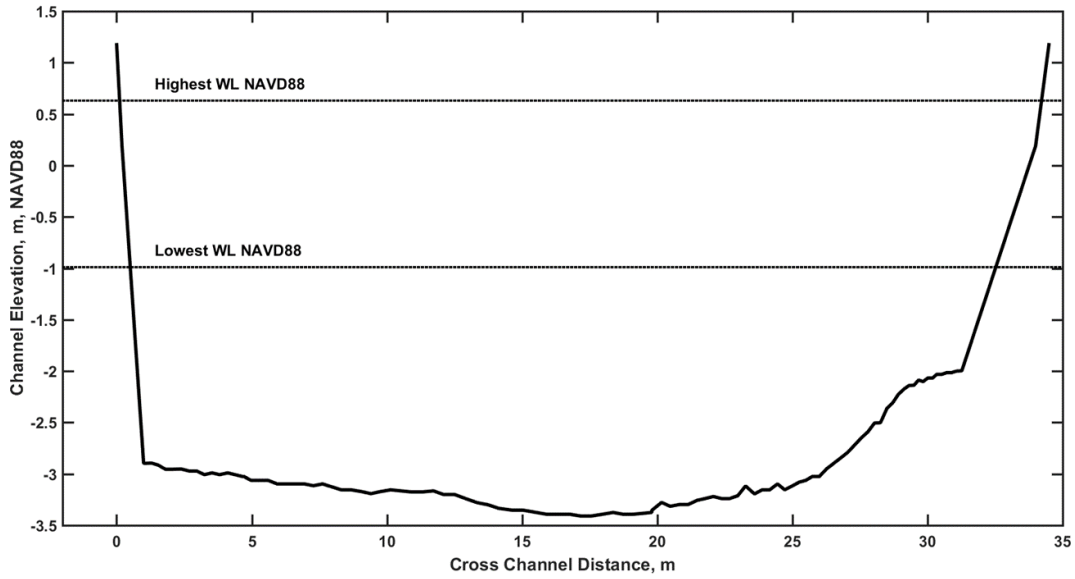

Figure 28. The cross-sectional surface area at KBM as measured by the boat-based ADCP and corrected for water elevation using pressure data recorded by the fixed YSI sensor at the station.

The calibrated YSI TSS time-series of suspended sediment concentration (calibrated from turbidities using bottle data collected at the station as outlined in Section 2.2.4) was multiplied by the discharge time-series to derive a sediment discharge time-series (in metric tons, referred to as 'tons' for the remainder of the report) (Figure 29, bottom). The YSI TSS time-series consists of a single water column measurement that is used to represent the sediment concentration for the entire water column. This means that our sediment discharge time series is depth-averaged and cannot account for stratification of sediment in the water column.

The cumulative discharge of water and sediment were used to derive annual net directional flux, or flux for a designated time-period. Data gaps in the time-series record of velocities, water levels, and turbidities (~suspended sediment concentrations) at the fixed sites were caused by instrument servicing and occasional instrument failure. Most of the gaps consist of an hour or less and were filled in using linear interpolation. However, as it is preferable to calculate cumulative fluxes with a gap-free record, longer data gaps were filled with a combination of other YSIs deployed by the Institute in the system and nearby NOAA and USGS gages. In only one longer gap at Station KBM was it necessary to fill the gap with a section of the existing gage record from the same lunar phase in a previous month. Turbidity and velocity gaps were typically filled using nearby YSI data, using a combination of replication of parts of the existing record and linear interpolation.

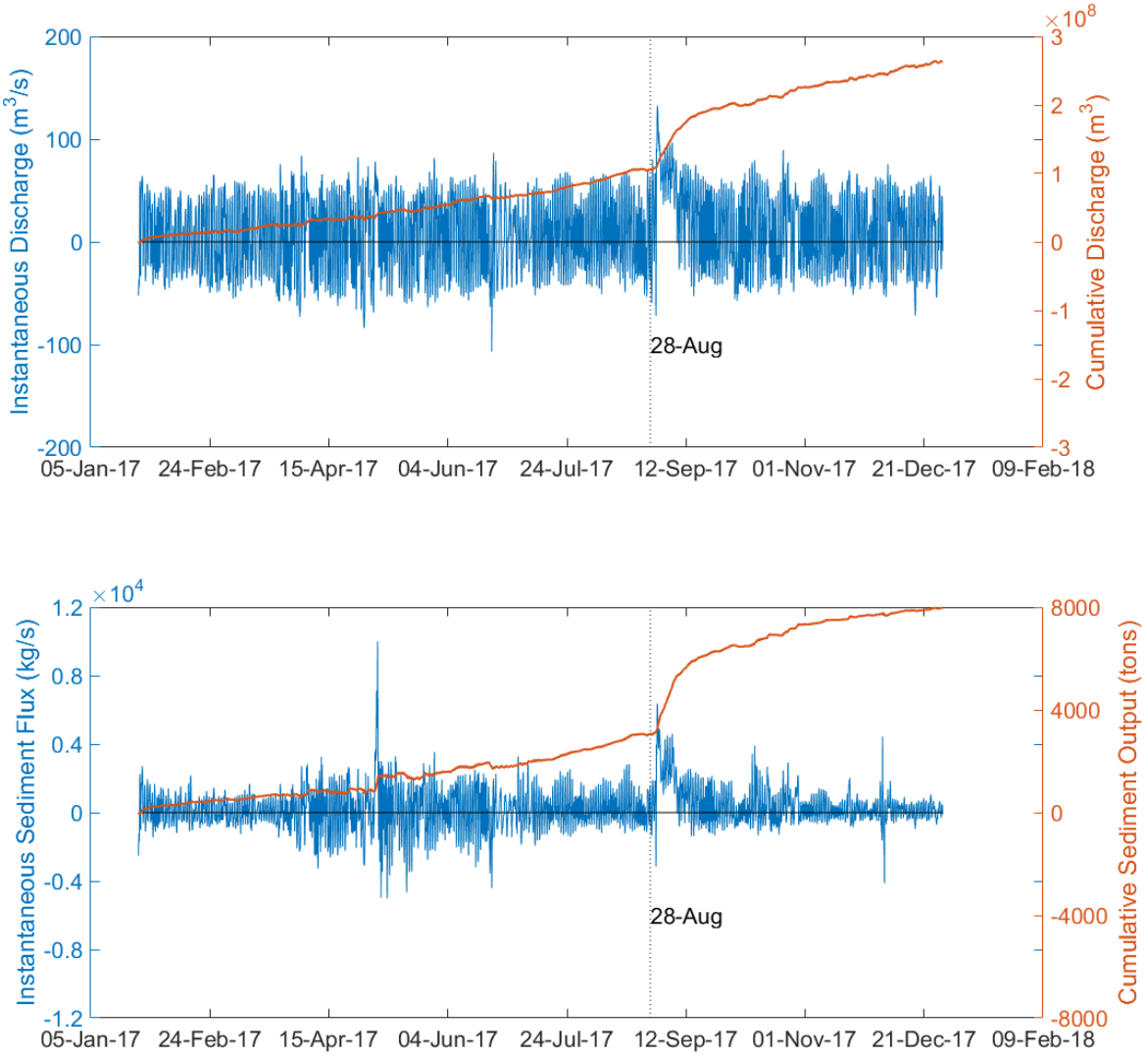

Figure 29. Example of calculated cumulative and instantaneous water (top) and sediment (bottom) discharges at Kelso Bayou (Station KBM). Instantaneous discharges are scaled on the left axes and plotted in blue, while cumulative discharges are shown on the right axes and are plotted in red.

Calcasieu River Input

At Station ILC, the YSI and a NOAA H-ADCP was used (Station ID lc0301, Lake Charles City Docks) to derive Calcasieu River water discharge (Figure 30). The CSC is well-confined here and provides a direct measurement of tidally modulated water velocity. The mean channel current velocity and direction from the NOAA gage were obtained from https://opendap.coops.nos.noaa.gov/axis/webservices/currents/index.jsp on a sub-hourly scale. These data were used in the same method as H-ADCP mean velocities and direction are used to derive the index velocities. No boat-based ADCP was available from NOAA from their gage site. Cross-channel ADCP transects were collected by the Institute at the location of the NOAA H-ADCP, which is approximately 1.7 miles downstream of the ILC station (Figure 30) and on the other side of Lake Charles. These transects were used for the index velocity calibration of this location.

Figure 30. Locations of the ILC boat-based ADCP transect and the NOAA Ports H-ADCP gage in the CSC below Lake Charles. Background image from Google Earth Pro.

The cumulative water and sediment discharge at ILC is predominantly in the downstream direction (toward the CSC and Gulf of Mexico) (Figure 31). The total 2017 record of net water discharge into the

CSC is 7.42 x 10^9 m^3, and sediment discharge is 3.63 x 10^5 tons. The Hurricane Harvey isolated discharges for the Calcasieu River input represent 8% and 11% of the annual water and sediment discharges, respectively. The modeling effort outlined in Chapter 3 uses the USGS Kinder gage (station 08015500) data multiplied by a factor of 1.8 (an estimated input to the Calcasieu River downriver of Kinder) to derive the riverine discharge at Lake Charles (ILC). Analytical results show that the modeling assumption produces estimates within a factor of 2 of that measured, but may be slightly underestimating discharge at the head of the CSC (Figure 31). The difference between the modeling assumption and the observational data may be due to (1) the model's estimate of input below Kinder may be too low, (2) boat-based ADCP transects directly at the NOAA Ports H-ADCP location might provide slightly different analytically derived water discharge for this station, (3), the NOAA Ports H-ADCP is located in the upper half of the water column and may not be capturing any deeper stratification effects (e.g., presence of a salt wedge).

Figure 31. Calculated cumulative and instantaneous water (top) and sediment (bottom) discharges at Calcasieu River (Station ILC). Instantaneous discharges are scaled on the left axes and plotted in blue, while cumulative discharges are shown on the right axes and are plotted in red. The model's calculation of the river water discharge (Kinder*1.82) is shown as a yellow line.

Kelso Bayou

The methods for calculating water and sediment input from Kelso Bayou (Station KBM) from the fixed H-ADCP (velocity) and YSI (stage and turbidity) are identical to those described for ILC and are plotted

in Figure 27, Figure 28, and Figure 29. The total 2017 record discharges at Kelso Bayou are 2.86 x 10^8 m^3 of water and 8,620 tons of sediment. The passage of Hurricane Harvey represented 21% and 27% of the total annual water and sediment discharges, respectively.

Southeastern Marshes

Water discharge data were not collected at the weirs at the lake entrances of the southeastern bayous that drain the Cameron marshes. The only data were obtained from a YSI placed at a platform about 200 ft into Calcasieu Lake opposite the Grand Bayou weir, which yielded water levels and turbidities. Bottle data for calibrating gage turbidities were collected at this station (GBW) and at the weir gates.

In order to provide an estimate of water and sediment flux from the southeastern marshes given the limited gaging at Grand Bayou and the other weir input points that were not gaged, the following strategy was used. Annualized water discharge data was obtained from a MIKE Flood model run of 2012 conducted by the Water Institute (Wang et al., 2018). This model gives water discharge inputs for Peconi Bayou, Mangrove Bayou, Grand Bayou, Lambert Bayou, and No-Name Bayou (Figure 32). Gaging inside and outside of the GBW by CPRA provided water level data. Model results estimate that the southeast marshes discharge approximately 3.41 x 10^8 m^3 of water annually (using the figure for 2012) to Calcasieu Lake. In order to derive a sediment flux into Calcasieu Lake, water elevation data from both sides of the Grand Bayou weir from December 2016 to January 2017 were utilized to determine the advantage in hydraulic head on either side of the weir. For 45 % of the time, water level was higher in the marshes and, therefore, it would be expected that the net flow direction would be toward Calcasieu Lake (Figure 33). During periods that the flow was into the lake, YSI gage records at the station were used to derive a mean suspended sediment concentration (calibrated from turbidities using the bottle data) of the marsh effluent. Given that the MIKE model results provide a net water influx, and assuming a similar suspended sediment concentration for lake to marsh periods of water motion, a sediment influx to the lake was calculated. The annual average TSS showed no difference with and without Hurricane Harvey: 38.63 mg/L and 38.41 mg/L, respectively. This exercise calculates that the southeastern marshes discharged approximately 13,186 tons of sediment in 2017.

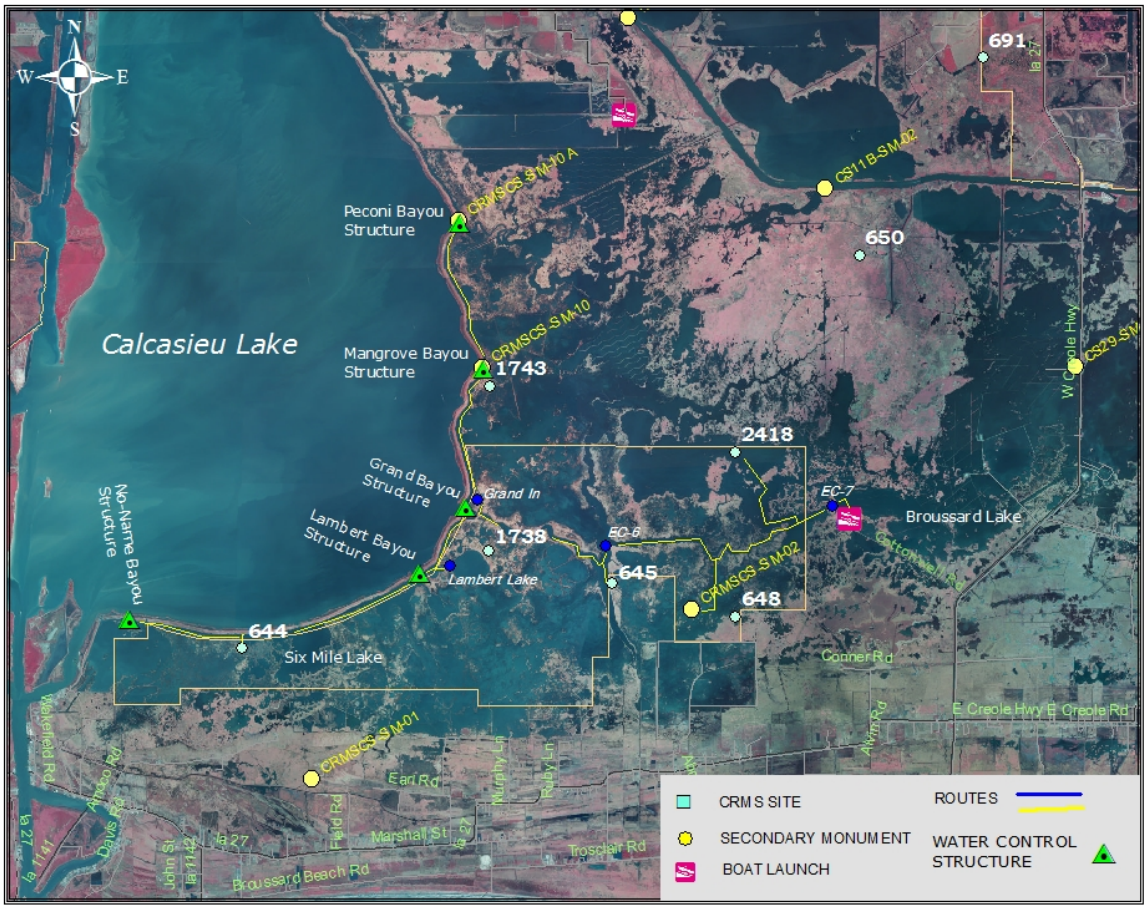

Figure 32. Southeastern marshes bayou structures monitored by CPRA in Calcasieu Lake. Map courtesy of CPRA.

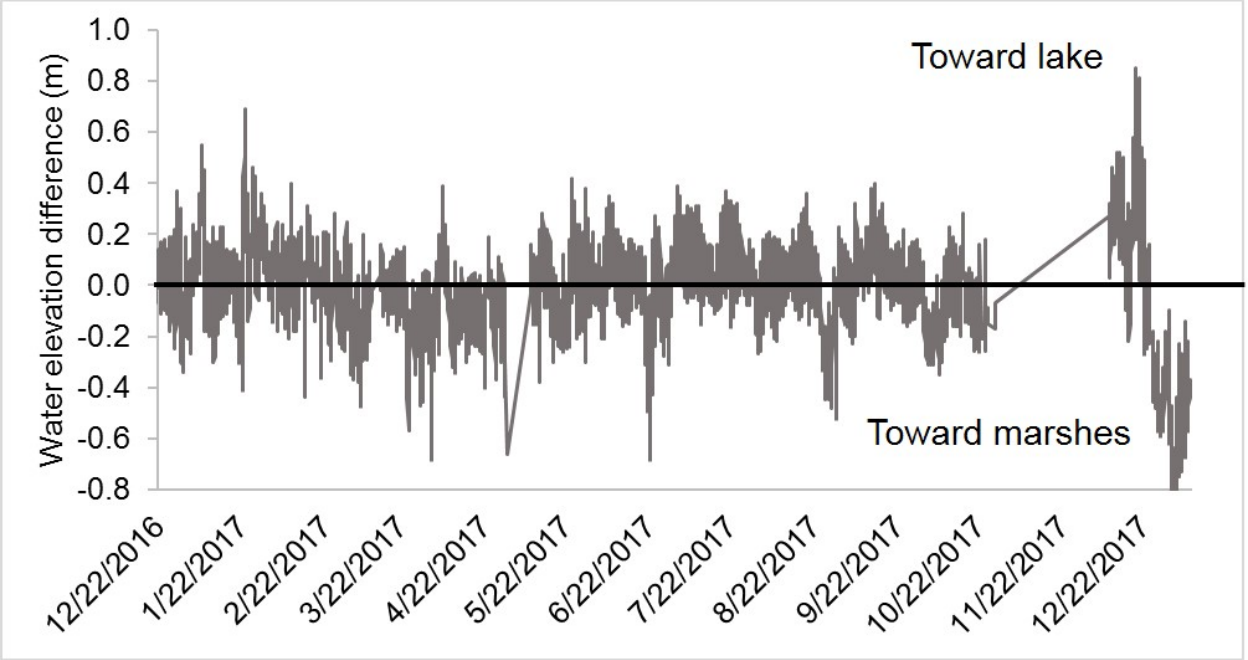

Figure 33. Difference in water level data from GBW in and out of weir.

The Gulf of Mexico

In the Lower CSC, water and sediment discharge are exchanged on tidal and meteorological forcing time-scales between the Gulf of Mexico, East Fork, West Fork, and the main CSC channel. In order to capture this exchange, annualized discharges were calculated from this study's instrument measurements at Station SCC, located south of the East and West Fork channel split, and at Station EPC at the Calcasieu Lake end of the East Fork channel. The annualized water and sediment fluxes at these two sites gave the total exchange with the Gulf and East Fork components directly and were used to derive a combined West Fork and main channel (north of the channel split) flux. The discharge calculations at SCC and EPC were more complicated than those described in for ILC and KBM and are described below.

At East Fork (Station EPC), the Institute's Aquadopp and YSI (see Section 2.2.6) provided the necessary up-looking water velocity and suspended sediment concentration (calibrated from YSI turbidity) data to calculate the discharge of water and sediment. Boat-based CTD casts demonstrate that during most of the station servicing the water column at EPC was well mixed with respect to sediment (Figure 34). However, periodically, extreme TSS measurements were present in the lowermost portion of the water column (e.g., a lutocline, or high concentration interface) where the fixed sensors were located (Figure 34). Using these values as a depth averaged sediment concentration yielded abnormally high fluxes relative to those observed at nearby stations at the same periods (e.g., SCC and SED). The origin of this lutocline is unresolved by our data but may relate to the estuarine and salt wedge dynamics of the system leading to temporary storage of fine sediments on the East Fork channel bottom during slack tides that are resuspended and advected toward the Lake during the incoming tide phase.

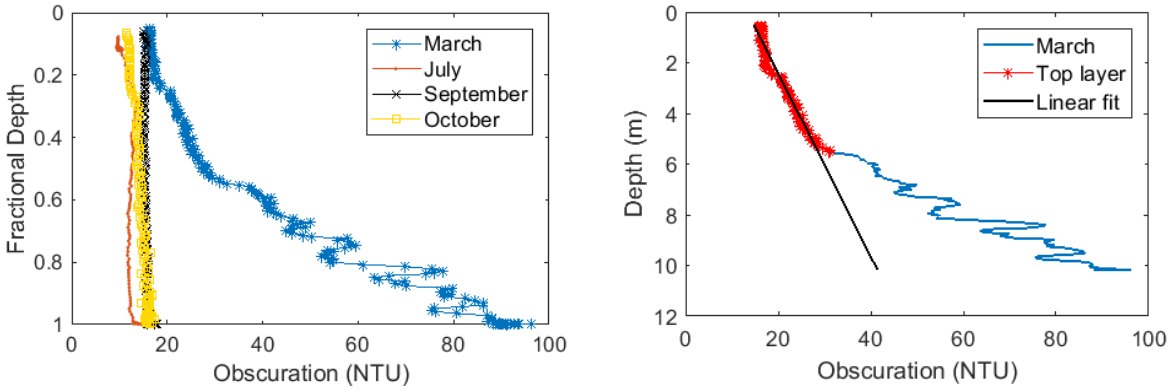

Figure 34. Suspended sediment concentrations at East Fork (Station EPC). Left, CTD casts from different months, with the cast in March cast at a time when a high concentration lutocline layer was present below 0.6 total depth. Right, the March cast extrapolation of near bottom turbidities if no lutocline had been present.

To arrive at an estimate of sediment concentration closer to a depth averaged value, we utilized the CTD cast at East Fork from March 2017 when a lutocline was observed to derive a correction factor (Figure 34). At approximately 6 m depth, the obscuration measured by the CTD begins to abruptly increase. This is interpreted as the beginning of the lutocline. A linear fit (Equation 5) to the obscuration data above 6 m was then used to estimate the obscuration at the 0.9 fractional depth without the influence of the high sediment "fluff" layer.

$$y = 2.76x + 13.35, R^2 = 0.95 \quad (5)$$

The measured CTD data with the lutocline was 2.1 times higher than the estimates without the lutocline. Peaks in TSS up to about 500 mg/L were common in the calibrated YSI time-series at EPC. Using 500 mg/L as a baseline, peaks higher than 600 mg/L were interpreted as periods in the record when the lutocline was present. TSS values from the YSI data above 600 mg/L were divided by 2.1 to correct the sediment concentration to values that were not skewed by the YSI recording the lutocline and are more representative of a depth averaged sediment concentration.

In the CSC south of the East and West Fork split (Station SCC), two Institute H-ADCPs and two YSI's (turbidity) were deployed at near surface and deeper in the water column to capture the salinity stratification, two-layer transport characteristic of the Lower CSC. It is apparent from the time-series record of the deeper H-ADCP that its depth (it was sited at about 40% total depth) did not capture the core of the salty layer entering from the Gulf in many instances. As a result, the ephemeral two-layer flow observed in CTD casts was not often captured in the continuous velocity record (Figure 35 and Section 2.2.5). Despite this limitation, the water and sediment discharge analysis, including the net flux of components when annualized, was conducted based on the record of deeper sensor (Figure 36).

Because the lower sensor was not located in the core of the bottom saline layer, which tends to flow inland through incoming freshwater due to its relatively high density, the net annualized offshore flux of water and sediment observed at Station SCC is probably an overestimate. In other words, depth of the

lower sensor recorded a downstream water flow, or a lower magnitude inland flow on occasions when the salt wedge was located in the CSC, and flow was actually at a higher magnitude upland.

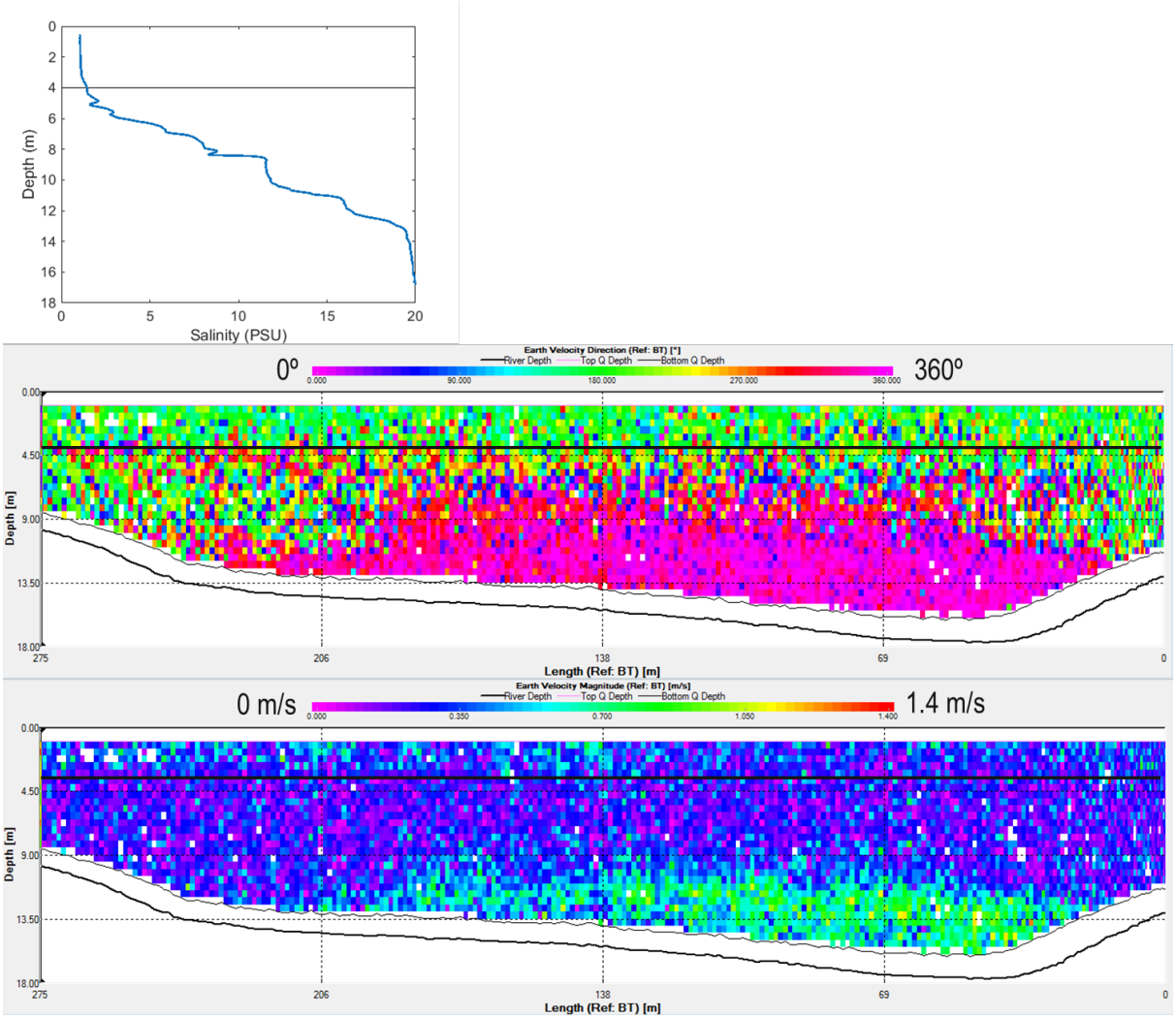

Figure 35. An example CTD cast of salinity with depth (upper plot) and a boat-based ADCP transect of velocity direction (middle plot) and magnitude (lower plot) taken on September 23, 2017 at 23:45 UTC at Station SCC. The black line indicates the approximate depth of the bottom H-ADCP at SCC. The approximate depth (~9 m) of the pycnocline between the fresh and saline layers can be estimated by the presence of a reversal in flow direction in the middle plot and an increase in flow velocities (the saline layer is flowing inland more rapidly than the overlying layer is flowing offshore) in the lower part of the water column (lower plot).

A comparison of the calculated water and sediment discharge rates for the trunk channel south of the split at Station SCC and East Fork (Station EPC) suggests that the East Fork channel is mainly a conduit for water to enter Calcasieu Lake, that is, it is a flood-tide dominated channel. At SCC, while water does flow toward the lake on certain days, the total annual cumulative flow, which is a combination of flow from the East Fork, West Fork, and Main CSC is towards the Gulf (Figure 36). This is a system response to the freshwater that enters the system north of the SCC from the Calcasieu River, Kelso Bayou, the

Southeastern Marshes and net precipitation over the coastal water bodies (e.g., Calcasieu Lake, West Cove, CSC). Episodic events, such as hurricanes, can have strong effects on the cumulative water discharge at SCC. Hurricane Harvey made landfall in Louisiana on August 30, 2017. Its effect on discharge from the CSC can be seen starting on August 28 when storm surge causes flow toward the lake, followed by large discharge toward the Gulf from record setting rainfall from the storm (Figure 36). Water levels at Calcasieu Pass reached 0.73 m above the predicted tide on August 28 (NOAA tide gauge 8768094 Calcasieu Pass, LA). The National Weather Service measured record amounts of rainfall in Lake Charles on August 27 and 28 (total of 10 inches) (http://w2.weather.gov/climate/index.php?wfo=lch).

Sediment flux at the trunk CSC channel and at East Fork is more complicated than water discharge because high water flux events do not necessarily contain large amounts of suspended sediment. Sediment imports and exports are highly dependent on episodic events as shown in Figure 36. Net cumulative sediment flux changes frequently toward the CSC or toward the Lake, which suggests that the net sediment flux is close to zero (Figure 36). Hence, short-duration events that suspend and transport large amounts of sediment can drastically influence the sediment budget. Tropical Storm Cindy made landfall near Calcasieu Lake on June 22, 2017 causing water levels to peak at 0.89 m above the predicted tide (NOAA tide gauge 8768094 Calcasieu Pass, LA). Concurrent high suspended sediment values, likely from the high winds associated with this event, caused an import of sediment (208,000 tons) from the Gulf into the ship and channel and lake. The effect of this sediment influx on the cumulative annual flux was later cancelled out by the offshore oriented fluxes associated with the high discharges from Hurricane Harvey rainfall. Suspended sediment values were much higher during Tropical Storm Cindy than during Harvey, resulting in similar amounts of suspended sediment flux even though Harvey had a much greater effect on the water budget.

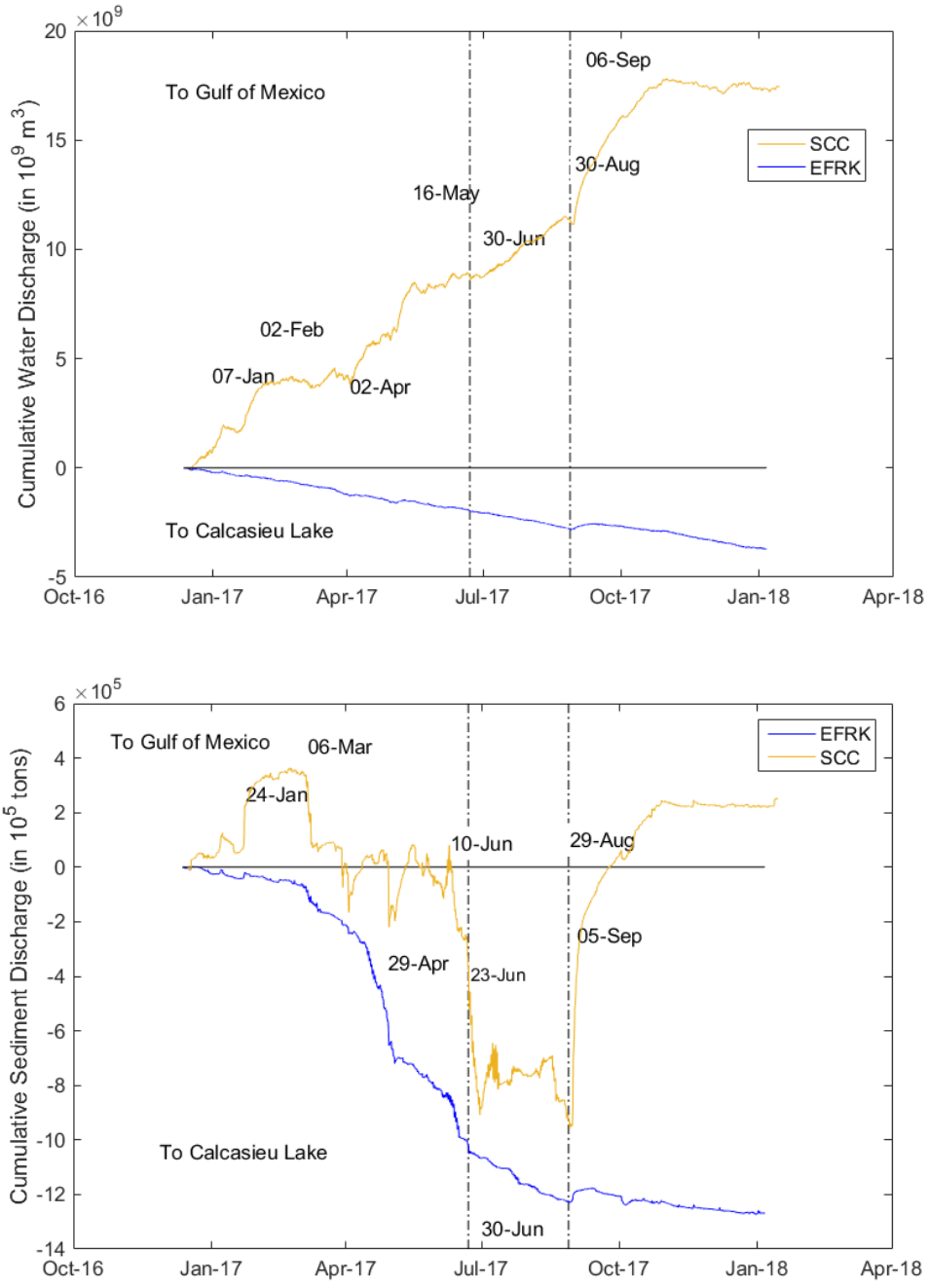

Figure 36. Water (top) and sediment (bottom) cumulative discharge plots in the trunk channel of the CSC (Station SCC) and at East Fork (Station EPC). Tropical Storms Cindy and Hurricane Harvey are indicated by black dashed lines.

The results of the water and sediment discharge calculations are shown in graphical form in Figure 37 for comparison. The cumulative water and sediment flows from data for the entire measurement period is included, as well the isolated effects from storms Cindy and Harvey. In the total annual record of the flux calculations (top plots in Figure 37), the CSC north of the split, and West Fork, have to be ebb dominated

in order to balance the influx of water through East Fork with the large (161 x 10^8 m^3) overall offshore water flux observed in the trunk channel at SCC. The sediment fluxes show sediment mass import into the lake (over 1 million tons) and some export to the Gulf (251,000 tons). The isolated effect of Tropical Storm Cindy is shown in the middle plots of Figure 37. The storm surge from this storm is clearly reflected in the import of both water and sediment into the CSC and the lake. In contrast, during Hurricane Harvey (lower plots in Figure 37), which was a large rainfall event, the CSC exported both water and sediment to the Gulf.

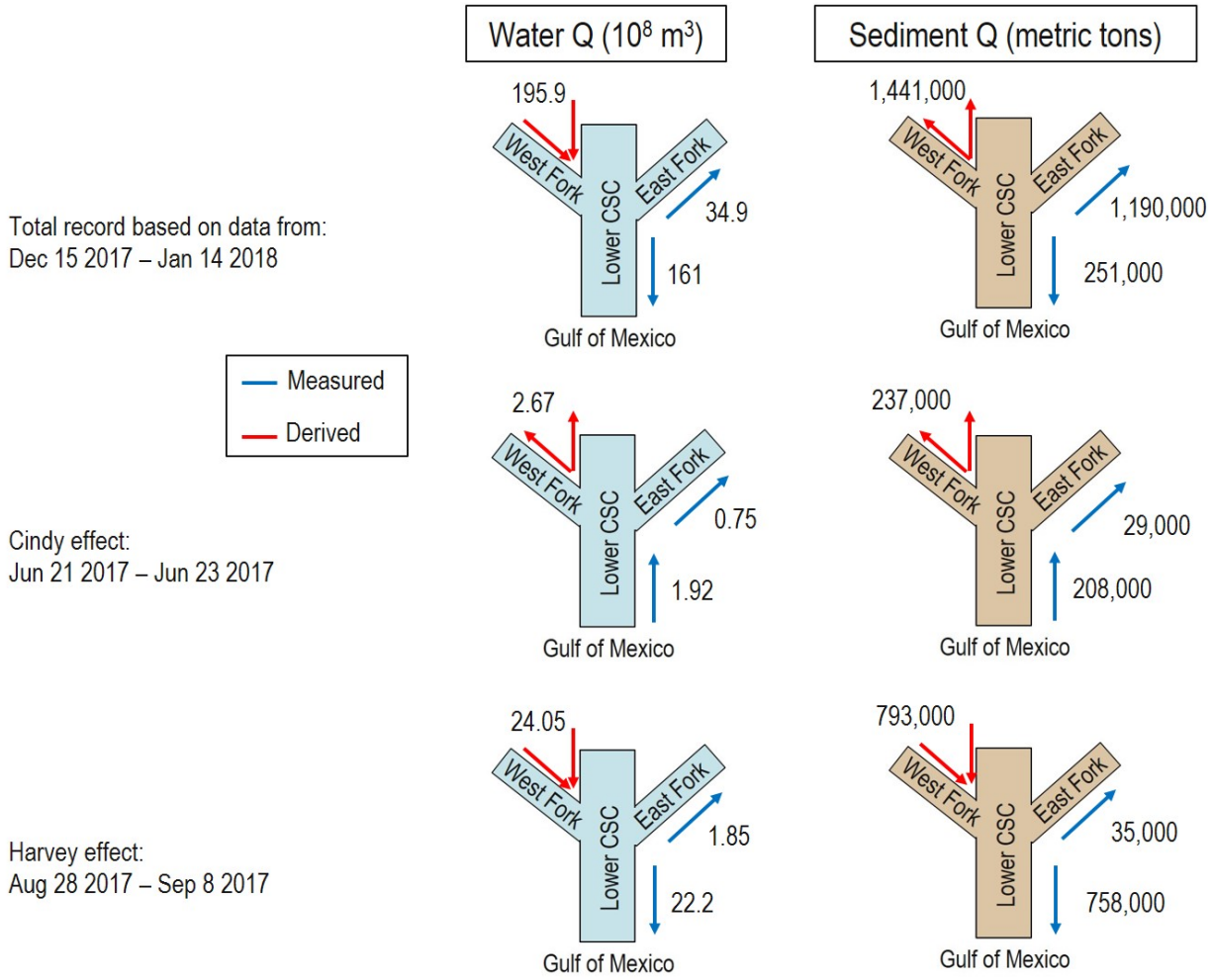

Figure 37. Water and sediment discharge exchange between Lower CSC, East Fork, and West Fork showing three records. Annual record values that include the Cindy and Harvey effect are shown in the top plots, a Cindy effect period is shown in the middle plots, and a Harvey effect period is shown in the lower plots. Water Q is in 10^8 m^3, and sediment Q is in metric tons.

Exchange with Calcasieu Lake and West Cove

In addition to the channelized exchange at East Fork and West Fork, water and sediment are exchanged between the Lake and the CSC throughout the Mid CSC. The largest openings are between the Lake and CSC at Miles 5 to 9 and 20 to 21 (Figure 25), although there are smaller (vessel cuts) exchange points at several other locations between the Lake and West Cove as indicated in the schematic in Figure 26.

Because of the number of cuts and the difficulty quantifying exchange across large channels, the experiment was not designed to constrain the magnitude of this sediment flux. However, several insights can be gleaned from the dataset.

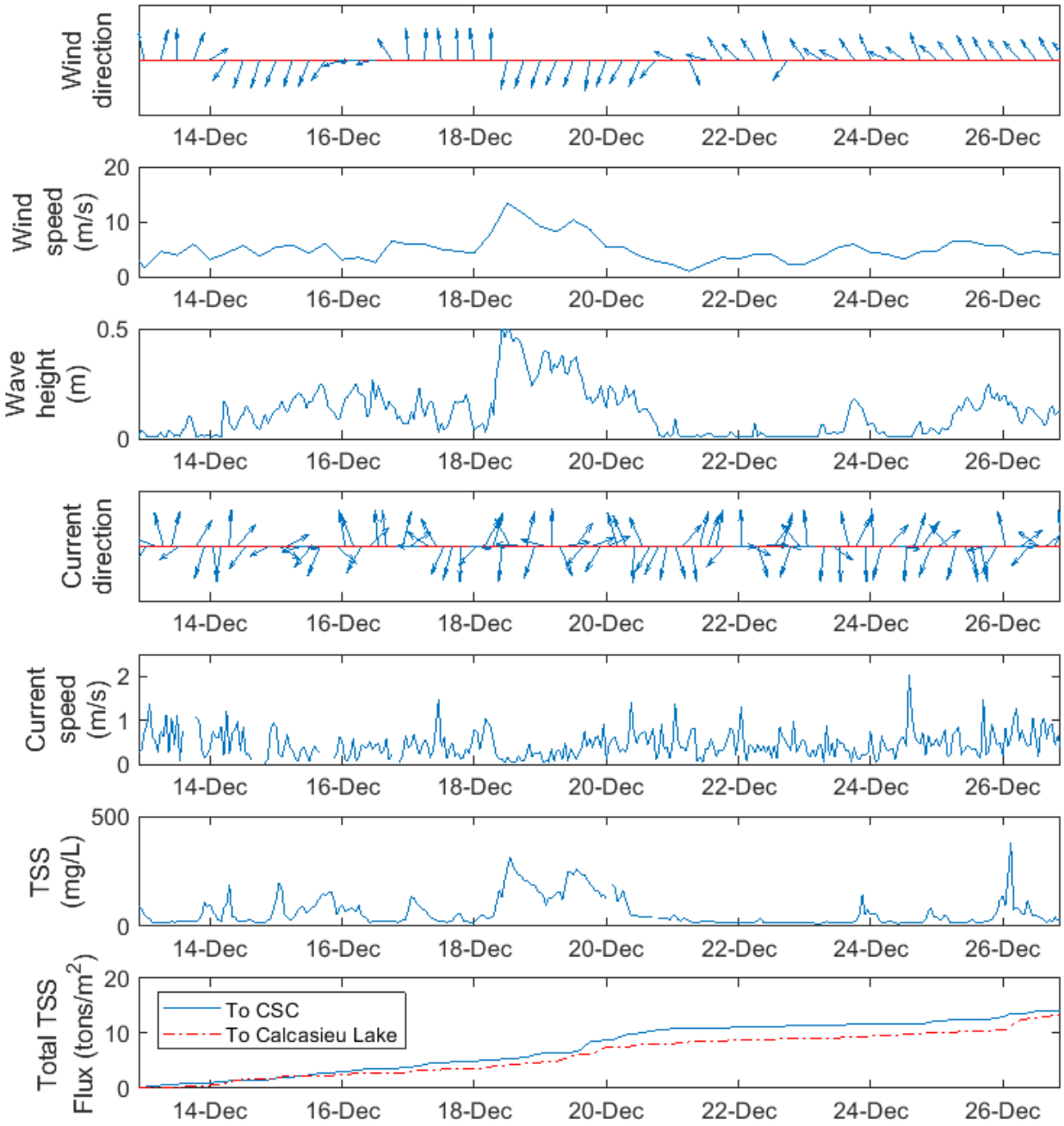

Figure 38. Wind, wave, and current direction and velocity plot at station SED in Calcasieu Lake opposite mile 7 of the CSC for the period 13-27 December 2016. TSS flux is calculated on a unit area basis for flow toward the CSC only. Flows toward the ship channel are defined as Azimuth direction 185° through 360° to 5°.

The SED station was located in the lake opposite the largest CSC opening with Calcasieu Lake (at about CSC Mile 7). Wave-current monitoring was conducted at this site to examine the nature and mechanisms of the exchange. Frontal passage during the winter months resulted in the highest TSS values in the Lake and in net sediment fluxes toward the CSC. An example can be seen in Figure 38, where strong pre-frontal (offshore) winds on December 17-18, 2016 resulted in large waves in the lake and resuspension of fines from the lake bottom. Large waves continued after the front passage on the 18th, through the end of the event on December 21st. Interestingly, the net currents at the site were not wind-dominated, but were more variable (Figure 38, currents) throughout the event, suggesting that tidal processes are equally important. Despite this temporal variability, cumulative sediment transport during the entire period of record shown in December 2016 was toward the CSC, with the front resulting in a step-wise increase in magnitude in the cumulative flux (Figure 38, Total TSS Flux). From December 2016 to March 2017, there was an Aquadopp sensor at station SED, which gives measurements of current speed and direction through the depth profile. In March it was switched for an ADV, which provided information about better wave directionality in this shallow setting but only single point current information. During the entire period that the Aquadopp was in place, there was continuously increasing cumulative sediment flux from the Lake toward the CSC (similar to that shown in the December period in Figure 38) that totaled 7.4 tons/m^2. An estimated 4.1 x 10^4 tons of sediment passed through the section of the Lake from RM 9 to 5, toward the CSC. Even if this value is compounded to an annual flux, this is a relatively small input into the CSC (<1 % of the annualized dredging amount). The data at SED suggest that Lake resuspension during strong wind events, and exchange through the openings with the CSC, may not be a significant sediment input to the CSC. The caveat to this is that SED is only a single site, and other locations in the Lake-CSC openings with different wind fetches, may behave differently. Short-period radiotracer (^{7}Be) results from the lake cores taken for the CPRA study (Allison et al., 2018) support the concept that the lake is an area of strong reworking and winnowing of material during high-energy events (fronts and tropical storms). While this generates a large flux of resuspended sediment, it is ultimately advected to multiple adjacent settings (e.g., offshore, fringing marshes, other portions of the lake), rather than just focused in the CSC.

CSC Sediment Inputs Summary

The results of the sediment source components outlined above are summarized in Table 5-7 below. The total annual record budget is shown in Table 5. Because of the importance of tropical storms, the isolated inputs and exchanges of storms Cindy and Harvey are separated into their periods of record, Table 6 and Table 7, respectively.

The results demonstrate that during “base conditions”, that is, without tropical storm impact, new sediment input by Kelso Bayou and the Southeastern marshes is a minor factor (~1% of total CSC sediment input). The results of this quantification show that over the 2017 monitoring period three measured sources together input 384,806 metric tons of sediment to the basin and CSC. These were the Calcasieu River (94.3%), Kelso Bayou (2.2%), and the weirs that exchange from water from the southeast bayous into Calcasieu Lake (3.5%). Over this same year, our measurements show that sediment was exported to the Gulf of Mexico (251,000 tons) equivalent to about 65% of the new sediment input from these sources (and potentially other, unmeasured sources). However, two tropical systems in 2017 had a dramatic impact on the annual sediment budget of the system. Hurricane Harvey was an extreme rainfall event, and the escape to the Gulf of that excess water overcame the storm surge effect (which tends to

import sediment from the Gulf), resulting in 758,000 tons of sediment export to the Gulf from August 28th to September 8th. Tropical Storm Cindy was a low rainfall, higher storm surge and wind event that brought 208,000 tons of sediment into the CSC from the Gulf in the period of June 21-23rd. If the effect of these two storms is subtracted from the annual monitoring record, this would indicate that the Gulf in 2017 would have been a net importer of sediment to the CSC – an estimated 299,000 tons. Harvey (but not Cindy) was also a major contributor to the new sediment input from the Calcasieu River (11%) and Kelso Bayou (27%) in 2017. Hence, without tropical storms, we conclude that the Calcasieu River and Gulf of Mexico were the dominant, and approximately equal in magnitude, sediment sources to the CSC and Calcasieu Lake in 2017.

Table 5. Total record of water and sediment budget flux results (including 2017 storms) for the period from December 20 2016 to January 14 2018.

Sediment transport	Location	Net water flux (10^8 m^3)	Dominant direction of water flux	% of water Q	Net sediment flux (tons)	Dominant direction of sediment flux
Input	Calcasieu River	74.20	to CSC	92.2	363,000	to CSC
Input	Kelso Bayou	2.86	to CSC	3.6	8,620	to CSC
Input	Southeast bayous	3.41	to Lake	4.2	13,186	to Lake
Export	Gulf of Mexico	161.00	to Gulf	-200.1	251,000	to Gulf
Input	**Total CSC Input**	80.47	-	-	384,806	-
Exchange	East Fork	34.90	to Lake	-	1,190,000	to Lake
Exchange	West Fork + Lower CSC	195.90	to Gulf	-	1,441,000	to Gulf

Table 6. Isolated water and sediment budget flux results for Tropical Storm Cindy for the period from June 21, 2017 to June 23, 2017.

Sediment transport	Location	Net water flux (10^8 m^3)	Dominant direction of water flux	% of water Q	Net sediment flux (tons)	Dominant direction of sediment flux
Input	Calcasieu River	0.07	to CSC	3.5	26	to above I-10
Input	Kelso Bayou	0.04	to marshes	2.2	200	to marshes
Input	Southeast bayous	n/d	n/d	n/d	n/d	n/d
Input	Gulf of Mexico	1.92	to mid CSC	94.3	208,000	to mid CSC
Input	**Total CSC Input**	2.04	-	-	208,226	-
Exchange	East Fork	0.75	to Lake	-	29,000	to Lake
Exchange	West Fork + Lower CSC	2.67	to mid CSC/WFRK	-	237,000	to mid CSC/WFRK

Table 7. Isolated water and sediment budget flux results Hurricane Harvey for the period from August 28, 2017 to September 8, 2017

Sediment transport	Location	Net water flux (10^8 m^3)	Dominant direction of water flux	% of water Q	Net sediment flux (tons)	Dominant direction of sediment flux
Input	Calcasieu River	6.21	to CSC	91.2	41,000	to CSC
Input	Kelso Bayou	0.60	to CSC	8.8	2,300	to CSC
Input	Southeast bayous	n/d	n/d	n/d	n/d	n/d
Export	Gulf of Mexico	22.20	to Gulf	-326.0	758,000	to Gulf
Input	**Total CSC Input**	6.81	-	-	43,300	-
Exchange	East Fork	1.85	to Lake	-	35,000	to Lake
Exchange	West Fork + Lower CSC	24.05	to Gulf	-	793,000	to Gulf

Sources of Uncertainty

The analytical budget study was designed to provide depth-averaged estimates of water and sediment flux in the Calcasieu Lake study area. In shallow, well mixed zones a time series of single water column measurements of TSS is expected to be representative of the entire water column. In the CSC and East Pass, the presence of a salt wedge and an ephemeral fluid mud layer complicates the sediment dynamics. While the Institute has used the best available information to estimate the water and sediment fluxes in this analytical sediment budget, further study of this area is needed to better characterize this dynamic part of the CSC system.

Additionally, the intersection of the CSC and GIWW was not considered as a sediment source in the analytical budget. At this confluence the water and sediment from several channels are exchanged in complex ways based on tide, wind, and river conditions. Locks across the GIWW and contributions to the GIWW from rivers outside the Calcasieu basin also affect the dynamics at this location. Fully characterizing the complexity of the water and sediment dynamics at this confluence would require a long-term, high resolution study of the area that is outside the scope of the analytical sediment budget. Estimates of inputs from the GIWW are considered in the modelling section of this report.

2.4.2. Shoreline Retreat Analysis

An analysis of shoreline retreat was conducted to examine the potential contribution of sediment from the CSC banks from 1998 to 2016. In this analysis, shorelines that were unarmored as of 2016 were considered – shorelines that were armored between 1998 and 2016 were not included. The focus of the analysis was on the average yearly retreat rate and the total sediment mass contribution from the unarmored shorelines over the two decades. In a draft report by Fischenich (2004), retreat rates were calculated along the CSC between RM 5 and 34 using orthophotos images from 1972 to 1998; and they calculated an average retreat rate of 1.9 ft/yr along the this reach of the CSC. They also found that bank line erosion from RM 5 to 34 contributes an average of about 200,000 cy/yr of sediment to the system. The imagery analysis here is performed to obtain comparable data for the period from 1998 to 2016. Additional imagery and analysis between 1998 and 2016 would help understand the effect of armoring the shoreline on the retreat rates on a more refined timeline. As this sub-activity was already beyond the scope of this study, an additional imagery analysis was not completed.

Imagery Analysis Methods

Methods used in the present analysis are comparable to those used in the draft report by Fischenich (2004). DOQQs and LiDAR imagery of the CSC were obtained from LSU Atlas (https://atlas.ga.lsu.edu/) and NOAA Digital Coast (https://coast.noaa.gov/digitalcoast/). The DOQQs used for comparison are from 1998 (02/08/1998), and from 2016 (10/01/2016). Elevation points of bank line, necessary to convert retreat rates to retreat volumes, were obtained from the 2003 LiDAR dataset. To derive retreat rates, a river centerline transect was drawn orthogonally between channel mile markers every 0.25 miles along the CSC. Distances from the centerline to the East and West bank lines were measured in both the 1998 and 2016 images. Figure 39 shows a sample of this analysis, from CSC river miles 9 to 12. Annually averaged land change rates per 0.25 miles for each bank are shown in Figure 41.

No timestamp record was found for the imagery, so water elevation was not resolved. The 2016 imagery resolution is of 0.5 m or 1.64 ft, while the 1998 imagery is of 1 m or 3.28 ft. Furthermore, where shallow shoals were visually recognized in the 1998 imagery, a careful attempt at identifying the true channel "edge" was made, with the goal of reducing potential water elevation differences. An example of this can be seen at River Mile marker 11 in Figure 40.

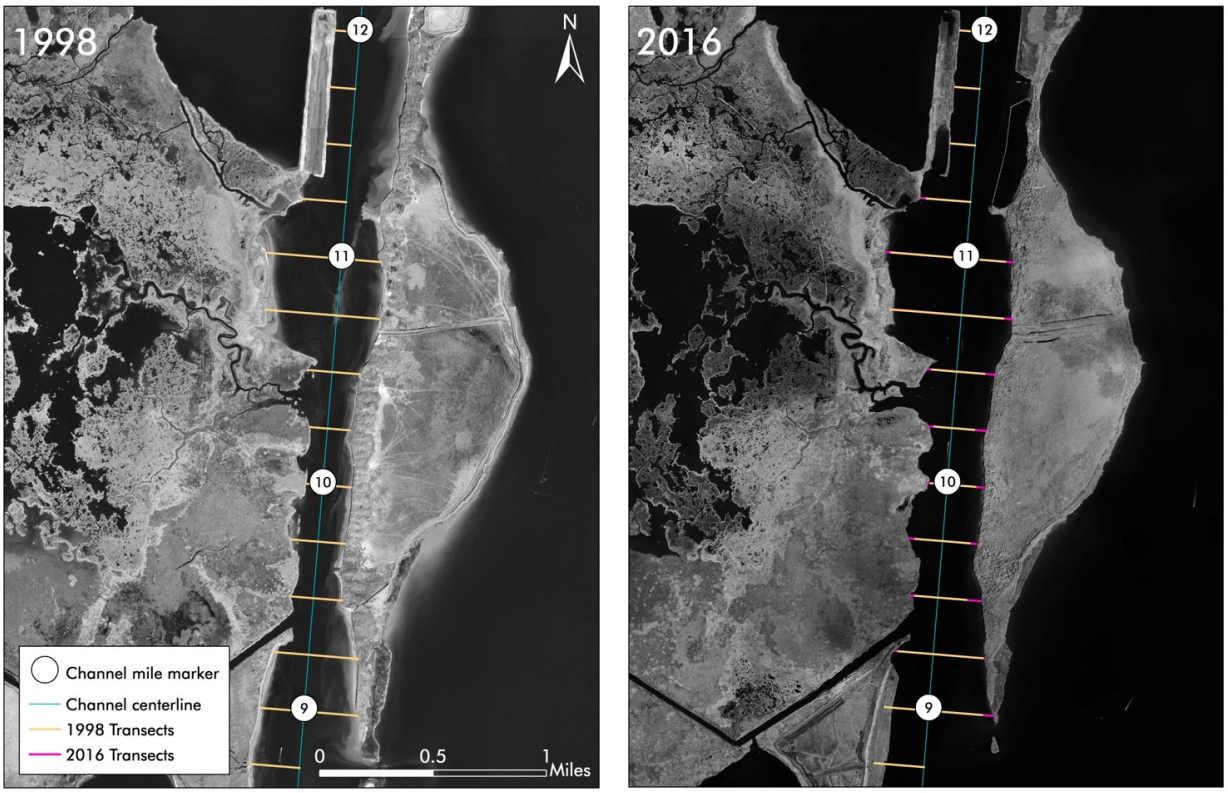

Figure 39. Transects from centerline to channel edge in 1998 (yellow) and 2016 (magenta) for river miles 9-12.

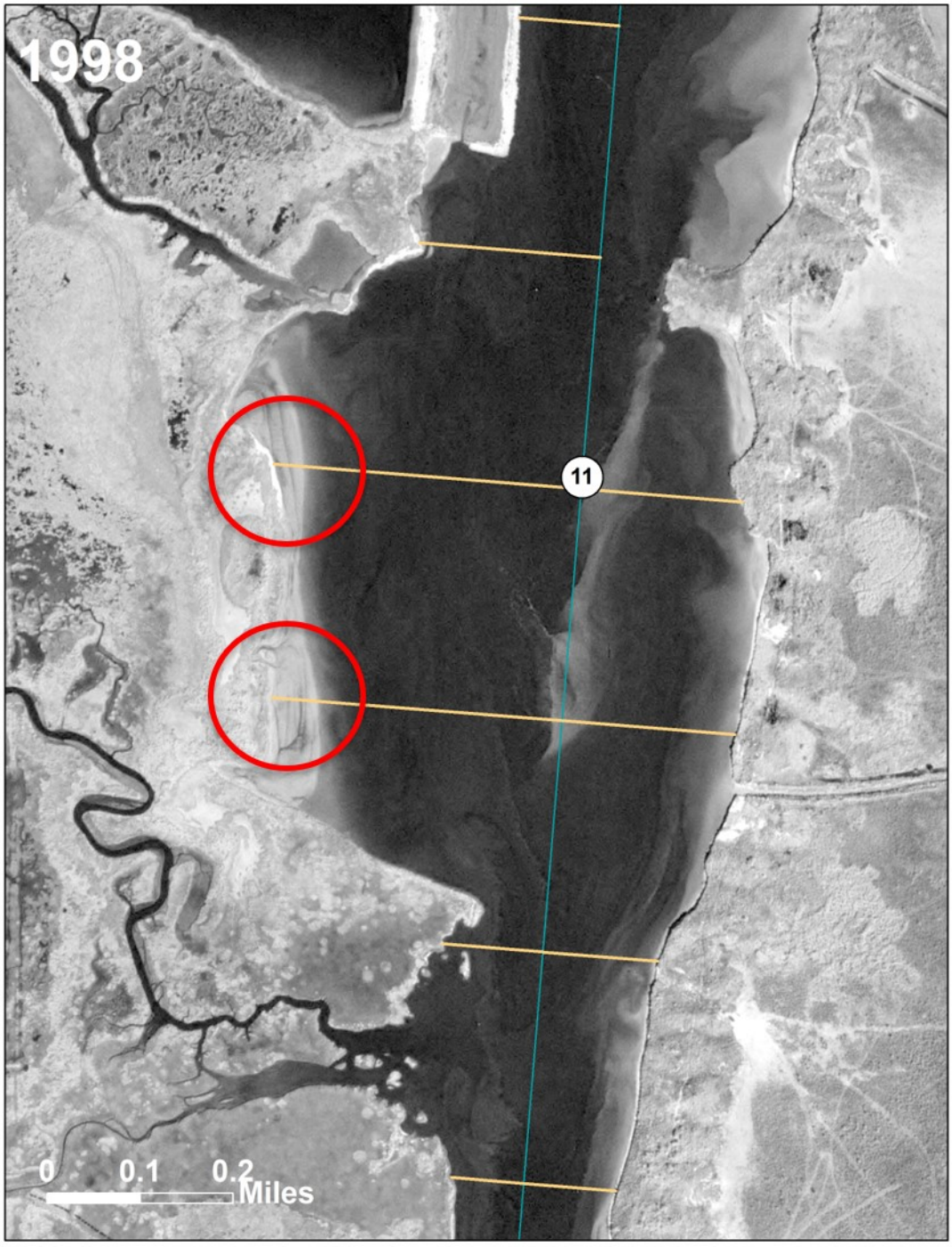

Figure 40. A close-up of the transect lines measured at River Mile marker on the 1998 image. The red circles highlight the edge of the transect line, which is drawn to what appears to be the hard edge of the channel bank, rather than the shallow shelf or plume of sediment that may at times be underwater during high water flow and/or high tide.

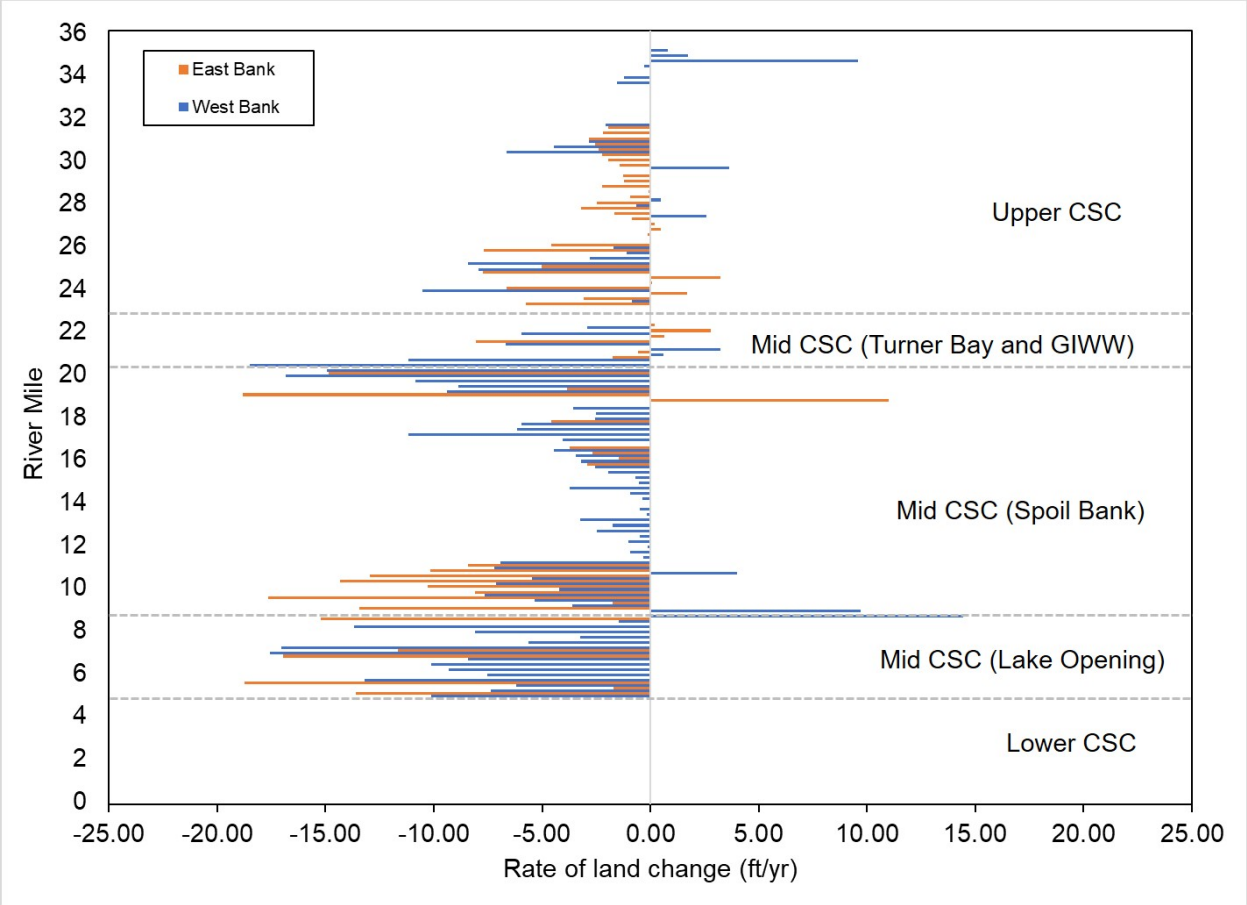

Figure 41. Rate of land change along CSC from 1998 to 2016, obtained every 0.25 mi from satellite imagery. The east bank is shown in orange, and the west bank is shown in blue.

In addition to measuring the channel bank lines, the land change rates for the spoil bank line facing Calcasieu Lake from river miles 9-20 were also measured (Figure 42). Transects were drawn from the channel centerline to the East bank line of the spoil. The average land change rates are shown in Figure 43.

Figure 42. Transects from centerline to spoil bank shoreline facing Calcasieu Lake in 1998 (yellow) and 2016 (magenta) for river miles 9-12.

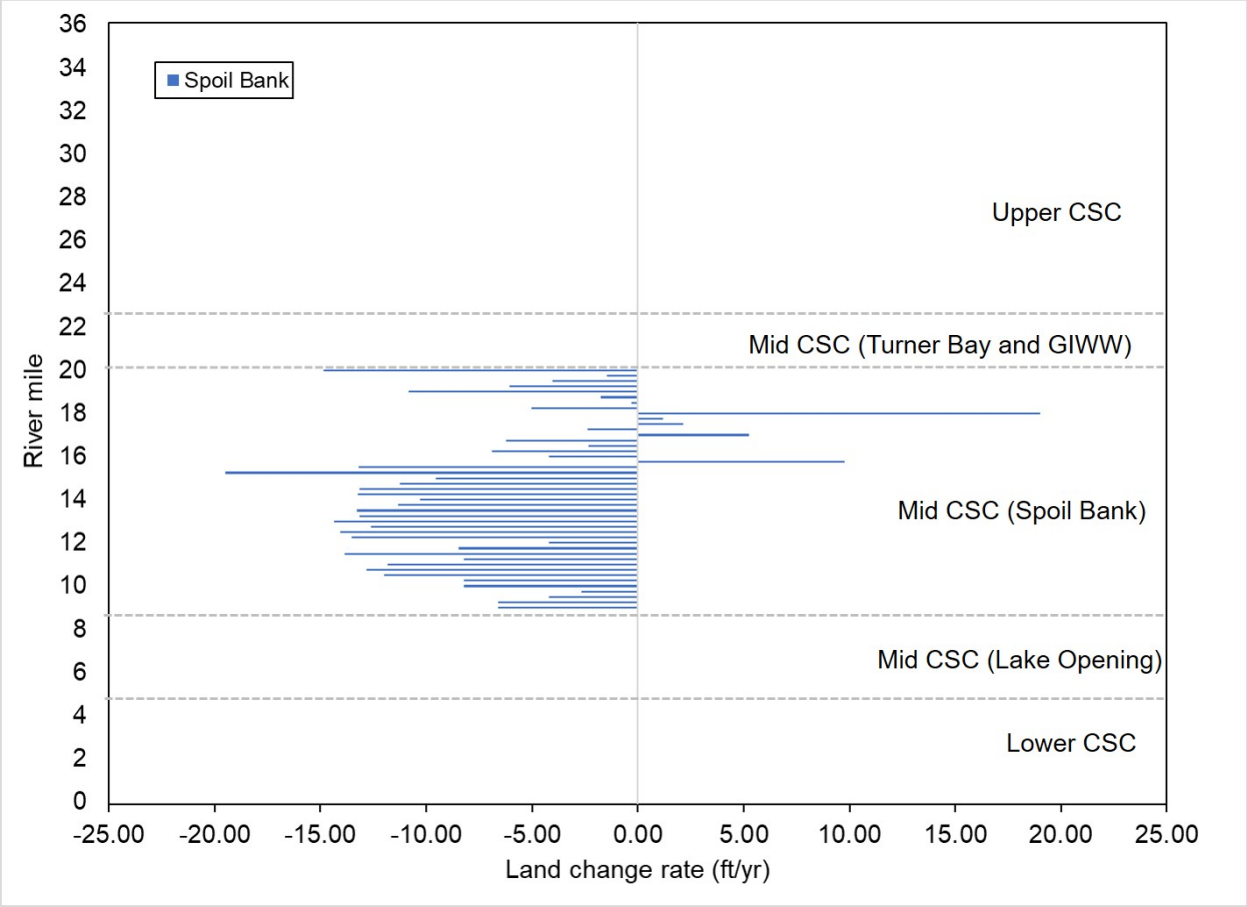

Figure 43. Rate of land change along spoil banks facing Calcasieu Lake from 1998 to 2016 obtained on 0.25 mi intervals from satellite imagery.

Shoreline Retreat Rates Calculations

To calculate the volume of sediment that the bank line retreat represented, it was necessary to approximate the thickness of the eroded land at the bank line. For this, elevation points from the 2003 LiDAR imagery were collected at the edge of each 1998 transect. The LiDAR elevation of the water surface in the images averaged approximately -1.6 ft NAVD88. Furthermore, an erodible depth needed to be determined. As no direct measurements were available, bracket estimates were made. A conservative value of 1.6 feet below the water surface (average tide range) was selected, and a value of 16 feet, an average value of the depth of the shelf margin of the CSC (Section 2.3.3) was used as a maximum, and volumes were calculated for each (Table 8). Only CSC-facing shorelines were utilized in this calculation to facilitate comparison with the Fischenich (2004) study, but basic trends for the Lake-facing shorelines can be examined in Figure 39. The eroded land thickness and volume for the CSC-facing shorelines were calculated according to the following equations.

Thickness = LiDAR land elevation – LiDAR water surface elevation + erodible depth

*Volume = land retreat * thickness * distance*

Table 8. Summary table of channel-facing shoreline retreat statistics from 1998 to 2016. Two volume retreat rates are calculated, using erodible depths (ED) of 1.6 ft and 16 ft. No data was measured or calculated for Lower CSC.

				Volume retreat rate (cy/yr) with ED 1.6 ft		Volume retreat rate (cy/yr) with ED 16 ft	
Section	**RM start**	**RM end**	**Description**	**West Bank**	**East Bank**	**West Bank**	**East Bank**
Upper CSC	22.5	36	GIWW to I-10	-15,697	-24,644	-24,412	-76,973
Mid CSC	20.25	22.25	GIWW	-35,847	-2,940	-79,497	-10,444
Mid CSC	8.25	20	Spoil	-78,085	-89,185	-206,919	-209,098
Mid CSC	5	8	Lake	-58,049	-21,125	-147,928	-66,607
Mid CSC Total	5	22.25	Lake to GIWW	-171,981	-113,250	-434,344	-286,148
Lower CSC	0	4.75	Gulf to Lake	N/D	N/D	N/D	N/D
Total				**-187,678**	**-137,894**	**-458,757**	**-363,121**
East + West				**-325,572**		**-821,877**	

In order to arrive at mass of sediment from bank line erosion, two porosity values from the literature for dredge spoil were used to represent the bulk density of spoil land areas – Porosity A (0.70) and Porosity B (0.74) were derived from HVJ Associates, Inc. (2007) in Table 9. The wet or dredged material porosity of 0.79 can be found using a void ratio of 3.72 (HVJ Associates, Inc., 2007). As no direct and recent measurements of porosities or erodible depths were available, and porosities likely varied spatially in any case, a range of mass of sediment from bank line retreat were calculated for the minimum and maximum erodible depth values, 1.6 ft and 16 ft, respectively, and for each porosity value (Table 9).

Table 9. CSC-facing shoreline annual retreat volume and range of mass for variable porosity values.

	Volume (cy/yr)	Mass (tons/yr) Porosity A	Mass (tons/yr) Porosity B
Porosity (dry sediment)		0.70	0.74
Shore retreat A (erodible depth = 1.6 ft)	325,572	197,889	171,504
Shore retreat B (erodible depth = 16 ft)	821,877	499,554	432,947
1998 bank retreat (Fischenich 2004)	200,000	121,564	105,356

From the report by Fischenich (2004), an estimate of 4 million cy/yr of sediment were being dredged, and 200,000 cy/yr of sediment annually resulted from bank line erosion between 1972 and 1998 (Table 9). This converts to an average of approximately 113,000 tons/yr eroded and nearly 2 million tons/yr dredged, which was nearly 7% of the amount dredged. Ranges are provided in Table 9.

The values calculated in this section are estimates and could be improved by performing geotechnical analyses of the spoil areas, shorelines, and channel slopes.

2.4.3. Sediment Storage

Two areas of sediment storage are considered: the CSC itself, as quantified using interannual dredging statistics averages, and Calcasieu Lake and West Cove on either side of the CSC, as quantified using radioisotope geochronology in the earlier CPRA project (Allison et al., 2018) (Figure 25). Water bodies that are hydrologically connected to the CSC (e.g., Lake Charles, turning basins, Devil's Elbow, etc.) are considered as part of the CSC dredging statistics analysis.

Sediment Burial in Calcasieu Lake and West Cove

Prior to the current work for the Port of Lake Charles, the Water Institute collected sediment cores in Calcasieu Lake and West Cove for CPRA and measured sediment burial rates using ^{210}Pb and ^{137}Cs radioisotopes. Radioisotope geochronology is a widely used method to measure and calculate ages of geologic materials, specifically, Pb^{210} and Cs^{137} radioisotopes are typically used to derive rates of sediment accumulation in marshes, estuarine water bodies, and continental shelves over the last 50-100

years. Detailed methods and assumptions can be found in the report delivered to CPRA (Allison et al., 2018), and the results are summarized in Table 10 (from the report).

Table 10. Annual accumulation rates and spatially integrated sediment storages for Calcasieu Lake and West Cove based on ^{210}Pb and ^{137}Cs geochronologies for the core sites.

Water Body	Annual average accumulation (cm yr^{-1})	Area (km^2)	Mass (metric tons)
West Cove	0.14	37	71,000
Calcasieu Lake	0.21	175	490,000
Total Storage	-	212	**556,000**

Channel Sediment Deposition Using Dredge Statistics

Making the assumption that dredging occurred at a frequency and removal rate necessary to maintain a constant bed elevation over time, then the volume of sediment removed from dredging can be used to approximate the volume of sediment that was deposited over the inter-dredge period. Sediment storage in the CSC was derived by utilizing two decadal USACE dredging datasets. Decadal dredge volume data from the U.S. Army Corps of Engineers (USACE) were available over two time periods: 1994-2005 (USACE, 2010) and 2006-2014 (from Jeff Corbino, personal comm.) These are shown in Table 11. An additional USACE dataset from 2017 (Austin Feldbaum, personal comm.) is illustrated in Figure 44, but is not included in the long term averaging in Table 11 as it is not representative of an annual average of sediment dredged from the channel. These dredge volume datasets represent very general estimates due to the lack of high fidelity data; dredging volumes are averaged over large channel reaches (> miles) and the dredging period is approximated from the project start and end date (which could span a period of multiple months). An alternate calculation of channel sedimentation derived from a time series of bathymetric survey data is also shown Figure 44. These data were initially reported by Tetra Tech, Inc. (2015), and were based on the assumption that measured bed elevation change was due to sedimentation (positive) or erosion (negative). The bathymetric surveys take place intermittently, at a frequency greater than one survey per year on average, over the years 2006-2014. Sedimentation rates derived from the bathymetric surveys, which are collected at channel cross sections less than 1000 ft apart, have a much higher resolution than those derived from dredging records, except for the 2017 dataset, which is reported at higher resolution intervals. Volumes for each dredging project conducted in the CSC were integrated to derive an annual average value (Figure 44). Table 11 shows the dredged quantity per distance for the two long-term USACE datasets, while Figure 44 normalized the dredged quantity per linear foot for all four datasets.

Sediment storage estimates derived by this dredging record method should be used cautiously. The method used to calculate the reported magnitudes of dredged material is dependent on the dredge operator, dredge configuration, and dredging contract. Calculating the total magnitude of sediment dredged over a dredging campaign, which may have had a duration on the order of months and may have been active episodically, often required significant spatial and temporal averaging methods that may not have been consistently applied. For this reason, this report emphasizes the comparison of the spatial patterns of dredged quantities, rather than absolute values.

Table 11. Annual average dredging volume in the CSC for the periods of 1994-2005, 2006-2014 obtained from USACE dredging records.

	USACE 1994-2005	USACE 2006-2014	Average 1994-2014
River Mile	Dredged quantity (cy/yr/mi)	Dredged quantity (cy/yr/mi)	Dredged quantity (cy/yr/mi)
5.50	175,000	135,285	155,142
6.50	175,000	135,285	155,142
7.50	175,000	135,285	155,142
8.50	175,000	135,285	155,142
9.50	175,000	135,285	155,142
10.50	125,000	135,285	130,142
11.50	125,000	135,285	130,142
12.50	225,000	135,285	180,142
13.50	225,000	135,285	180,142
14.50	225,000	135,285	180,142
15.50	225,000	163,124	194,062
16.50	175,000	163,124	169,062
17.50	175,000	256,445	215,723
18.50	175,000	256,445	215,723
19.50	175,000	256,445	215,723
20.50	175,000	256,445	215,723
21.50	225,000	256,445	240,723
22.50	175,000	256,445	215,723
23.50	175,000	27,839	101,419
24.50	175,000	108,673	141,836
25.50	175,000	108,673	141,836
26.50	75,000	108,673	91,836
27.50	75,000	108,673	91,836
28.50	75,000	108,673	91,836
29.50	75,000	140,895	107,948
30.50	25,000	140,895	82,948
31.50	25,000	140,895	82,948
32.50	25,000	60,062	42,531
33.50	25,000	60,062	42,531
34.50	25,000	49,652	37,326
35.50	25,000	49,652	37,326

It should be noted that, while extensive agitation dredging is carried out in the CSC offshore extension to Mile -19.2 (Jeff Corbino, personal comm.), this dredging is not included in the analysis as it is likely sourced from alongshore coastal currents as well as the CSC, and hence, not directly associated with the inshore CSC sediment budget. In addition, the exchange of this material inland of Mile -1.7 should be reflected in the annualized exchange of sediment measured at fixed site SCC (see Section 2.4.1).

The total mass storage in the channel based on the dredging records is on the order of 1.85 million tons/y with the porosity value of 0.79 from (HVJ Associates, Inc., 2007) (Table 12). This compares to a calculated total storage in Calcasieu Lake and West Cove from the core geochronology of about 0.56 million tons/yr, or about 23% of the combined masses sediment dredged in the CSC and sediment stored in Calcasieu Lake. Together, with the channel and lake sediment storage combined, we calculate a total sediment storage in the system of 2.4 million tons/yr. No dredging took place between RM 0 and RM 4.5 in the 2006 to 2014 period, and since authorized depth was maintained, this indicates that there is enough hydrodynamic energy to scour or maintain an equilibrium depth profile in the channel in this restricted channel reach, and no significant storage is taking place. The dredge statistics from the 1994-2014 datasets are only slightly larger than the volume reported by Fischenich (2004), estimated at approximately 1.7 million tons/yr (Table 12). However, there is a 1.6 to 4 times scale offset in the bank line retreat volumes calculated by Fischenich (2004) compared to those calculated by the present study (Table 9). This is reasonable because Fischenich (2004) did not include an erodible depth when calculating the thickness of the eroded bank, so the offset can likely be accounted for by the range of possible erodible depths.

Table 12. Long term dredge statistics data by volume and converted mass values.

	Volume (cy/yr)	Mass (tons/yr)
Wet/Dredge Porosity		0.79
USACE 1994-2005	4,275,000	1,818,903
USACE 2006-2014	4,431,084	1,885,313
Average 1994-2014	4,353,042	1,852,108
1998 dredged (Fischenich 2004)	4,000,000	1,701,898

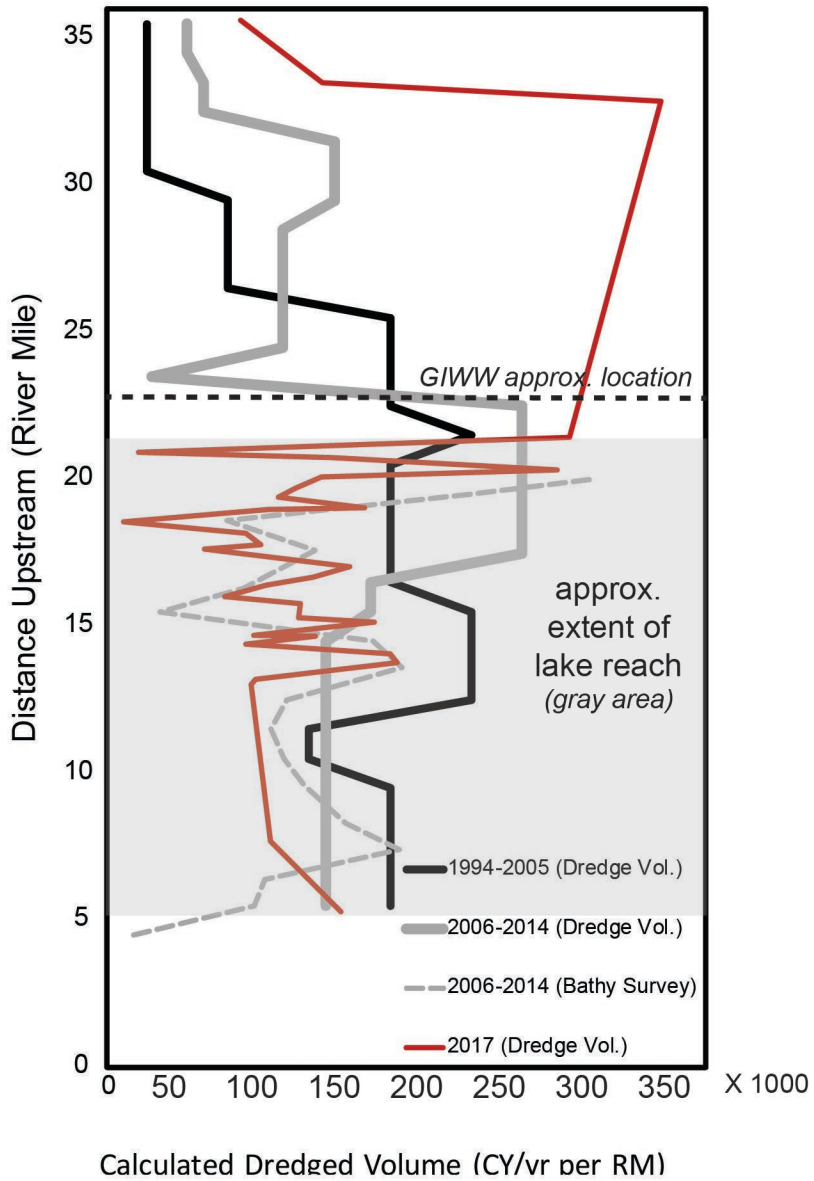

Figure 44. Calculated sedimentation rates in cubic yards per year per channel mile in the CSC. The 2006-2014 bathymetric survey was derived from Tetra Tech (2015).

The areas of highest dredged volume (and mass) are concentrated from the GIWW to the northern section of where the CSC is open to Calcasieu Lake (RM 17.5-22.5; Figure 25); this is observed in all three multi-year averaged datasets (Table 11; Figure 44). The fourth dataset, from 2017 has artifacts that are a result of plotting a single year of dredging activity, and, thus are less indicative of overall dredging pattern as it is used by assumption as a proxy for sedimentation rate. Areas of lower mass dredged (< 100,000 cy/yr per mile) are observed in the upper reaches of the CSC, RM 30.5-35.5. The spatial pattern of dredging need for two of the three multi-year datasets (i.e., 1994-2005 Dredge Vol., 2006-2014 Bathy Survey) display a [1] decrease in need from the River Mile (RM) 5-7 channel reach to the RM 10-11

reach and an [2] increase in need from the RM 10-11 reach to the RM 13-14 reach. The dataset that does not indicate these trends (i.e., 2006-2014 Dredge Vol.), had a very coarse spatial resolution that may not resolve these dredging need gradients. Figure 45 shows the reach of the CSC from miles 5 to 11 where the CSC is largely open to exchange with Calcasieu Lake.

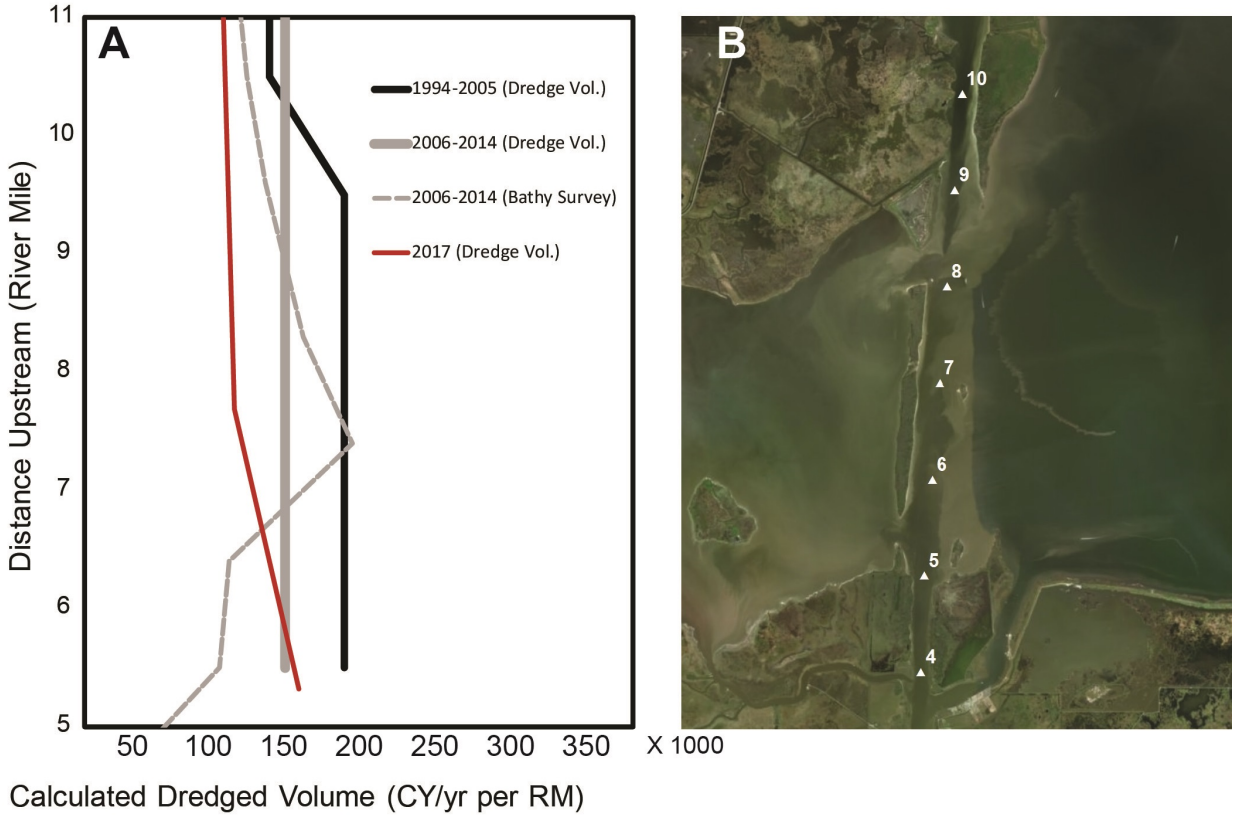

Figure 45. Calculated sedimentation rates for River Miles 5-11 A) plot and B) map of the same section of the CSC.

If the two large new sediment sources in the system (Gulf and Calcasieu River) are the major contributors to the dredging need in the CSC, then spatial records of dredging volume (Table 12, Figure 44) would likely show larger dredging volumes adjacent to these inputs. This is not the case in the northern CSC, opposite the Calcasieu River entrance; where dredging rates are low in the most proximal reach to the riverine input (e.g., CSC Mile 34-36; Figure 44), despite lower tidal energies for remobilization this far inland. Lake Charles and other interconnected water bodies (e.g., turning basins) in the Upper and Mid CSC are potential sequestration points for river-delivered sediment other than the CSC – but burial in these areas was not quantified in the present study. In the Lower CSC (CSC Mile -1.7 to 4.5), no dredging was conducted during the 1994-2014 period, suggesting this highly confined reach is sufficiently energetic to serve as a bypass for Gulf-derived sediment (as is confirmed by the modeling in Chapter 3). Dredging volumes do increase from CSC miles 5 to 8 (Figure 44), however, this does not definitively equate to a sediment focusing point for the Gulf input as this is also the reach which is exchanging sediment with the Lake and West Cove, as is discussed in Section 2.4.1.

2.4.4. Analytical Sediment Budget Implications

The primary purpose of the analytical budgeting exercise is to compare the magnitude of the sediment inputs (bank retreat, Calcasieu River, and bayous, shown in Table 13) with the magnitude of the dredging record from 1994 to 2014 as shown in Table 11. This comparison reveals that the estimated mass of new sediment inputs in 2017 from the Calcasieu River (including Kelso Bayou and the southeast bayous) is only 18% (including storms) to 21% (excluding storms) of the sediment dredged from the CSC. The annual bank retreat measured from the 1998 to 2016 imagery analysis (Table 9) can account for an additional 9% to 27%, depending on the spoil bank porosity and erodible depth (Table 13). This suggests that approximately 50% to 70% of the sediment entering the CSC remains unaccounted for by the analytical sediment budget and the shoreline retreat imagery analysis.

This comparative methodology requires using dredge records as the only available measure of sediment mass reaching the CSC on an annual basis. Though the observed trends are of value here, the absolute quantities, and the apparent "missing fraction" can be misleading for several reasons. The dredging and the shoreline retreat are averages of nearly two decades of record, whereas the CSC inputs budget calculations are from year 2017 only. Additionally, tropical systems had a major impact on the 2017 budget triggering a large sediment import from Cindy (Table 6) and an even larger sediment export from Harvey (Table 7). Mass of shoreline bank retreats and dredge material are subject to some variability depending on selected porosity of the wet and dry sediment (Table 9).

Another method for examining causality (Figure 46) involves using the sediment volume yield of shoreline bank retreat (1998-2016) against the dredged volumes (1994-2014). This conversion of bank retreat rates to volume, allows a volume versus volume comparison, overcoming the issues with volume:mass conversion - and the time averages are similar. An examination of Figure 46 reveals that higher dredging volume is positively correlated with retreat volume for areas north of about CSC Mile 16: this suggests that spoil bank retreat is a major control on dredging need in this reach, and that it is deposited near the point that it inputs into the system (as opposed to being diffused up and down channel). This concurs with model results (Chapter 3, Section 3.3) that show that sediment delivered to the CSC from banks that erode above Mile 10 is unlikely to be transported large distances and will need to be removed from the ship channel by dredging activities near the source. Tetra Tech (2015) outlines the erosional retreat of existing dredge spoil mounds that line the channel as a major contributor. The dredging records shown in Figure 46 do show a correlation of high dredging volumes with areas that are unlined by rip-rap and have undergone significant retreat. In the area from CSC mile 16 to 5, the correlation is less positive. The area of the opening with Calcasieu Lake, which today has large open water sections, shows both spoil bank retreat volumes and dredging need are high from mile 5-9. Some of these spoil banks completely retreated and are shallow submerged banks, resulting in a retreat rate of zero. Note that Figure 46 shows the sum of the east and west banks, but the channel section opening to the lake is mostly open water on the east bank, so the retreat volume is largely due to the west bank erosion (see Figure 41 to distinguish the retreat rates from either bank). There is an offset from the highest dredged volumes slightly north of mile 10-11, which may reflect the fact that although shorelines are moving back rapidly in the 5-9 mile reach, they are already discontinuous, so that the total volume removed is smaller. The offset at miles 10-11 is also at the transition between storage and flushing of sediment to the Gulf. In mile 5-9, unlike for the upstream, the CSC does have the transport capacity to

move sediment that is delivered from the banks, so the retreat areas exceeding the dredged quantities in this section could indicate flushing to marine.

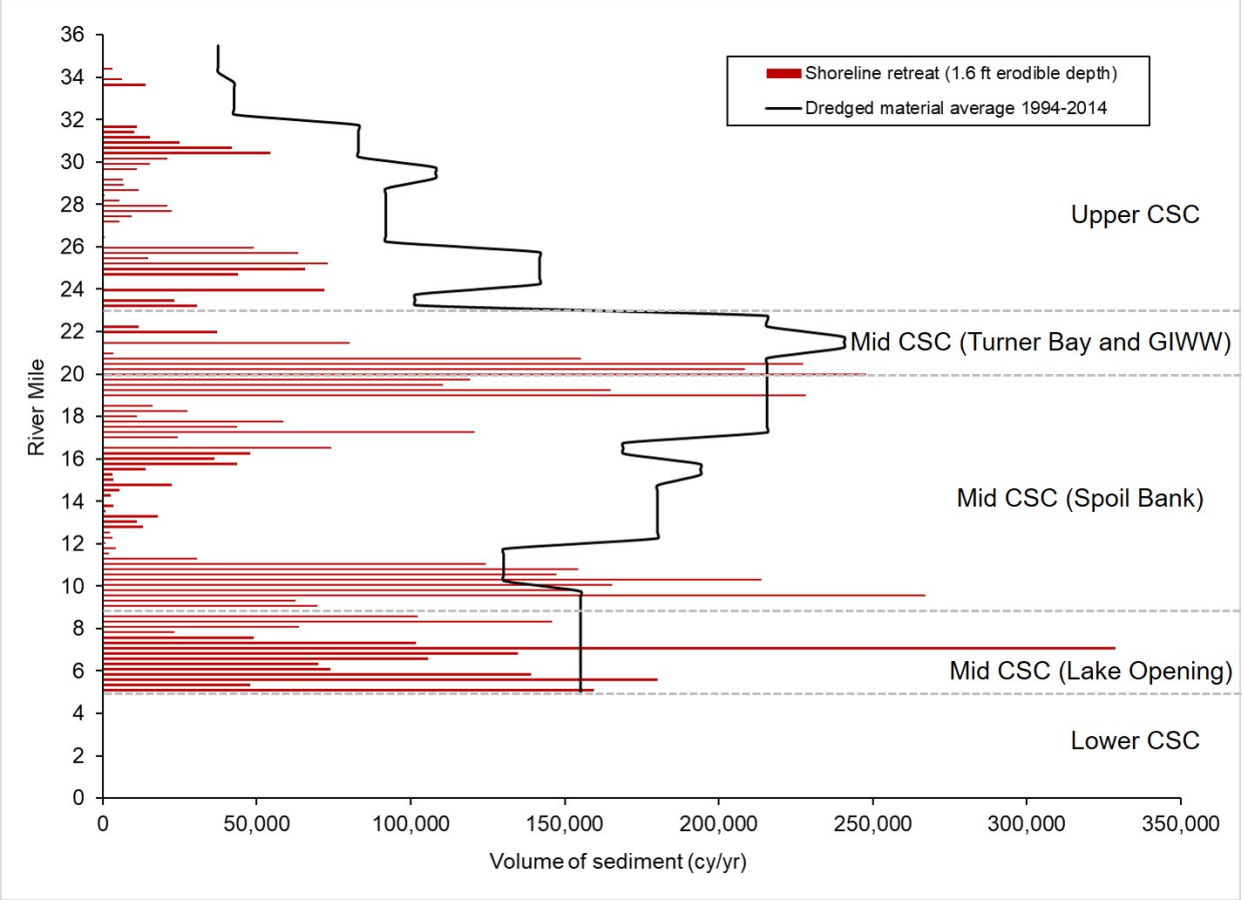

Figure 46. Combined plot of CSC-facing shoreline retreat and dredged material volumes. The shoreline retreat is based on 1998-2016 imagery for the sum of east and west bank retreat. Refer to Figure 41 retreat rate per bank. An erodible depth of 1.6 ft is shown here. The dredged material average was obtained from USACE records for 1994-2014.

From the sediment budgeting exercise, even using the most favorable volume:mass conversions, sediment sourcing (natural + bank retreat) is less than the annualized dredging mass. This differential between sources and sinks in the system is potentially produced by multiple factors. The first is the aforementioned generalized constraint of volume:mass conversion for the bulk density of dredge spoil and bank spoils. There may also be unmeasured additional natural sediment sources (e.g., Contraband Bayou, Bayou D'Inde, Big Lake). However, given their small water contribution relative to the measured sources, these are likely to be small contributors in our estimation. Finally, the analytical budget does not include the inputs from the GIWW or the fluid mud layer from the Gulf as both were beyond the scope of this study.

Table 13. Summary table of the % CSC sediment inputs relative to average dredged quantities (1994-2014). The bank retreat range reflects the variability from the two spoil bank porosities (0.70 and 0.74) and the two erodible depths (1.6 ft and 16 ft).

CSC Sediment Inputs	% Sediment Input
Total Record 2017	**20.8**
Calcasieu River	19.6
Kelso Bayou	0.5
Southeast bayous	< 0.1
Total Record 2017 (minus storms)	**18.4**
Calcasieu River	17.4
Kelso Bayou	0.3
Southeast bayous	< 0.1
Bank Retreat Range	**9.3-27.0**

2.5. SHIP WAKE RESUSPENSION STUDY

A ship wake resuspension study was conducted to characterize the effects of passing vessels in the CSC. The object of this study was to establish whether [1] vessels resuspended sediment along the marginal submerged shelf of the CSC [2] resuspension, if taking place, is restricted to vessels of a given size, and [3] insights can be gleaned about the source(s) of the resuspended sediment. The study was not focused on calculating the magnitude of this process in the overall sediment budget analysis or establishing if this is a major mechanism for advecting sediment into the CSC. Even without this element, a better understanding of the effects of vessel passage timing, draft, and speed relative to the tidal cycle can inform CSC navigation operations, and can give insight into establishing a link between wake resuspension and dredging need.

2.5.1. CSC Instrument Deployment

Arrays of fixed-station instrumentation were deployed for durations on the order of a few days (Table 14). The arrays were submerged along the navigation submerged channel margins (e.g., shelf) and were deployed to place individual instruments at a range of depths and distances from the shoreline (Table 15). YSIs (described in Section 2.2.2) and RBR Duos (a product of RBR, Inc. www.rbr-global.com) were used to monitor water level using pressure-sensing transducers; water-level data was collected at a frequency capable of resolving the passage and properties of significant waves (i.e., 6 hz). A data file log is listed under Appendix F.

The RBRs and YSIs that composed the fixed-station instrument arrays contained sensors to monitor optical turbidity. Turbidity is a common proxy for suspended sediment concentration. Conversion of turbidity to suspended sediment concentration was not possible due to the brief deployments limiting the ability to collect water samples to derive a conversion calibration (and hence a quantitative flux). However, the time series of turbidity measurements from spatially distributed instruments does allow users to investigate the movement and timing of suspended sediment remobilized from the channel bed due to the wake of large vessels.

Three deployments were conducted during this study, however the first deployment in October 2017 resulted in instrument displacement likely due to the impact of large ship wakes. Two more deployments were executed in January 2018 with a different bottom mounting strategy designed to curtail instrument displacement – their site locations are indicated in Figure 47. For the present report of results, only the observations from deployments at sites 2 and 3 (January 2018) are explored.

Table 14. Ship wake study instrument deployment dates and parameters.

Site #	Channel edge type	Shoreline type	Deployment Dates	Instruments Deployed	Parameters Measured
1	Muddy shallow shelf	Terrace	10/22/2018	RBR (4)	Water-level, turbidity
2	Muddy steep shelf	Beach and marsh	1/10-13/2018	RBR (6), YSI (1)	Water-level, turbidity
3	Muddy shallow shelf	Terrace and beach	1/13-15/2018	RBR (3), YSI (1)	Water-level, turbidity

Table 15. Ship wake study instrument coordinates in NAVD83 UTM 15N.

Site #	String	Station	Easting	Northing	Latitude	Longitude
1	A	D	467245.5	3308927.6	29.910601	-93.339304
		C	467263.2	3308926.4	29.910590	-93.339121
		B	467275.8	3308934.9	29.910667	-93.338991
		A	467290.7	3308927.5	29.910601	-93.338836
2	A	F	468500.9	3328230.9	30.084835	-93.326870
		C	468532.1	3328229.1	30.084820	-93.326546
		A	468549.5	3328229.1	30.084820	-93.326366
	B	B	468476.9	3328047.8	30.083182	-93.327114
		D	468528.1	3328041.5	30.083127	-93.326582
		E	468510.8	3328040.8	30.083120	-93.326762
		G	468711.4	3328022.9	30.082964	-93.324680
3	A	B	467333.7	3310975.2	29.929082	-93.338453
		C	467352.9	3310973.4	29.929066	-93.338254
		E	467363.3	3310968.2	29.929019	-93.338146
	B	G	467329.7	3310504.3	29.924832	-93.338480
		D	467345.4	3310478.3	29.924598	-93.338317
		K	467356.7	3310494.7	29.924746	-93.338200

Figure 47. The red polygon shows approximate site locations of instrument deployments(A. Site 2; B. Site 3). Navigation channel river mile shown for reference.

2.5.2. Vessel Traffic

Vessel traffic properties were quantified using Vessel Finder (www.vesselfinder.com) traffic datasets. These data included ship location by time, course, speed, and draft. During the deployment of fixed-station instruments, an automated digital camera (GoPro Hero 5 with HD camera) was set to visually record all traffic through the monitored reach at 1 min intervals (Figure 48).

Figure 48. Photograph of a vessel passing through the study area recorded from the deployed automatic camera. The picture is from Event 4 in Table 16.

During the approximately three-day-long fixed-station instrument deployment at Site 2, Vessel Finder reported the passage of 34 vessels; 14 of these vessels are classified as large (i.e., draft > 5 m). During an approximate 1.5-day deployment at Site 3, 17 vessels were identified, and 15 vessels were classified as large. The camera used to visualize vessel traffic during deployment indicated that the Vessel Finder dataset did not catalogue all channel traffic and, therefore, the dataset should be considered a conservative estimate of channel traffic.

2.5.3. Observations During Vessel Passage

Table 16 shows vessel and wake data for ten large vessel passage events. Study measurements suggest that the wake from large vessels produce a sizeable impact on water level and the resuspension of bed sediment. Figure 49 shows the typical hydrodynamic and sediment response to the passage of a large vessel in the two study areas. The ship produces a water level drawdown followed by a sudden water-level increase (i.e., a ‘surge’) that translates away, in the approximate normal direction, from the vessel’s course. This can be thought of as a pressure wave of water carried along with the vessel when it enters a

waterway confined on both banks, as typifies much of the CSC. The ship may produce a series of wake waves that also translate away from the vessel's course (sometimes both bow and stern wakes). These wake waves are of a much smaller amplitude and period than the initial drawdown and surge (Figure 49a). Stations mounted on the shelf floor during these passages show that the turbidity levels significantly increase upon the passage of the initial drawdown and remain elevated above background values (i.e., the ambient levels prior to vessel passage) for periods of tens of minutes (Figure 50). The smaller waves that compose the vessel wake do not have a clear influence on turbidity. While some events showed an apparent positive relationship between wake magnitude and turbidity, other events exhibited no systematic trend between the two variables (e.g., the event illustrated in Figure 49b) shows little indication of the presence of a significant vessel wake and wake impact on turbidity at the instrument location). A previous study on ship wakes in the CSC (i.e., USACE, 2010), speculated that the relative low amplitude and sediment transport capacity of the wake waves was likely due to the vessel's low rate of speed in the study area.

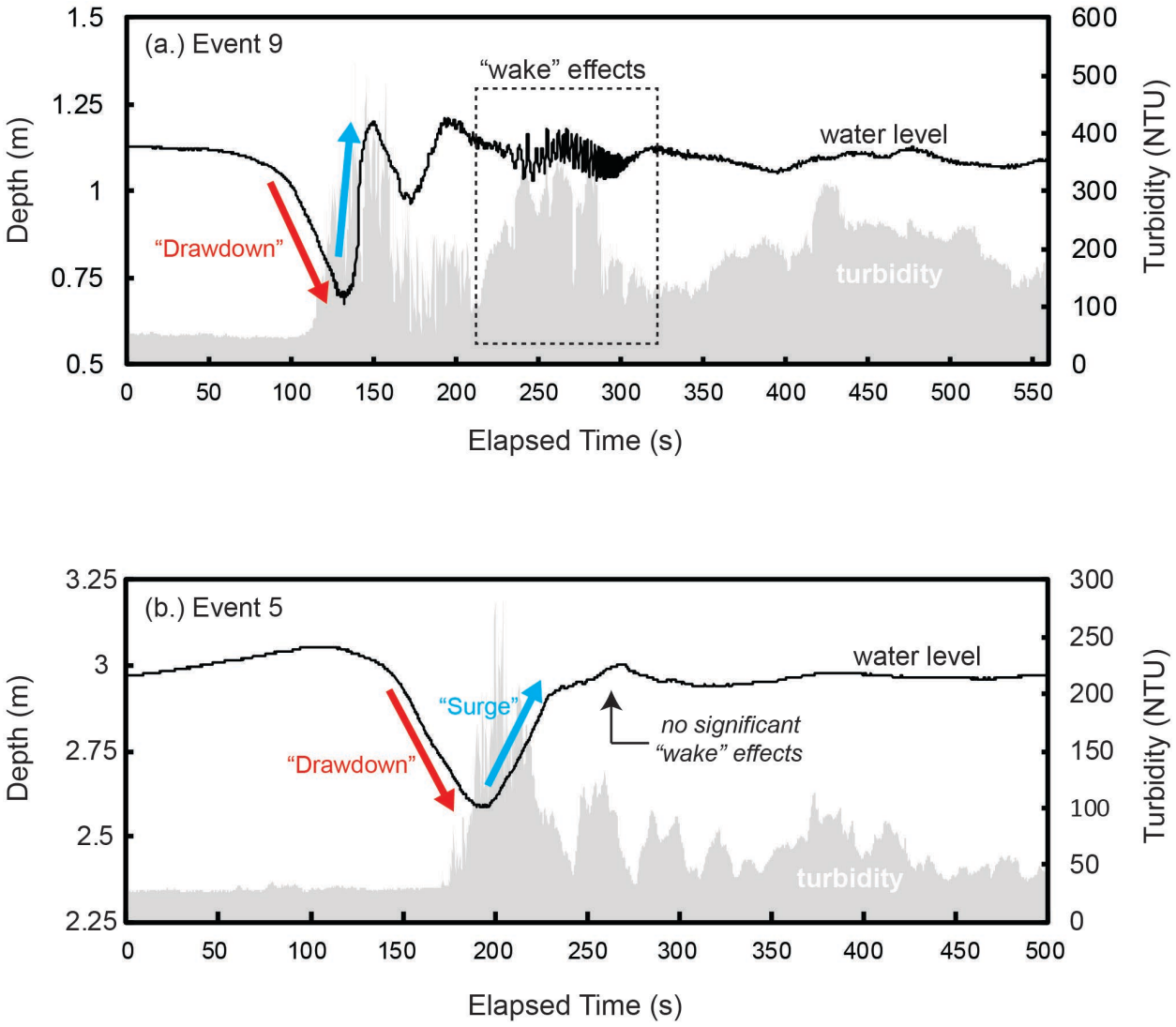

Figure 49. Plot of water-level, in terms of flow depth, (black line) and turbidity (gray filled region) showing typical responses after the passage of a large vessel: (a.) with a significant vessel wake and (b.) without a significant vessel wake visually discernable within the observed datasets.

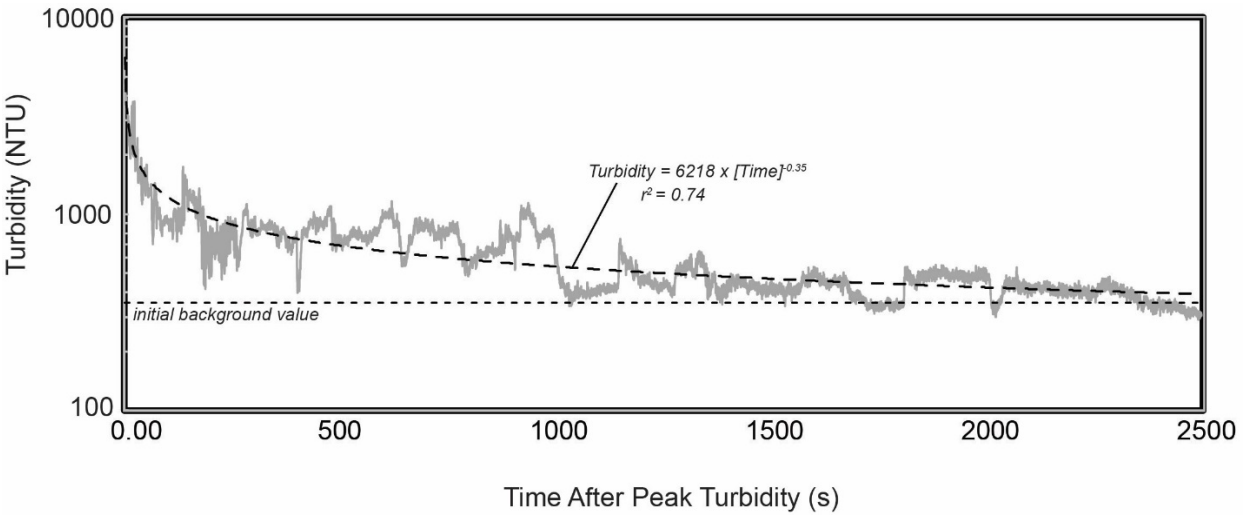

Figure 50. Plot shows the typical recovery time of channel turbidity after the passage of a large vessel (Event 10 from Table 16 shown). The plot shows the trend in turbidity relative to the passage of the peak value that corresponds to the water level draw-down and surge. Note that the drawdown/surge process typically initiates on the order of 30 to 60 seconds prior to peak turbidity. Data are shown from an instrument positioned in relatively deep water and is in log scale.

Table 16. Summary data for ten large vessel passage events.

Event	Date (UTC)	Site	Tide[1]	Vessel Info			Depth			Turbidity (NTU)		
				Draft (m)	Speed (kn)	Direction (Upstream/ Downstream)	Bkg[2] Depth (m)	Max Surge Event Amp.[3] (m)	Event Duration[4] (s)	Bkg Turbidity	Event Avg.	Event Max
1	1/11/2018 16:48	2	High Flood	11.4	7.4	Up	3.14	0.60	164	22	43	173
2	1/12/2018 4:35	2	Mid Ebb	10.7	5.7	Down	3.32	0.61	117	18	284	752
3	1/12/18 5:05	2	Mid Ebb	11.9	5.7	Down	3.45	0.55	200	19	159	341
4	1/12/2018 17:47	2	Mid Flood	11.2	5.9	Down	2.80	0.38	99	95	320	512
5	1/13/2018 7:28	2	High Ebb	11.9	6.9	Down	2.97	0.47	152	28	77	281
6	1/14/2018 6:12	3	High Flood	11.3	8.6	Down	1.26	1.29	141	24	246	783
7	1/14/2018 9:57	3	Mid Ebb	8.7	9.1	Up	1.29	1.05	136	27	319	881
8	1/14/2018 13:37	3	Low Ebb	9.8	7.8	Up	1.16	0.50	167	21	286	562
9	1/14/2018 15:02	3	Low Flood	9.0	8.5	Down	1.11	0.54	246	50	191	521
10	1/14/2018 22:38	3	High Flood	11.3	7.4	Down	1.40	2.09	288	18	91	417

[1]High = near local peak, Mid = in transition, low = near local low; [2]Bkg (background) = mean pre-event value; [3]Max event amplitude = max surge crest – min draw-down trough; [4]Event duration = period of significant water level disturbance; Note: data are from instruments located in the middle of an array (located between the channel-most and shoreline-most instruments).

Figure 51 shows how the flow and sediment signal generated from the vessel passage translates shoreward over time from the deepest instrument station to the closest to the shoreline. While the drawdown begins almost simultaneously at both instrument locations, the drawdown trough is offset by approximately 30 seconds. The peak turbidity values do not show a clear pattern and can occur higher at either instrument location; however, once the turbidity values are elevated, the turbidity values at the channel-ward most instrument are sustained at significantly higher levels than the shoreward locations. It is also notable that the background turbidities in the channel-ward most instrument locations are greater than in the shore-ward locations.

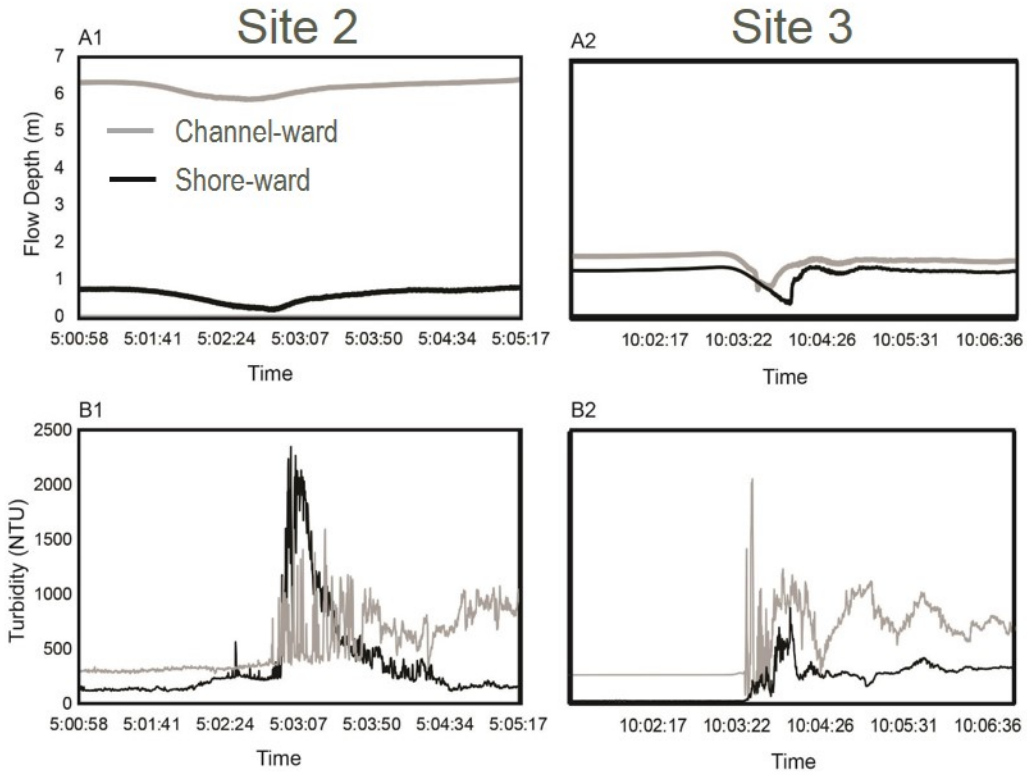

Figure 51. Figures A1 and A2 show the flow depth response to the draw-down and surge after the passage of a large vessel at Site 2 (A1) and Site 3 (A2). The gray line shows the measured change in depth over the instrument nearest the deep CSC and the black line shows the depth nearest the spoil bank shoreline instrument. B1 and B2 show the corresponding measured turbidities for the same time period and locations. The two instruments shown were located approximately 50 m apart. Note that the secondary wake waves are too small to be shown in the A plot vertical scale.

Smaller vessels (e.g., drafts significantly less than 5 m) do not appear to generate wakes capable of significantly influencing the resuspension of bed sediment. Small vessel wakes were low amplitude (i.e., on the order of centimeters at the instruments), high frequency waves that lasted tens of seconds (Figure 52). That is, there was no significant drawdown and surge associated with these events. During passages of these small vessel wakes, measured turbidities did not appear affected (e.g., turbidities remained at background values).

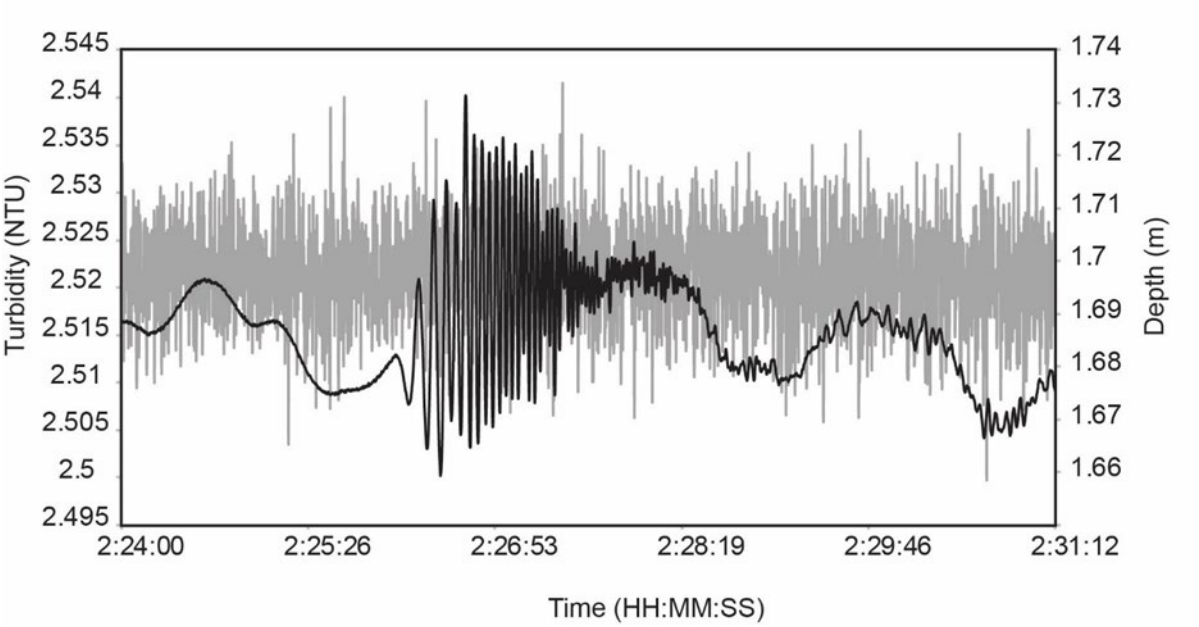

Figure 52. Example measurements after the passage of a small vessel (data from a 1.8 m draft vessel traveling at 20.4 knots). The gray line is the turbidity, and the black line shows the water level.

2.5.4. Discussion and Preliminary Conclusions for Wake Experiment

Deployments in this resuspension study were limited to muddy shelves of varying slopes behind beach, marsh, and terrace shorelines. This ship wake resuspension study offered several preliminary conclusions. During vessel passage, there is wake resuspension occurring, and it is primarily restricted to larger vessels. The size of the vessel (indicated by the draft) appears to be the dominant factor. The vessel direction and speed (at normal speeds), and tide phase seem to have minimal impact on magnitude and direction of sediment resuspension. Two types of waves were observed – surges and wake waves – both of which generate resuspension. Events can generate turbidities up to an order of magnitude above background, and elevated turbidities remain for up to 5 minutes, suggesting that there is significant time for ambient currents to advect or diffuse resuspended material to significant distances along channel or across channel from the resuspension site.

Additional information is needed in order to determine whether the resuspension energy changes from the deeper channel margin to the shoreline. Without a clearer pattern of higher resuspension on the deeper versus nearshore areas, it is difficult to discern whether shoaling waves are losing energy (by dissipation) at rates greater than the increased shear stress on the bed caused by the surge/wake wave passage through shallowing water. Furthermore, a clear pattern of timing and direction of resuspension turbidities is needed. In Figure 51, both the sensors near the shoreline show a rapid drop-off in turbidities post-disturbance. This suggests the increased turbidity was dependent on energy from surge/wake to resuspend local bed sediment in shallow areas. In deeper areas, the period of increased turbidity was much longer and appeared to last well beyond the period of flow disturbance. Turbidity in this region could be subject to transport to other areas; further information detailing currents could help define how the elevated turbidities may be affecting sedimentation within the shipping channel.

Given these preliminary observations and insights, future questions need to be addressed to better constrain importance of wake resuspension on sediment dynamics in the CSC. These include:

- How does the resuspension energy change from the deeper channel margin to the shallower shoreline edge? How fast do shoaling waves (i.e., waves headed shoreward) lose energy compared to rate that the waves increased bed shear stress?
- What is the directional flow of the resuspended material? Is the resuspended material from local adjacent eroding shoreline, from the channel bed, or brought in with the ship surge?
- Once resuspended, where does the sediment eventually come to rest—vectored toward the shoreline, the channel, or largely redeposited in place?
- How much do the refractory waves from the ship wake affect the shoreline erosion? Put another way, how many large ship passages are required to result in a measurable erosion of the shoreline?
- How do all of the above vary by shoreline bank type? Do the armored shorelines significantly alter the direction and magnitude of sediment resuspension?

3.0 Chapter 3: Delft3D Numerical Modeling

3.1. INTRODUCTION AND OBJECTIVES

This chapter describes the calibration and implementation of a depth averaged Delft3D model of the CSC and its surroundings (Task 2). The primary purpose of the work described herein is to document and understand the sediment dynamics of the CSC. This includes a quantitative accounting of sediment exchange with the Gulf of Mexico and with Calcasieu Lake, patterns of sedimentation and erosion along the ship channel, and a comparison with historical dredging activities as presented in Section 2.4. The model is also used to predict the sedimentary response to the CSC system as a result of CPRA's proposed salinity control structure, and two sea level rise scenarios.

This model was developed by the Institute, was initially presented to CPRA by Pereira and Meselhe (2015), was then further modified by Esposito et al. (2018), and is modified and improved for its current use. The model simulates depth averaged flow, salinity, and sediment transport throughout Calcasieu Lake, the Calcasieu Ship Channel from the jetties to the I-10 bridge, and portions of the Gulf Intercoastal Waterway. Four discharge boundary conditions are included to provide inland flows to and from the ship channel, and a water level boundary is imposed at the marine end of the computational domain. Wind and precipitation are included, but waves are not.

In this report the model is calibrated to an observational data set collected by the Institute during 2017 and described in Chapter 2. This newly calibrated model provides insight into the flow and sediment transport dynamics that are relevant to sedimentation in the CSC. The model is then run for four other conditions. First, a long-term simulation from 2006 to 2014 was conducted in order to compare the model results with historical dredging records. Then the model is re-run for the year 2017 with structures emplaced along the ship channel to restrict exchange with Calcasieu Lake. These structures are based on salinity control structures that the CPRA is proposing to reduce salinity intrusion in to Calcasieu Lake. The structures also affect flow and sediment transport in the ship channel and could be considered as possible locations for beneficial use of dredge spoil. Finally, the 2017 model is re-run with an increased sea level to provide an estimate of the influence that sea level rise will have on future dredging activity.

The results from each of the four models are evaluated in order to explain the process basis for observations in the CSC, and to provide recommendations to the Port of Lake Charles for long term strategies of dredging and disposal.

3.2. MODEL DESCRIPTION

3.2.1. Computational Grid and Bathymetry

The model grid used for the simulations presented in this report is shown in Figure 53. The maximum grid spacing in Calcasieu Lake is 475 ft, with the resolution generally being finer closer to the Calcasieu Ship Channel. The finest resolution is in approximately 65 ft, in the tidal channel that connects Calcasieu Lake to the Gulf of Mexico.

The model bathymetry is derived from public sources and from Institute surveys conducted in 2014 and 2017. A key feature of this model is in the treatment of the initial bathymetry. The model is first initialized using the bathymetry derived from public sources and from Institute surveys. For each case, the model is first run with bed morphology active for eight months (January 3rd to August 22nd, 2017), and we then use the resulting bathymetry as the initial bathymetry for the production runs. This choice is made so that the starting bed morphology is more nearly in equilibrium with the hydrodynamics, and thus avoids any shocks to the morphology that show up as excessive deposition or erosion.

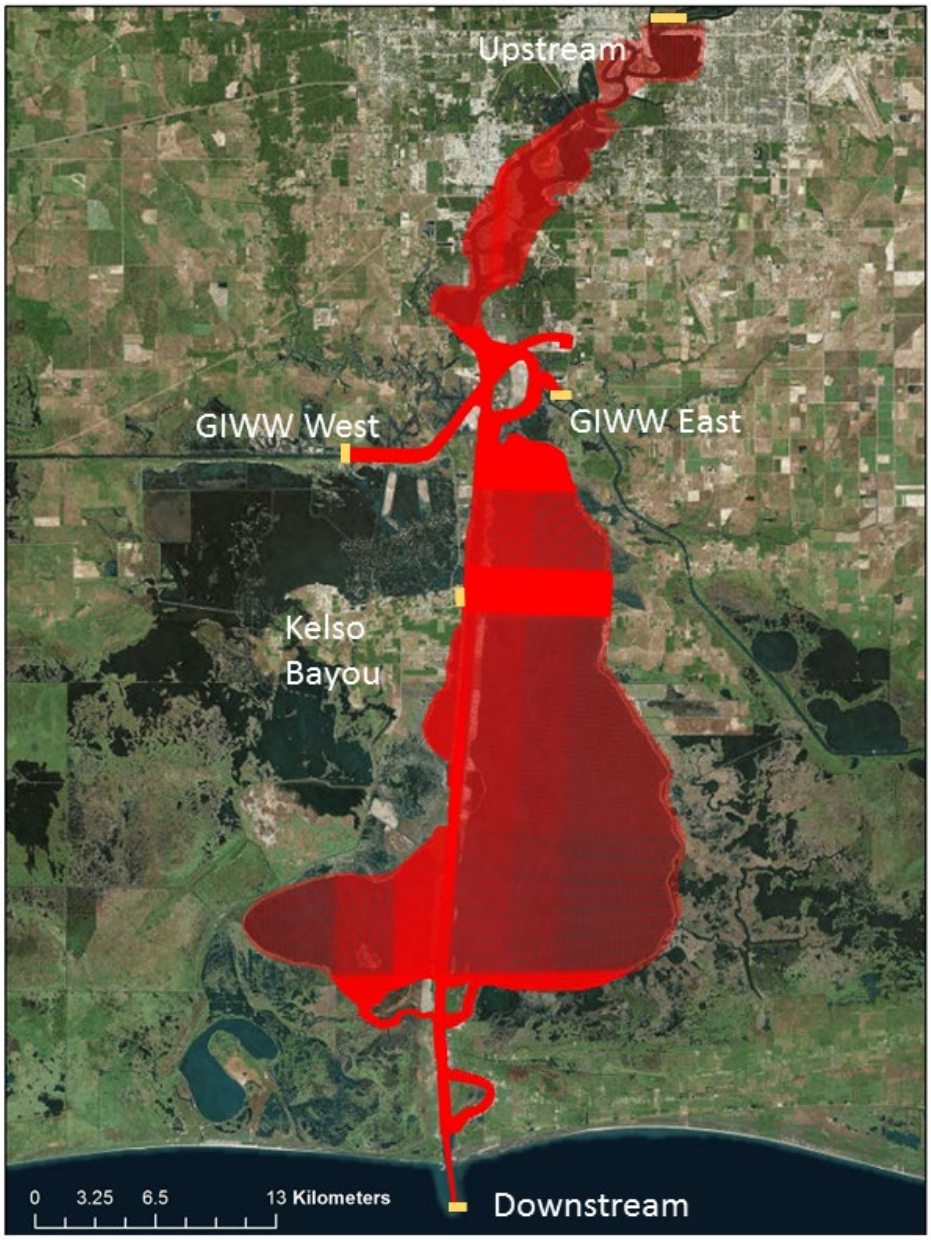

Figure 53. Delft3D Model Domain showing the four open model boundaries.

3.2.2. Boundaries

The model is driven by four discharge boundaries and one tidal boundary. The discharge boundaries (Figure 54) enter Calcasieu Lake through the Calcasieu River, the East and West entrances to the Gulf Intercoastal Waterway, and Kelso Bayou. The tidal boundary (Figure 55) imposes the downstream water level in the Gulf of Mexico. Delft3D allows the user to set a reflection parameter at water level boundaries to minimize oscillations originating from the boundary. We apply a reflection parameter of α=500 s2 to the downstream boundary. Each of the five boundaries has a time series of salinity and of sediment defined, which are shown in the following sections.

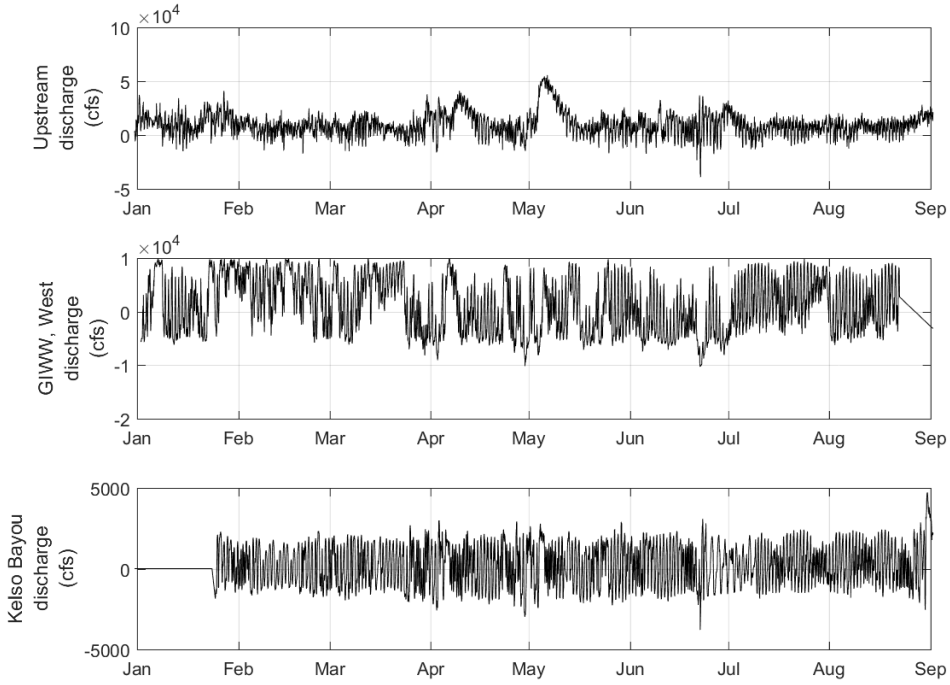

Figure 54. Total discharge boundary condition time series used at the Upstream, GIWW West, and Kelso Bayou Boundaries. The GIWW East boundary is set to a constant zero discharge for this model run due to uncertainty in lock operations. This does not have a significant impact on the model results in the southern portions of the ship channel.

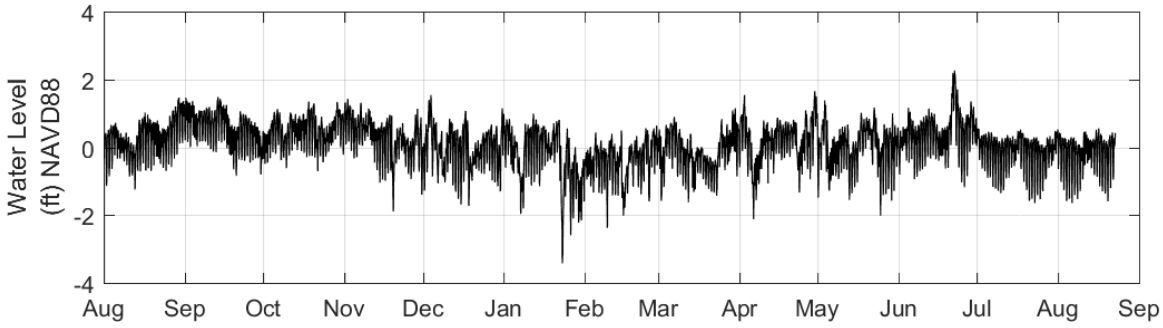

Figure 55. Water level boundary condition used at the downstream boundary.

Salinity

All salinity boundary conditions are shown in Figure 56. The salinity at the downstream boundary is based on the USGS salinity gauge at Cameron, but is compressed towards the open Gulf value of 35 ppt using the following formula.

$$Sal\_boundary = Sal\_cameron + (35-Sal\_cameron)*0.6$$

This technique provides a salinity timeseries that agrees with the salinity modeled offshore of Calcasieu Lake by the ICM Master Plan model.

The salinity timeseries at GIWW East and GIWW West are both taken to be the salinity as the USGS gauge at Hackberry increased by 10%.

The salinity condition at the Upstream boundary is defined as a function of the discharge in the Calcasieu River as measured by the USGS station at Kinder (not shown, Kinder is to the north of the model domain), and the salinity measured by the Water Institute at the I10 station. (Figure 6).

$$Sal\_upstream = Sal\_I10+(SalMax-Sal\_I10)*(1-Q\_Kinder/QMax)$$

SalMax, which is the maximum depth averaged salinity is set to 25 ppt, and QMax, which is the approximate maximum discharge at Kinder, is set to 3500 ft^3/s. This formula provides a salinity that decreases during periods of high discharge, but is always less than 25 ppt. This condition was implemented to account for the fact that the salinity measured at the Water Institute I10 station is from high in the water column, and therefore provides a salinity value that is usually lower than the depth averaged value. This formula assumes that the Kinder discharge never exceeds QMax, and that the depth averaged salinity never exceeds SalMax, which is true during the period that we model.

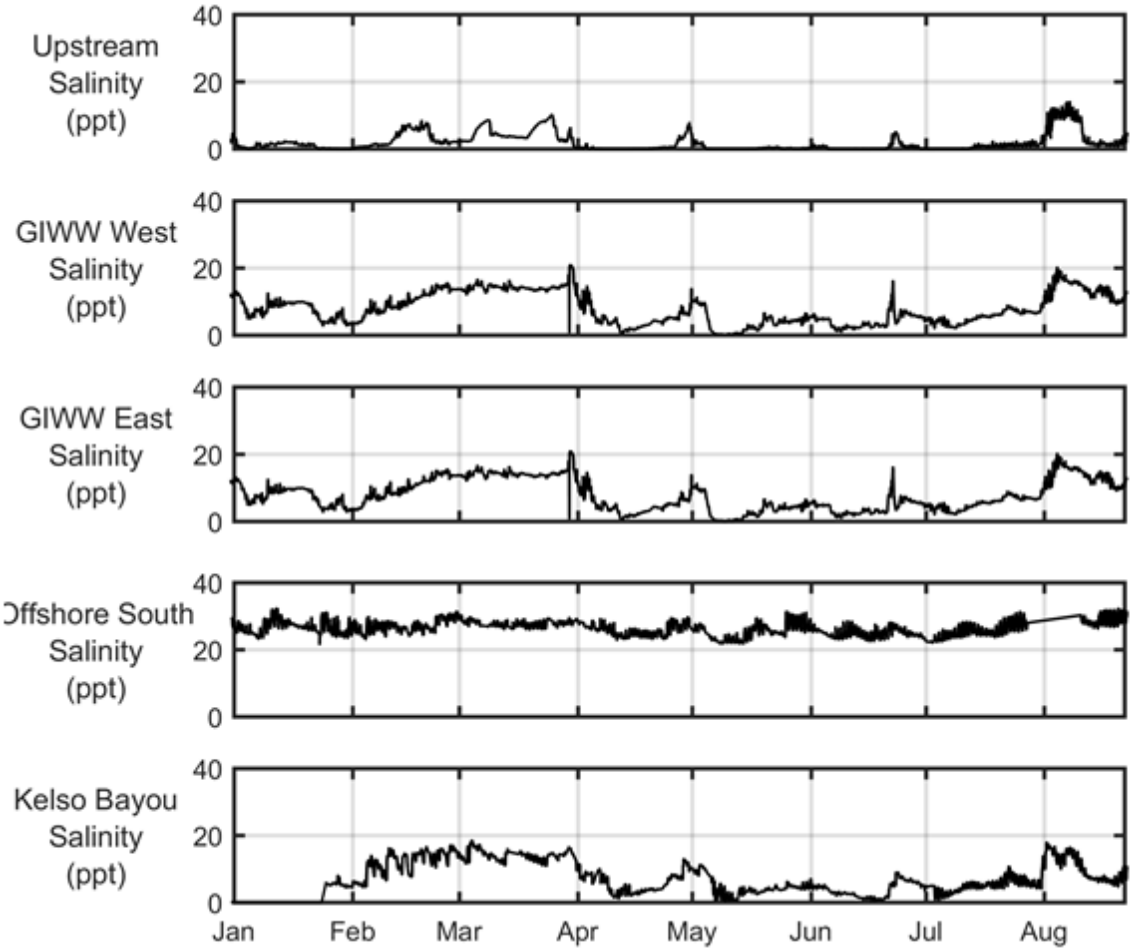

Figure 56. Salinity boundary conditions.

Sediment

The total suspended sediment input at the upstream boundary is given by a relationship developed by the Water Institute using historical data and Water Institute field data.

TSS_US= 4.2889232*(KinderQ*1.82)^0.2878-2.5485

TSS_US is the concentration of suspended sediment applied at the upstream boundary, in mg/L, and is estimated as a function of the discharge at Kinder in cubic meters per second.

The total load is divided into 55% silt and 35% clay, consistent with other Gulf Coast rivers near their mouth. The sand concentration input at this boundary is set to be equal to the transport capacity of the incoming flow. The silt and clay concentrations used in the upstream boundary are also applied to the two GIWW boundaries, as is the sand equilibrium boundary. This model uses a constant concentration of clay at the downstream boundaries.

Sediment boundary condition timeseries are shown in Figure 57.

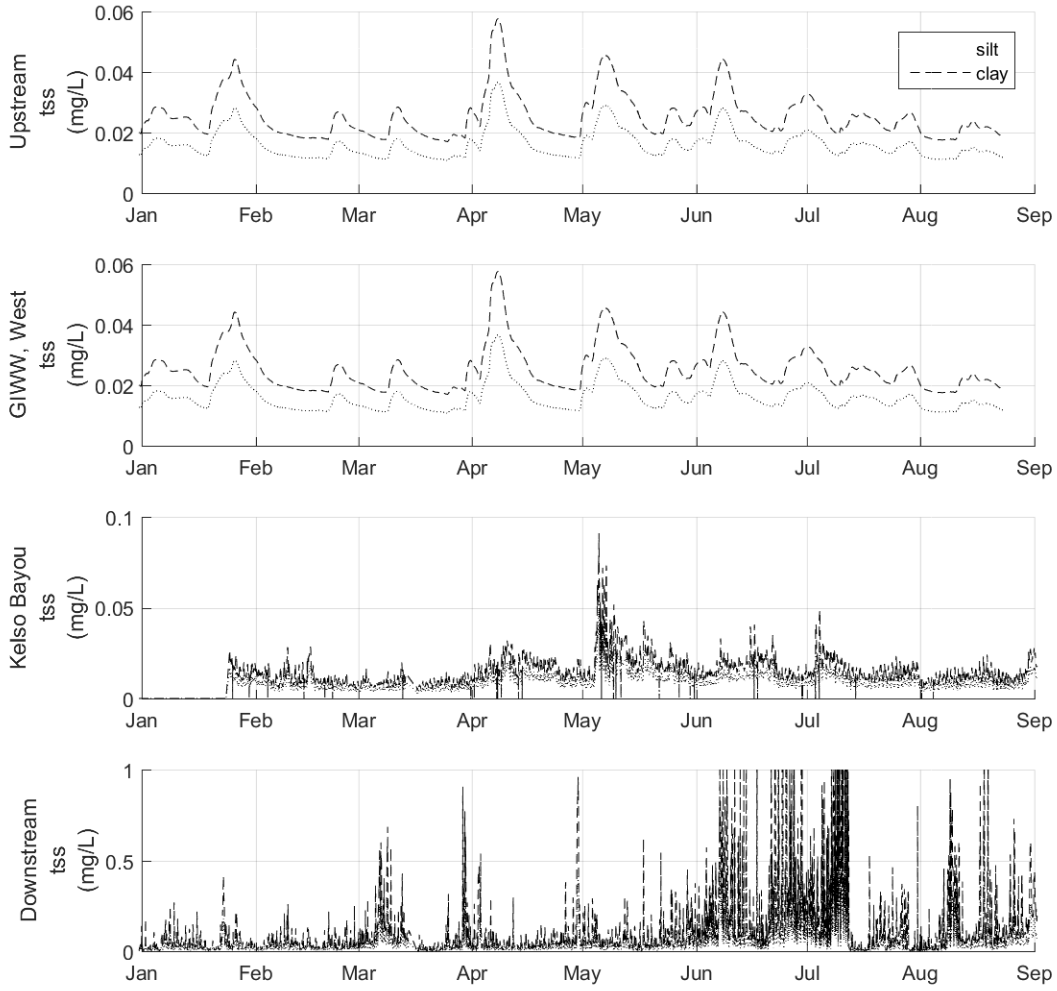

Figure 57. Suspended sediment boundary conditions.

3.2.3. Meteorological Forcing

Wind and precipitation are both included, but evapotranspiration is not considered. Wind and precipitation data are downloaded from NOAA's National Centers for Environmental Information and then interpolated to the model grid.

3.2.4. Initial Bed Composition

The model's initial bed composition was generated based on Water Institute grab samples collected in 2014, and compiled USACE grab samples from 2007 to 2014. The reach from the end of the jetties (which is the downstream boundary for the present model) to Mile 5 is composed of coarse sediment compared to the rest of the ship channel, lake, and offshore region. In our model the initial composition of this reach is a 10 m thick layer of sand; the rest of the domain begins as a 10 m thick layer that is equal parts sand, silt, and clay.

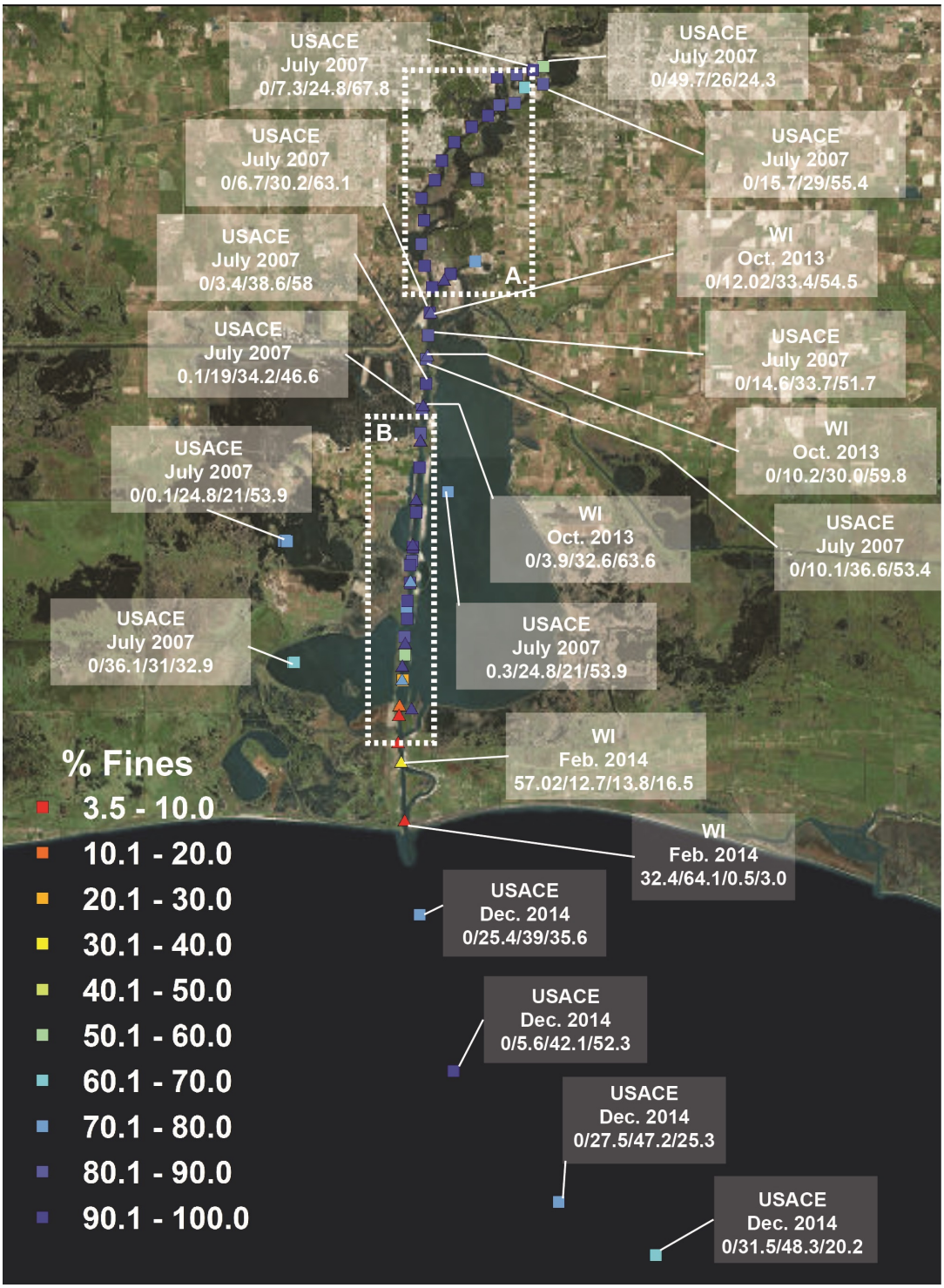

Figure 58. Grab sample sediment composition from offshore to the intersection of the Calcasieu Ship Channel with I-10. Data source and date are indicated in the boxes, as is sediment composition in the form gravel/sand/silt/clay. The gravel fraction occasionally seen in Water Institute cores is crushed oyster shells. Data from insets A and B are shown in Figures Figure 59 and Figure 60, respectively

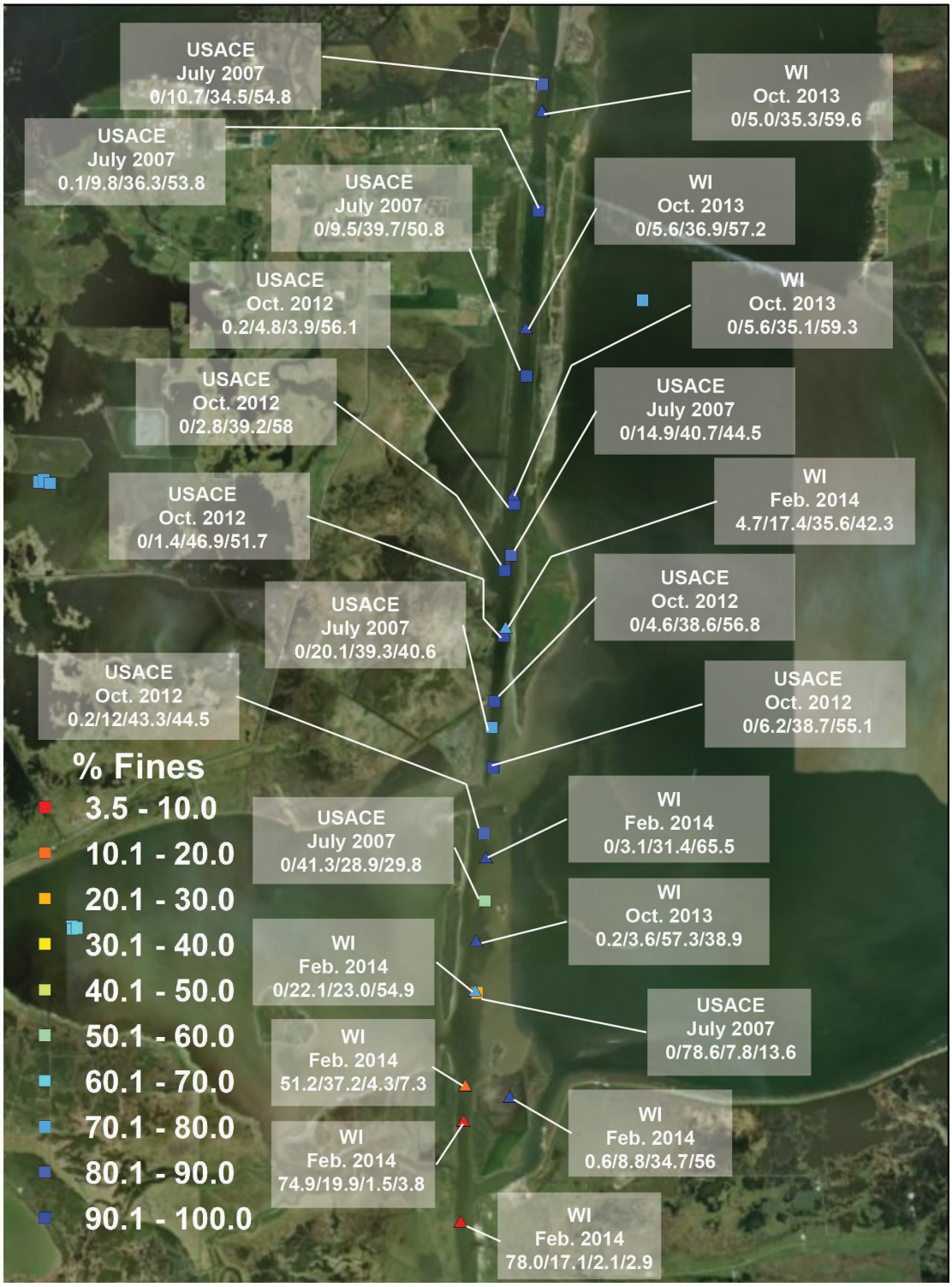

Figure 59. Grab sample composition in the middle ship channel.

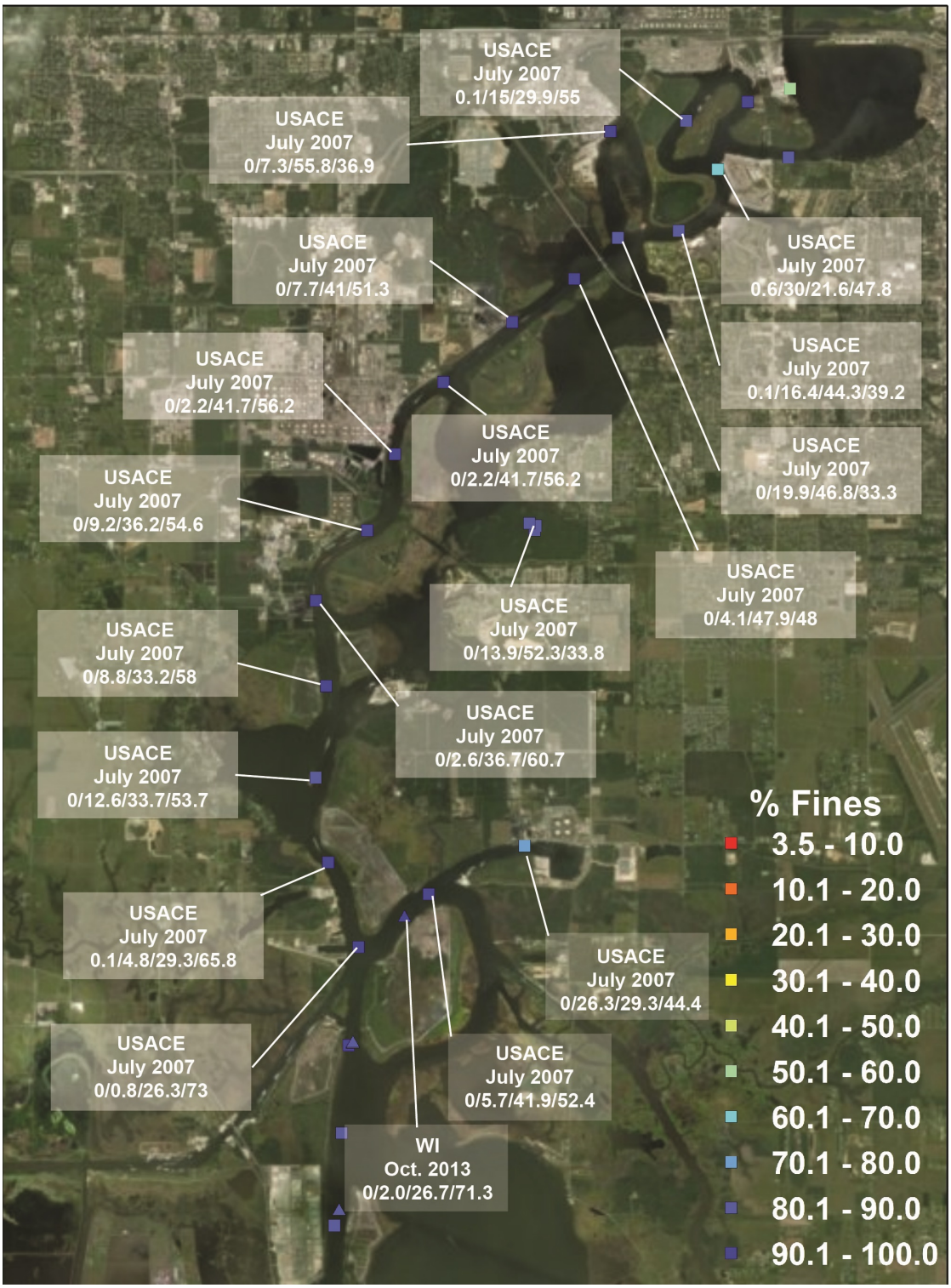

Figure 60. Grab sample composition in the upper ship channel.

3.2.5. Drivers of Modeled Sediment Transport

Delft3D allows users to model sediment erosion, deposition, and transport for cohesive and non-cohesive sediments. In this model we include two cohesive sediment classes (silt and clay) and one non-cohesive sediment class (sand). Transport of cohesive and non-cohesive sediment is equivalent for sediments that are suspended in the water column, and is calculated with the advection-diffusion equation in the same way as any other conservative constituent. The difference between cohesive and non-cohesive sediment transport lies in their interaction with the bed, however in both cases erosion and deposition are controlled by the bed shear stress that is calculated in the hydrodynamic model. We use bed shear stress in this report to indicate conditions that are conducive to sediment deposition. Further details can be found in the Delft3D user's manual (Deltares, 2014).

Cohesive sediments are modeled using the Parthinedes-Krone formulation. Erosion from the bed is allowable only when the bed shear stress exceeds a user defined threshold. We define this threshold to be 0.35 N/m^2 for both silt and clay, consistent with other locations on the Gulf Coast (Meselhe, 2016). Deposition is constant, but in the presence of erosive conditions the material that is deposited is immediately eroded. For the purposes of understanding cohesive sediment transport in this model we can say that silt and clay can both be eroded from the bed under similar conditions (bed shear > 0.35 N/m^2), but that clay has a lower fall velocity, and travels farther once in suspension.

Non-cohesive sediments (sand) can be transported either in suspension or as bedload, but the definition of the initiation of motion threshold is calculated within Delft3D rather than imposed by the user. Sand transport is also dependent on the modeled bed shear stress. Sand settles out of suspension faster than either silt or clay, and so requires persistent high bed shear conditions to be transported. We use the technique of Van Rijn (2004), as implemented in Delft3D (Deltares, 2014).

3.2.6. Model Runs

Five separate runs of the Delft3D model are used in this report to investigate the sediment dynamics in the Calcasieu Ship Channel.

The first case, CSC_108, simulates the year 2017 from January 3rd through August 22nd, ending shortly before Hurricane Harvey. This is the base case model and is used for model calibration and validation. Model calibrations to 2017 field data were performed using CSC_108. Calibrations to water level, salinity, total suspended sediment, and discharge are shown in Appendix G: Model Calibrations to 2017 Field Data. Results from CSC_108 are also used to validate model performance with respect to regional sediment budgeting by comparison to the Water Institute's analytical sediment budget in the Lower CSC reach. This comparison is shown in Section 3.3.1. CSC_108 is then used to generate sediment budgets for other regions of the CSC where field data are not available.

Models CSC_113 and CSC_114 both include some version of CPRA's proposed set of salinity control structures. Model CSC_113 includes all five of the features shown in Figure 61. These include an 8-part wall along the east side of the ship channel, and constrictions to four other points of exchange between the ship channel and the lake. Model CSC_114 includes the Lake Wall, 9 Mile Cut, and Joe's Cut, but

does not include the constrictions to East Pass or West Pass. Salinity control structure features are shown in Figure 61.

Models CSC_115 and CSC_116 simulate the sedimentary performance of the CSC under conditions of 0.5 of sea level rise and 1.0 m, respectively.

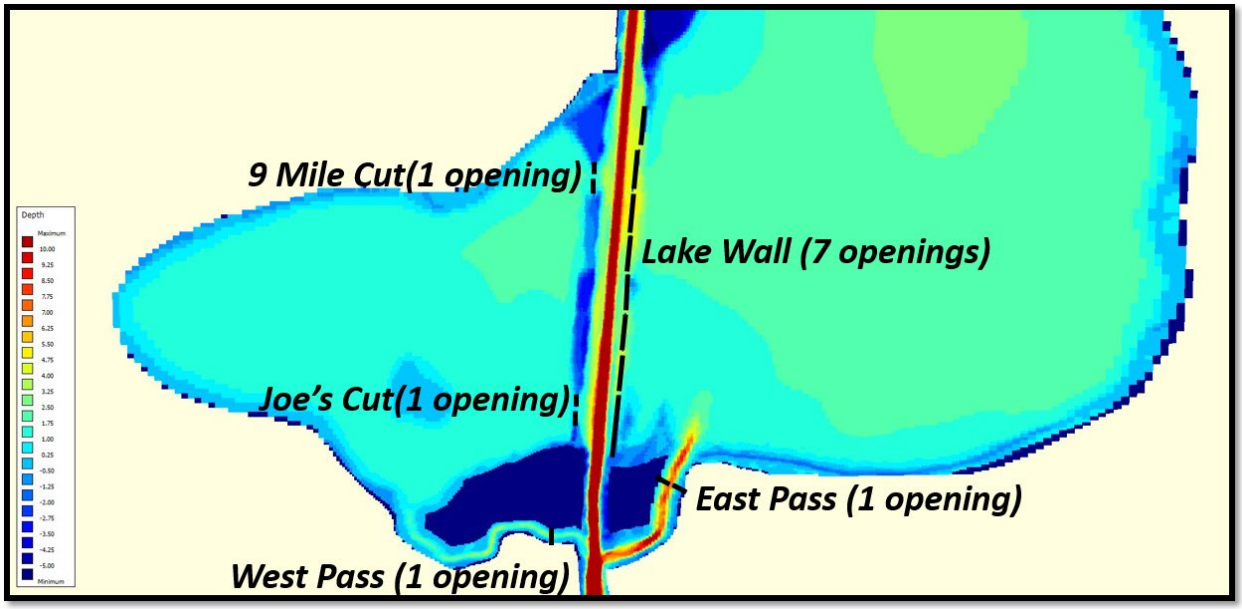

Figure 61. CPRA's proposed salinity control structures. Background contour are for depth (invert of surface elevation)

3.3. MODELED SEDIMENT DYNAMICS IN THE CALCASIEU SHIP CHANNEL

3.3.1. Modeled Sediment Budget

Using the Delft3D model it is possible to break down sedimentation by channel reach. In Table 17 we show the annualized transport into and out of four reaches of the CSC, and the net accumulation into each reach. The base case model, CSC_108, is compared to the analytical sediment budget primarily based on results from the Lower CSC. In our model the Lower CSC is the reach between Mile 2, where the Water Institute SCC station marked the downstream end of the analytical sediment budget, and Mile 5, where the ship channel enters the unconfined reach in Lake Calcasieu. In this reach the model lost a total of 23,679 tons of sediment between January 1 and August 22, 2017. The planform area of this reach is 1.5 km^2. Assuming a porosity of 30% and a sediment density of 2650 kg/m^3, this equates to an annualized erosion of 8.5 mm in the Lower CSC. We interpret this low value to indicate that the modeled morphology in the Lower CSC is stable, as it is in the real system, and that the model is robust for morphological analysis. The borders of the Lower and Lower-Mid CSC reaches are shown in Figure 62, along with the locations and names of the cross sections used in Delft3D to measure sediment transport into and out of the reaches.

As with the analytical sediment budget, the model results show that much more sediment is dredged from the ship channel than can be explained by the sediment inputs included in the model. In Section 3.3.3 we use the Delft3D model to investigate the transport capacity of the CSC along reaches that are prone to bank erosion. Here we use the Delft3D model to identify the reaches that are prone to deposition in the absence of additional bank-derived sediments. The results from model run CSC_108 show that while Lower CSC and Upper CSC are stable or slightly erosional with no bank inputs, the two reaches of the Mid-CSC (Lower-Mid and Upper-Mid) are prone to deposition even if no sediment is input from the bank. In particular, the Upper-Mid CSC, which runs from Mile 10 to Mile 22, accumulates more sediment than any other reach under base case conditions. The two largest inputs to the Upper-Mid CSC are 6-ab and East_Stage_2, indicating that the sediment that accumulates in the Upper-Mid CSC comes from upstream (see cross section locations in Figure 63). By contrast, the largest input to the Lower-Mid CSC is L5-b, indicating that sediment deposited in this location comes from downstream.

		Sediment Inputs: Modeled 2017 (CSC_108)	Sediment Inputs: Modeled Deposition with Control Structures (CSC_113)	Sediment Inputs: Modeled Deposition with Limited Control Structures (CSC_114)
Lower CSC	L2-b	1,473,319	237,703	594,286
	L5-b	-1,377,512	455,346	-297,105
	West_Flow_6	-10,192	-9,126	-10,161
	East_Flow_4	-109,220	-380,529	36,037
	NET DEPOSITION	-23,605	303,394	323,057
Lower-Mid CSC	L5-b	1,377,512	-455,346	297,105
	L8-b	-154,097	-21,430	-90,720
	West_Flow_4	-337,146	-57,550	-73,030
	West_Flow_5	16	-160,381	-173,649
	East_Flow_Lake_1	19,239	1,844	1,703
	East_Flow_Lake_2	-29,964	192,265	180,258
	East_Flow_Lake_3	-543,797	-155,242	-304,808
	NET DEPOSITION	331,763	-655,840	-163,141
Upper-Mid CSC	6-ab	631,227	650,815	651,576
	L8-b	154,096	21,437	90,720
	West_Flow_2	-48,258	-37,755	-41,812
	West_Flow_3	5,378	6,194	6,015
	East_Stage_2	451,560	414,438	450,779
	Kelso_Bayou	-34,679	-24,942	-28,720
	NET DEPOSITION	1,159,324	1,030,187	1,128,558
Mid CSC combine		1,491,087	374,347	965,417
Upper CSC	6-ab	-631,227	-650,815	-651,576
	U/S	472,444	471,339	472,354
	West_Flow_1	76,680	76,322	76,726
	East_Flow_1	-85,210	-60,072	-68,158
	NET DEPOSITION	-167,313	-163,226	-170,654
		1,300,169	514,515	1,117,820

Table 17. Modeled Sediment Budget for each model broken down by reach, in metric tons. Positive numbers represent net transport into the reach through the given cross section, and negative numbers represent transport out of the reach. The "Net Deposition" line for each reach shows the total mass of sediment delivered the given reach, with negative numbers indicating erosion.

Figure 62. Cross sections (yellow) that are used to display model results in the Lower and Lower-Mid budget regions.

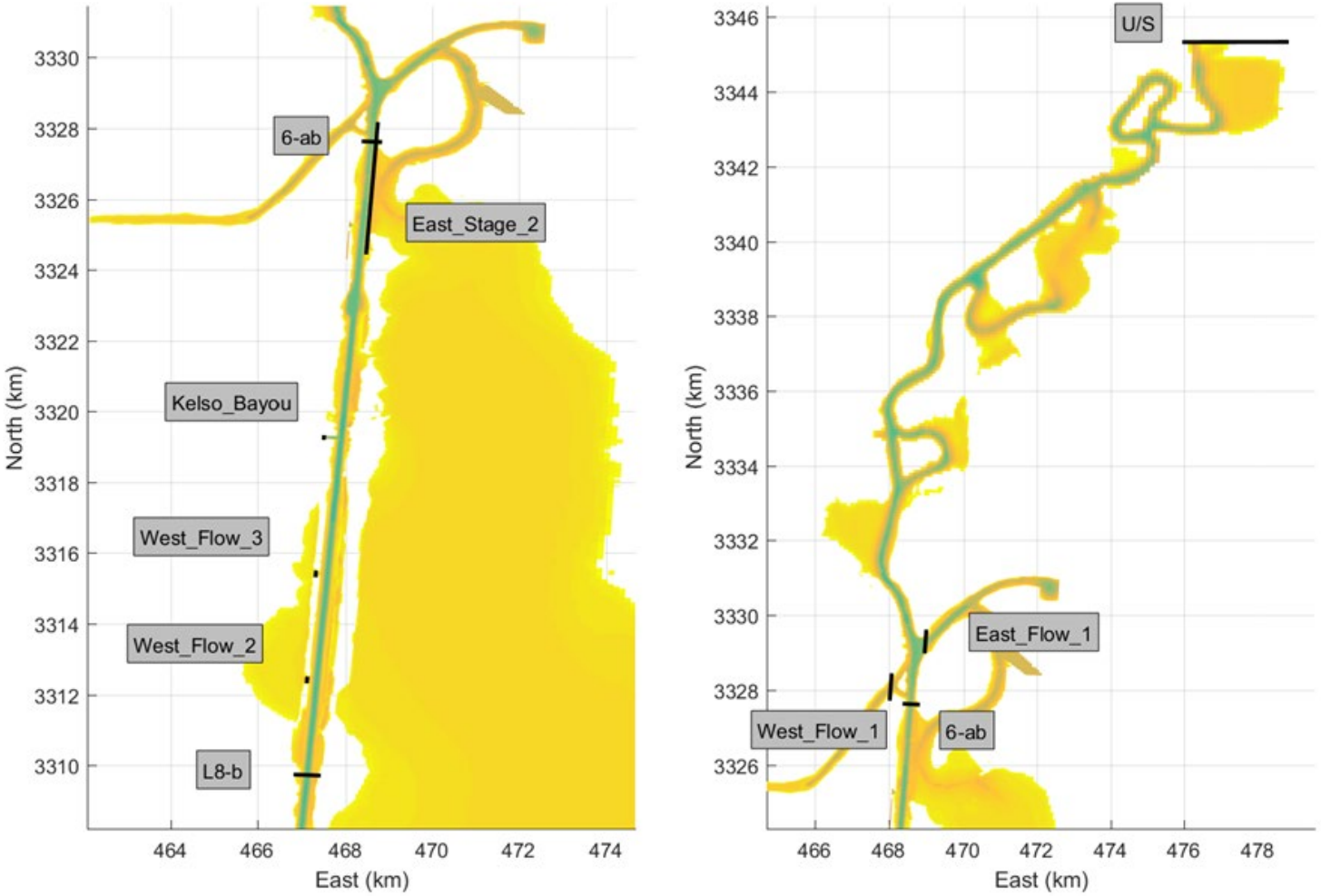

Figure 63. Cross sections that define the Upper-Mid (left) and Upper (right) budget regions.

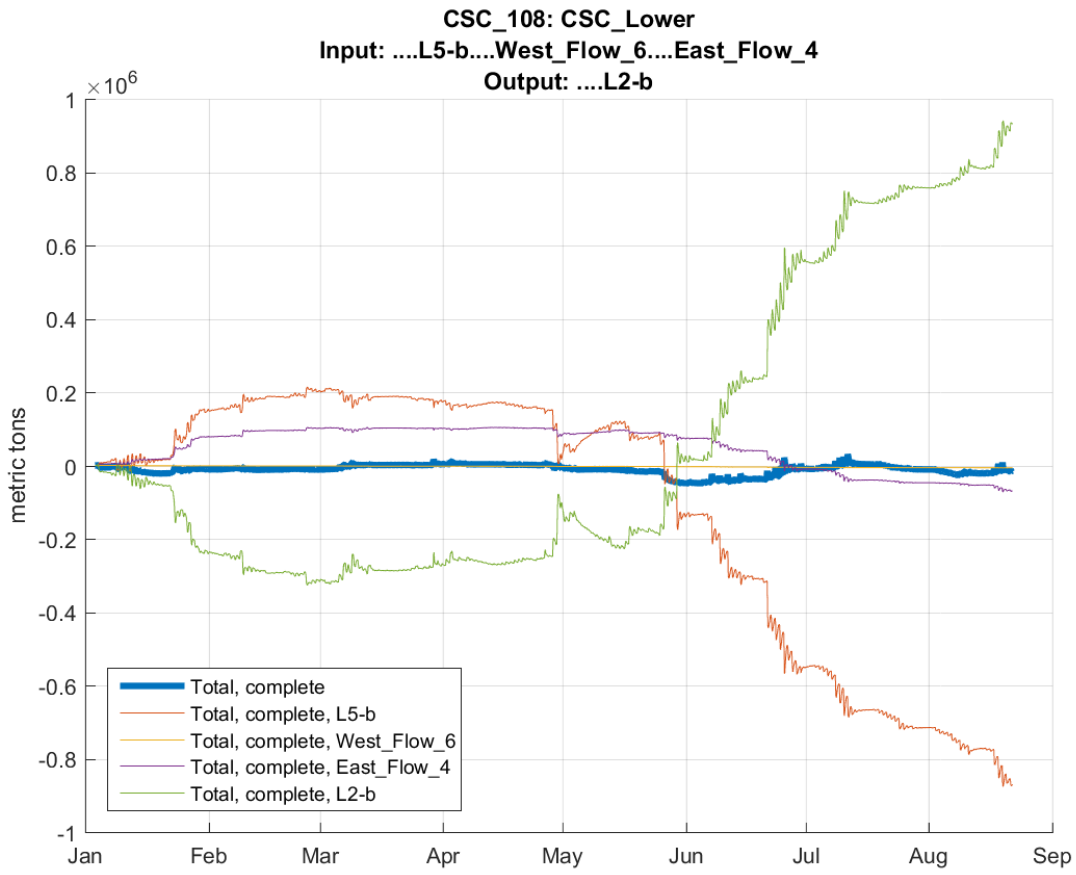

Figure 64. Time series of sediment inputs to the Lower region of the Calcasieu Ship Channel for CSC_108. The integrated sediment input to the region is shown in the bold line.

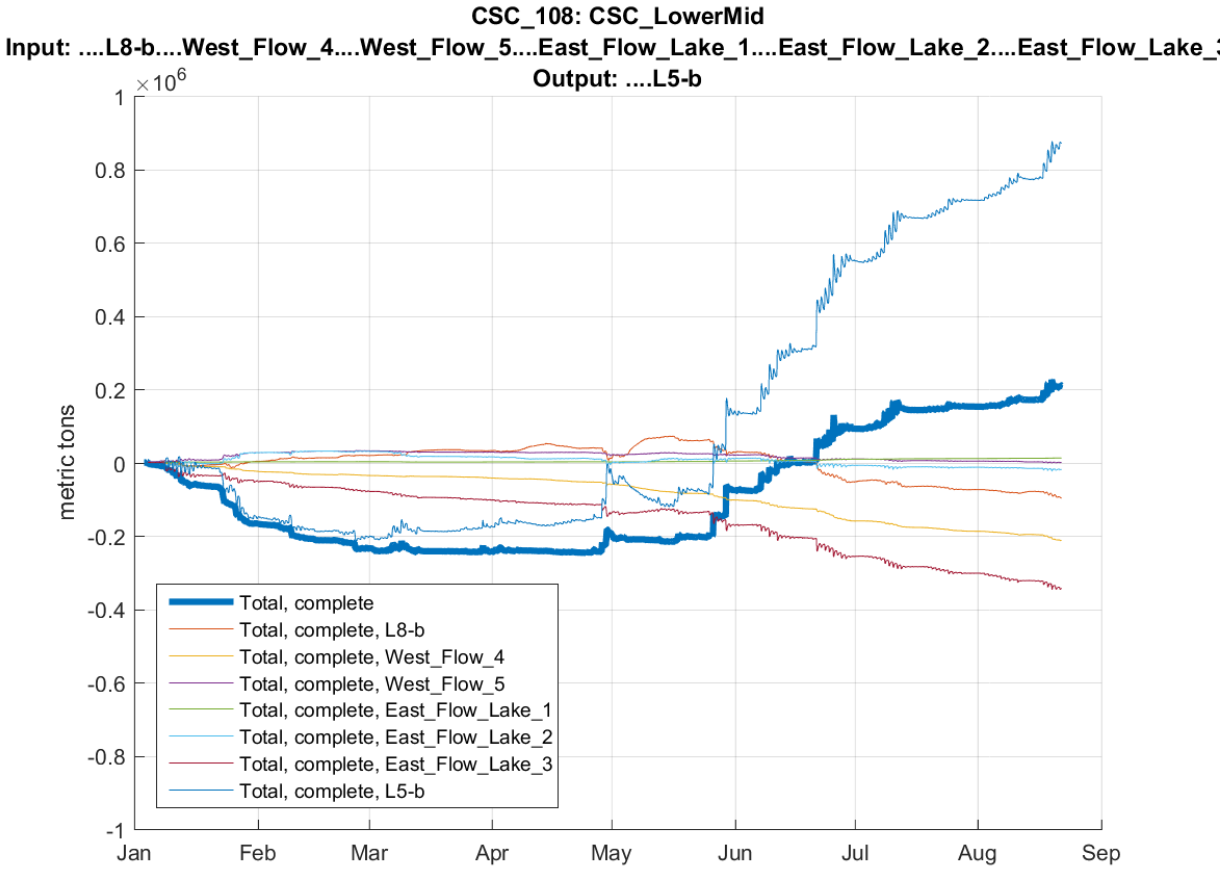

Figure 65. Time series of sediment inputs to the Lower-Mid region of the Calcasieu Ship Channel for CSC_108. The integrated sediment input to the region is shown in the bold line.

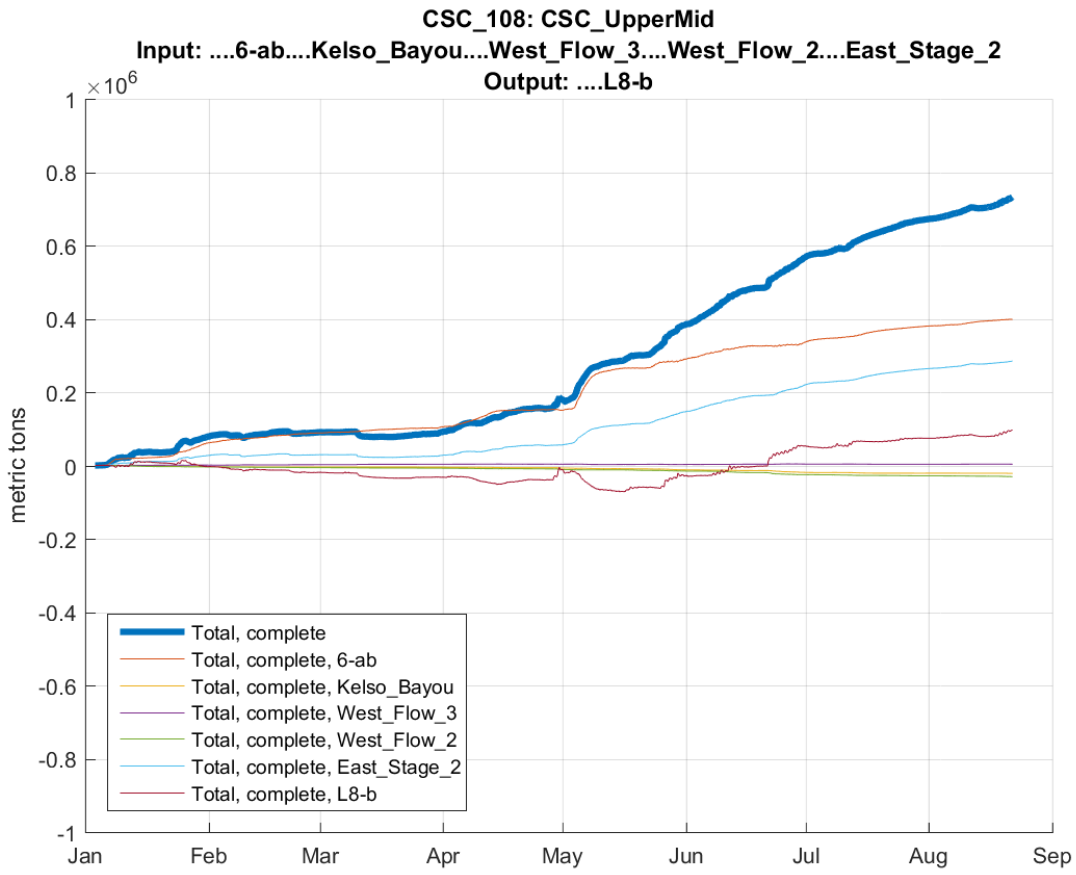

Figure 66. Time series of sediment inputs to the Upper-Middle region of the Calcasieu Ship Channel for CSC_108. The integrated sediment input to the region is shown in the bold line.

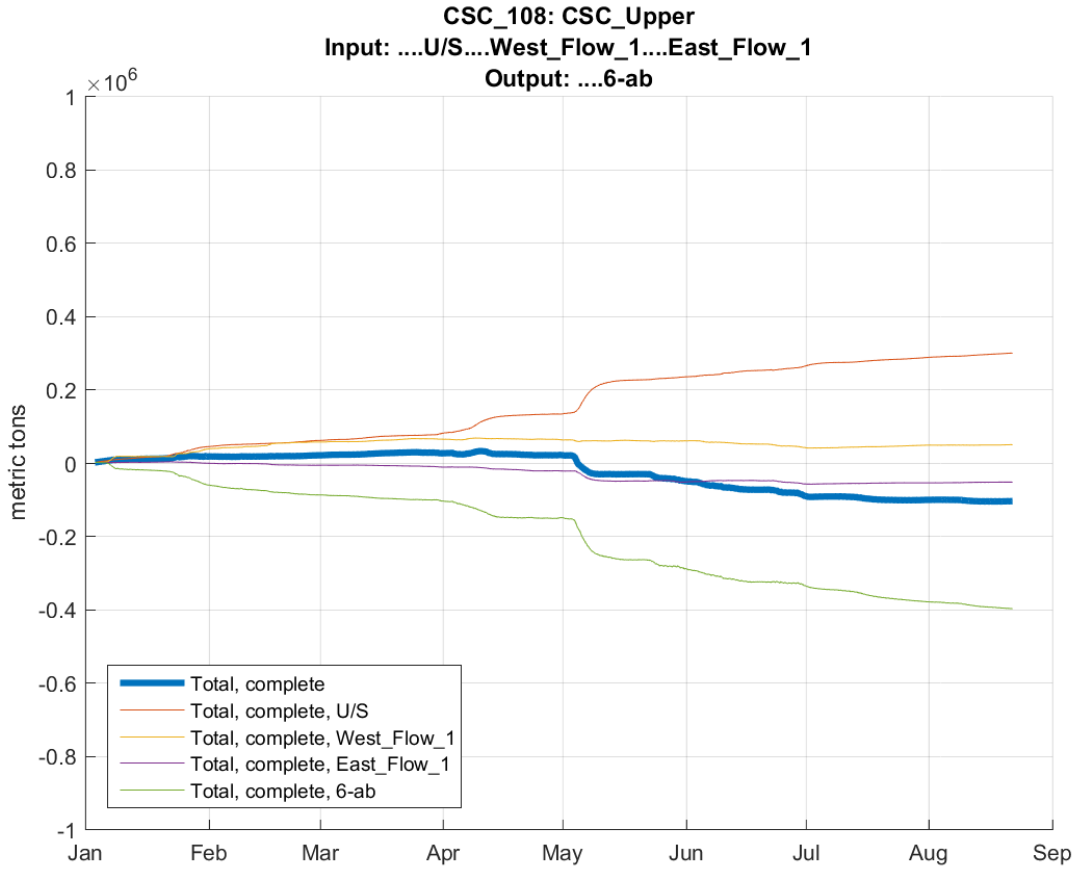

Figure 67. Time series of sediment inputs to the Upper region of the Calcasieu Ship Channel for CSC_108. The integrated sediment input to the region is shown in the bold line.

3.3.2. Flow Confinement in the CSC

The Port of Lake Charles is interested in exploring options for beneficial use of dredged material. One potential location would be along in the Lower-Mid CSC reach between Miles 5 and 10, where the ship channel is exposed to Lake Calcasieu to the East, and partially exposed to the West. This reach is also the location of a salinity control structure that is proposed by CPRA. In this section we model the proposed CPRA control structure to examine the influence that flow confinement along this reach has on the hydrodynamics and sediment budget throughout the CSC. We display results here from two models. The first, CSC_113, contains all of the control structures shown in Figure 61. The second, CSC_114, leaves out the flow constrictions on the East and West Fork channels.

Influence on Hydrodynamics

To demonstrate the influence that the proposed salinity control structure has on the sediment transport environment in the Lower and Lower-Mid CSC, we show modeled bed shear stress from June 1st to June 15th of 2017 at select locations in Figure 68. This time period includes both spring and neap tidal conditions and does not contain any significant meteorological events. These are considered typical "day-to-day" conditions for the CSC.

For all model runs velocity and shear stress are greatest at L2-b, which is in the confined section between the Gulf of Mexico and Calcasieu Lake. This reach is also notable for the coarsest bed sediments, as the fine material is often flushed away by the high velocity associated with the daily tides (see Section 3.2.4). The velocity and bed shear stress that are available to mobilize sediment drops significantly at L7-b and L8-b, which are both in the Lower-Mid CSC region, where the ship channel exchanges flow with Calcasieu Lake to the East.

A regional view of velocity and shear stress distribution in the Lower and Lower-Mid CSC shows why the restrictions in exchange between the ship channel and the lake result in the patterns seen at L2-b, L7-b, and L8-b. Figures Figure 69 and Figure 70 show the distribution of bed shear stress in order to highlight locations of flow exchange between the CSC and Calcasieu Lake from Miles 5 to 10. Exchange across the western boundary of the ship channel occurs at two discrete locations. The exchange across the eastern boundary occurs through numerous cuts and via widespread shallow overbank flow. Loss of water from the ship channel results in a reduction of bed shear stress along that reach of the ship channel, and thus a reduction in sediment transport capacity that results in deposition.

Flow confinement as a result of the salinity control structure affects the Lower CSC reach (L2-b) differently than the Lower-Mid CSC reach (L7-b and L8-b) in a way that is important to sediment transport and to dredging operations. Limiting the exchange of water between the ship channel and Calcasieu Lake through the five salinity control structures modeled here reduces the total tidal prism that is exchanged with the Gulf of Mexico. But flow is concentrated in the ship channel where it would otherwise be lost to the lake above Mile 5. In the Lower CSC reach, this manifests as a reduction in discharge volumes, and therefore station L2-b experiences lower velocity and lower bed shear stress in CSC_113 and CSC_114 than in CSC_108. But in the Lower-Mid CSC reach, limiting exchange with the lake means that more water stays in the ship channel. In this case velocity and bed stress are increased. This is particularly true near L7-b, where the channel is currently open to Calcasieu Lake, and experiences substantial lateral flow loss. The increase in flow as a result of the control structures is sufficient to expand the region of bed shear stress that is capable of mobilizing sediment to areas that are farther up the channel. Deposition is thus inhibited in the reach that is currently open to exchange with the lake. In the annualized sediment budget this results in a reduction in deposition in the Lower-Mid CSC reach.

Flow constriction is important both on a falling tide and on a rising tide. The figures below show that velocity and bed stress for both tides is increased high in to the Lower-Mid CSC. On a rising tide the effect is to prevent deposition throughout the reach. On a falling tide the effect is to flush sediments to the Lower CSC and then to the Gulf. In Section 3.3.1 we explore the impact that these patterns have on the sediment budget.

The differential response to flow confinement with respect to dredging is quantified in Section 3.3.1, and forms the basis of our recommendation that the Port of Lake Charles work with CPRA to determine a configuration for the salinity control structure that meets the needs of both organizations.

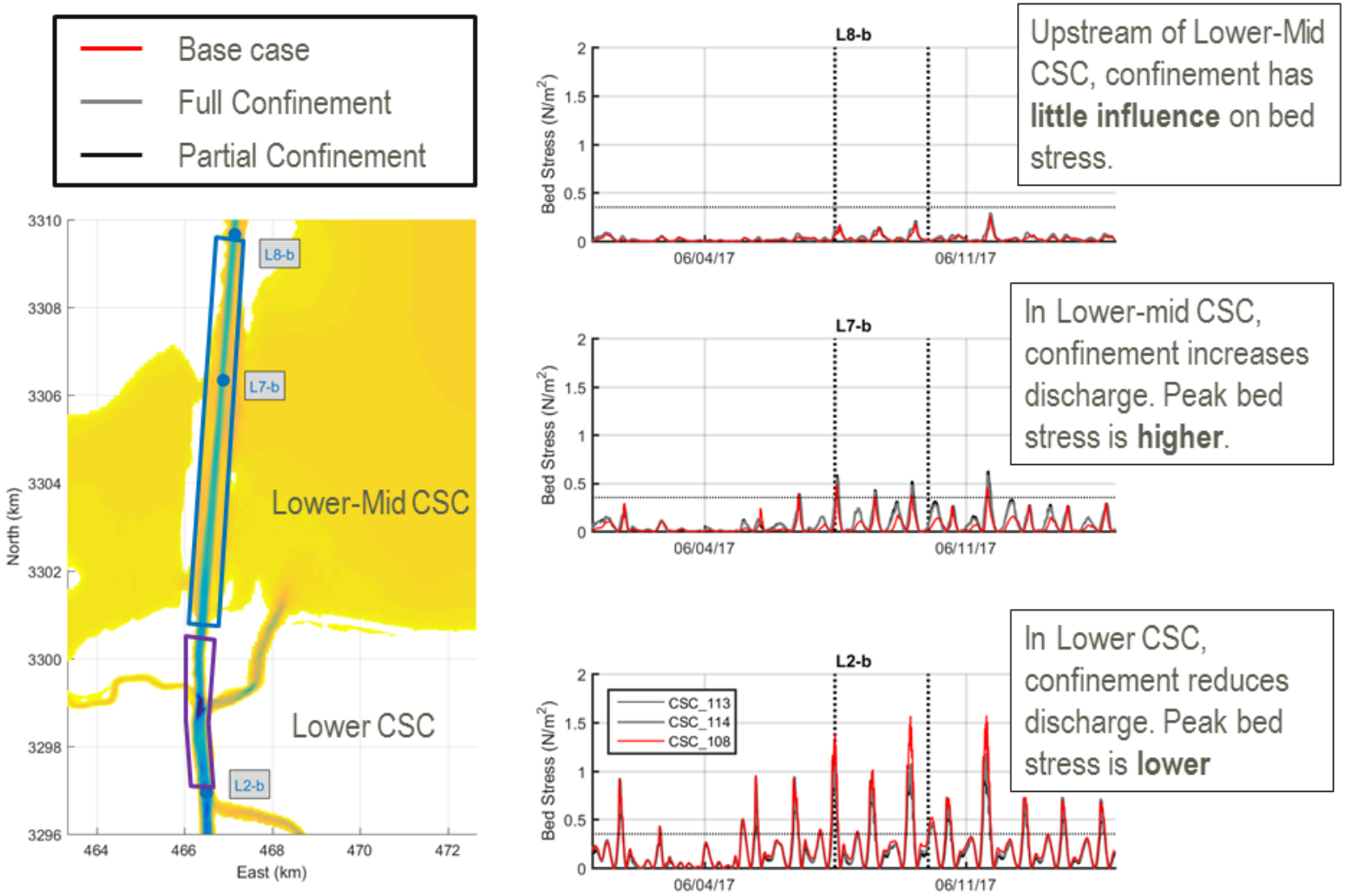

Figure 68. Modeled bed shear stress in the Lower and Lower-Mid CSC with and without flow confinement. Bed shear stress is higher in the Lower CSC for all cases. Adding the salinity control features reduces bed shear stress in the Lower CSC as a result of reduced tidal exchange, but increases it in the Lower-Mid CSC as a result of flow constriction.

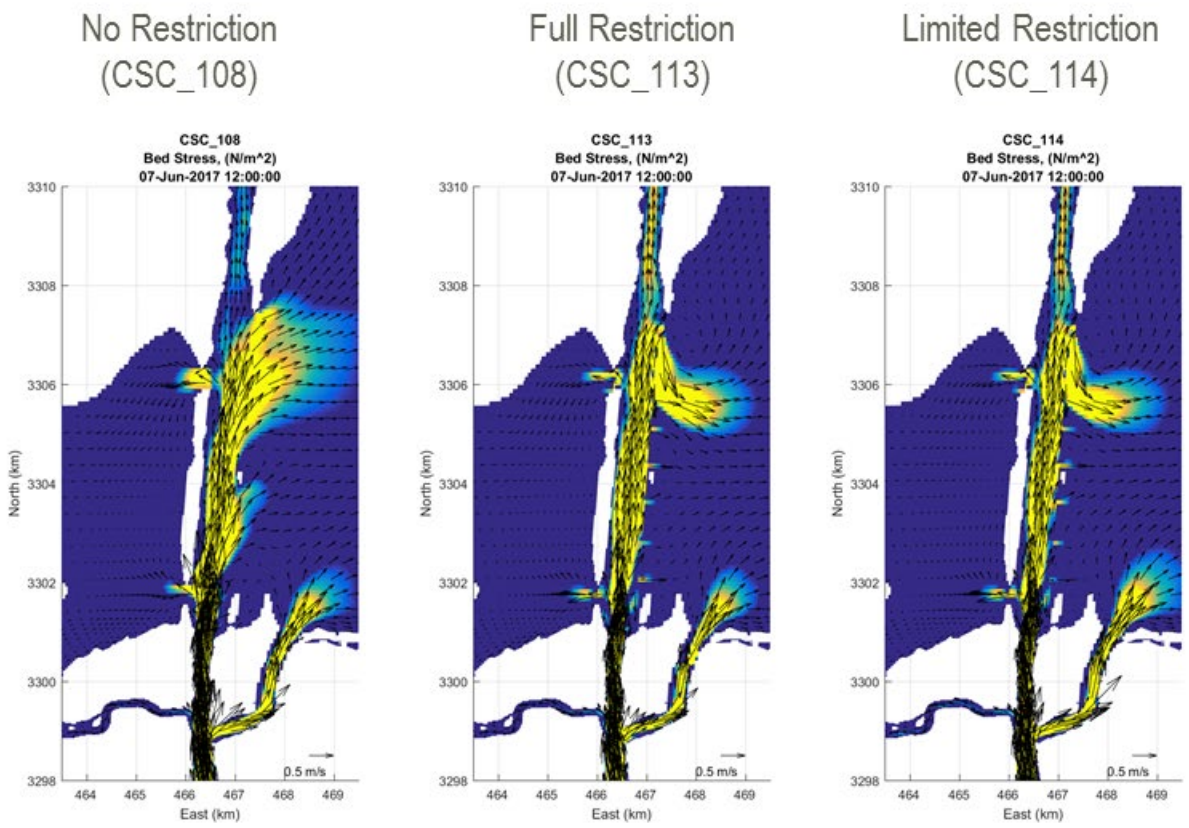

Figure 69. Velocity and bed stress in the Lower-Mid CSC during a rising tide. The time of this figure is indicated by a dotted line in Figure 68.

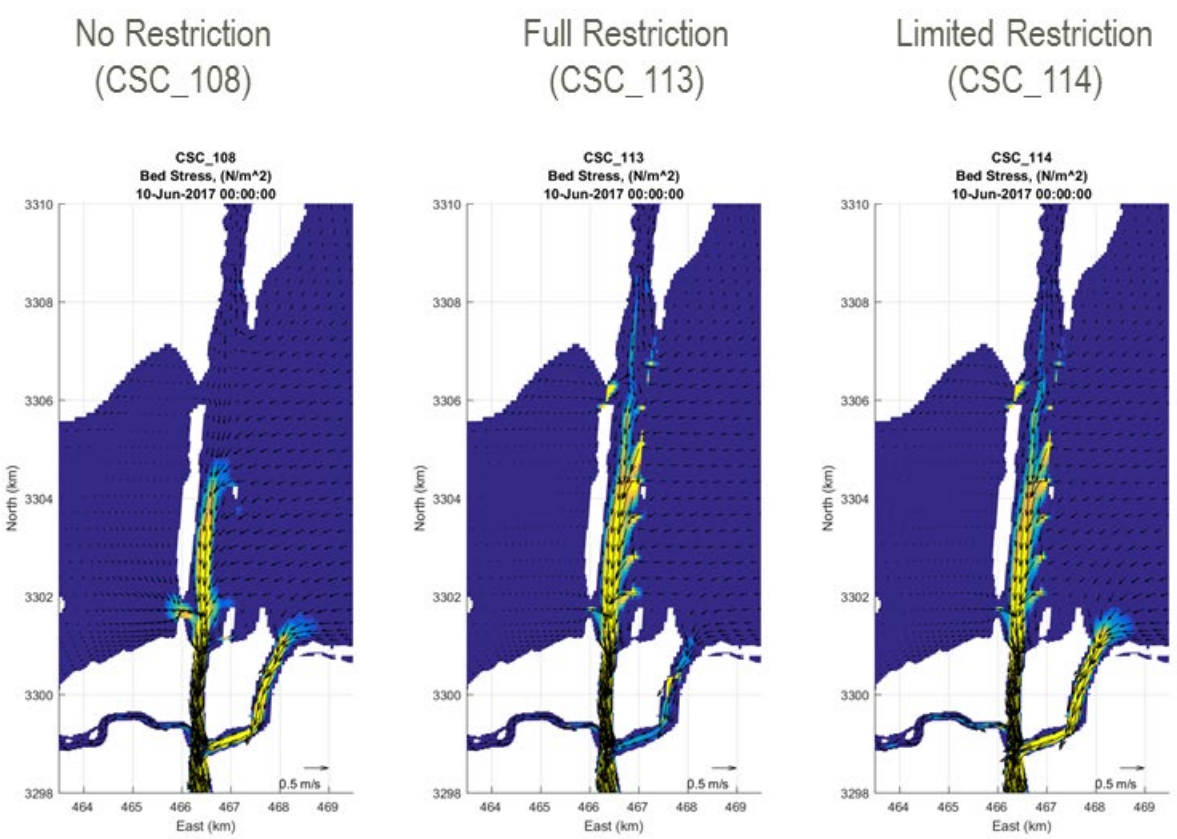

Figure 70. Velocity and bed stress in the Lower-Mid CSC during a falling tide. The time of this figure is indicated by a dotted line in Figure 68.

Influence on Sediment Budget

In the Lower CSC, adding the salinity control structures leads to an increase of nearly 330,000 tons of sediment deposited each year, changing the reach from slightly erosional (-23,605 tons) to depositional (303,394 tons). The increase reflects the reduced tidal prism, and therefore reduced velocity through this reach as a result of restricted exchanges with the lake, which results in lower bed shear stresses.

In the Lower-Mid CSC however, the flow restrictions on either side of the ship channel result in increased in-channel velocity and bed stress, and a reduction in deposition. For CSC_113, which includes the full set of five salinity control structures, the salinity control structures result in the erosion of 655,840 tons of sediment, which is a benefit of nearly 1,000,000 tons of sediment that does not need to be dredged relative to the base case. It is important to note that this benefit is only realized when East and West Passes are constricted in addition to restricting direct exchange with the lake. In CSC_114, which only includes direct restrictions with the lake, the resistance to flow in the Lower-Mid CSC reach forces water through East Fork. The result is that the Lower-Mid CSC reach does not experience the same increased flow velocity or reduction in deposition that CSC_113 experiences.

The reaches to the north of Mile 10 (Upper-Mid CSC and Upper CSC) are not significantly affected by the salinity control structures. While it might seem that an increase in transport capacity in the Lower-Mid ship channel would lead to increased transport towards, and therefore deposition in, the Upper-Mid CSC, this is not the case. To see why, it is instructive to look at the cross sections that experienced the largest change in transport between CSC_108 and CSC_113. First, L2-b, which represents the downstream boundary of the Lower-CSC, imports 84% less sediment with the full salinity control structures in place. This means that substantially less marine sediment enters the system to be distributed upstream in the first place. Further, time series plots of sediment transport at L2-b and L5-b (Figure 71) show that sediment transport is reduced on the flood tide, but relatively unchanged on the ebb, resulting in a net flushing of sediments towards the Gulf of Mexico.

The salinity control structures therefore reduce deposition above the Lower-Mid CSC by 1) reducing the total mass of marine sediments that are input to the system, and 2) changing the net direction of sediment transport in the Lower-Mid CSC from North to South.

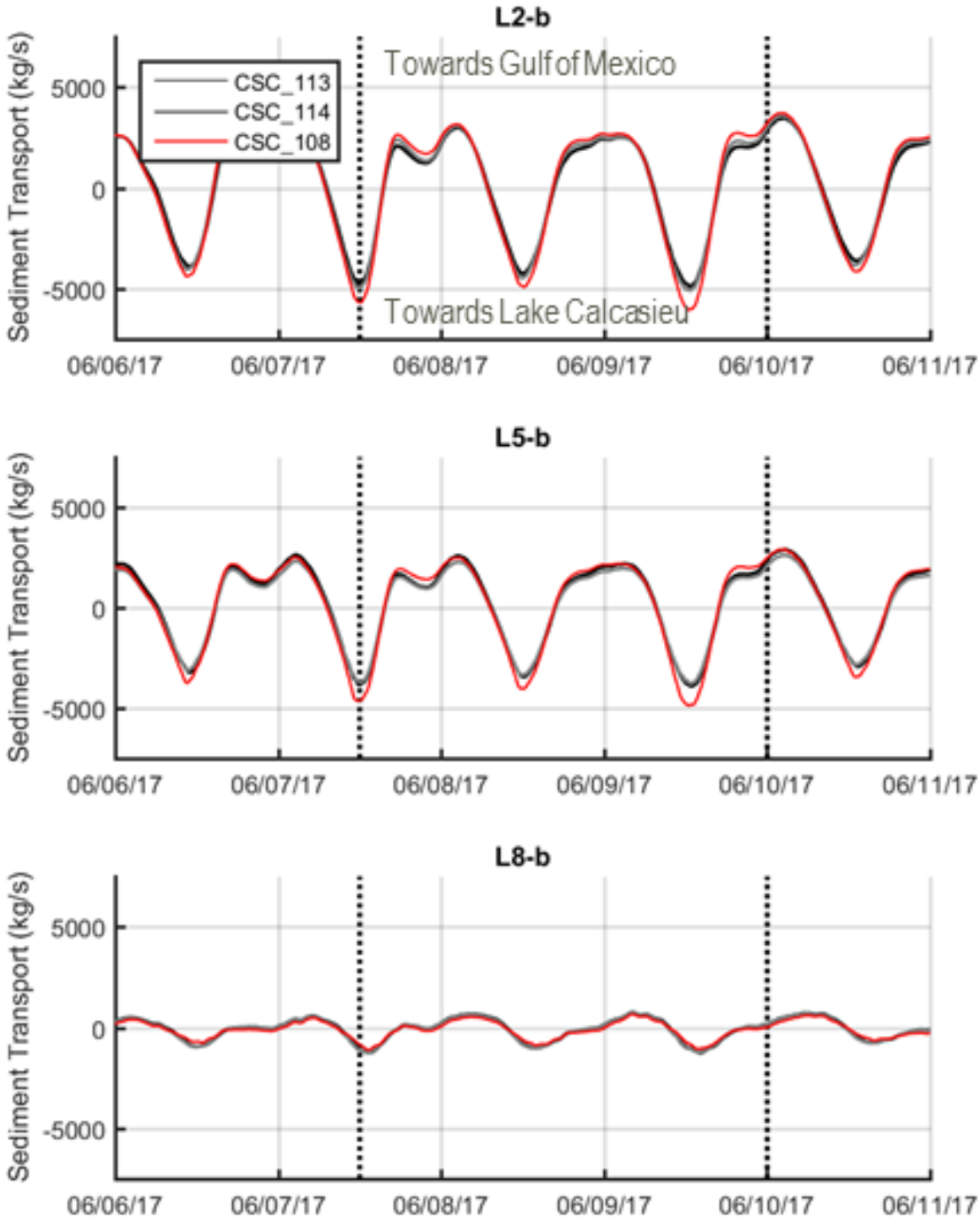

Figure 71. Sediment Transport between Lower and Lower-Mid CSC. The direction of flow is indicated in the top frame, and consistent throughout. Flood tide (towards Lake Calcasieu) is shown by positive numbers, and ebb tide (towards the Gulf of Mexico) by negative numbers.

3.3.3. Transport of Sediment Derived from Bank Erosion

In the context of historical dredge records, the modeled and analytical data collection efforts show that the mass of sediment dredged from the CSC over decadal timescales is several times greater than the mass supplied from the upstream and downstream inputs, and from exchange with Calcasieu Lake. While conclusive evidence identifying the source of the additional sediment is not yet available, some contribution is likely associated with bank erosion (of dredge material containment areas) along the channel.

To examine the likely fate of sediments that are derived from such bank erosion we conducted a model run in which we added ten sediment sources in the ship channel between Kelso Bayou and the Gulf Intracoastal Waterway. Bank erosion is documented to be common in this reach (Fischenich, 2004). The total rate of sediment added to the system by these ten sources is $3.75X10^6$ tons/yr, which is in the range of the mass of sediment that remains unaccounted for in the empirically based analytical sediment budget. The sources input sediment at a constant rate, directly into the center of the ship channel. This model run is intended to show whether sediments that are derived from bank erosion are likely to be transported long distances from their sources in the Upper-Mid and Upper CSC.

To set our expectations, we first show a timeseries of modeled bed shear stress in the Upper-Mid CSC from January to August of 2017 in Figure 72. The horizontal dashed line at 0.35 N/m^2 indicates the critical shear stress necessary to mobilize silt and clay particles from the bed. Shear stress only exceeds this value once during the first eight months of 2017, and then at only two of the three measurement locations shown along the Upper-Mid CSC. This indicates that the flow conditions in this reach are only energetic enough to move sediments that enter the channel via bank erosion.

The results of the model run with additional sediment sources (Figure 73) are consistent with the results of the bed shear stress analysis; the modeled sediment input by sources was deposited in close proximity to the source itself. This indicates that sediment that is input to the ship channel through bank erosion does not travel long distances along the channel, and usually is reworked and deposited locally.

Historical dredge records are therefore likely to be highly correlated with sources of sediment input. A region that requires frequent dredging is likely to be a region where bank erosion is common and productive. This analysis is consistent with the analysis of bank line retreat rates (Chapter 2, Section 2.4.2) showing that dredging is most frequent near unprotected bank lines.

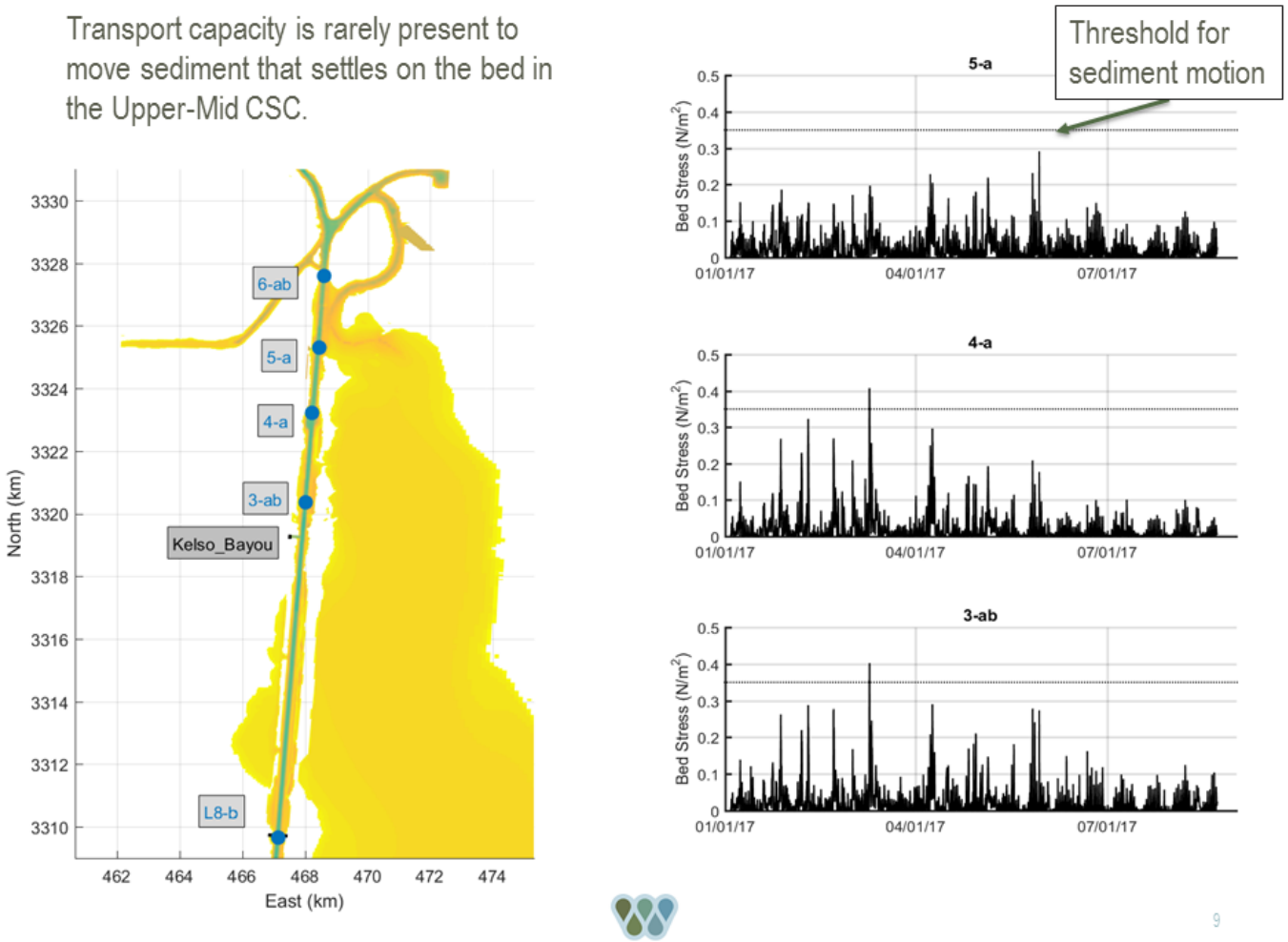

Figure 72. Bed shear stress at select locations in the Upper-Mid CSC. The horizontal dashed line at 0.35 N/m^2 indicates the critical shear stress necessary to mobilize silt and clay particles that have settled onto the bed.

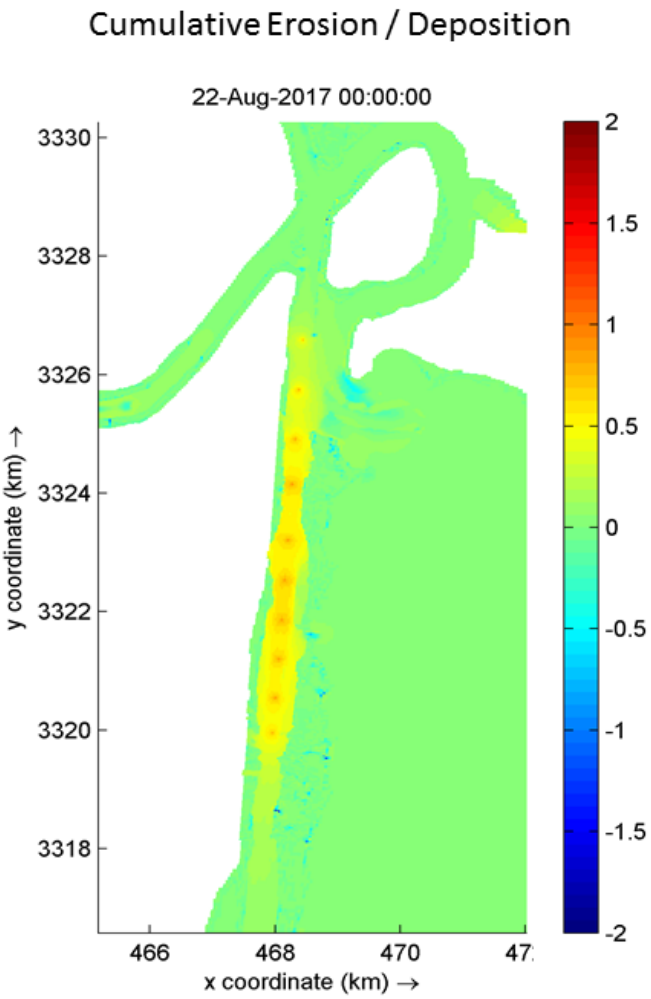

Figure 73. Sediment derived from additional sediment sources remains between the Gulf Intracoastal Waterway and Kelso Bayou.

3.3.4. Effects of Sea Level Rise

In order to test the influence of Sea Level Rise on the sediment dynamics of the CSC, the model was re-run with a 50 cm increase, and then with a 100 cm increase in the downstream boundary condition. The median current rate of Relative Sea Level Rise in the Western Chenier plain is approximately 0.88 cm/yr, so 50 and 100 cm are meant as an upper limit for the amount of sea level rise that might be experienced by the CSC over the next 50 to 100 years, respectively. The influence of relative sea level rise on the sediment budget is understandably greatest near the coast. The full sediment budgets for the two sea level rise runs are shown in Table 18.

		Sediment Inputs: Modeled 2017 (CSC_108)	Sediment Inputs: SLR 0.5 m (CSC_115)	Sediment Inputs: SLR 1 m (CSC_116)
Lower CSC	L2-b	1,473,319	2,952,110	6,667,480
	L5-b	-1,377,512	-2,388,694	-4,728,140
	West_Flow_6	-10,192	-11,014	-18,585
	East_Flow_4	-109,220	-360,250	-844,796
	NET DEPOSITION	-23,605	192,152	1,075,959
Lower-Mid CSC	L5-b	1,377,512	2,388,694	4,728,144
	L8-b	-154,097	-468,658	-1,036,916
	West_Flow_4	-337,146	-494,660	-745,931
	West_Flow_5	16	-24,777	-80,789
	East_Flow_Lake_1	19,239	56,927	124,001
	East_Flow_Lake_2	-29,964	-109,078	-205,056
	East_Flow_Lake_3	-543,797	-653,194	-1,137,933
	NET DEPOSITION	331,763	695,254	1,645,520
Upper-Mid CSC	6-ab	631,227	432,177	297,667
	L8-b	154,096	468,568	1,036,916
	West_Flow_2	-48,258	-87,947	-171,239
	West_Flow_3	5,378	7,197	-7,612
	East_Stage_2	451,560	473,829	536,144
	Kelso_Bayou	-34,679	-38,738	-71,212
	NET DEPOSITION	1,159,324	1,255,086	1,620,664
Mid CSC combine		1,491,087	1,950,340	3,266,184
Upper CSC	6-ab	-631,227	-432,177	-297,667
	U/S	472,444	449,612	436,307
	West_Flow_1	76,680	30,076	9,950
	East_Flow_1	-85,210	-150,983	-221,908
	NET DEPOSITION	-167,313	-103,472	-73,318
		1,300,169	2,039,020	4,268,825

Table 18. Influence of relative sea level rise on sediment budget. Modeled Sediment Budget for each model broken down by reach, in metric tons. Positive numbers represent net transport into the reach through the given cross section, and negative numbers represent transport out of the reach. The "Net Deposition" line for each reach shows the total mass of sediment delivered the given reach, with negative numbers indicating erosion.

3.3.5. Model Summary and Conclusions

- Flow constriction resulting from the CPRA-proposed salinity control structure reduces sedimentation in the Lower-Mid CSC (Mile 5 to Mile 10), and slightly increases sedimentation in the Lower-CSC (Mile 2 – 5). When the Lower and Lower-Mid CSC reaches are taken together the five southernmost salinity control structures result in a reduction in deposition of 660,604 tons. When the East and West Fork structures are not included the result is 148,242 tons less than the base case.

- The salinity control structure has little effect on sedimentation patterns north of the Lower-Mid CSC.

- The capacity to transport sediment that is derived from the banks is not often present north of the Lower-Mid CSC. This means that sediment that enters the channel from bank remains close to the source. Bank stabilization is therefore recommended in locations with high dredging activity.

- Sea Level Rise increases deposition throughout the CSC, but the increase is greatest in the Lower and Lower-Mid CSC reaches. A base level rise of 0.5 meters of increases deposition in the Lower and Lower-Mid CSC by 579,248 tons. A one-meter increase leads to 2,413,321 more tons of deposition in the same reach.

4.0 Chapter 4: Explore Regulatory Efficiencies

4.1. INTRODUCTION AND BACKGROUND

Under this Task, the Institute was to explore new regulatory efficiencies pursuant to White House Council of Environmental Quality and Office of Management and Budget Memorandum M-17-10 (https://obamawhitehouse.archives.gov/sites/default/files/omb/memoranda/2017/m-17-10.pdf) and the President's January 24, 2017 Executive Order "Expediting Environmental Reviews and Approvals For High Priority Infrastructure Projects" (https://www.whitehouse.gov/presidential-actions/executive-order-expediting-environmental-reviews-approvals-high-priority-infrastructure-projects/). Since this study was initiated, the Administration has promulgated several new Executive Orders and associated processes to expedite regulatory review. The most promising of these approaches are discussed below.

As noted previously, this study focused more on modifications to the system that would reduce dredging needs than the examination of preferred alternatives for the placement of dredge material. Consequently, our recommendations focus on engaging directly with the U.S. Army Corps of Engineers (USACE) and the CPRA around pursuing such modifications. The Institute, however, recognizes that future engagement with federal and state regulatory bodies will occur around the question of the placement of dredge material for potential beneficial use. The following analysis proceeds from that assumption.

As the scope of this study was coming together in late summer of 2017, the Institute was invited to Washington, D.C. to present to senior officials in the White House Council on Environmental Quality (CEQ), Office of Management and Budget, USACE and the U.S. Department of the Interior. The discussions focused around using regulatory efficiency mechanisms – some specific to the Gulf of Mexico – to speed up the process of permitting projects beneficially using dredge material and protecting critical infrastructure. While these discussions focused on other geographies in coastal Louisiana, the Institute flagged the needs around the Port of Lake Charles and was invited to future discussions (in particular, with the Port's industry stakeholders) to explore opportunities in such a critically important area. This Administration is quite interested in expediting the regulatory process to use dredge material to protect critical infrastructure while also realizing important community and ecosystem service benefits.

4.2. EXECUTIVE ACTIONS: CONSIDER UTILIZING THE NEW *ONE FEDERAL DECISION* POLICY

Several recent Executive Orders have been issued to improve the efficiency of the environmental permitting and review process. On January 24, 2017, Executive Order 13766 "Expediting Environmental Reviews and Approvals for High Priority Infrastructure Projects," was signed by President Trump. This Executive Order focuses on expediting environmental reviews and approvals for "high priority infrastructure projects" as identified by the CEQ Chairman. While promising, this Executive Order did not include much detail or specific direction on how efficiencies would be achieved.

Additional detail and clarification on what projects may be considered priorities and how their permitting timelines may be expedited can be found in Executive Order 13807 "Establishing Discipline and Accountability in the Environmental Review and Permitting Process for Infrastructure," singed by the President on August 15, 2017 (https://www.whitehouse.gov/presidential-actions/presidential-executive-order-establishing-discipline-accountability-environmental-review-permitting-process-infrastructure/. Executive Order 13807 contains provisions designed to improve the efficiency and effectiveness of

environmental permitting and review for "major infrastructure projects." A major infrastructure project is defined in the Executive Order as "an infrastructure project for which multiple authorizations by federal agencies will be required to proceed with construction, the lead federal agency has determined that it will prepare an environmental impact statement (EIS) under the National Environmental Policy Act (NEPA), 42 U.S.C. 4321 et seq., and the project sponsor has identified the reasonable availability of funds sufficient to complete the project." (Exec. Order No. 13807, 3 C.F.R. 1 (2017).)

The Executive Order also establishes that major infrastructure projects will now fall under the *One Federal Decision* policy and establishes that all project reviews and authorizations should be completed within two years, and that each individual project should have a single EIS and a single Record of Decision.

Under *One Federal Decision*, a single federal agency is identified as the lead agency for the entire regulatory process. This is an important development and has the promise to greatly improve an often-disjointed regulatory process. As the Port moves forward with discussions with the USACE, we recommend that, as appropriate, discussions begin around the USACE serving as the lead federal agency for future regulatory activities. The USACE has already served as lead agency on other projects in Louisiana, gaining experience in how to coordinate and collaborate with other federal regulatory staff in the region. In addition to serving as the agency responsible for channel maintenance and navigation, the USACE has important recent experience with shortening regulatory review timelines.

Under the *One Federal Decision* policy, as the lead federal agency, the USACE would work with other federal agencies such as the U.S. Fish and Wildlife Service (USFWS) and the National Oceanic and Atmospheric Administration (NOAA). While more analysis needs to be done to consider the range of potential alternatives, it is quite likely that the following permits/authorizations could be required:

USACE

- EIS (NEPA)
- Section 404 Permit (Clean Water Act)
- Section 408 Permit (Rivers and Harbors Act)
- Section 10 Permit (Rivers and Harbors Act)

USFWS

- Endangered Species Act Consultation (Endangered Species Act)
- Fish and Wildlife Coordination Act Review (Fish and Wildlife Coordination Act)

NOAA

- Endangered Species Act Consultation (Endangered Species Act)
- Essential Fish Habitat Consultation (Magnuson-Stevens Act)
- Marine Mammal Protection Act Authorizations (Marine Mammal Protection Act)

The *One Federal Decision* policy is designed to improve coordination across federal agencies in the permitting and review process. Ideally, all of the above agencies could coordinate their efforts to provide the permits and authorizations they are responsible for by statute in a timely manner.

On March 20, 2018, the CEQ and the Office of Management and Budget released a joint memorandum: M-18-13, "One Federal Decision Framework for the Environmental Review and Authorization Process for Major Infrastructure Projects under Executive Order 13807." (https://www.whitehouse.gov/wp-content/uploads/2018/04/M-18-13.pdf) This memorandum outlines that federal agencies involved in the environmental permitting and review of a major infrastructure project should enter into a Memorandum of Understanding to ensure implementation of the *One Federal Decision* framework, including establishing a project timeline with critical permitting and review milestones needed to issue a final Record of Decision for a project. M-18-13 includes an example MOU available here: https://ceq.doe.gov/docs/ceq-regulations-and-guidance/One_Federal_Decision_Framework_Guidance_(M-18-13)_2018-03-20.pdf

Memoranda can benefit a project sponsor by clearly outlining their role and the role of federal agencies, identifying key points of contact to improve coordination, and establishing critical dates and milestones to ensure a project stays on track to meet or exceed goals for environmental permitting and review. Examples of other relevant MOUs are available here:

http://www.mvn.usace.army.mil/Portals/56/docs/regulatory/permits/EIS/2017-09-11_MBSD_FED_MOU_fpw.pdf

http://www.mvn.usace.army.mil/Portals/56/docs/regulatory/permits/EIS/2018-01-25_MBSD_FED-STATE-MOU_fpw.pdf

The Institute recommends that the Port consider approaching the USACE to develop a Memoranda of Understanding signed by all relevant federal agencies (*e.g.*, USFWS and NOAA) with equities and responsibilities around the Port.

4.3. ADOPTION OF OTHER RELEVANT NEPA DOCUMENTS

White House CEQ NEPA regulations allow and thus encourage the adoption of existing environmental compliance documentation. One of the most costly and time-consuming errors that can be made when seeking regulatory approvals is to fail to consider "adopting" timely and previously completed environmental compliance documentation. There is great opportunity around the Gulf and, specifically in coastal Louisiana, to find time and cost savings by incorporating relevant information and analysis in recently completed NEPA documents. Some of these documents could be incorporated in whole or by citation into a draft Environmental Assessment or EIS for new work in and around the Port. In particular, building on the technical analysis completed by the Institute, there may be opportunities to incorporate elements of the "Final Programmatic Damage Assessment and Restoration Plan and Final Programmatic Environmental Impact Statement" completed by the Natural Resources Damages Assessment Trustee Council (http://www.gulfspillrestoration.noaa.gov/restoration-planning/gulf-plan). In addition, a great deal of work has been completed around the system for the Calcasieu Salinity Control Measures and, based upon the final set of alternatives to be explored, this information and analysis should be considered for citation and/or incorporation.

4.3.1. Other Regulatory Efficiency Opportunities

- **USACE Nationwide Permit on Living Shorelines**
    - As noted throughout this section, the best regulatory efficiency strategy is contingent upon the ultimate set of alternatives examined. With that important caveat in mind, we believe that there may be an opportunity to take advantage of a recently completed USACE Nationwide Permit. In 2017 the USACE finalized Nationwide Permit 54, which addresses and covers opportunities around living shorelines (https://usace.contentdm.oclc.org/utils/getfile/collection/p16021coll7/id/6765). More work would need to be done to determine the utility of this Nationwide Permit, but should it be found that it applies, important cost and time saving could be realized.
- **Utilizing Categorical Exclusions via Partnership with the RESTORE Council**
    - Federal agencies that are members of the Gulf Coast Ecosystem Restoration Council (RESTORE Council) can utilize certain Categorical Exclusions to advance specific projects. The RESTORE Council was the first federal agency in the nation to advance the practice of using the Categorical Exclusion of a federal agency for use in a partner's project (https://restorethegulf.gov/council-selected-restoration-component/environmental-compliance). RESTORE funds are being using in the Calcasieu system and there may be an opportunity to explore partnerships that generate additional cost and time efficiencies.
- **Post-*Deepwater Horizon* Gulf of Mexico Regulatory Efficiency Workgroup**

In 2016, the previous Administration issued Memorandum M-17-01, "Federal Coordination, Permitting and Review of Gulf Coast Ecosystem Projects." (https://www.whitehouse.gov/sites/whitehouse.gov/files/omb/memoranda/2017/m-17-01.pdf). This Memorandum was cited in a recent letter from the Acting Chair of the White House CEQ to the Louisiana Governor and sets forth a helpful precedent of establishing a locally-based interagency review team that is to improve coordination and communication across federal agencies to expedite environmental permitting and review. While the *One Federal Decision* method may moot the need to pursue this avenue, the interagency regulatory team established by the Memorandum continues to meet and it would be worthwhile to request that the Port's proposed future activities receive the attention of this group.

4.3.2. A Regulatory Path Forward

Ultimately, whatever set of alternatives are explored and ultimately decided upon, a proactive engagement strategy with the relevant federal and state agencies would help the Port to benefit from the new Executive Orders and other recent policy initiatives noted above. The analysis completed by the Institute in this study will enhance the Port's ability to engage with these agencies and structure a productive conversation around efficiently moving forward with the regulatory process.

The *Deepwater Horizon* settlement has provided a large influx of funding for restoration and protection projects, many of which require federal permits and authorizations. This has led to an increase in permit applications submitted to federal agencies, while the number of regulatory staff available to process these applications has stayed roughly the same. With increased workloads and pressure to prioritize many new projects, it is easy for important projects to fall to the bottom of the pile. To ensure that the important work around the Port receives the attention that it deserves, we recommend and could assist the Port with engaging the following:

- While House CEQ
- White House Office of Management and Budget
- US Army Corps of Engineers Headquarters
- Federal Permitting Improvement Steering Council
- USACE New Orleans District
- Coastal Protection and Restoration Authority
- Governor's Office of Coastal Activities
- RESTORE Council

Given the growing economic importance of the Port and the stated priorities of the Trump Administration, there are opportunities to use new regulatory efficiency tools. The State of Louisiana and CPRA leadership have a strong desire to move forward with implementation of restoration and protection projects contained in the Coastal Master Plan. In complex systems, the regulatory process is often the most time-consuming piece. By generating regulatory efficiencies, the process of modifying existing plans is reduced and thus more viable. There are important future opportunities to explore with relevant officials in Washington, D.C. and Baton Rouge.

5.0 Chapter 5: Overall Report Summary and Recommendations

To adequately maintain channel dimensions for navigation traffic in the CSC, the US Army Corps of Engineers implements a rigorous dredging plan. However, the possibility of constructing channel salinity control structures, as proposed by LA CPRA, could alter the current dredging needs and strategy. An effective dredging plan is needed to address these changes. This requires an understanding of the sediment dynamics and characteristics along the CSC and surrounding areas as well as an investigation of a path forward for dredge material placement. To this end, the Institute conducted a study to quantify the sources of sediment to the channel and the physical processes that induce deposition that requires dredging in specific locations.

The study was divided into five technical tasks designed to accomplish these objectives.

- *Task 1: Data Collection in the CSC and Calcasieu Lake*
- *Task 2: Model Refinements and Validation*
- *Task 3: Detailed Sediment Dynamic Analysis*
- *Task 4: Results Synthesis and Draft Reporting*
- *Task 5: Explore Regulatory Efficiencies*

5.1. TASKS 1 AND 2: DATA COLLECTION AND NUMERICAL MODELING

The observational data collection and the numerical model improvement tasks were critical to achieving the other analytical-modeling objectives of the present project. The data collection period (December 2016 to January 2018) was used to validate (test the accuracy of) the model by comparison with the real-world conditions. In addition, the multibeam bathymetric survey was used to update the model grid to the most recent bathymetry. The observational data were used to calibrate and validate the Delft3D model and demonstrate that it performs well for predictive simulations.

The first application of the Delft3D sediment model was to assess the impact to dredging of the proposed CPRA salinity control measures. Model results indicate that the structures would result in flow constriction that reduces sedimentation in the Lower-Mid CSC section (Mile 5 to Mile 10), and slightly increases sedimentation in the Lower-CSC (Mile 2 – 5). If these two segments are combined, the CPRA project will result in a reduction in deposition of 660,604 metric tons. If the East and West Fork proposed structures (part of the CPRA proposed project) are not included, the reduction in deposition is diminished by 148,242 metric tons compared to the full project implementation. The model also indicated that the CPRA-proposed salinity control measures have little effect on sedimentation patterns north of the Lower-Mid CSC (north of Mile 10).

Further model studies were conducted to examine the mobility of sediment that potentially enters the CSC from bank erosion. Based on the model results that include point source sediment inputs to represent hypothesized bank erosion, the sediment transport capacity north of Mile 10 is rarely sufficient to remobilize sediment that is derived from the banks. Sediment that enters the channel from the banks in this reach is unlikely to be moved to a different location. High dredging needs are therefore good spatial indicators of increased local sediment sources, possibly from eroding channel banks. We recommend that banks are inspected and stabilized when necessary in locations with high dredging activities.

The model was then used to examine the impact of plausible sea level rise (SLR) rates on the sediment dynamics within the Calcasieu Ship Channel. Two scenarios were used to examine the impact of SLR; an increase in the Gulf water level by 50 and 100 cm. The increase in sea level resulted in an increase in sediment net deposition especially in the Channel segments nearest to the Gulf. The model indicates that the additional deposition induced by SLR might negate the increase in draft depth created by the increase in sea level.

The ship wake field experimental results confirmed that sediment resuspension was caused by vessel passage in the CSC. These occurrences and the resulting magnitude of the increase in turbidity was linked to vessel size, speed, and displacement (smaller vessels did not show a significant effect). Resuspended sediment was sourced from the submerged margin (shelf) areas of the CSC, but may have also been sourced from the adjacent shoreline (e.g., wave impact): The latter is likely linked to shoreline type (e.g., armored versus unarmored). The wake effect was complex, and resuspension was as much or more due to a surge-drawdown effect associated with a ship's passage as it was from the wake wave translation.

5.2. TASK 3: DETAILED SEDIMENT DYNAMIC ANALYSIS

Using the data collected in the boat-based field campaigns, the Delft3D model that those data informed, and data mined from other sources, an effort was undertaken to identify sediment sources and sinks of sediment in the Calcasieu Basin. This involved exploring potential solutions to increase the efficiency of the CSC in order to minimize the dredging needs, evaluate the impact of relative sea level rise on the frequency and pattern of dredging, and, if needed, to evaluate alternatives of deepening and/or widening the CSC.

The analytical effort focused, first, on developing a sediment source budget. The results of this quantification show that over the monitoring period of December 20, 2016 through January 14, 2018, three measured sources combined contributed 384,800 metric tons of sediment to the basin and CSC. These were the Calcasieu River (94.3%), Kelso Bayou (2.2%), and the water control structures along the southeast rim of Calcasieu Lake (3.4%). Over the same time period, our measurements show that sediment was exported to the Gulf of Mexico (251,000 metric tons) equivalent to about 65% of the new sediment input from these sources (and potentially other, unmeasured sources). However, two tropical systems in 2017 had a dramatic impact on the annual sediment budget of the system. Tropical Storm Harvey was an extreme rainfall event, and the escape to the Gulf of that excess water overcame the storm surge effect (which tends to import sediment from the Gulf). Harvey resulted in a next export of 758,000 metric tons of sediment to the Gulf during the period of August 28, 2017 through September 8, 2017. Tropical Storm Cindy was a low rainfall, higher storm surge and wind event that brought 208,000 metric tons of sediment into the CSC from the Gulf in the period of June 21 to June 23, 2017. If the effect of these two storms is subtracted from the one-year monitoring record, this would indicate that the Gulf in 2017 would have been a net importer of sediment to the CSC – an estimated 299,000 metric tons. Harvey (but not Cindy) was also a major contributor to the new sediment input from the Calcasieu River and Kelso Bayou, where it represented 11% and 27% of the annual input, respectively, in 2017. Hence, without tropical storms, we conclude that the Calcasieu River and Gulf of Mexico were the dominant, and approximately equal in magnitude, new sediment sources to the CSC and Calcasieu Lake in 2017.

A compilation of dredging records was utilized to derive an average annual volume of sediment dredged from the CSC for the period 1994 to 2014 (4.3 million cubic yards) to serve as a proxy for sedimentation rate. To allow comparison with the sediment source magnitudes expressed as a mass (e.g., metric tons), requires an understanding of the porosity of the dredged material. In the absence of direct measurements of the CSC dredged material, literature values were employed and produced a "volume to mass" conversion – 1.85 million tons. Hence, we conclude that the estimated annual mass of new sediment inputs in 2017 from the Calcasieu River (including Kelso Bayou and the southeast bayous) is only 18% (including storms) to 21% (excluding storms) of the annual average mass of sediment dredged from the CSC.

A number of factors could combine to produce the calculated difference between source and sink mass. The first is an additional sediment source that has been recognized in previous CSC studies – the erosional retreat and sediment input from the dredge material containment areas that line the greater portion of the CSC. We conducted an additional analysis of the magnitude of this spoil retreat using a GIS methodology. Again, the volume to mass conversion and shoreline retreat volume estimate is hampered by an absence of direct measurements of sediment parameters (e.g., porosity, bulk density, and erodible depth). Porosity ranges derived from literature result in a calculated mass input of 0.17 to 0.49 million metric tons per year. Thus, the spoil bank retreat may account for an estimated 9% to 27% of the sediment deposited in the CSC.

The results from the analytical sediment budget and the shoreline retreat imagery analysis suggest that approximately 52% to 73% of the sediment that is dredged from the CSC remains unaccounted for. This mass of sediment might enter the CSC via the GIWW, which is not well measured by our observational data, or via salt wedge propagation from the fluid mud stream that exists in the Gulf of Mexico. Additional data collection and modeling efforts could be targeted to improve our understanding of sediment inputs and circulation near the very complex GIWW / Devil's Elbow / CSC intersection. Further, a targeted study of 3D flow structure and flocculation dynamics at the marine end of the CSC system could be used determine whether fluid mud input from the Gulf is adding to dredging costs. Another potential source of sediment introduced into the channel could possibly be related to lateral "creep" of the substrate material into the CSC excavation, a process that would be exacerbated by loading and pressure gradients induced by passing vessels. Existing geotechnical and geological data could be analyzed to determine potential for high water-content strata prone to lateral displacement into unconfined excavations.

5.3. TASK 4: RESULTS SYNTHESIS AND DRAFT REPORTING

The results of the data collection and modeling reported on herein provide input for decision makers on strategic solutions relating to (1) placement and storage of dredge material, (2) optimizing dredging volumes and locations, (3) minimizing vessel traffic impact on sediment infilling of the dredged channel, and (4) possible alterations to the geometry of the CSC to improve any of the aforementioned issues. The present report and the associated Executive Summary are the primary outputs of this task.

5.4. TASK 5: EXPLORE REGULATORY EFFICIENCIES

The objective of this task was to explore new regulatory efficiencies pursuant to recent Executive Orders and White House Council on Environmental Quality (CEQ) and Office of Management and Budget

(OMB) guidance. As this study focused more on modifications to the system that would reduce dredging needs than the examination of preferred alternatives for the placement of dredge material, our recommendations focus on engaging directly with the U.S. Army Corps of Engineers (USACE) and CPRA around pursuing such modifications. The Institute, however, recognizes that future engagement with federal and state regulatory bodies will occur around the question of the placement of dredge material for potential beneficial use and our analysis proceeds from that assumption.

As the scope of this study was coming together in late summer of 2017, the Institute was invited to Washington, D.C. to present to senior officials in the White House CEQ, OMB, USACE and the U.S. Department of the Interior (DOI). The discussions focused around using regulatory efficiency mechanisms to speed up the process of permitting projects beneficially using dredge material and protecting critical infrastructure. While these discussions focused on other geographies in coastal Louisiana, the Institute flagged the needs around the Port of Lake Charles and was invited to future discussions (in particular, with the Port's industry stakeholders) to explore opportunities in such a critically important area.

In the report, we suggest that future work in and around the Port could be deemed "major infrastructure projects" that will now fall under the new *One Federal Decision* policy that established that all project reviews and authorizations should be completed within two years, and that each individual project should have a single Environmental Impact Statement (EIS) and a single Record of Decision. Under *One Federal Decision*, a single federal agency is identified as the lead agency for the entire regulatory process. This is an important development and has the promise to greatly improve an often-disjointed regulatory process. As the Port moves forward with discussions with the USACE, we recommend that, as appropriate, discussions begin around the USACE serving as the lead federal agency for future regulatory activities. In the report, we recommend that the Port consider approaching the USACE to develop a Memoranda of Understanding signed by all relevant federal agencies (*e.g.*, USFWS and NOAA) with equities and responsibilities around the Port.

In addition, we recommend that the Port explore several other mechanisms to explore future regulatory reviews and approvals including: (a) adoption of relevant NEPA documents created for other relevant projects; (b) USACE Nationwide Permits; (c) utilization of Categorical Exclusions via partnership with the RESTORE Council; and (d) the post-*Deepwater Horizon* Gulf of Mexico Regulatory Efficiency Workgroup.

Given the growing economic importance of the Port and the stated priorities of the Trump Administration, there are opportunities to use new regulatory efficiency tools. The State of Louisiana and CPRA leadership have a strong desire to move forward with implementation of restoration and protection projects contained in the Coastal Master Plan. In complex systems, the regulatory process is often the most time-consuming piece. By generating regulatory efficiencies, the process of modifying existing plans is reduced and thus more viable. There are important future opportunities to explore with relevant officials in Washington, D.C. and Baton Rouge.

5.5. PROPOSED NEXT STEPS

The study conducted by the Institute was designed to assist in developing solutions to the challenges currently facing the Port of Lake Charles and its stakeholders. Accordingly, the following next steps are suggested for consideration. We suggest that the steps follow the order set out below – engage with the state and federal government first and then convene the port's stakeholders based on the results of the governmental discussions.

1. **Convene the USACE and CPRA to discuss the Institute study and the potential actions that one or both agencies could take to minimize future CSC dredging needs.** We believe that both agencies will be interested in the results and more open to potential action than in the past. Given the fact that CPRA has been conducting public meetings regarding the Salinity Control Measures, engaging with CPRA – potentially with the support of local and industry stakeholders – could be important and compelling. Through our existing models, the Institute could examine and quantify the potential benefits of options such as strategic armoring or design alternatives. If there is interest, the Institute could complete additional tasks such as fieldwork to gain a better knowledge of dredged material and bottom sediment bulk properties, develop focused research on salt wedge dynamics and role in sediment delivery, focused analysis on the role of GIWW in sediment import from outside of the Calcasieu basin, and geotechnical analysis of potential input of substrate material via lateral flow induced by loading or vessel passage.

2. **Following the state and federal discussions, convene the port's stakeholders to discuss creation of a Public-Private Partnership (P3) to implement any of the proposed modification(s) noted above that cannot be implemented with state and/or federal dollars.** The port's stakeholders have a vested economic interest in maintaining channel depth and avoiding the uncertainty of the annual "plea for dredging funds." With the partners like the port and Louisiana Mid-Continent Oil and Gas Association, the Institute could outline how the implementation of proposed modification(s) set forth in this study could generate a "return on investment" for the port's stakeholders and minimize future uncertainty – one-time investments in the system could yield dredging cost-savings for many years to come. Such a P3 could concurrently provide beneficial ecosystem services that are important to a number of the port's major corporate stakeholders. The Institute has experience structuring and implementing P3s designed for similar purposes. In addition, the P3 could serve as an important advocate for the regulatory efficiencies discussed in Task 5.

3. **Informed sediment management of the CSC will require sustained monitoring, modeling, data analysis, and coordination of such activities with regional stakeholders.** The Institute has the experience in facilitating coordination of technical and management activity among local, federal, and state level stakeholders that is necessary to assist the Port of Lake Charles in this effort.

Should the Port and its stakeholders wish to continue pursuing these ideas, we could work together to conceive of how to best minimize dredging costs while yielding environmental benefits.

Appendices

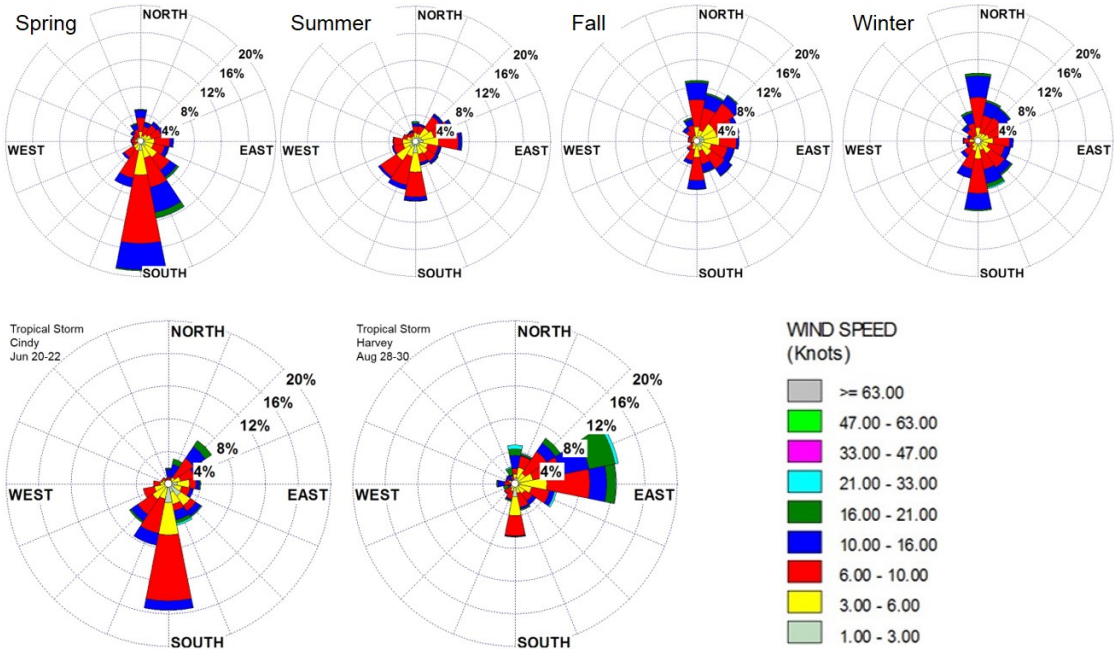

Figure 74. Wind plots from the Lake Charles regional airport (NOAA WBAN station: 03937). Top, average seasonal wind plots from 2008-2016. Bottom, wind plots for Tropical Storm Cindy (Jun 20-22) and Hurricane Harvey (Aug 28-30). Data obtained from: https://www.ncdc.noaa.gov/data-access.

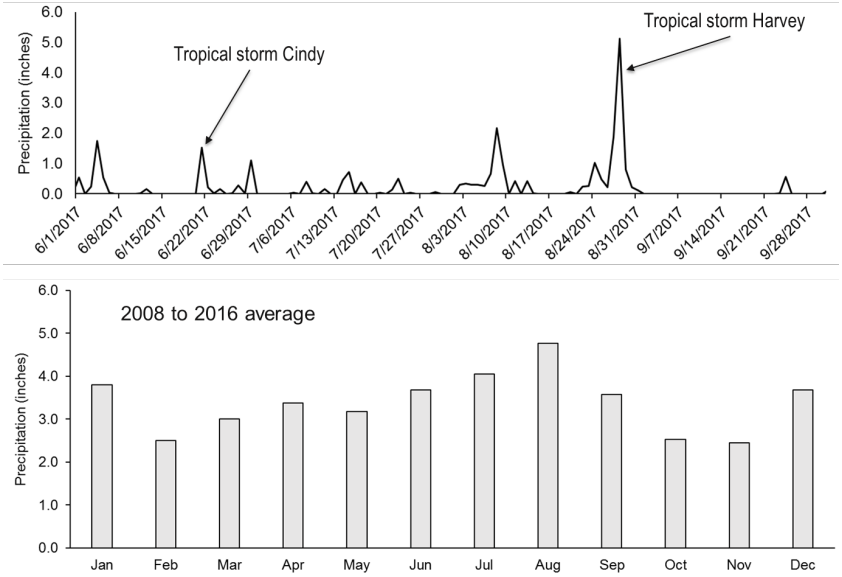

Figure 75. Precipitation plots from the Lake Charles regional airport (NOAA WBAN station: 03937). Top, precipitation plot for Summer 2017, Tropical Storm Cindy and Hurricane Harvey are indicated. Bottom, monthly average of precipitation from 2008 to 2016. Data obtained from: https://www.ncdc.noaa.gov/data-access.

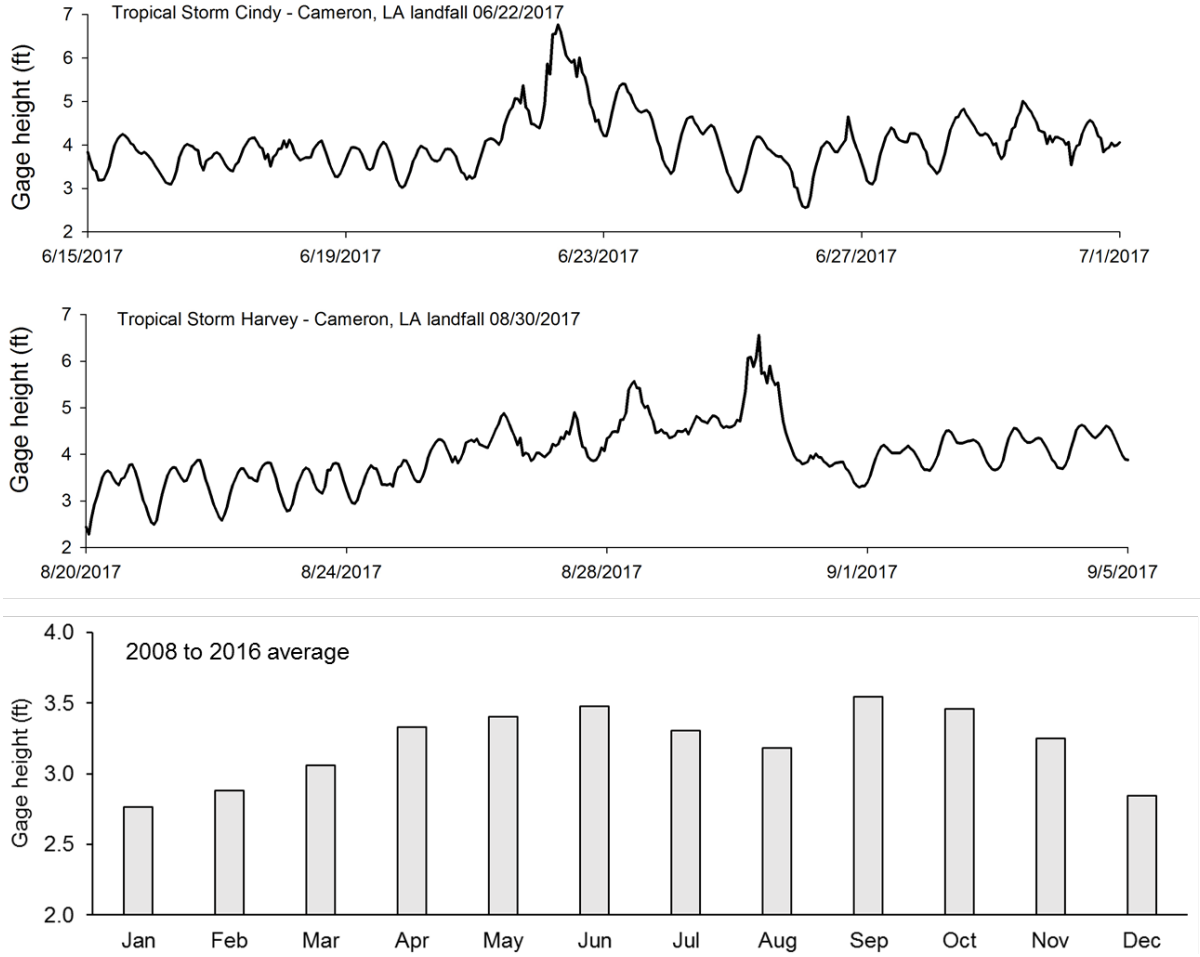

Figure 76. Water gage height plots for Calcasieu Lake (USGS station 08017095). Top, water gage height for Tropical Storm Cindy and Hurricane Harvey. Bottom, monthly average gage height from 2008 to 2016. Data obtained from: https://waterdata.usgs.gov/nwis/uv?site_no=08017095).

APPENDIX B: FIXED STATION INSTRUMENTS FILE LOG

Station name	Date	Instrument	Filename	Notes
ILC	9/6/2017	AWS	CR800_SamplerStat20170906	
ILC	9/6/2017	OMS YSI	ILC4.txt	
NCC	9/7/2017	EXO2 YSI	NCC_14C101014_090717_151200.bin	
KBM	9/6/2017	SL500	KBM10001.arg	
KBM	9/6/2017	EXO2 YSI	KBM_14D102161_090917_160000.bin	
SCC	9/6/2017	AWS	CR800SCC10232017_SamplerStat	
SCC	9/6/2017	SL500 top	SCT08001.arg	
SCC	9/6/2017	SL500 bot	SCB07003.arg	No Data
SCC	9/6/2017	EXO2 YSI top	SCT_14D102306_090617_192400.bin	
SCC	9/6/2017	EXO2 YSI bot	SCB_14D102134_090617_191200	
SED	9/7/2017	EXO2 YSI	SED_14C101015_090717_173600.bin	
SED	9/7/2017	ADV	SED8001.tri	
EPC	9/7/2017	EXO2 YSI	EPC_14D102136_090717_174800.bin	
EPC	9/7/2017	AQD	EPC0508	
SLC	9/7/2017	EXO2 YSI	SLC_14M101280_090717_180000.bin	
SLC	9/7/2017	AQD	SLC0802	
GBW	9/7/2017	EXO2 YSI	GBW_14C101837_090717_234800.bin	
ILC		AWS		No Data
ILC	10/21/2017	OMS YSI	NONAME4	
NCC	10/24/2017	EXO2 YSI	NCC_14D102135_102417_222400	
KBM	10/21/2017	SL500	KBM11001	
KBM	10/21/2017	EXO2 YSI	KBM_14D102161_102117_220000	
SCC	10/23/2017	AWS	CR800SCC01142018_SamplerStat	
SCC	10/23/2017	SL500 top	SCT09001	
SCC	10/23/2017	SL500 bot	SCB09001	

Station name	Date	Instrument	Filename	Notes
SCC	10/23/2017	EXO2 YSI top	SCT_14D102306_102317_182400	
SCC	10/23/2017	EXO2 YSI bot	SCB_14D102134_102317_181200	
SED	10/20/2017	EXO2 YSI	SED_14C101015_102017_141200	
SED	10/20/2017	ADV	SED8004	
EPC	10/20/2017	EXO2 YSI	EPC_14D102136_102017_140000	
EPC	10/20/2017	AQD	EPC90009	
SLC	10/19/2017	EXO2 YSI	SLC_14M101280_101917_184800	

APPENDIX C: ADCP TRANSECTS FILE LOG AND DISCHARGES

Station	Transect Name	Date Time (UTC)	Filename	Transect direction	Good or junk file	MBT Corrected Q (m^3/s)	Flow direction (positive = toward Gulf)
ILC	Transect 011	10/21/2017 15:29	ILC_0_011_17-10-21_151034.PD0	W to E	Good	55.340	pos
	Transect 012	10/21/2017 15:32	ILC_0_012_17-10-21_152819.PD0	E to W	Good	61.515	pos
	Oct average 3	10/21/2017 15:30				58.428	
ILC*	Transect 007	10/21/2017 14:32	ILC_0_007_17-07-14_155819.PD0	N to S	Junk	104.394	neg
	Transect 008	10/21/2017 14:34	ILC_0_008_17-10-21_143135.PD0	S to N	Junk	85.089	neg
	Oct average 1	10/21/2017 14:33				94.742	
	Transect 009	10/21/2017 15:09	ILC_0_009_17-10-21_143345.PD0	N to S	Good	133.840	neg
	Transect 010	10/21/2017 15:11	ILC_0_010_17-10-21_150811.PD0	S to N	Good	128.502	neg
	Oct average 2	10/21/2017 15:10				131.171	
	Transect 013	10/21/2017 19:26	ILC_0_013_17-10-21_153116.PD0	S to N	Good	205.177	pos
	Transect 014	10/21/2017 19:30	ILC_0_014_17-10-21_192556.PD0	N to S	Good	195.499	pos
	Oct average 4	10/21/2017 19:28				200.338	
NCAL	Transect 006	9/7/2017 21:29	NCAL_0_006_17-07-13_215323.PD0		Junk	18.503	
	Transect 007	9/7/2017 21:36	NCAL_0_007_17-09-07_212928.PD0	R to L	Good	560.324	pos
	Transect 008	9/7/2017 21:40	NCAL_0_008_17-09-07_213611.PD0	L to R	Good	560.359	pos
	Sep average	9/7/2017 21:38				560.342	
	Transect 004	10/24/2017 20:16	NCAL_0_004_17-03-17_193647.PD0	E to W	Good	674.558	pos
	Transect 005	10/24/2017 20:25	NCAL_0_005_17-10-24_201533.PD0	W to E	Good	645.164	pos

Station	Transect Name	Date Time (UTC)	Filename	Transect direction	Good or junk file	MBT Corrected Q (m^3/s)	Flow direction (positive = toward Gulf)
	Transect 006	10/24/2017 20:30	NCAL_0_006_17-10-24_202433.PD0	W to E	Good	710.447	pos
	Oct average	10/24/2017 20:24				692.503	
ICWW	Transect 007	9/7/2017 22:34	ICWW_2_0_007_17-07-13_220732.PD0		Junk	20.878	
	Transect 008	9/7/2017 22:40	ICWW_2_0_008_17-09-07_223449.PD0	L to R	Good	344.978	pos
	Transect 009	9/7/2017 22:43	ICWW_2_0_009_17-09-07_224041.PD0	R to L	Good	366.871	pos
	Sep average	9/7/2017 22:42				355.925	
	Transect 001	10/24/2017 19:41	ICWW_2_0_001_17-03-17_191414.PD0	N to S	Good	560.294	pos
	Transect 002	10/24/2017 19:43	ICWW_2_0_002_17-10-24_194053.PD0	S to N	Good	563.418	pos
	Oct average	10/24/2017 19:42				561.856	
MCAL	Transect 007	9/7/2017 23:22	MCAL_0_007_17-07-13_201039.PD0		Junk	12.828	neg
	Transect 008	9/7/2017 23:24	MCAL_0_008_17-09-07_232235.PD0	R to L	Junk	1.282	neg
	Transect 009	9/7/2017 23:28	MCAL_0_009_17-09-07_232430.PD0	R to L	Good	110.676	pos
	Transect 010	9/7/2017 23:31	MCAL_0_010_17-09-07_232806.PD0	L to R	Good	125.161	pos
	Sep average	9/7/2017 23:29				117.9185	
	Transect 004	10/24/2017 17:49	MCAL_0_004_17-03-17_201544.PD0	E to W	Good	663.047	pos
	Transect 005	10/24/2017 17:53	MCAL_0_005_17-10-24_174816.PD0	W to E	Good	668.541	pos
	Oct average	10/24/2017 17:51				665.794	
KBM	Transect 019	10/20/2017 22:23	KBM_0_019_17-07-13_142831.PD0	S to N	Good	24.027	neg
	Transect 020	10/20/2017 22:24	KBM_0_020_17-10-20_222226.PD0	N to S	Good	23.449	neg
	Oct average	10/20/2017 22:23				23.738	

Station	Transect Name	Date Time (UTC)	Filename	Transect direction	Good or junk file	MBT Corrected Q (m^3/s)	Flow direction (positive = toward Gulf)
SCAL	Transect 011	10/20/2017 21:02	SCAL_0_011_17-07-13_191859.PD0	W to E	Good	298.316	neg
	Transect 012	10/20/2017 21:04	SCAL_0_012_17-10-20_210107.PD0	E to W	Good	306.545	neg
	Oct average	10/20/2017 21:03				302.431	
WFRK	Transect 013	10/20/2017 20:12	WFRK_0_013_17-07-13_172008.PD0	S to N	Good	129.441	neg
	Transect 014	10/20/2017 20:14	WFRK_0_014_17-10-20_201147.PD0	N to S	Good	127.757	neg
	Oct average	10/20/2017 20:13				128.599	
EFRK	Transect 018	9/8/2017 22:38	EFRK_0_018_17-07-13_162832.PD0	E to W	Good	148.433	neg
	Transect 019	9/8/2017 22:42	EFRK_0_019_17-09-08_223823.PD0	W to E	Good	122.734	neg
	Sep average 1	9/8/2017 22:40				135.584	
	Transect 020	9/8/2017 22:50	EFRK_0_020_17-09-08_224237.PD0	E to W	Good	142.854	neg
	Transect 021	9/8/2017 22:57	EFRK_0_021_17-09-08_225000.PD0	W to E	Good?	74.032	neg
	Sep average 2	9/8/2017 22:53				108.443	
	Transect 022	10/20/2017 18:03	EFRK_0_022_17-09-08_225755.PD0	W to E	Good	174.774	neg
	Transect 023	10/20/2017 18:05	EFRK_0_023_17-10-20_180222.PD0	E to W	Good	136.278	neg
	Oct average 1	10/20/2017 18:04				155.526	
	Transect 024	10/20/2017 18:17	EFRK_0_024_17-10-20_180456.PD0	R to L	Good	47.852	pos
	Transect 025	10/20/2017 18:20	EFRK_0_025_17-10-20_181638.PD0	L to R	Good	43.475	pos
	Oct average 2	10/20/2017 18:18				45.664	

Station	Transect Name	Date Time (UTC)	Filename	Transect direction	Good or junk file	MBT Corrected Q (m^3/s)	Flow direction (positive = toward Gulf)
SCC	Transect 022	9/9/2017 0:05	SCC_0_022_17-09-09_000104.PD0	R to L	Good	242.073	neg
	Transect 023	9/9/2017 0:07	SCC_0_023_17-09-09_000527.PD0	L to R	Good	338.393	neg
	Transect 024	9/9/2017 0:11	SCC_0_024_17-09-09_000746.PD0		Good	242.477	neg
	Sep average	9/9/2017 0:08				274.314	
	Transect 025	10/20/2017 19:26	SCC_0_025_17-09-09_001106.PD0	W to E	Good	1106.869	neg
	Transect 026	10/20/2017 19:30	SCC_0_026_17-10-20_192559.PD0	E to W	Good	1156.462	neg
	Oct average	10/20/2017 19:28				1131.666	

*ILC: These transects were taken south of the ILC station, at the NOAA PORTS side-looker: https://tidesandcurrents.noaa.gov/stationhome.html?id=8767816

APPENDIX D: CTD/LISST CASTS FILE LOG

Station	Date	Time (UTC)	CTD Filename	LISST Filename
EFRK	9/8/2017	23:26	2017-09-EFRK005	
ICWW	9/7/2017	22:53	2017-09-ICWW003	L2502253
MCAL	9/7/2017	23:35	2017-09-MCAL004	L2502335
NCAL	9/7/2017	21:51	2017-09-NCAL002	L2502151
SCC	9/8/2017	23:43	2017-09-SCC006	

Fixed stations water samples.

Station	Bottle	Bottle Date Time	TSS (mg/L)
NCC	0.1	09/07/2017 20:35:00	81.58
GBW	0.1	09/07/2017 23:48:00	27.20
SLC	0.1	09/08/2017 18:30:00	62.70
EPC	0.1	09/08/2017 20:33:00	19.39
GBW	0.1	10/19/2017 15:43:00	10.70
GBW Weir	0.1	10/19/2017 17:05:00	3.89
SLC	0.1	10/19/2017 17:54:00	17.07
SED	0.1	10/19/2017 20:55:00	30.30
EPC	0.1	10/19/2017 21:40:00	30.72
SED	0.1	10/20/2017 16:15:00	100.10
EPC	0.1	10/20/2017 16:40:00	42.22

Automated water sampler at ILC.

Station	Bottle	Bottle Date Time	TSS (mg/L)
ILC	1	09/08/2017 00:00:00	60.78
ILC	2	09/10/2017 00:00:00	9.21
ILC	3	09/12/2017 00:00:00	24.34
ILC	4	09/14/2017 00:00:00	16.39

Automated water sampler at SCC.

Station	Bottle	Bottle Date Time	TSS (mg/L)
SCC	1	09/08/2017 00:00:00	61.22
SCC	2	09/10/2017 00:00:00	13.27
SCC	3	09/12/2017 00:00:00	21.63
SCC	4	09/14/2017 00:00:00	67.96
SCC	5	09/16/2017 00:00:00	106.12
SCC	6	09/18/2017 00:00:00	66.33
SCC	7	09/20/2017 00:00:00	24.49
SCC	8	09/22/2017 00:00:00	23.88
SCC	9	09/24/2017 00:00:00	34.49
SCC	10	09/26/2017 00:00:00	30.41
SCC	11	09/28/2017 00:00:00	23.47
SCC	12	09/30/2017 00:00:00	44.90
SCC	13	10/02/2017 00:00:00	101.63
SCC	14	10/04/2017 00:00:00	64.69
SCC	15	10/06/2017 00:00:00	86.12
SCC	16	10/08/2017 00:00:00	76.33
SCC	17	10/10/2017 00:00:00	107.96
SCC	18	10/12/2017 00:00:00	41.63
SCC	19	10/14/2017 00:00:00	28.16
SCC	20	10/16/2017 00:00:00	43.88
SCC	21	10/18/2017 00:00:00	24.29
SCC	22	10/20/2017 00:00:00	55.71
SCC	23	10/22/2017 00:00:00	157.96
SCC	24	10/24/2017 00:00:00	41.84

Van Dorn casts water samples.

Station	Fractional Depth	Date Time (UTC)	Sed. Concentration (mg/L)
NCAL	0.1	09/07/2017 21:51:00	14.76
NCAL	0.5	09/07/2017 21:51:00	19.43
NCAL	0.9	09/07/2017 21:51:00	21.63
ICWW	0.1	09/07/2017 22:53:00	40.72
ICWW	0.5	09/07/2017 22:53:00	40.95
ICWW	0.9	09/07/2017 22:53:00	144.69
MCAL	0.1	09/07/2017 23:36:00	69.24
MCAL	0.5	09/07/2017 23:36:00	52.32
MCAL	0.9	09/07/2017 23:36:00	124.63
EFRK	0.1	09/08/2017 23:26:00	21.86
EFRK	0.5	09/08/2017 23:26:00	57.00
EFRK	0.9	09/08/2017 23:26:00	8.96
SCC	0.1	09/08/2017 23:43:00	40.62
SCC	0.5	09/08/2017 23:43:00	18.83
SCC	0.9	09/08/2017 23:43:00	48.85

APPENDIX F: SHIP WAKE INSTRUMENT FILE LOG

Deployment #	Instrument deployed	Instrument retrieved	String	Station	Instrument	Folder name
1	10/22/2017 22:00	10/23/2017 23:00	A	D	RBR	052638_20171106_1638_D
	10/22/2017 22:00	10/23/2017 23:00		C	RBR	052637_20171106_1611_C
	10/22/2017 22:00	10/23/2017 23:00		B	RBR	052639_20171103_2133_B
	10/22/2017 22:00	10/23/2017 23:00		A	RBR	052636_20171103_2050_A
2	1/10/2018 17:00	1/13/2018 17:00	A	F	RBR	052636_20180113_1949_F
	1/10/2018 17:00	1/13/2018 17:00		C	RBR	052640_20180113_1941_C
	1/10/2018 17:00	1/13/2018 17:00		A	RBR	052639_20180329_1035_A_shortened_data
	1/10/2018 17:00	1/13/2018 17:00	B	B	RBR	052641_20180113_2003_B
	1/10/2018 17:00	1/13/2018 17:00		D	RBR	052637_20180113_1955_D
	1/10/2018 17:00	1/13/2018 17:00		E	RBR	052638_20180113_1915_E
	1/10/2018 17:00	1/13/2018 17:00		G	YSI	PLCa_14C101014_010918_150000
3	1/13/2018 23:00	1/15/2018 0:00	A	B	RBR	052638_20180116_0126_B
	1/13/2018 23:00	1/15/2018 0:00		C	RBR	052640_20180116_0134_C
	1/13/2018 23:00	1/15/2018 0:00		E	RBR	052637_20180116_0132_E
	1/14/2018 16:00	1/15/2018 0:00	B	G	YSI	PLC3_14C101014_011418_160000
	1/14/2018 16:00	1/15/2018 0:00		D	RBR	052636_20180116_0123_D
	1/14/2018 16:00	1/15/2018 0:00		K	RBR	052641_20180116_0129_K

APPENDIX G: MODEL CALIBRATIONS TO 2017 FIELD DATA

This section presents the calibration effort for water level, salinity, total suspended sediment, and for the discharge through the southern passes. All calibrations have been conducted by comparing output from CSC_108 to observed data that was collected by the Water Institute or publicly available through the USGS. Total suspended sediment calibrations are presented as daily averages, while all other parameters are hourly or more frequent.

For water level, salinity, and total suspended sediment, the full record of calibration from January through August of 2017 is shown, and is then followed with figures showing the data in more detail for selected timespans. For discharge records, which are collected only during field deployments, only the detailed figures are shown. The calibration data is presented separately for the stations in the northern and southern ends of the domain.

The locations of all calibration data are shown in Figure 6.

Northern Stations

Water Level

Figures Figure 77 and Figure 79 show water level calibrations throughout the northern stations. Model output is generally in agreement with the calibration data, including the magnitude of water level fluctuations. Water Level data from Water Institute stations is shown as blue dots, and is regarded as having better absolute elevation control than nearby USGS stations. Where Water Institute data is not available the model is calibrated to USGS water level data (black dots). Model output is shown as a red line.

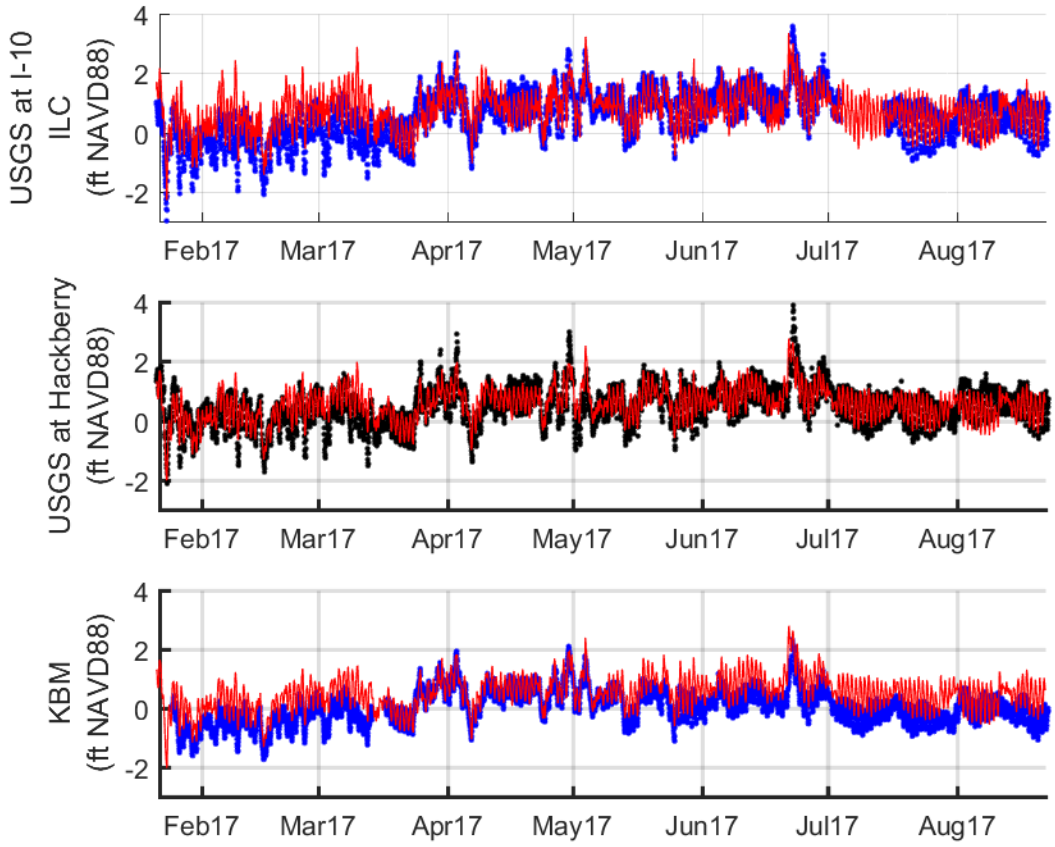

Figure 77. Water Level calibrations at selected northern stations.

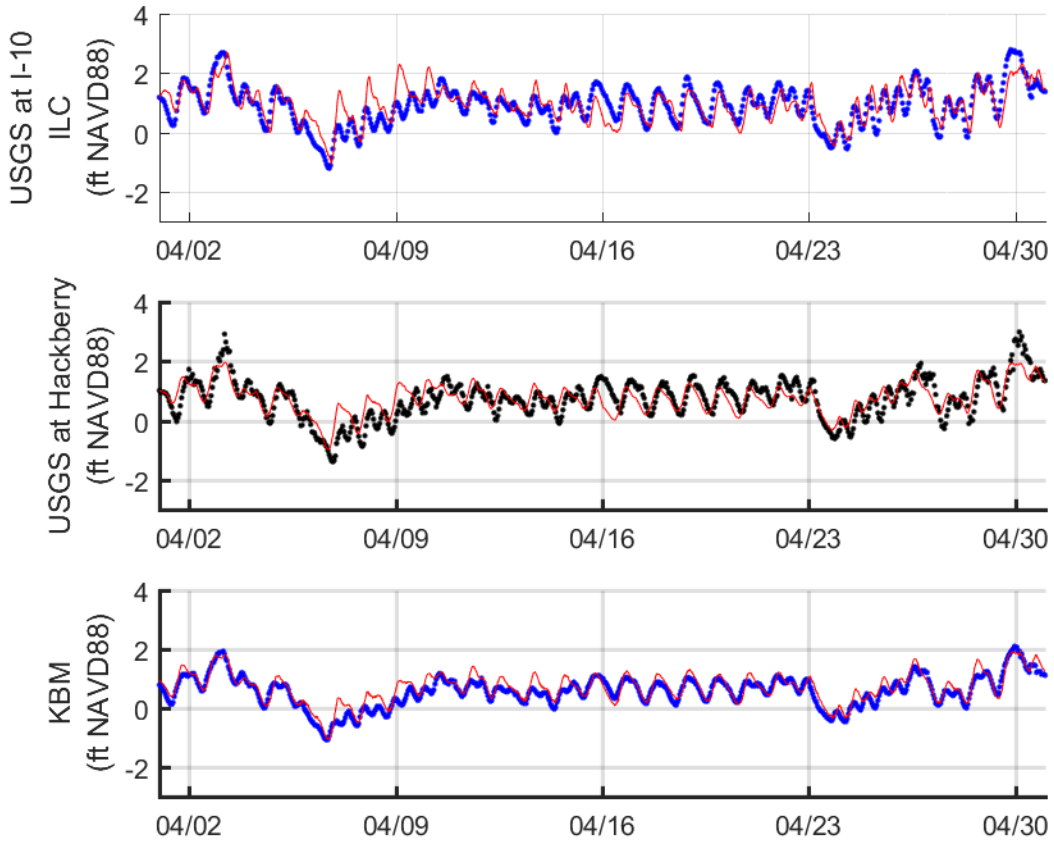

Figure 78. Water Level calibrations at selected northern stations for the month of April.

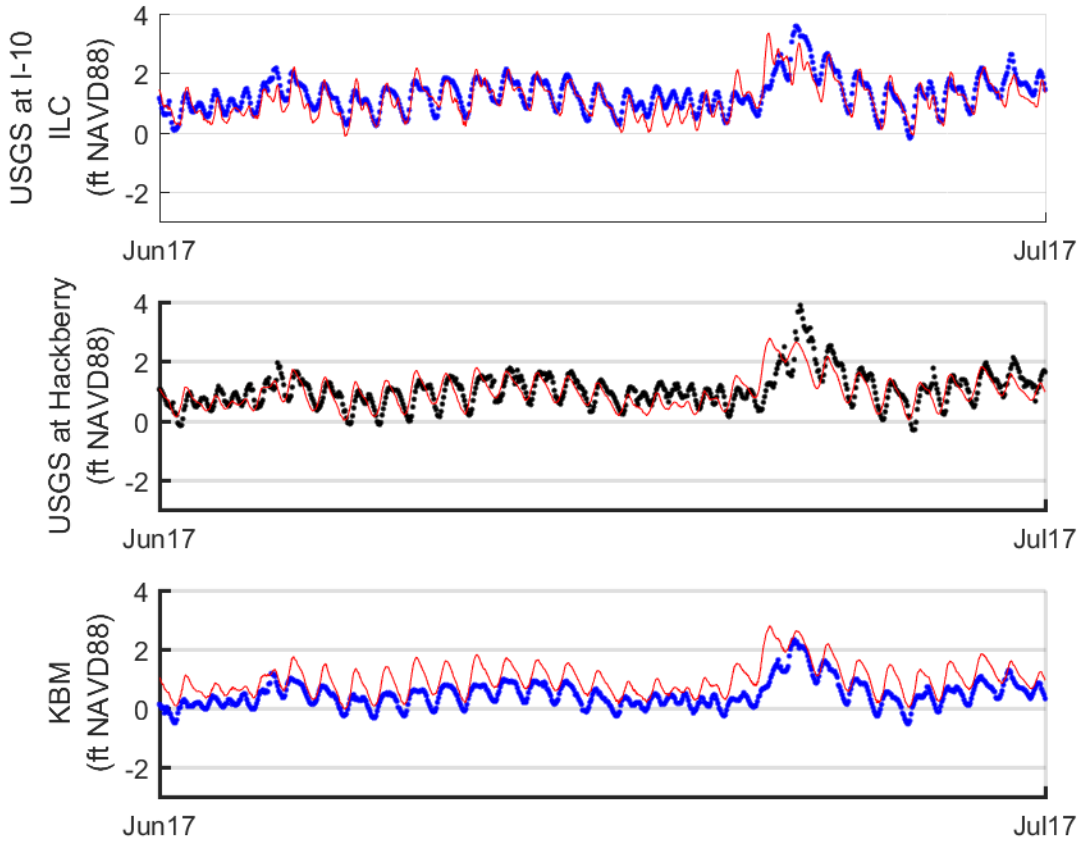

Figure 79. Water Level calibrations at selected northern stations for the month of June.

Salinity

The salinity at the upstream boundary, which is imposed by the function shown in Section 2.2, drives the salinity signal at the USGS I-10/ILC location. The data below show that this boundary condition accurately represents the average salinity, but not the tidal fluctuations. This is to be expected, since the boundary condition is partially a function of discharge upstream at Kinder, which is not subject to tidal fluctuations. The model underpredicts salinity in the northern part of Calcasieu Lake (at USGS Hackberry) during periods of prolonged high salinity.

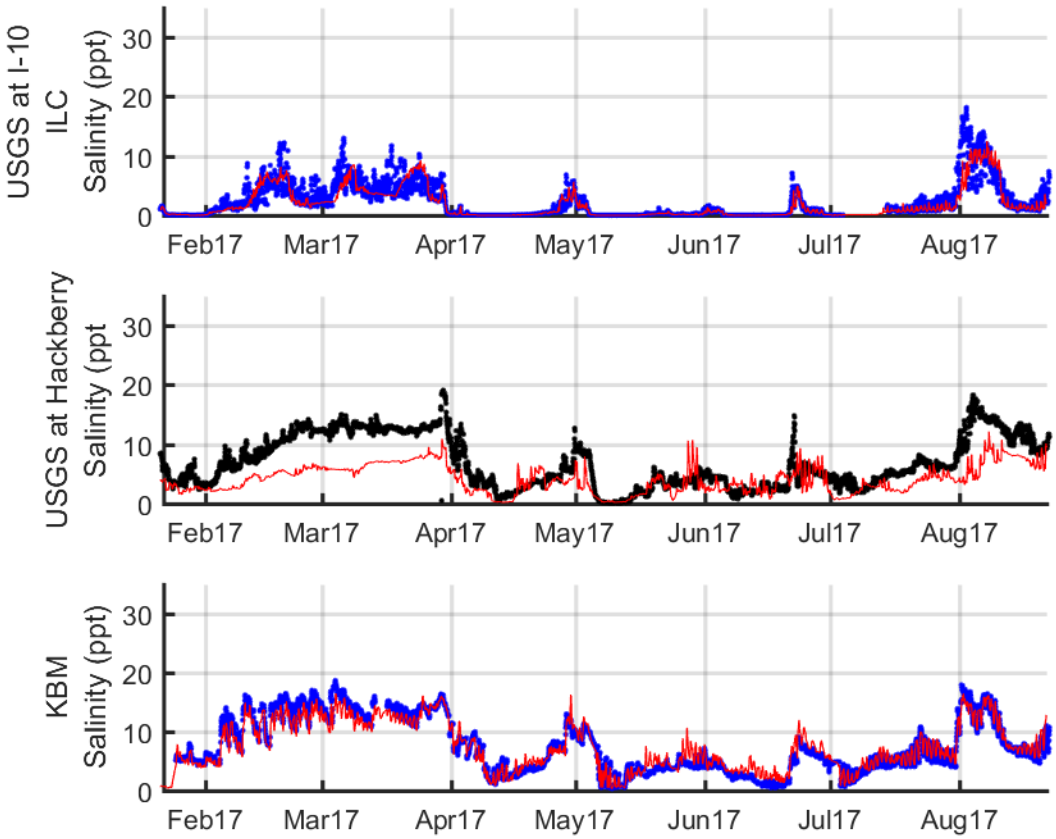

Figure 80. Salinity calibrations at selected northern stations. Model output is shown with a red line, USGS data shown as black dots, and Water Institute data shown as blue dots.

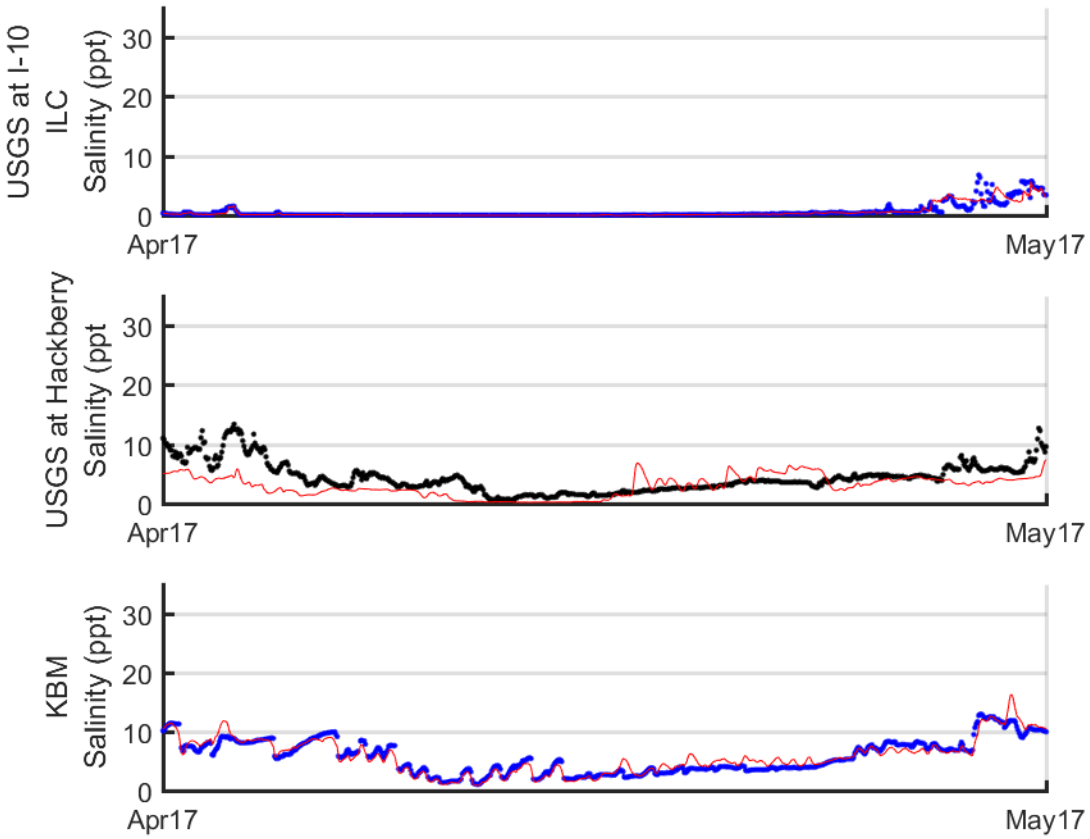

Figure 81. Salinity calibrations at selected northern stations for the month of April.

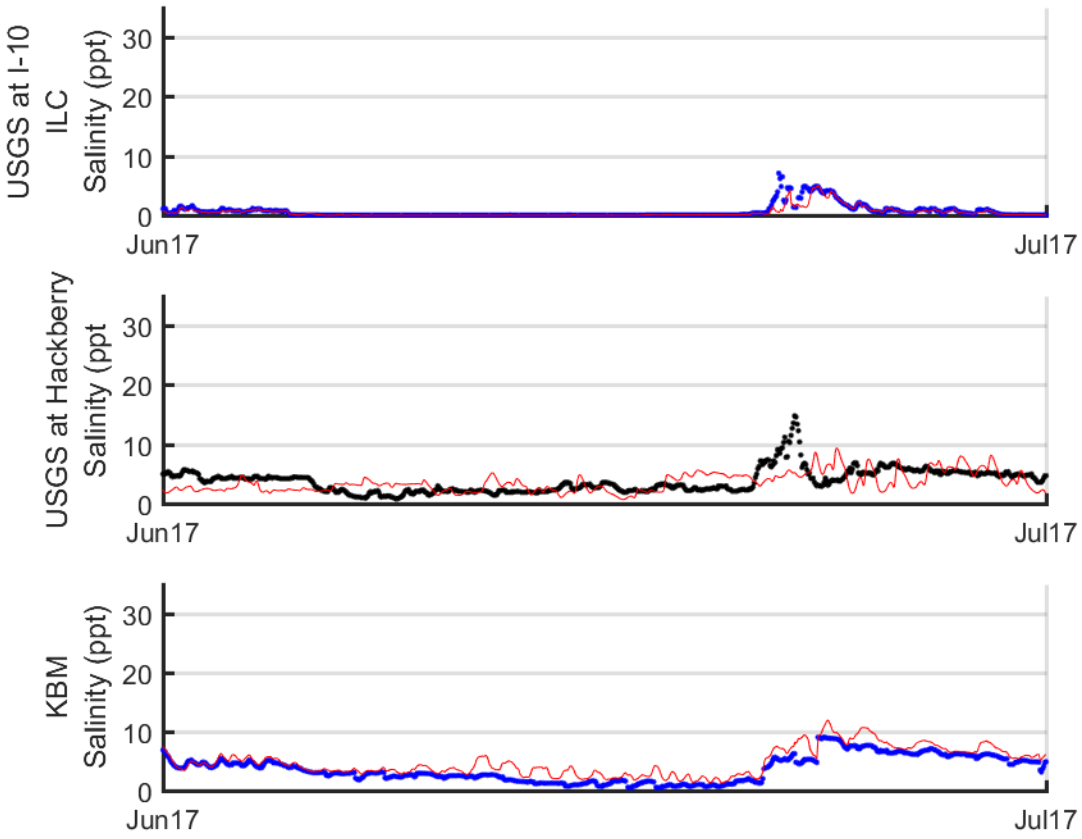

Figure 82. Salinity calibrations at selected northern stations for the month of June.

Total Suspended Sediment

This section shows the total suspended sediment concentration modeled at ILC, along with Water Institute calibration data. The suspended sediment concentration at ILC is driven by the upstream boundary condition, so these plots show the performance of the sediment rating curve developed by Pereira and Meselhe (2015) and used here. The rating curve accurately predicts day to day suspended sediments through most of the time period modeled.

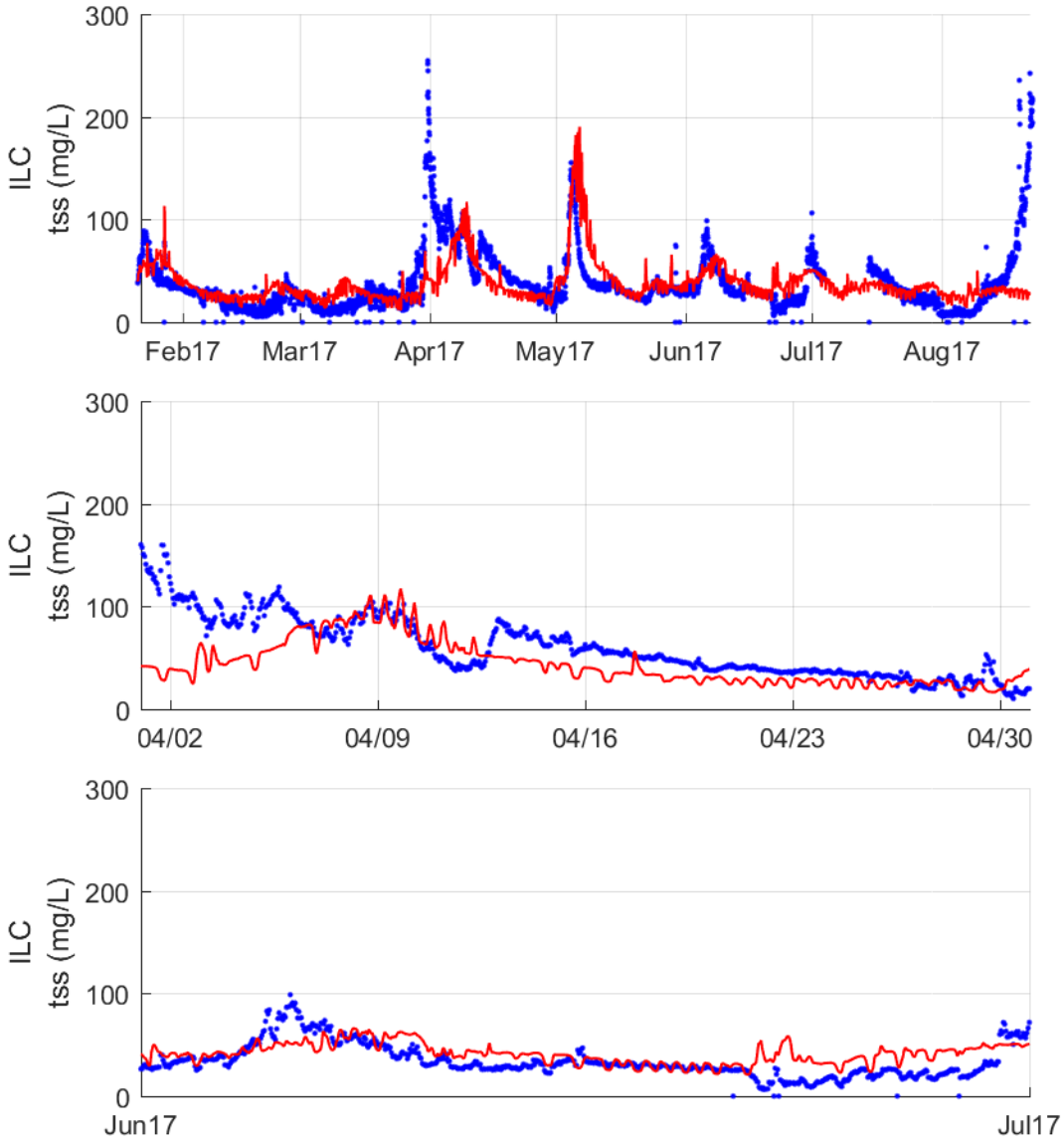

Figure 83. Total suspended sediment calibrations at ILC. Model output is shown with a red line and Water Institute data shown as blue dots.

Discharge

Discharges through the northern stations are well calibrated.

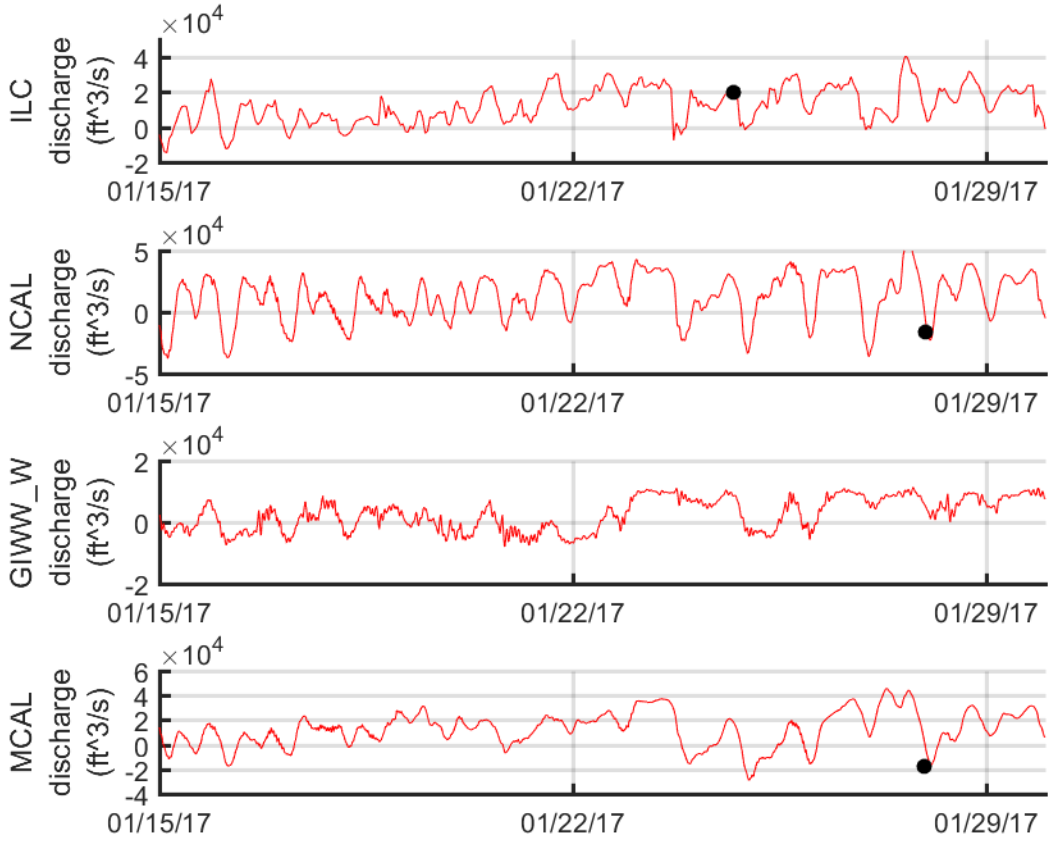

Figure 84. Discharge calibrations at northern stations during January 2017 visit.

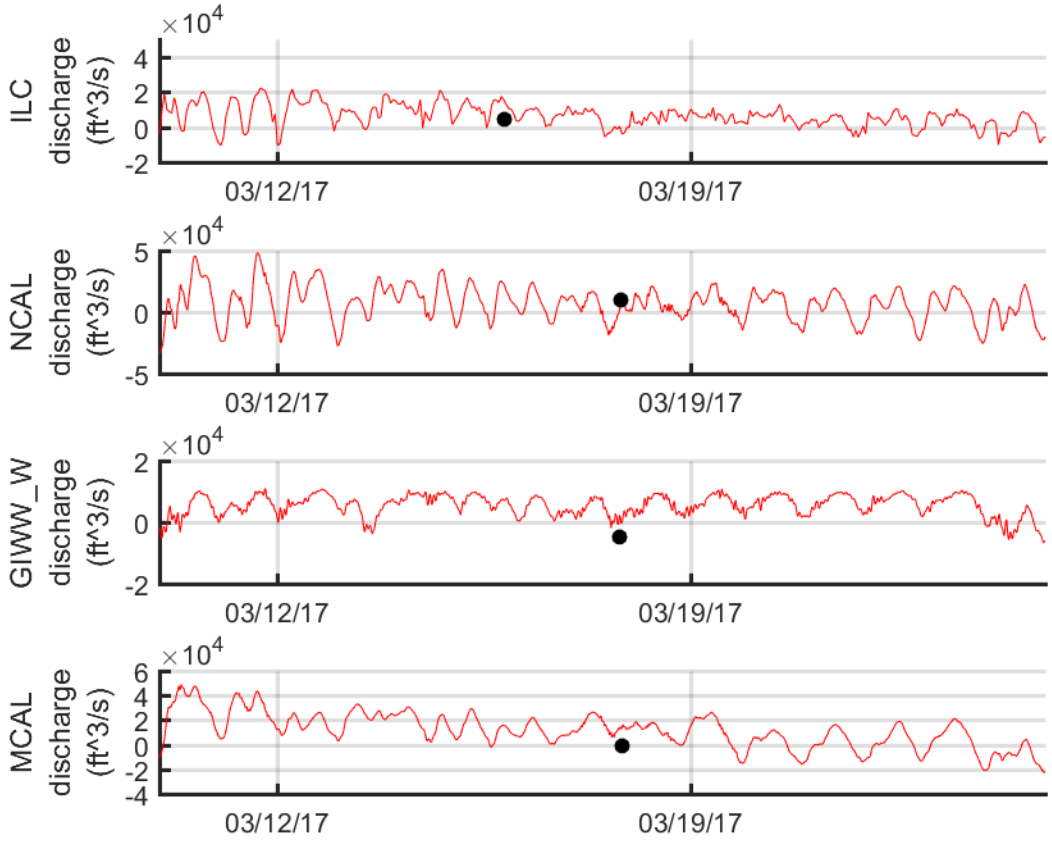

Figure 85. Discharge calibrations during March 2017 field visit.

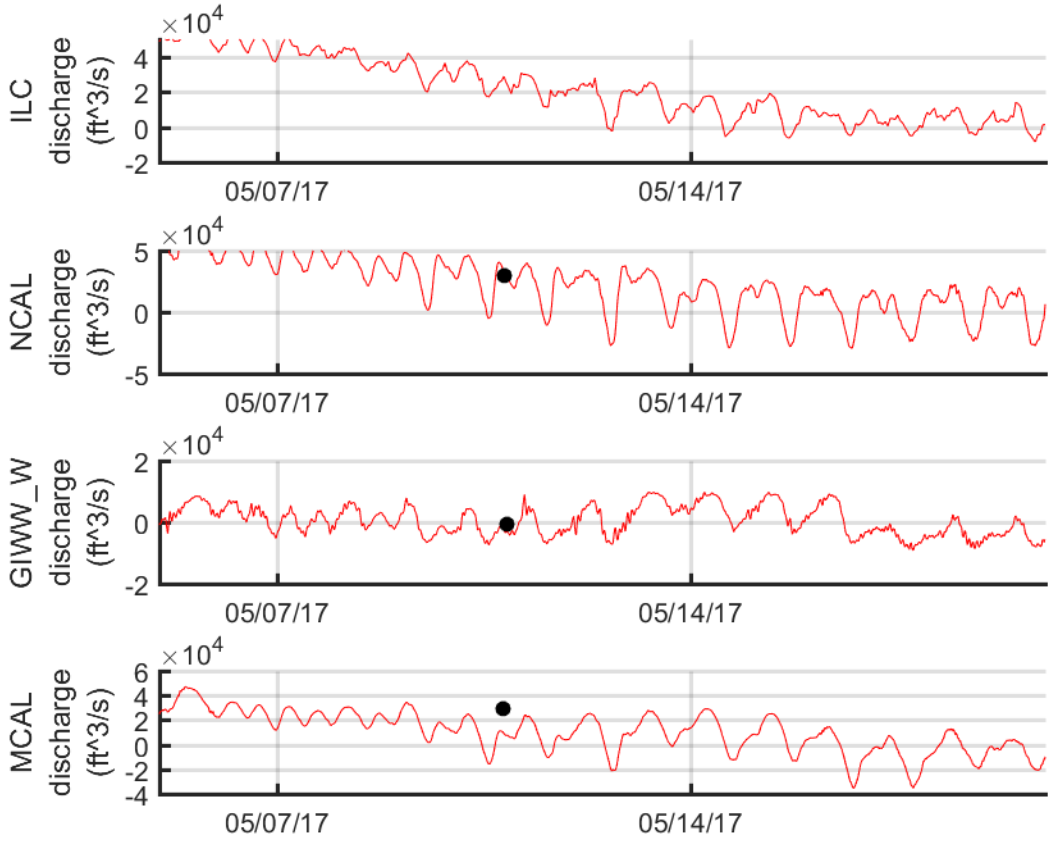

Figure 86. Discharge calibrations at Northern stations during May 2017 field visit.

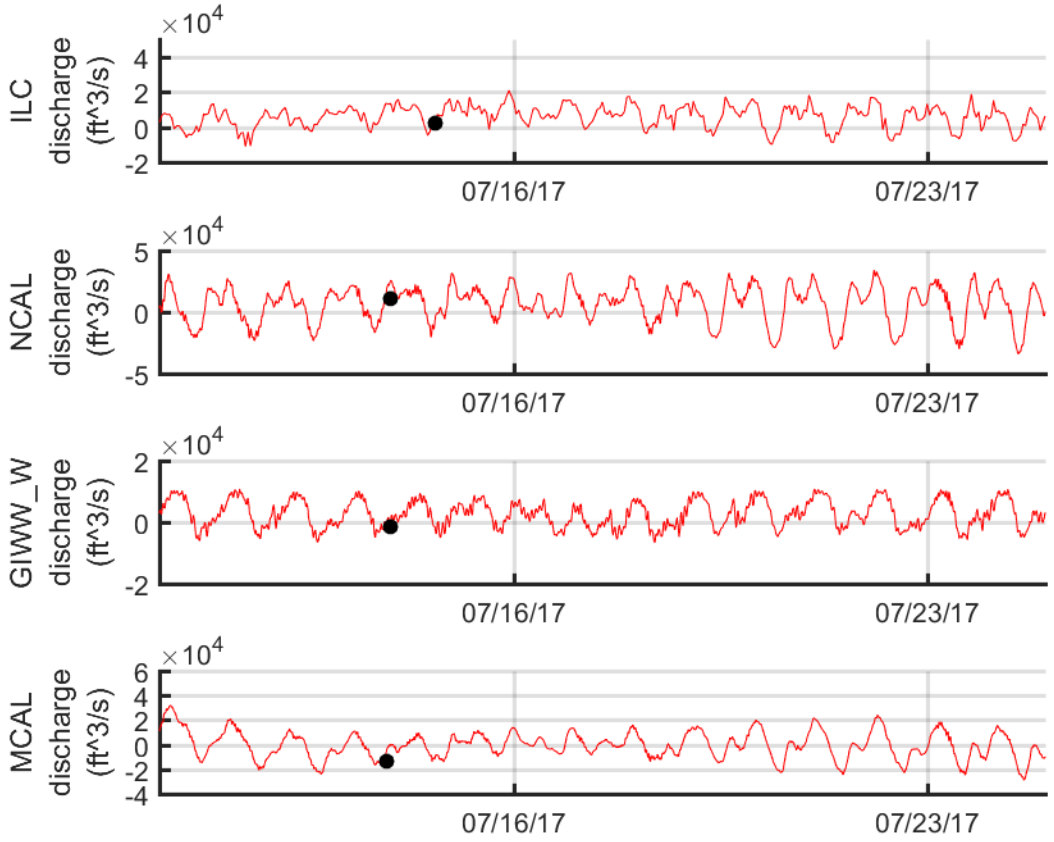

Figure 87. Discharge calibrations at northern stations during July 2017 field visit.

Southern Stations

Water Level

Water levels throughout the southern stations are in good agreement with the calibration data, including the magnitude of tidal water level fluctuations, and the influx of water associated with Tropical Storm Cindy in late June.

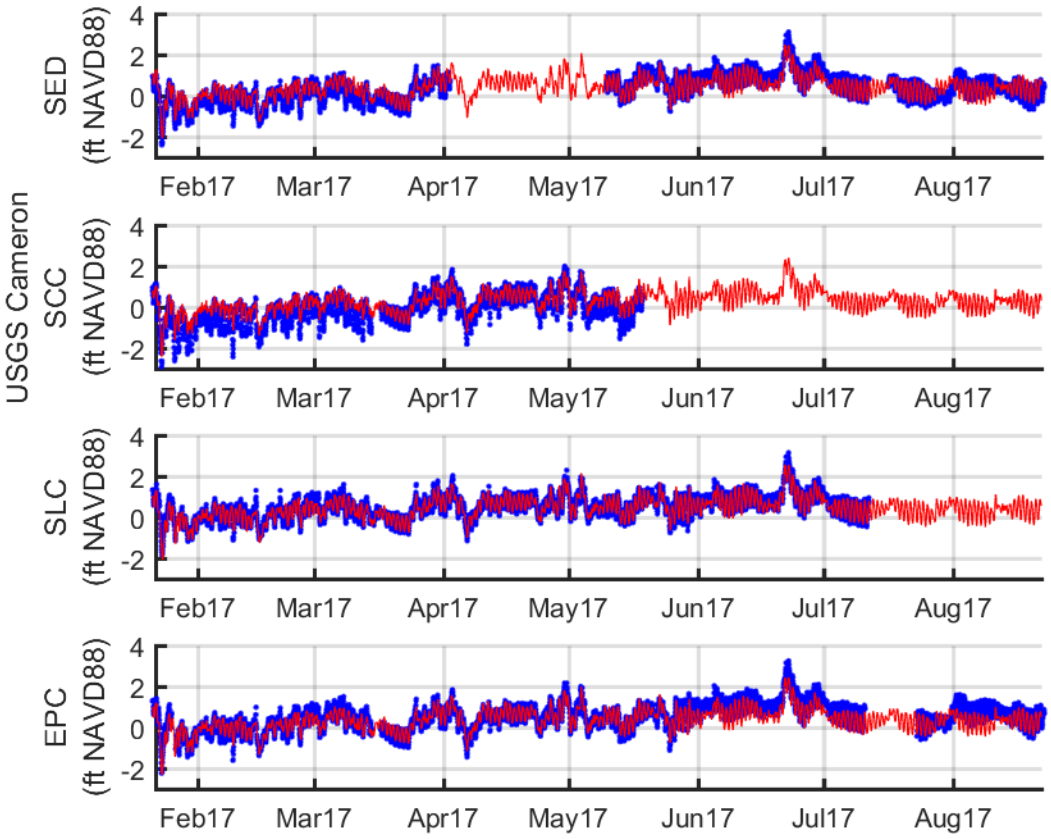

Figure 88. Water level calibrations at selected southern stations.

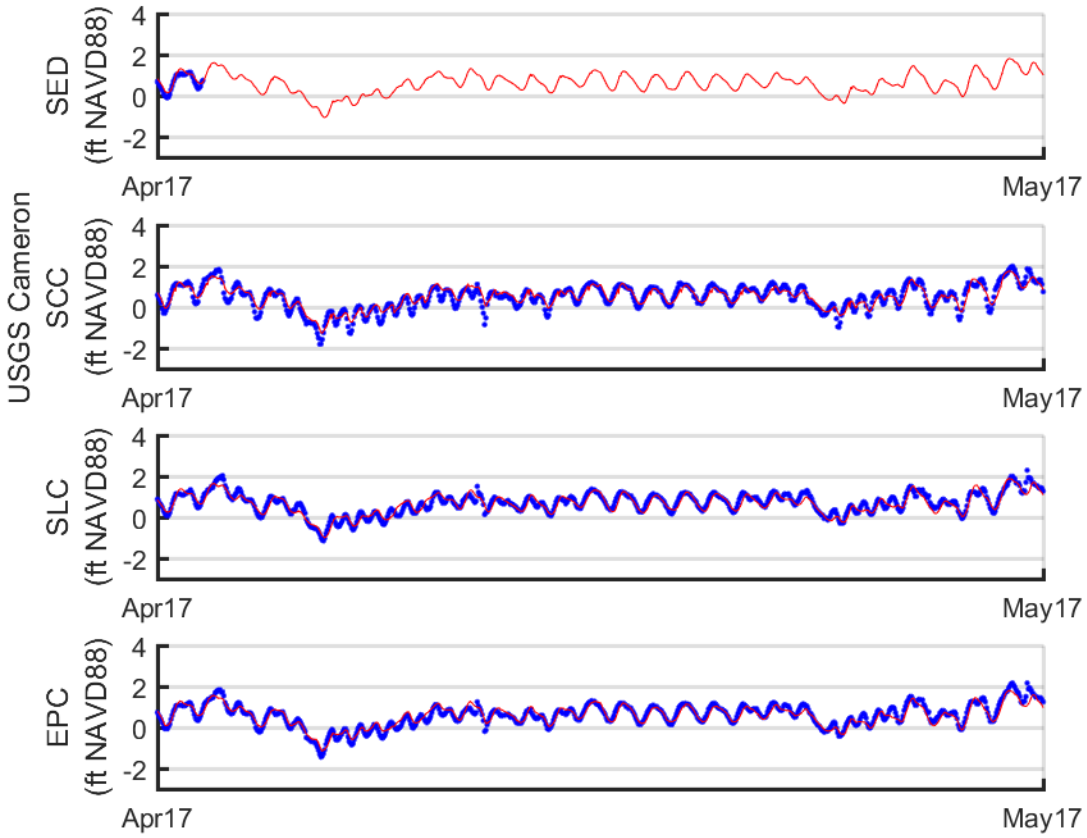

Figure 89. Water level calibrations at selected southern stations during the month of April.

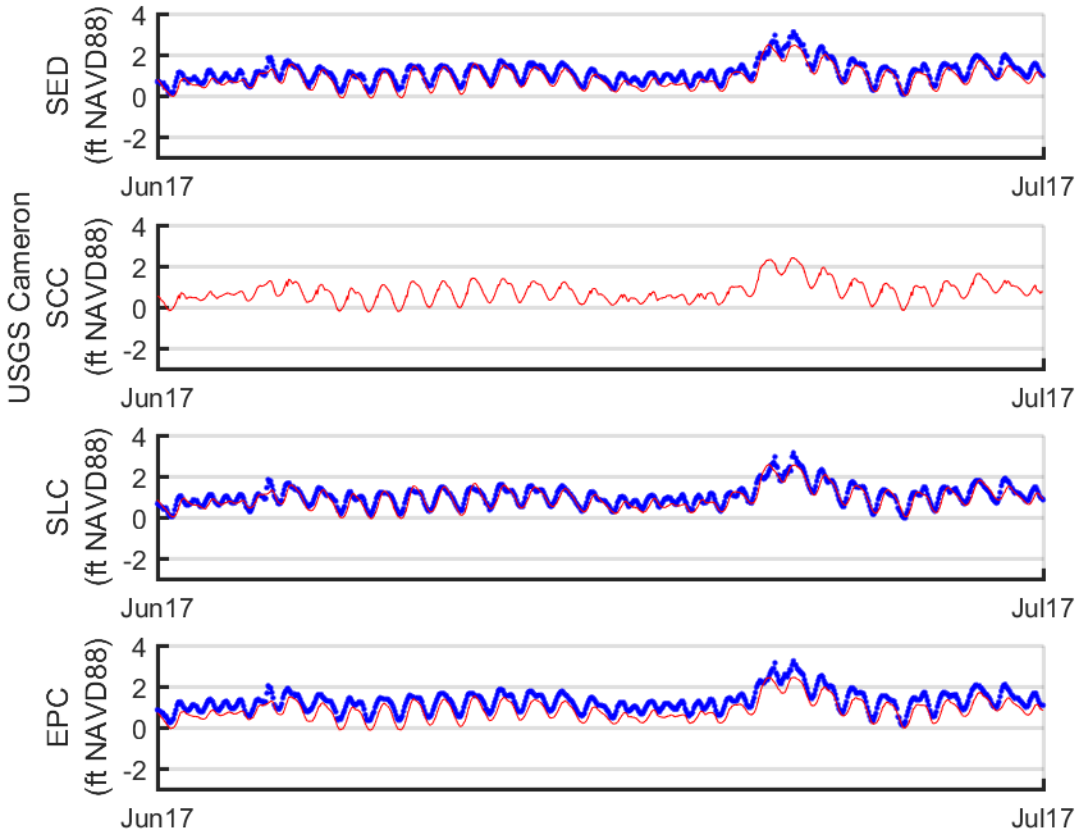

Figure 90. Water level calibrations at selected southern stations during the month of June.

Salinity

This section shows the salinity calibration throughout the southern stations. The magnitude of salinity fluctuations, including transitions between spring and neap tides, is well represented during most time periods. A period of prolonged low modeled salinity relative to data is seen at EPC from the start of the simulation through the flood in April. This is likely due to a persistent salt wedge that is not represented in this depth averaged model.

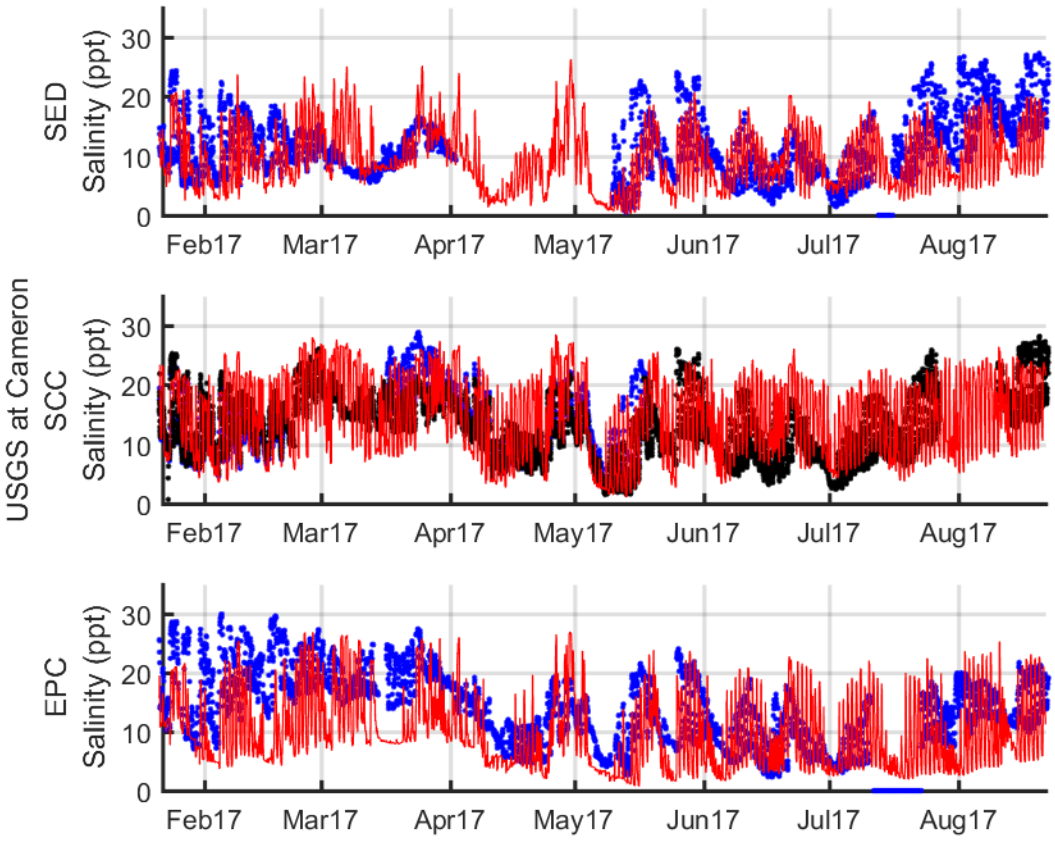

Figure 91. Salinity calibrations at selected southern stations. Model output is shown with a red line, USGS data as black dots, and Water Institute data shown as blue dots.

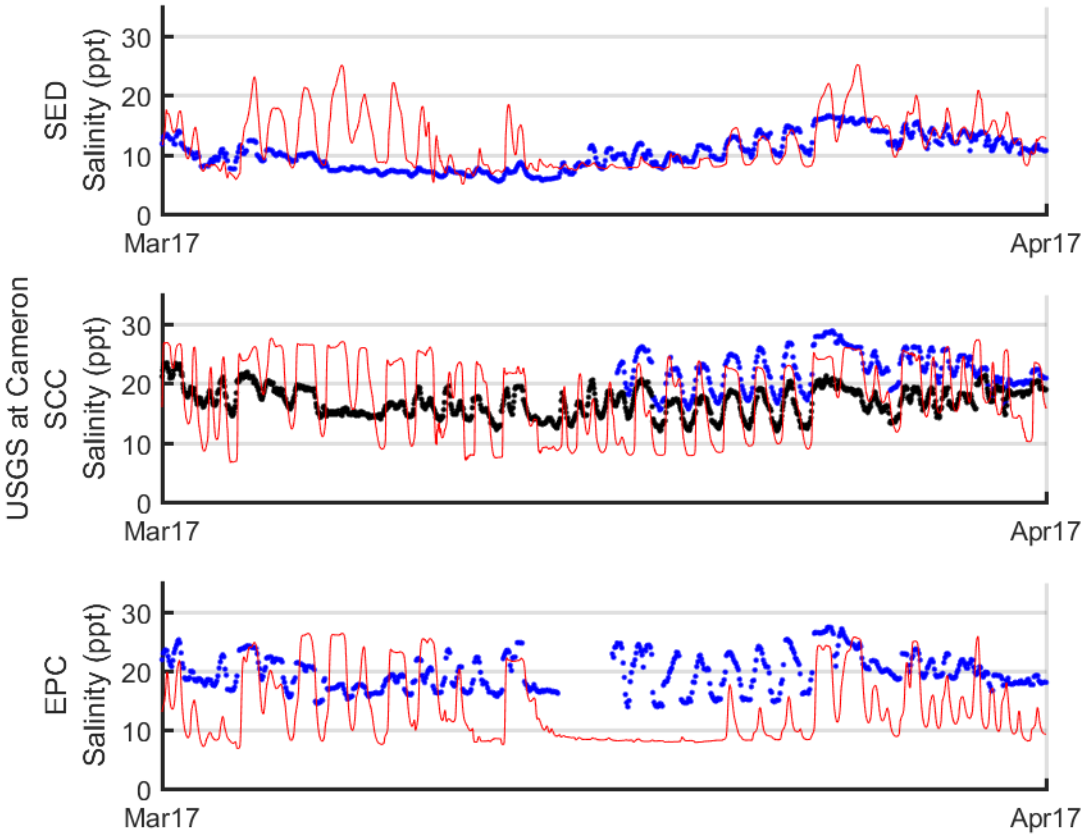

Figure 92. Salinity calibrations at selected southern stations during the month of March. Model output is shown with a red line, USGS data as black dots, and Water Institute data shown as blue dots.

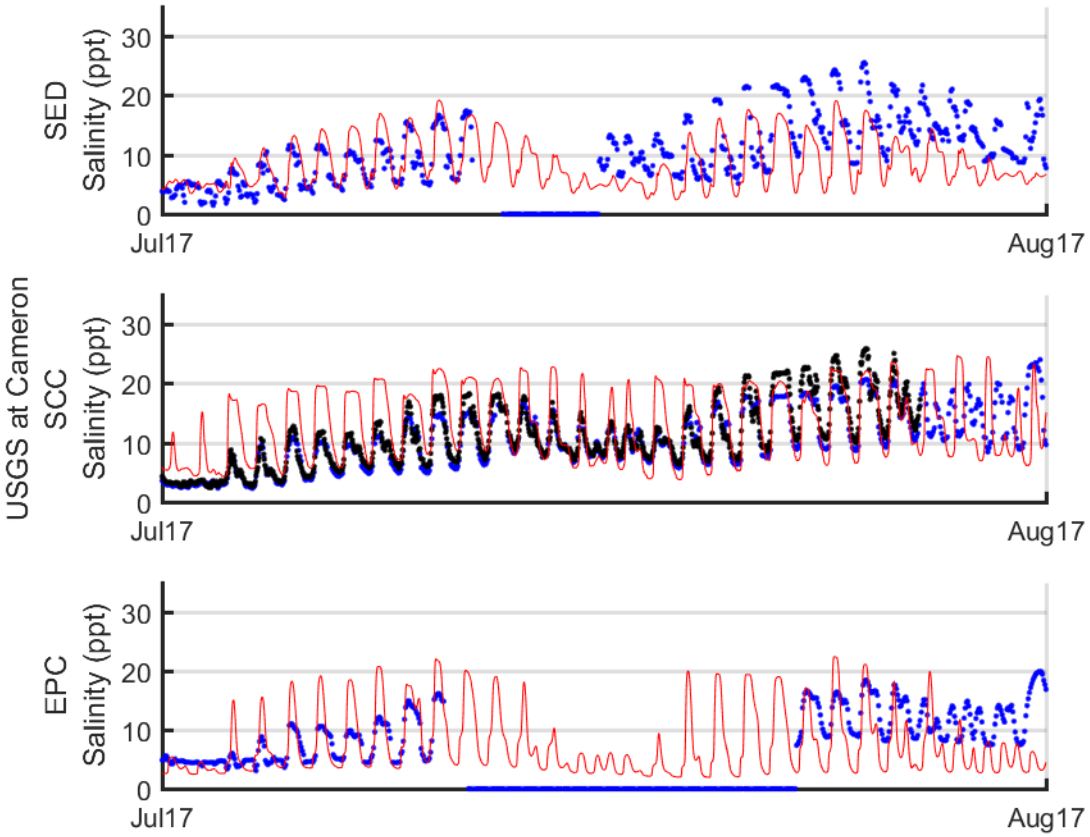

Figure 93. Salinity calibrations at selected southern stations during the month of July. Model output is shown with a red line, USGS data as black dots, and Water Institute data shown as blue dots.

Total Suspended Sediment

Total suspended sediment concentrations agree well with data at SCC, indicating that the downstream boundary is accurately represented in the model; and at SED, which indicates that sediment resuspension from the bed, and transport along the channel is accurate.

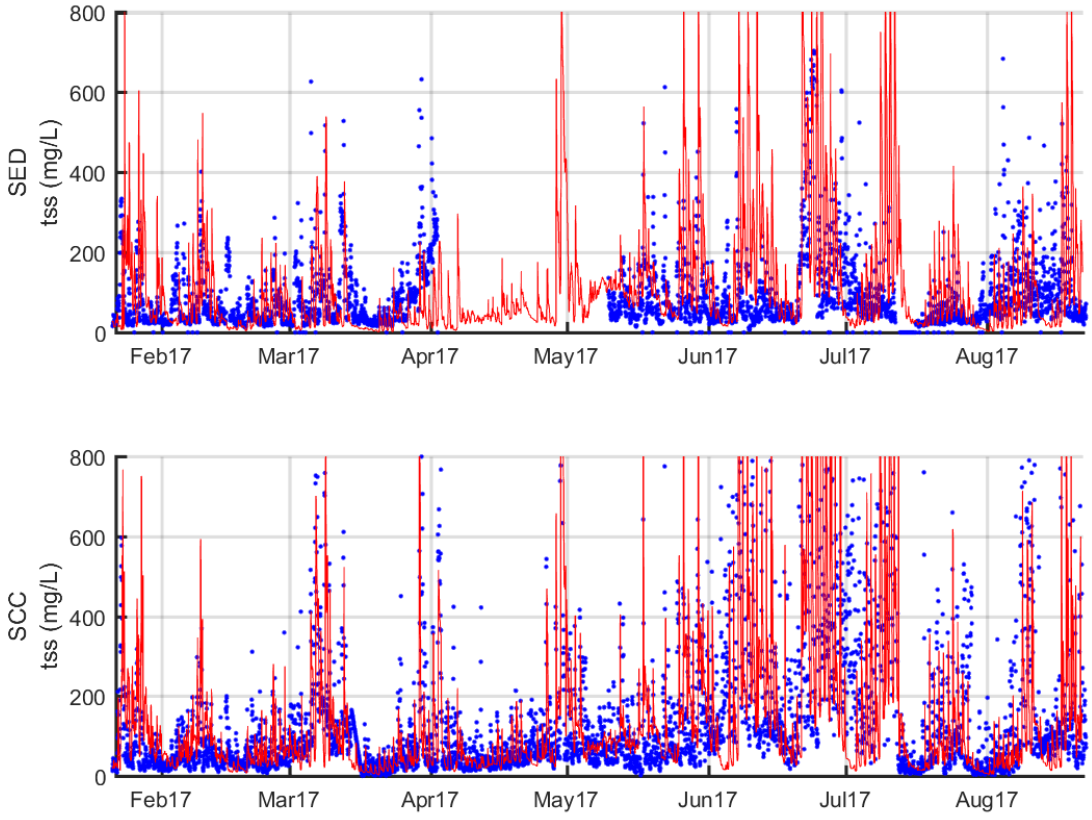

Figure 94. Total suspended sediment calibrations at selected southern stations. Model output is shown with a red line, USGS data as black dots, and Water Institute data shown as blue dots.

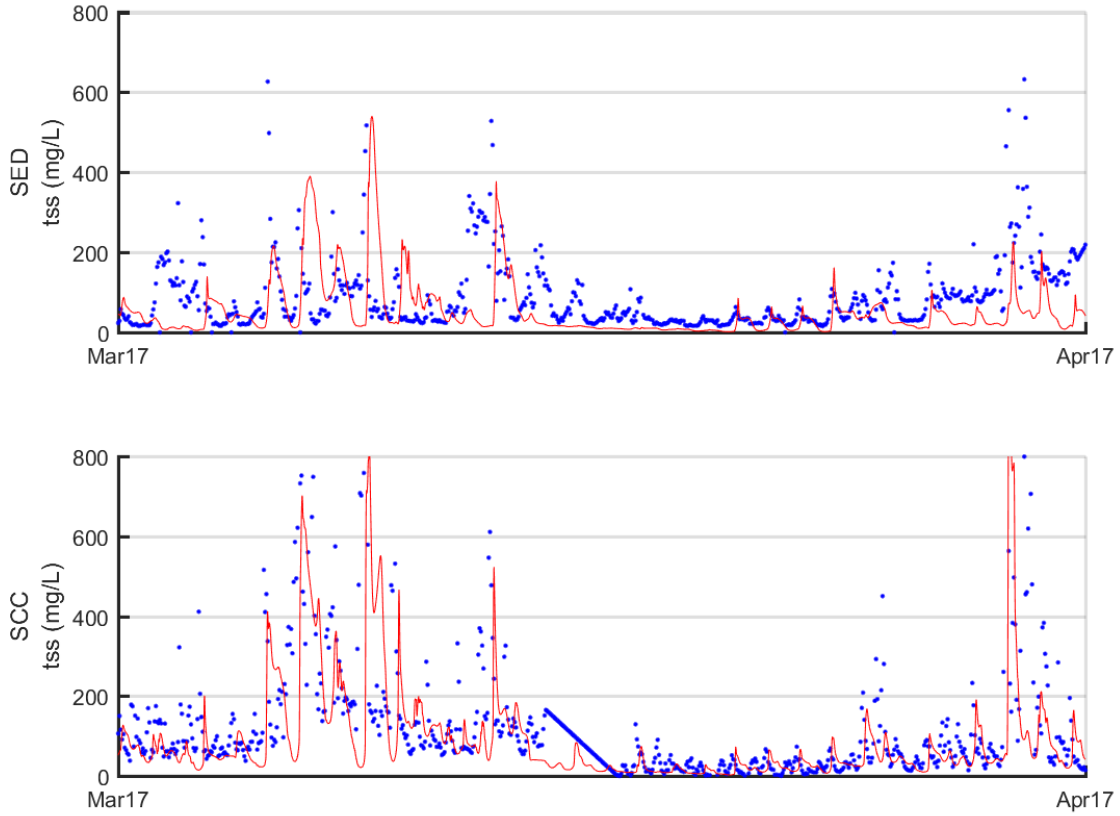

Figure 95. Total suspended sediment calibrations at selected southern stations during the month of March.

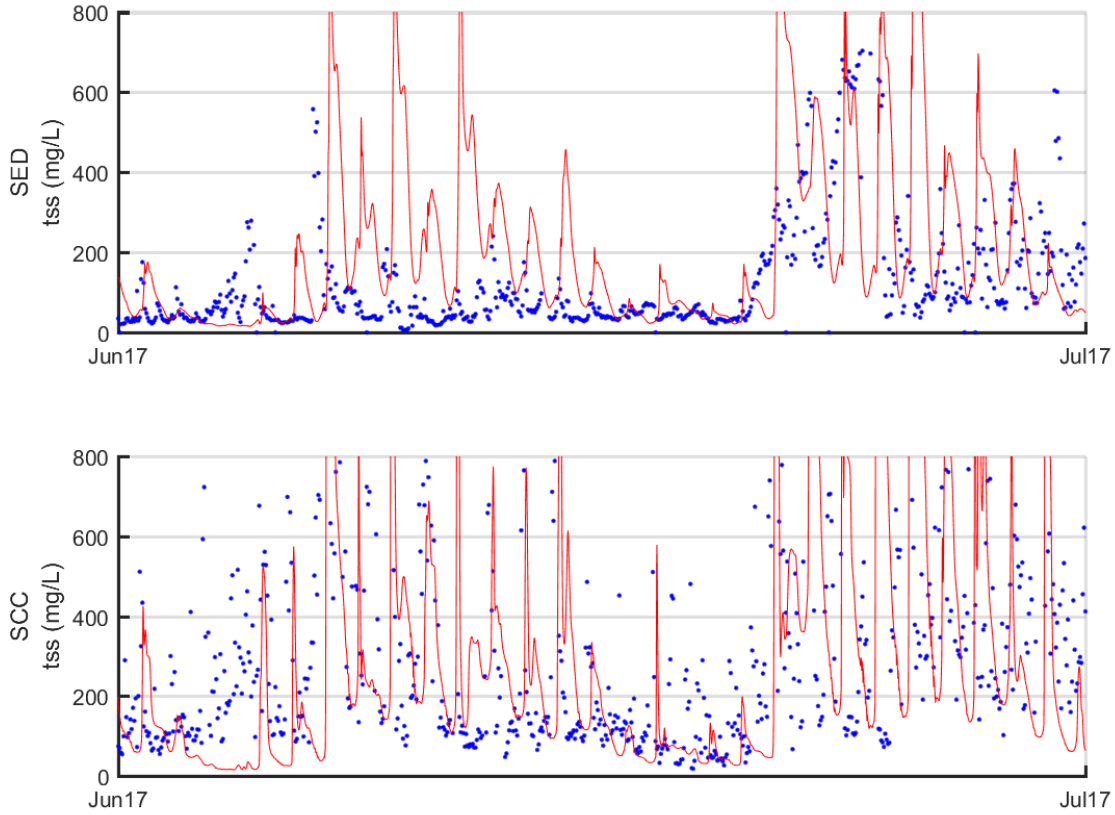

Figure 96. Total suspended sediment calibrations at selected southern stations during the month of June.

Discharge

The model is in very close agreement with the discharge calibration data throughout the southern passes. This lends credence to the modeled impacts on flow distribution shown in Section 4.5.

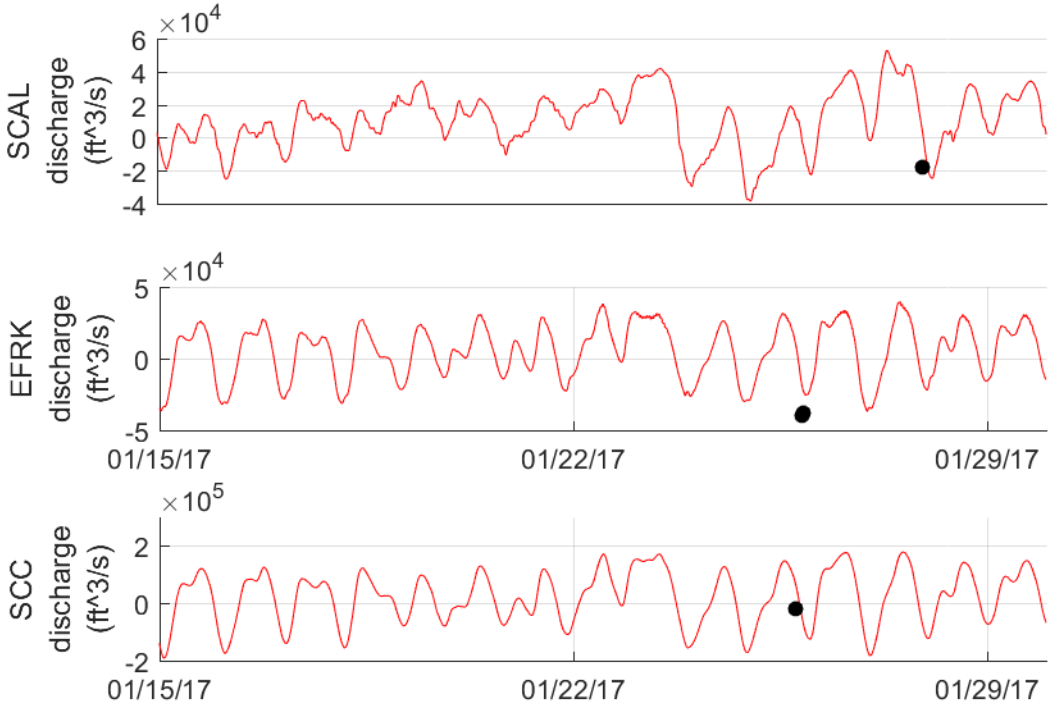

Figure 97. Discharge calibration through the southern passes during January 2017.

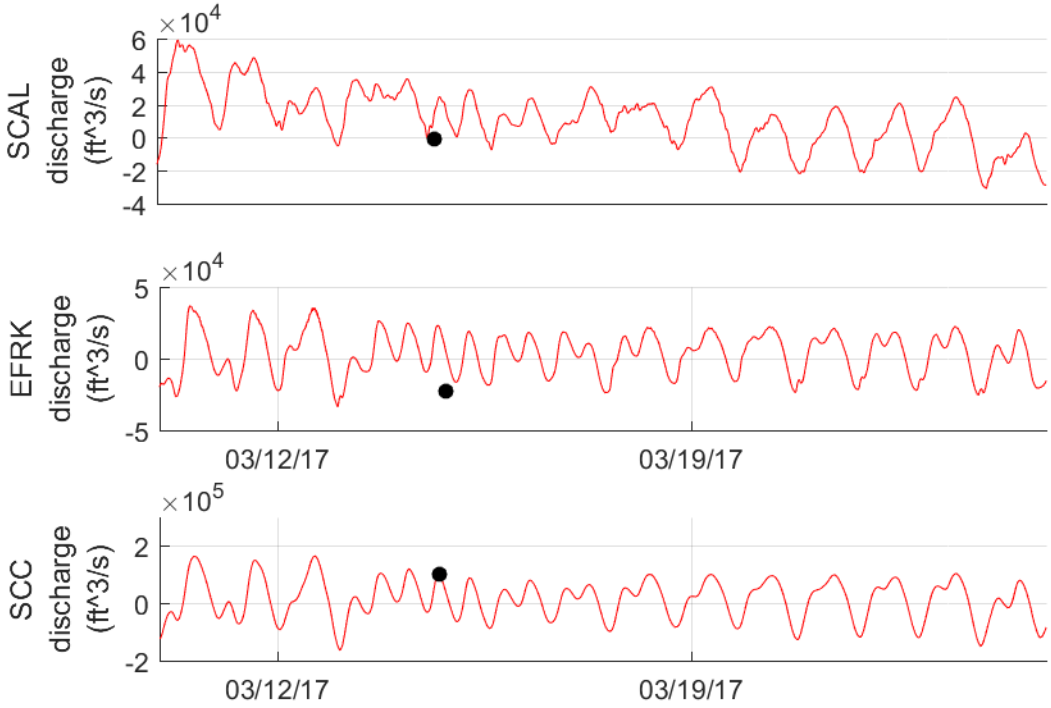

Figure 98. Discharge calibration through the southern passes during March 2017.

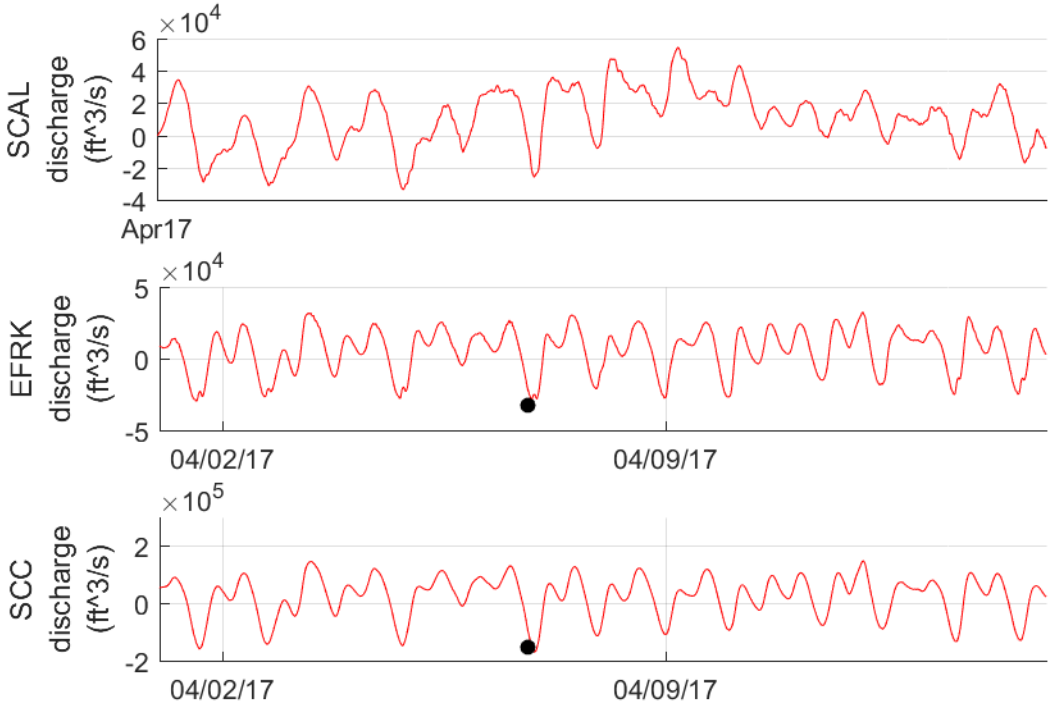

Figure 99. Discharge calibration through the southern passes during April 2017.

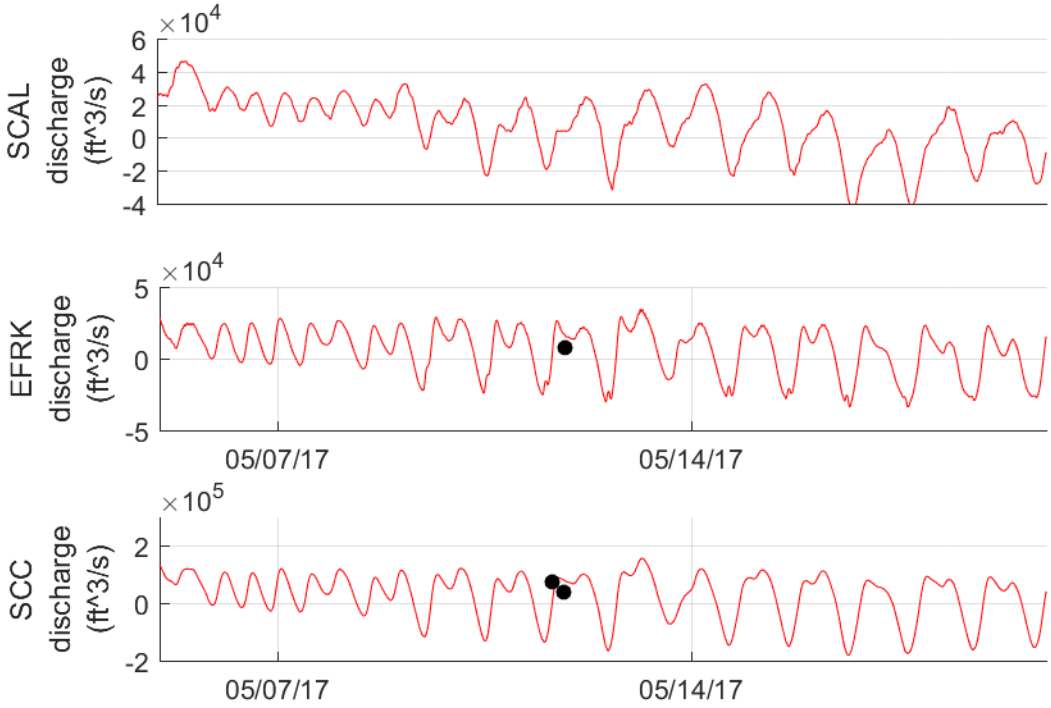

Figure 100. Discharge calibration through the southern passes during May 2017.

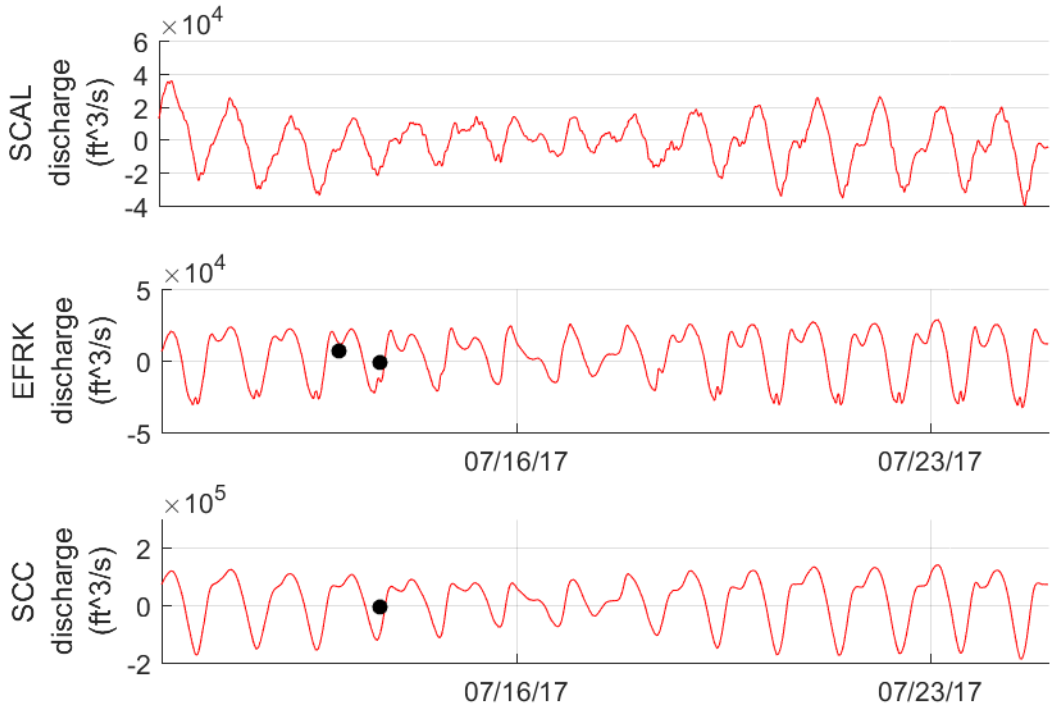

Figure 101. Discharge calibration through the southern passes during July 2017.

References

Agrawal, Y. C., & Pottsmith, H. C. (2000). Instruments for particle size and settling velocity observations in sediment transport. *Marine Geology*, *168*, 89–114.

Agrawal, Y. C., Whitmire, A., Mikkelsen, O. A., & Pottsmith, H. C. (2008). Light scattering by random shaped particles and consequences on measuring suspended sediments by laser diffraction. *Journal of Geophysical Research*, *113*(C4).

Al Ani, S., Dyer, K. R., & Huntley, D. A. (1991). Measurement of the influence of salinity on floc density and strength. *Geo-Marine Letters*, *11*(3), 154–158.

Allison, M. A., Ramatchandirane, C., Di Leonardi, D. R., Esposito, C. R., Meselhe, E. A., & Weathers, H. D. (2018). *Calcasieu Salinity Control Project: Data Collection Phase II (Draft)* (p. 97). Baton Rouge, LA: The Water Institute of the Gulf. Funded by the Coastal Protection and Restoration Authority.

Burban, P.-Y., Lick, W., & Lick, J. (1989). The flocculation of fine-grained sediments in estuarine waters. *Journal of Geophysical Research: Oceans*, *94*(C6), 8323–8330.

CPRA. (2017). *Louisiana's comprehensive master plan for a sustainable coast: committed to our coast* (p. 392). Coastal Protection and Restoration Authority.

Deltares. (2014). Delft3D-FLOW User Manual: Simulation of multi-dimensional hydrodynamic flows and transport phenomena, including sediments. Deltares.

Dyer, K. R., & Manning, A. J. (1999). Observation of the size, settling velocity and effective density of flocs, and their fractal dimensions. *Journal of Sea Research*, *41*(1–2), 87–95.

Fischenich, J. C. (2004). *Calcasieu River and ship channel erosion and sediment impact assessment (phase I) (draft)*. Vicksburg, MS: U.S. Army Engineer Research and Development Center Environmental Laboratory.

HVJ Associates, Inc. (2007). *Geotechnical analysis report DMMP Study Calcasieu River & Pass* (No. HG-06-17340) (p. 322). Houston, TX: HVJ Associates, Inc. Prepared for Gahagan & Bryant Associates Inc. and funded by the U.S. Army Corps of Engineers.

Kineke, G. C., Higgins, E. E., Hart, K., & Velasco, D. (2006). Fine-sediment transport associated with cold-front passages on the shallow shelf, Gulf of Mexico. *Continental Shelf Research*, *26*(17–18), 2073–2091.

Kranck, K., & Milligan, T. G. (1992). Characteristics of suspended particles at an 11-hour anchor station in San Francisco Bay, California. *Journal of Geophysical Research: Oceans*, *97*(C7), 11373–11382.

Levesque, V. A., & Oberg, K. A. (2012). *Computing discharge using the index velocity method: U.S. Geological Survey Techniques and Methods 3–A23* (p. 148). Reston, VA: U.S. Geological Survey.

Manning, A. J., Bass, S. J., & Dyer, K. R. (2006). Floc properties in the turbidity maximum of a mesotidal estuary during neap and spring tidal conditions. *Marine Geology*, *235*(1–4), 193–211.

McBride, R. A., Taylor, M. J., & Byrnes, M. R. (2007). Coastal morphodynamics and Chenier-Plain evolution in southwestern Louisiana, USA: A geomorphic model. *Geomorphology*, *88*, 2007.

McLachlan, R. L., Ogston, A. S., & Allison, M. A. (2017). Implications of tidally-varying bed stress and intermittent estuarine stratification on fine-sediment dynamics through the Mekong's tidal tiver to estuarine reach. *Continental Shelf Research*, 43.

Meselhe, E. (2016). *TO15/16: Sediment erodibility in outfall areas of Barataria and Breton Sound*. Baton Rouge, LA: The Water Institute of the Gulf. Funded by the Coastal Protection and Restoration Authority under Task Orders 15/16.

Mikkelsen, O. A., & Pejrup, M. (2000). In situ particle size spectra and density of particle aggregates in a dredging plume. *Marine Geology*, *170*, 443–459.

Mikkelsen, O., & Pejrup, M. (2001). The use of a LISST-100 laser particle sizer for in-situ estimates of floc size, density and settling velocity. *Geo-Marine Letters*, *20*(4), 187–195.

Ralston, D. K., Geyer, W. R., & Warner, J. C. (2012). Bathymetric controls on sediment transport in the Hudson River estuary: Lateral asymmetry and frontal trapping: SEDIMENT-LATERAL ASYMMETRY AND FRONTS. *Journal of Geophysical Research: Oceans*, *117*(C10), n/a-n/a.

Ramatchandirane, C. G., Allison, M. A., & Weathers, D. H. (2014). *Water and sediment surveys of the Calcasieu Ship Channel in October 2013, February 2014, and March 2014.* (p. 30). Baton Rouge, LA: The Water Institute of the Gulf. Funded by the Coastal Protection and Restoration Authority.

Ruhl, C. A., & Simpson, M. R. (2005). *Computation of discharge using the index-velocity method in tidally affected areas: U.S. Geological Survey Scientific Investigations Report 2005-5004* (p. 31). Reston, VA: U.S. Geological Survey.

Small, L. F., & Prahl, F. G. (2004). A particle conveyor belt process in the Columbia River estuary: evidence from chlorophylla and particulate organic carbon. *Estuaries*, *27*(6), 999–1013.

Tetra Tech. (2015). *Calcasieu Salinity Control Measures Project Feasibility Decision Document, Appendix B Engineering Appendix*.

USACE. (2010). *Hydrodynamic and sediment transport study - Calcasieu River and Pass, Louisiana - Dredged Material Management Plan Phase II: Technical Report Appendix C - Hydrodynamic Studies*. New Orleans, LA: U.S. Army Corps of Engineers.

Wang, Y., White, E., & Meselhe, E. (2018). *Calcasieu Ship Channel Salinity Control Measures Project Phase I Subtask III: Numerical Modeling with MIKE*. Baton Rouge, LA: The Water Institute of the Gulf. Funded by the Coastal Protection and Restoration Authority.

Wells, J. T., & Roberts, H. H. (1980). Fluid mud dynamics and shoreline stabilization: Louisiana chenier plain. *Coastal Engineering Proceedings*, *1*(17), 1382–1401.

Wolanski, E., Huan, N. N., Dao, L. T., Nhan, N. H., & Thuy, N. N. (1996). Fine-sediment dynamics in the Mekong River estuary, Vietnam. *Estuarine, Coastal and Shelf Science*, *43*(5), 565–582.

Wolanski, E., Nhan, N. H., & Spagnol, S. (1998). Sediment dynamics during low flow conditions in the Mekong River estuary, Vietnam. *Journal of Coastal Research*, *14*(2), 472–482.

INTEGRATING APPLIED RESEARCH | LINKING KNOWLEDGE TO ACTION | BUILDING PARTNERSHIPS

THE WATER INSTITUTE
OF THE GULF®

1110 RIVER ROAD S., SUITE 200
BATON ROUGE, LA 70802

(225) 448-2813
WWW.THEWATERINSTITUTE.ORG